University of Kentucky
UKnowledge

Theses and Dissertations--Physiology | Physiology

2021

Rad Modulation of the L-type Calcium Channel Confers Systolic Advantage in the Heart

Brooke Mildred Ahern
University of Kentucky, brooke.ahern@gmail.com
Author ORCID Identifier:
https://orcid.org/0000-0003-2649-6000
Digital Object Identifier: https://doi.org/10.13023/etd.2021.146

Right click to open a feedback form in a new tab to let us know how this document benefits you.

Recommended Citation

Ahern, Brooke Mildred, "Rad Modulation of the L-type Calcium Channel Confers Systolic Advantage in the Heart" (2021). *Theses and Dissertations--Physiology*. 50.
https://uknowledge.uky.edu/physiology_etds/50

This Doctoral Dissertation is brought to you for free and open access by the Physiology at UKnowledge. It has been accepted for inclusion in Theses and Dissertations--Physiology by an authorized administrator of UKnowledge. For more information, please contact UKnowledge@lsv.uky.edu.

STUDENT AGREEMENT:

I represent that my thesis or dissertation and abstract are my original work. Proper attribution has been given to all outside sources. I understand that I am solely responsible for obtaining any needed copyright permissions. I have obtained needed written permission statement(s) from the owner(s) of each third-party copyrighted matter to be included in my work, allowing electronic distribution (if such use is not permitted by the fair use doctrine) which will be submitted to UKnowledge as Additional File.

I hereby grant to The University of Kentucky and its agents the irrevocable, non-exclusive, and royalty-free license to archive and make accessible my work in whole or in part in all forms of media, now or hereafter known. I agree that the document mentioned above may be made available immediately for worldwide access unless an embargo applies.

I retain all other ownership rights to the copyright of my work. I also retain the right to use in future works (such as articles or books) all or part of my work. I understand that I am free to register the copyright to my work.

REVIEW, APPROVAL AND ACCEPTANCE

The document mentioned above has been reviewed and accepted by the student's advisor, on behalf of the advisory committee, and by the Director of Graduate Studies (DGS), on behalf of the program; we verify that this is the final, approved version of the student's thesis including all changes required by the advisory committee. The undersigned agree to abide by the statements above.

Brooke Mildred Ahern, Student

Dr. Jonathan Satin, Major Professor

Dr. Kenneth S. Campbell, Director of Graduate Studies

RAD MODULATION OF THE L-TYPE CALCIUM CHANNEL CONFERS SYSTOLIC ADVANTAGE IN THE HEART

DISSERTATION

A dissertation submitted in partial fulfillment of the
requirements for the degree of Doctor of Philosophy in the
College of Medicine
at the University of Kentucky

By
Brooke Mildred Ahern
Lexington, Kentucky
Director: Dr. Jonathan Satin, Professor of Physiology
Lexington, Kentucky
2021

Copyright © Brooke Mildred Ahern 2021
https://orcid.org/0000-0003-2649-6000

ABSTRACT OF DISSERTATION

RAD MODULATION OF THE L-TYPE CALCIUM CHANNEL CONFERS SYSTOLIC ADVANTAGE IN THE HEART

Heart failure is a major public health problem and a leading cause of mortality. This clinical condition affects populations of all ages, and is the result of various cardiomyopathies. Almost half of these patients suffer specifically from heart failure with reduced ejection fraction; these hearts have decreased performance due to a failure of the heart to contract with sufficient force to meet demand. While there are therapies available to increase contractility, none of these enhance contraction without also further promoting pathological signaling and remodeling.

Under normal physiological conditions, the body elevates cardiac output through the fight-or-flight response. This response activates β-adrenergic receptors (β-AR) at the level of individual cardiomyocytes, which leads to enhanced calcium handling in order to increase contraction. One of the major targets of β-AR downstream signaling is the L-type calcium channel (LTCC). The influx of calcium through the LTCC ($I_{Ca,L}$) provides the trigger for calcium induced calcium release from the sarcoplasmic reticulum in order to produce a contraction; LTCC activity is significantly increased when β-ARs are activated. However, β-ARs are chronically activated in heart failure, leading to pathological remodeling and further development of heart failure. This has served as a foundation to establish dogma that increasing $I_{Ca,L}$ in a manner that reflects β-AR activation necessarily promotes pathology. Because β-AR signaling is a principle physiological mechanism to increase cardiac output, understanding this pathway and how to increase calcium safely is critical to successfully treating heart failure. Discovering a mechanism to increase cardiac output downstream of β-AR signaling would be ideal so as to preserve the fight-or-flight response while also boosting cardiac performance in order to meet demand.

The mechanism by which LTCC activity is increased under β-AR signaling, known as modulation, has been a major focus of study for many years; however, it remains unknown. The LTCC is a heteromultimeric protein complex, and is inhibited by an endogenous small monomeric GTPase called Rad. Studies in heterologous expression systems show overexpression of Rad blocks calcium current through the LTCC; absence of Rad yields a significant increase in calcium current. Whole-body Rad knock out mouse models demonstrate calcium current that mirrors calcium current stimulated by β-AR signaling; however, this also promoted significant growth of the heart. To investigate the effect of Rad deletion without contributions from non-cardiac tissue, a cardiomyocyte-restricted inducible Rad knock out mouse model was created. The work of this

dissertation utilizes this mouse to better understand the mechanism by which Rad inhibits the LTCC by studying the effects on channel function, cellular calcium handling, and overall cardiac structure and function in the absence of Rad.

Using an array of methods and techniques, the studies in this dissertation establish Rad as a critical target of the LTCC to respond to β-AR stimulation. When Rad is depleted specifically from cardiomyocytes, $I_{Ca,L}$ is increased in a safe, stable manner that mirrors LTCC modulation, both in sinoatrial node and in the ventricle. This regulation is governed specifically by the C-terminus of Rad. Elevated $I_{Ca,L}$ in the absence of Rad promotes enhanced calcium handling and increased cardiac output without progression to heart failure, and occurs independently of β-AR activation. Enhanced calcium cycling in the absence of Rad is balanced by accelerated inactivation of the LTCC so as to promote positive inotropy without instigating arrhythmogenesis. This allows for cardiac protection under conditions of pressure-overload induced heart failure. In summary, the work of this dissertation supports Rad deletion specifically from cardiomyocytes as an ideal positive inotrope for heart failure treatment due to the novel mechanism to increase $I_{Ca,L}$ in a manner that preserves structure, function, and the fight-or-flight response within the heart.

KEYWORDS: L-type calcium channel, Rad, β-adrenergic receptor signaling, Fight-or-flight response, Heart Failure

Brooke Mildred Ahern

(Name of Student)

04/23/2021

Date

RAD MODULATION OF THE L-TYPE CALCIUM CHANNEL CONFERS SYSTOLIC ADVANTAGE IN THE HEART

By
Brooke Mildred Ahern

Jonathan Satin, Ph.D.
Director of Dissertation

Kenneth S. Campbell, Ph.D,
Director of Graduate Studies

04/23/2021
Date

To *my parents, my grandparents, and my sister*

ACKNOWLEDGMENTS

Completing this dissertation work would not have been possible for me without the help and guidance from my support system. I would like to acknowledge the following people who have helped me succeed and grow as a student and individual.

First, thank you to my mentor, Dr. Jonathan Satin. Thank you for challenging me daily to become a better scientist, critical thinker, writer, electrophysiologist, and person. Your passion for all things cardiac and calcium quickly convinced me to switch mindsets from neuroscience to studying the mechanisms of the heart, and I am very grateful for that. Thank you for seeing my potential, and helping me to succeed and grow these past five years.

I would also like to express sincere gratitude for the members of my committee: Dr. Doug Andres, thank you for pushing me to think differently (not always as an electrophysiologist) and to see both science and life from a different perspective. Dr. Brian Delisle, thank you for always providing a listening ear and a sounding board for my projects and my life; also, thank you for teaching me how to patch-clamp – a technique that has taught me the true meaning of patience and perseverance. Dr. Ahmed Abdel-Latif, thank you for providing helpful feedback on my work from a clinical perspective, and giving me career advice as I have tried to navigate my future. Dr. John McCarthy, thank you for your support of my work, my love for space, and for allowing me to be an honorary member of your lab. And to Dr. Sanda Despa, thank you for serving as my outside examiner and taking the time to review my dissertation.

Thank you to the American Heart Association for awarding me a pre-doctoral fellowship that funded me for two years. I am sincerely grateful for the time and service

by volunteers within that wonderful organization that provided the financial support so I could pursue my passion for understanding Rad. I am also very grateful for the NIH T32 that I was given my first year within the department and the work from faculty within the department to have that available for students.

I have also been blessed to share the lab with two amazing women, Bryana Levitan and Andrea Sebastian. Thank you Bryana (aka lab mom) for your support and teaching me what you have learned about the heart and about life. Thank you Andrea (the science fairy) for your constant support in all of my experiments, for all of the therapy sessions while isolating cells or making solutions, and for being a great friend. I am a much better person for knowing both of you.

I was also very lucky to join the best department on campus, the Physiology Department. The faculty and staff made each day great – thank you to all those that have given me advice over the years, shared a laugh or taught me both in and out of the classroom. I also appreciate that we had the best lunches, best seminar treats (always had Diet Coke!), and the best holiday parties. I will cherish the fun I had with all of you.

To all of the friends I have made in graduate school: Ben Shaw, Beth Oates, and Sarah Sternbach – the original dream team of first year and the reason I survived. Ryan Cloyd, Brandon Farmer – the wonderful additions to the crew. Our adventure lunches, Mario Kart, parties, therapy sessions and of course the pet therapy from all of you have helped me maintain my sanity throughout the years here. Words do not truly express my gratitude; thank you guys for being a major part of my support system. To Taylor Valentino, Yuan Wen, Ivan Vechetti, and Brooks Mobley – thank you for all of your support while I figured out my life and career, teaching me, letting me vent, always

providing chocolate and Diet Coke, and giving me honorary member status in the lab. I am lucky to have been able to call your lab, as well as the Satin lab, home. To those that I have met in graduate school but have not mentioned thank you for supporting me! I have been very blessed to meet many wonderful people, and call them friends.

To Kate Holbrook and Trent Simmons – friends who have known me for a long time and have been critical support for much of my life. Thank you for the late night phone calls, the supportive texts, and for being the best cheerleaders even though you both are so far away. I would not have gotten this far without you two.

And last, but certainly not least, I want to thank my family. To my wonderful parents, David and Heidi Ahern – thank you for always pushing me to be the best I can be. You have always believed in me, encouraged me to follow my passions, and given me confidence when I doubted myself. I cannot express in words how grateful I am for your sacrifices so that I could make it this far. To my amazing grandparents, Donald and Abbey Schluter and Rel Ahern, who have always been the most supportive of anything I do in life, especially in graduate school. Thank you for always being there, whether in person, in spirit, or on Facetime; I am so grateful to have you in my life. And to the best sister anyone could ask for, Alexandra Ahern – thank you for being my best friend through everything, for understanding all aspects of my life (including getting a PhD), and for inspiring me daily to be better than I was the day before. Thank you for always being the ideal example in my life.

To those that I have not mentioned but have helped me, given me advice, and made my life better, thank you!

TABLE OF CONTENTS

ACKNOWLEDGMENTS ..... **iii**

LIST OF FIGURES ..... **x**

CHAPTER 1 Introduction **1**

1.1 Significance *1*

1.2 L-Type Calcium Channels *3*

1.2.1 Voltage Gated Calcium Channels 3

1.2.2 Structure of the L-type Calcium Channel 4

1.2.2.1 The pore-forming subunit: α_{1C} 4

1.2.2.2 $Ca_V\beta$ subunit 5

1.2.2.3 $\alpha_2\delta$ subunit 5

1.2.2.4 γ subunit 6

1.2.2.5 Calmodulin 6

1.2.3 Function of the L-type Calcium Channel 7

1.2.3.1 Excitation Contraction Coupling 7

1.2.3.2 Activation of the L-type Calcium Channel 8

1.2.3.3 Inactivation of the L-type Calcium Channel 10

1.2.3.4 L-type Calcium Channel Regulation by Facilitation 12

1.2.3.5 Modulation of the L-type Calcium Channel 13

1.2.4 Role of the L-type Calcium Channel in Cardiac Pathophysiology 17

1.2.4.1 Arrhythmias 17

1.2.4.2 Early After Depolarizations 18

1.2.4.3 Timothy Syndrome 19

1.2.4.4 Brugada Syndrome 20

1.2.4.5 Heart Failure 21

1.2.4.5.1 Cardiac Hypertrophy 22

1.2.4.5.2 Loss of β–Adrenergic Receptor Stimulation 23

1.3 Rad *24*

1.3.1 RGK Proteins 24

1.3.2 Structure of Rad 25

1.3.3 Function of Rad 26

1.4 Working Hypothesis *29*

CHAPTER 2. Materials and Methods **33**

2.1 Animal Model *33*

2.2 TAC *34*

2.3 Immunoblotting *35*

2.4 Quantification of myofibril protein phosphorylation *36*

2.5 Ventricular myocyte isolation *36*

2.6 Electrophysiological recordings *37*

2.7 Calcium Transients *38*

2.8 Single Cell Database Analysis *39*

2.9 Quantitative Proteomics Database Analysis *40*

2.10 RNA In Situ Hybridization *41*

2.11 Quantitative RT-PCR *41*

2.12 Histology *42*

2.13 Echocardiography *42*

2.14 Radiotelemetry *43*

2.15 Surface ECG *44*

2.16 Open Behavioral Assessment *44*

2.17 Statistical Analysis *44*

CHAPTER 3. Myocardial-Restricted Ablation of the GTPase RAD Results in a Pro-Adaptive Heart Response in Mice 46

3.1 Preface *46*

3.2 Introduction *46*

3.3 Results *48*

3.3.1 Development of conditional cardiac-restricted RAD-deficient transgenic mice 48

3.3.2 Cardiac-restriced RAD-deficient mice (*RAD*$^{\Delta/\Delta}$) show improved function with no changes in heart dimensions 49

3.3.3 *RAD*$^{\Delta/\Delta}$ modification of voltage-gated calcium current, $I_{Ca,L}$ 51

3.3.4 *RAD*$^{\Delta/\Delta}$ enhances cellular calcium homeostasis 52

3.3.5 Basal $I_{Ca,L}$ in *RAD*$^{\Delta/\Delta}$ cardiomyocytes reflects a modulated $I_{Ca,L}$ 54

3.3.6 *RAD*$^{\Delta/\Delta}$ basal heart function is elevated *in vivo*, yet retains a partial ISO response 54

3.3.7 *RAD*$^{\Delta/\Delta}$ retains β−adrenergic receptor modulation of calcium and sarcomere dynamics 55

3.4 Discussion *56*

3.4.1 Increased calcium does not necessarily promote cardiac hypertrophy 57

3.4.2 Myocardial-restricted RAD deletion differs from whole body RAD deletion 60

CHAPTER 4. Rad-GTPase Contributes to Heart Rate Via L-type Calcium Channel Regulation 76

4.1 Preface *76*

4.2 Introduction *76*

4.3 Results *78*

4.3.1 SANcm express Rad 78

4.3.2 L-type calcium current ($I_{Ca,L}$) in SANcm 80

4.3.3 RAD reduction increases intrinsic heart rate 81

4.3.4 Rad-deletion effects on HR are greatest when Sympathetic Drive is Relatively Low 82

4.4 Discussion *83*

4.4.1 Rad is a key contributor to SANcm $I_{Ca,L}$ modulation 84

4.4.2 Relationship among SANcm heterogeneity, Rad expression, and SAN function 86

4.4.3 Diurnal impact and ANS drive with Rad reduction 87

4.5 Limitations *88*

4.6 Conclusions *89*

CHAPTER 5. Enhanced Inactivation Balances Increased Peak L-Type Calcium Current in the Absence of Rad 99

5.1 Preface 99

5.2 Introduction 99

5.3 Results 102
5.3.1 cRadKO mirrors modulated LTCC 102
5.3.2 Increased Ca^{2+} and Rad both contribute to CDI 103
5.3.3 Rad does not alter the late component of LTCC decay 104
5.3.4 Faster kinetics in cRadKO prevent alterations in cardiac electrophysiology 105
5.3.5 cRadKO yields modulated kinetics of LTCC downstream of β–AR signaling 107

5.4 Discussion 109
5.4.1 Rad contributes to regulation of LTCC inactivation 110
5.4.2 Rad is a key contributor to LTCC Modulation 111
5.4.3 Rad regulation of LTCC is independent of β–adrenergic receptor signaling 113

5.5 Limitations 114

5.6 Conclusions 114

CHAPTER 6. Alterations to Rad Structure Modulate LTCC Gating 129

6.1 Preface 129

6.2 Introduction 129

6.3 Results 131
6.3.1 Rad-Flag A277X increases cardiac function and wall thickness 131
6.3.2 Rad-Flag A277X enhances LTCC gating 132

6.4 Discussion 133

CHAPTER 7. Myocardial Rad deletion Preserves Cardiac Function in Pressure-Overload Induced Heart Failure 141

7.1 Preface 141

7.2 Introduction 141

7.3 Results 143
7.3.1 cRadKO protects *in vivo* heart function from pressure-overload induced heart failure 143
7.3.2 cRadKO enhances *in vivo* heart function after pressure-overload 144
7.3.3 cRadKO maintains elevated calcium cycling after pressure-overload 145
7.3.4 Response to β–adrenergic receptor stimulation remains blunted in cRadKO after pressure-overload 147
7.3.5 cRadKO promotes recovery of function in advanced stages of pressure-overload 147
7.3.6 cRadKO prevents progression of cardiac dysfunction in advanced stages of pressure-overload 148
7.3.7 cRadKO improves quality of life in advanced stages of pressure-overload 150

7.4 Discussion 150
7.4.1 Myocardial-restricted Rad deletion preserves cardiac function in pressure-overload induced heart failure 151
7.4.2 Myocardial-restricted Rad deletion differs from whole-body knockout of Rad 153

CHAPTER 8. Discussion 172

8.1 Rad is a critical regulatory site for LTCC modulation *172*
8.2 Rad governs $I_{Ca,L}$ by multiple mechanisms *173*
8.3 Hypertrophic signaling is not exclusively dependent on elevated $I_{Ca,L}$ *176*
8.4 Enhanced $I_{Ca,L}$ does not necessarily promote electrical dysfunction *178*
8.5 Targeting Rad represents the ideal positive inotrope *180*
8.6 Future directions *182*
8.7 Limitations *184*
8.8 Conclusions *184*

APPENDIX **186**

REFERENCES **192**

VITA **213**

LIST OF FIGURES

Figure 1.1 L-type Calcium Channel Complex. 31
Figure 1.2 L-type Calcium Channel pore-forming subunit α_{1C}. 32
Figure 3.1 Myocardial deletion of Rad. 62
Figure 3.2 Cardiomyocyte-restricted Rad deletion does not induce markers of myocardial pathology. 63
Figure 3.3 Figure 3.3. Myocardial Rad deletion results in a rapid, stable gain of cardiac function without pathological structural remodeling in vivo. 64
Figure 3.4 Myocardial Rad deletion results in increased calcium current ($I_{Ca,L}$)..... 65
Figure 3.5 Rad$^{\Delta/\Delta}$ enhances cellular calcium handling. 66
Figure 3.6 RAD$^{\Delta/\Delta}$ enhances sarcomere shortening and increases the tension-integral. 67
Figure 3.7 ISO does not alter RAD$^{\Delta/\Delta}$ $I_{Ca,L}$. 68
Figure 3.8 β-AR-mediated responsiveness retained following Rad deletion *in vivo* 69
Figure 3.9 Cardiomyocyte cytosolic Ca^{2+} handling responds to β-AR-mediated activation in RAD$^{\Delta/\Delta}$..... 70
Figure 3.10 Sarcomere dynamics and proteins respond to β-AR-mediated activation in RAD$^{\Delta/\Delta}$..... 71
Supplemental Figure 3.11 Myocardial Rad deletion results in increased calcium current ($I_{Ca,L}$). 72
Supplemental Figure 3.12 RAD$^{\Delta/\Delta}$ $I_{Ca,L}$ response after β-adrenergic receptor stimulation. 73
Supplemental Figure 3.13 RAD$^{\Delta/\Delta}$ cellular response after β-adrenergic receptor stimulation. 74
Supplemental Figure 3.14 No effect on sarcomere dynamics after treatment with ISO. 75
Figure 4.1 RRAD is expressed in SANcm. 90
Figure 4.2 RAD is expressed in SANcm. 91
Figure 4.3 Rad reduction increases SANcm $I_{Ca,L}$. 92
Figure 4.4 β-AR stimulation has no significant effect on cRadKO SANcm ICa,L. 93
Figure 4.5 Intrinsic heart rate increases after Rad deletion. 94
Figure 4.6 Rad deletion increases heart rate in the sleep phase. 95
Figure 4.7 Rad deletion demonstrates preserved Heart Rate Variability (HRV). 96
Supplemental Figure 4.8 No significant difference between males and females of $I_{Ca,L}$ in CTRL and cRadKO. 97
Figure 4.9 Rad Deletion Increases Sinus Heart Rate..... 98
Figure 5.1 Rad deletion $I_{Ca,L}$ phenocopies modulated $I_{Ca,L}$. 116

Figure 5.2 Rad deletion accelerates fast component of $I_{Ca,L}$ decay. 117
Figure 5.3 Rad regulation of ICa,L kinetics requires SR Ca^{2+} release. 118
Figure 5.4 Rad does not alter slow component of $I_{Ca,L}$ decay. 119
Figure 5.5 Rad deletion enhances VDI. 120
Figure 5.6 Rad deletion does not prolong action potential duration or QT interval. 121
Figure 5.7 Rad deletion increases heart function exclusive of β1β2-Adrenergic Receptors. 122
Figure 5.8 Rad deletion yields modulated $I_{Ca,L}$ in the absence of $\beta_1\beta_2$-Adrenergic Receptors. 123
Figure 5.9 Rad modulates $I_{Ca,L}$ independent of $\beta_1\beta_2$-Adrenergic Signaling to Confer Systolic Advantage. 124
Supplemental Figure 5.10 Two-way ANOVA 95% confidence intervals and tabular results. 125
Supplemental Figure 5.11 Two-way ANOVA 95% confidence intervals and tabular results. 126
Supplemental Figure 5.12 Surface ECG Measurements. 127
Supplemental Figure 5.13 Whole Heart measurements of dKO and tKO. . 128
Figure 6.1 Schematic of Rad-Flag and Rad-Flag A277X transgenic mice. . 137
Figure 6.2 Rad-Flag A277X enhances cardiac function and increases wall thickness. 138
Figure 6.3 Rad-Flag A277X enhanced LTCC function 139
Figure 6.4 Rad-Flag A277X enhanced inactivation. 140
Figure 7.1 Loss of cardiomyocyte Rad before pressure overload prevents progression of cardiac dysfunction. 155
Figure 7.2 ANOVA 95% confidence intervals and tabular results. 156
Figure 7.3 Loss of cardiomyocyte Rad before pressure overload does not protect all pathological signaling. 157
Figure 7.4 One-way ANOVA 95% confidence intervals and tabular results. 158
Figure 7.5 Loss of cardiomyocyte Rad before pressure overload promotes survival and enhances cardiac function. 159
Figure 7.6 ANOVA 95% confidence intervals and tabular results. 160
Figure 7.7 Loss of cardiomyocyte Rad increases ICa,L after pressure-overload. 161
Figure 7.8 ANOVA 95% confidence intervals and tabular results. 162
Figure 7.9 Loss of cardiomyocyte Rad enhances cellular calcium handling after pressure-overload. 163
Figure 7.10 Loss of cardiomyocyte Rad does not alter sarcomere dynamics after pressure-overload. 164
Figure 7.11 β-AR stimulation does not alter $I_{Ca,L}$ in Rad deletion after pressure-overload. 165

Figure 7.12 β-AR stimulation response in cellular calcium handling is blunted after pressure-overload. 166
Figure 7.13 Loss of cardiomyocyte Rad after pressure overload prevents progression of cardiac dysfunction..... 167
Figure 7.14 ANOVA 95% confidence intervals and tabular results. 168
Figure 7.15 Loss of cardiomyocyte Rad after pressure overload prevents progression of cardiac dysfunction..... 169
Figure 7.16 ANOVA 95% confidence intervals and tabular results. 170
Figure 7.17 Loss of cardiomyocyte Rad after pressure overload improves locomotive activity. 171

CHAPTER 1. INTRODUCTION

1.1 Significance

The incidence of heart failure (HF) is steadily increasing, with projections putting heart failure as the leading cause of mortality and morbidity in developed countries by the year 2030 [1, 2]. Many cardiovascular disorders, including atherosclerosis, cardiomyopathy, and hypertension, result in the development of HF. Of these patients, ~45% suffer from HF with reduced ejection fraction (HFrEF). HFrEF results in a decrease in cardiac performance due to a failure of the heart to contract with sufficient force to meet demand; this is soon followed by problems in other organ systems, such as neurohormonal, circulatory, and renal systems [3, 4]. Current therapies are limited to increasing survival and reducing symptoms, but are accompanied by side effects and ultimately fail to increase systolic function or inhibit HF progression [3-5].

Cardiac contractility is governed by calcium cycling within individual cardiomyocytes. During a cardiac action potential, calcium enters the cell via voltage-gated calcium channels, specifically L-type calcium channels (LTCC). This calcium triggers calcium release from the sarcoplasmic reticulum (SR), raising cytosolic calcium concentration ~ten-fold to activate muscle contraction. Upon relaxation, calcium is either taken back up into the SR via SERCA2a (Sarco/endoplasmic reticulum calcium ATPase) or extruded from the cell via the Na^+/Ca^{2+} exchanger (NCX) [3, 4, 6]. In HF, calcium transients are depressed, resulting in decreased contractile function,[6, 7]. Logically, it would follow that a treatment for HF would therefore be to increase calcium within the cardiomyocyte in order to increase contraction. Indeed, the body naturally increases

cardiac contractility by increasing sympathetic drive and activating the β-adrenergic receptor (β-AR) signaling cascade. However, chronic stimulation of this cascade triggers pathological remodeling of the heart, thereby promoting the development of HF ([4, 6, 8, 9]. Studies focusing on the utilization of positive inotropes have proven to be acutely effective, but chronically induce further damage on the heart by initiating hypertrophic signaling and triggering arrhythmias [5-7, 9, 10]. It has therefore become dogma that increasing calcium within a cardiomyocyte directly causes pathology and ultimately results in HF.

Many studies have focused on the SR, [3-5, 7] the pathways associated with β-AR signaling [8, 11], or certain components of the LTCC complex [12-15] as potential therapeutic targets for HF; unfortunately, they have yet to find a target that increases contraction without instigating more pathology as a side effect. A recent new potential therapeutic target that has emerged is Rad, a small monomeric GTPase that serves as an endogenous inhibitor to the LTCC [16-24]. The studies of this dissertation focus primarily on the mechanism by which the absence of Rad confers systolic advantage on the heart independently of β-AR signaling, thereby preserving the cardiac response to autonomic input without pathological structural remodeling.

β-AR stimulation is the principle physiological mechanism whereby contractility and cardiac output is increased; the guiding principle for treating heart failure, and this dissertation, is that enhancing systolic function exclusive of adrenergic activation is safe and beneficial [5].

1.2 L-Type Calcium Channels

1.2.1 Voltage Gated Calcium Channels

Voltage-gated calcium channels (VGCC) are found in all excitable cells; these channels support longer depolarizing responses because they can maintain inward current, and also are the only link between non-electrical components and excitation [25, 26]. Calcium entering via VGCCs serves as an elemental secondary messenger that initiates numerous intracellular events, including contraction [25, 27-31]. Signal transduction via VGCCs differs depending on cell type, thereby requiring different molecular subtypes of channels to have unique physiological, pharmacological and regulatory properties [25, 28]. VGCCs were first differentiated based on activation threshold, classified as either low-voltage-activated (LVA) or high-voltage-activated (HVA) [25, 28, 29]. Calcium channels are also large heteromeric proteins and are categorized based on structure of the complex [29]. The first purified calcium channel was isolated from skeletal muscle and comprised of five components: α_1 (170 kDa), α_2 (150 kDa), β (52 kDa), δ (17-25 kDa), and γ (32 kDa) in an approximately stoichiometric ratio (**Figure 1.1A**; [28-30]. This complex was also termed the dihydropyridine receptor for its sensitivity to 1,4-dihydropyridines (DHPs); because α_1 was identified as the subunit of the complex that bound DHPs, it was established that it was the pore-forming subunit [29]. As of now, there are 10 different α_1 subunits that have been discovered and all exhibit distinct functions (**Figure 1.1B,C**). These include L-type, P/Q-type, N-type, R-type, and T-type calcium channels [25, 28, 29]. HVA channels that were sensitive to DHPs were identified as 'long-lasting' or L-type channels because of slow voltage dependent inactivation and are long lasting when barium is used as the charge carrier [25,

28]; these channels form the Ca_V1 family [25, 28, 29, 32, 33]. $Ca_V1.1$ expression is restricted to skeletal muscle, while $Ca_V1.4$ expression is restricted to the retina [29]. $Ca_V1.2$ and $Ca_V1.3$ are found in many different excitable cell types with both often expressed in the same cell [29], such as adrenal chromaffin cells, neurons, and sinoatrial and atrial cardiomyocytes [29]. The remainder of this chapter will focus primarily on $Ca_V1.2$ and its role in cardiac function.

1.2.2 Structure of the L-type Calcium Channel

1.2.2.1 The pore-forming subunit: α_{1C}

The α_1 subunit that comprises $Ca_V1.2$ is encoded by the gene cacna1c [34]. The α_1 subunit is approximately 2000 amino acid residues and is organized into four repeated domains (I-IV) that each contain six transmembrane segments (S1-S6) and a membrane-associated loop between transmembrane segments S5 and S6 (**Figure 1.2**; [29, 35]. The domains are connected by intracellular loops linking domain I-II, domain II-III, and domain III-IV [36], and end in NH_2- and COOH-terminal intracellular segments [34]. In each domain, S1-S4 segments form a voltage-sensing domain [37], with S4 being the primary 'voltage sensor' for activation [25, 28, 29]. In every third position within the helix of the S4 are positively charged Arg or Lys that sense depolarization of the membrane [37]. Changes in the electric field of the membrane cause the S4 segment to rotate outwards, thereby changing the conformation of the channel to open the pore [25, 28]. The S5 and S6 segments and the associated loop form the pore lining of the channels [25, 28, 29, 38]. The external portion contains a pair of glutamate residues within the pore loop that act as the selectivity filter for the channel so that it is calcium-specific; the

inner pore is formed by the S6 segments and contains the receptor sites for antagonist, pore-blocking drugs specific for L-type calcium channels [25, 28, 29, 38]. Though a structural model of the $Ca_V1.2$ pore has been suggested [39], a detailed three-dimensional structure of calcium channels is not known [25, 28]. For clarity and consistency, the remainder of the dissertation will refer to $Ca_V1.2$ simply as LTCC (L-type calcium channel).

1.2.2.2 $Ca_V\beta$ subunit

A requirement for normal LTCC function is the auxiliary $Ca_V\beta$ subunit [40]. There are four distinct genes that encode four subfamilies of $Ca_V\beta$ (β_1-β_4), each of which regulate LTCC differently [29, 40]. Each consist of a core region, composed of two highly conserved regions homologous to the SRC homology 3 (SH3) and guanylate kinase (GK) domains; these are joined together by the HOOK region [25, 40]. $Ca_V\beta$ binds to the α_1 subunit in a 1:1 stoichiometric fashion with high affinity to a single site within the α-interaction domain (AID), the first half of the cytoplasmic linker connecting domains I and II of the α_1 subunit (**Figure 1.2**; [25, 28, 40, 41]. The AID forms an α-helix that binds tightly to a groove within the GK domain of $Ca_V\beta$, and is critical for $Ca_V\beta$ regulation of calcium channels [25, 40]. The GK domain of $Ca_V\beta$ also contains the interaction sites for other proteins that regulate channel function, such as RGK GTPases [20, 40]. The interaction between $Ca_V\beta$ and LTCC is crucial for normal channel function, and modulates channel activity [25, 28, 40, 41], which will be further discussed in the next section.

1.2.2.3 $\alpha_2\delta$ subunit

The LTCC complex also contains the $\alpha_2\delta$ subunit (**Figure 1.1A**). $\alpha 2$ and δ are produced from a single gene and proteolytically cleaved to form separate proteins but still attached via a disulfide bond [25, 29, 40, 42]. There are also four distinct genes that encode $\alpha_2\delta$ ($\alpha_2\delta$1-4), that correspond to specific tissues, with $\alpha_2\delta$1 highly expressed in skeletal muscle [42, 43]. The δ peptide of the subunit anchors the subunit to the extracellular membrane via a glycosylphosphatidylinositol linker [41, 42]. The main function of $\alpha_2\delta$ is to increase calcium channel expression and retention within the membrane, and contributes minorly to channel gating properties [25, 28, 29, 40, 42].

1.2.2.4 γ subunit

The γ subunit of LTCC complex is a glycoprotein that has four transmembrane segments and intracellular amino and carboxy termini (**Figure 1.1A**) [25, 28, 41]. There are eight different genes that encode γ subunits that all have diverse functions, depending on the tissue in which they are expressed, though the function of each subunit is not fully known [41]. Of these eight genes, only $Ca_V\gamma$1 and $Ca_V\gamma$6 are considered to be a subunit of voltage-gated calcium channels [34]. In regards to calcium channel function, γ subunits primarily contribute to voltage dependence of activation and inactivation in a small but significant manner [25, 28, 41, 44]. Although $Ca_V\gamma$1 was found in skeletal muscle, it appears there are no $Ca_V\gamma$ subunits expressed in the heart [13].

1.2.2.5 Calmodulin

A critical protein that associates with the LTCC complex is a ubiquitous calcium-sensing protein called calmodulin (CaM) [45]. CaM associates with the carboxyl-

terminus of the α_1 subunit within the EF hand, pre-IQ, and IQ regions and serves as a key regulator of channel function and targeting LTCC to the cell surface (**Figure 1.2**; [45-47]. For every channel, there is one CaM molecule in association [48, 49]. Each molecule of CaM is composed of two lobes, each made of two EF hands [49]. The N-terminal lobe acts as a 'global' calcium sensor for the channel, sensing an elevation of calcium within the couplon or junction; the C-terminal lobe acts as a 'local' calcium sensor, triggering regulatory signaling of the channel based on calcium flowing through individual channels [49]. Specific interactions within the IQ domain and the two lobes cause different calcium-dependent regulatory processes to occur within the channel [46], which will be discussed in the next section.

1.2.3 Function of the L-type Calcium Channel

1.2.3.1 Excitation Contraction Coupling

Calcium is a critical intracellular second messenger that initiates multiple signaling pathways within the cell [5, 6]. In a cardiomyocyte, the membrane is depolarized in response to an action potential and LTCCs open to provide an influx of calcium needed for excitation contraction coupling [6]. LTCCs also maintain membrane depolarization during the plateau phase of the cardiac action potential [44]. Because alterations in calcium influx affect action potential duration and refractory period duration, the LTCC contributes to electrical balance that allows contraction and relaxation of the myocardium [44, 50].

LTCCs are expressed within the transverse tubules of the membrane in close proximity (~12-20 nm) to ryanodine receptors (RyR2) so that the calcium influx from the channel induces calcium induced calcium release (CICR) from the sarcoplasmic reticulum

(SR) [6, 45]. This provides the necessary elevation in cytosolic calcium to activate myofilaments and generate contractile activity [6, 51]. At the junction between plasma membrane and the sarcoplasmic reticulum, ~25 LTCCs and ~100 individual RyR2 form a unit known as the couplon [51]. Couplons are spaced between 1-2 µm away from each other so that neighboring couplons can activate calcium release synchronously and provide a unified contraction within the entire cardiomyocyte [6, 51].

There is also a subset of LTCCs that are expressed within the caveolae of ventricular myocytes, a type of lipid raft that create small invaginations within the plasma membrane and characterized by the expression of caveolin-3 [45]. The fraction of LTCCs found in the caveolae range depending on species, but it is estimated that in mice, ~50% of LTCCs are found in the caveolae; the mechanisms by which LTCCs are sorted either to transverse tubules versus caveolae remain unknown [45]. It is unclear whether LTCCS that exist in the caveolae contribute to excitation contraction coupling within the entire cardiomyocyte, or rather in a more localized fashion [45]. However, studies have shown these channels play a critical role in NFAT signaling and β_2-adrenergic signaling [52, 53]. Because cardiac LTCCs are expressed in multiple microdomains within the plasma membrane and play a major role in critical signaling pathways within the cardiomyocyte, channel activity is tightly regulated to prevent cellular and cardiac dysfunction [45].

1.2.3.2 Activation of the L-type Calcium Channel

The activation of a channel occurs via charge movement in four domains, with a resulting ‘concerted’ step of opening the pore [54]. Modifications in activation could occur due to changes in the four domains, or in the step of the pore opening [55]. For LTCCs, channels

activate once the membrane has depolarized to about -30 mV [46]. Gating charge movement is governed by the S4 segments within each domain, though the specific segment contributions is unclear. One study suggests S4 from domain I and domain III determine the voltage dependence of channel opening and channel closing, while all four voltage sensors contribute to stabilizing the channel in an open state [55]; a different study observed that S4 segments from domain II and III played a major role in activation, while domain I only played a minor role [37]. The cooperative step of opening the pore results from the interaction between the S4 segments in domain I, II, and III with the S6 segment in all four domains [55]. The specific S6 segments that contribute to activation of the LTCC still remain undetermined, though studies suggest the binding of Cavβ to the AID induces a conformational change between the S6 of domain I and the linker between domain I and II that contributes to activation [34, 56]. Cavβ causes a hyperpolarized shift in voltage dependence of activation, ~10-15 mV, accelerates activation, and increases the open probability of the channel when present in the complex [40, 41].

An emerging hypothesis is that individual LTCCs can activate additional channels in close proximity through physical tethers between their C-terminal tails [57-59]. When multiple channels are adjoined, the resulting clusters coordinate activity to open synchronously to provide a larger calcium influx, thereby causing a larger calcium release from the SR [57, 58]. The clustering is dictated by calcium complexing with CaM [58]. When one channel opens during an action potential, the resulting calcium sparklet[1] induces binding between calcium and CaM; this promotes the physical interaction between the C-

1Footnote: A sparklet is a local calcium release event by a single RyR2 (190).

termini of the open channel and a neighboring LTCCs [57, 58]. As more channels physically interact as more calcium flows in, clusters form; once individual channels begin to inactivate, coupled channels begin to disassemble and activity decreases [58]. Some channels remain clustered, forming a 'molecular memory' and instant increases in calcium influx upon subsequent action potentials [58]. This mechanism of cooperativity is hypothesized to be a way that LTCCs are regulated, either during β-adrenergic receptor stimulation or during facilitation [58, 59]. These regulatory processes will be discussed later.

1.2.3.3 Inactivation of the L-type Calcium Channel

Inactivation of the LTCC is a key regulatory mechanism to concomitantly control action potential plateau duration and levels of intracellular calcium [46]. During depolarization, calcium current ($I_{Ca,L}$) decays in a non-exponential fashion but is divided into two components; investigators have described this complex process by fitting a double exponential function to the data [34, 60]. These studies have yielded a fast component and a slow component with time constants of 10 ms and 90 ms, respectively [34, 50, 60-63]. $I_{Ca,L}$ decay occurs by two distinct processes: calcium dependent inactivation (CDI) and voltage dependent inactivation (VDI) [64, 65].

CDI is hypothesized to dominate the early, fast component of $I_{Ca,L}$ [60, 66]. Calcium induced inactivation was first proposed by Eckert and Tillotson; their experiments illustrated that the depression of calcium currents seemed to be based on a calcium dependent mechanism [67]. It is now known that this is dictated by calcium directly associating with CaM [34, 49]. Calcium complexes with CaM and the LTCC undergoes a

conformational change to induce rapid inactivation [45, 48, 49, 68-72]. For LTCC, the C-lobe of CaM is responsible for the rapid phase of CDI [45, 48, 49, 68-72]; the N-lobe of CaM contributes minimally to CDI [72]. CaM binds to the IQ motif on the C-terminus of LTCC α_{1C}, specifically amino acids 1624-1635; disruption of this region abolished CDI [34, 49, 72]. Amino acid 1624 of this region is isoleucine, and is required for CaM binding; studies in heterologous expression systems demonstrated that the mutation I1624A decreased the affinity of CaM binding and abrogated CDI [34, 49]. Two other elements that are essential for CDI are $Ca_V\beta$ and a rigid IS6-AID linker; mutations that disrupted the α-helix of IS6-AID linker or that disrupted $Ca_V\beta$ binding to $Ca_V\alpha_1$ both drastically slowed CDI [41, 73]. The source of calcium to induce CDI can be from the sarcoplasmic reticulum (SR) or from entry through the LTCC [45, 48, 49, 66, 68-72]. Calcium released from the SR is thought to control CDI in the initial phase of the action potential, and calcium entering through the channel is suggested to control CDI in the remainder of the action potential [66].

It is generally accepted that the late, slow component of $I_{Ca,L}$ decay is dominated by VDI [60, 66]; however, some studies claim that VDI contributes to both components but is dampened when calcium influx increases [60, 74-76]. Early studies demonstrated that inactivation of the LTCC occurred independent of ion permeation, and displayed a monotonic dependency on membrane potential [77-79]. Many of these experiments used barium as the charge carrier in order to isolate inactivation dependent on calcium [34, 77] [78, 79]. The mechanism by which VDI occurs remains controversial. Key players involved in the mechanism include: the S4 segments of α_1, the cytosolic ends of the S6 segments of α_1, the linker between domain I and II, the N- and C-termini of LTCC, the

AID of LTCC, and Cavβ [34, 55, 67, 80]. One hypothesis has been that all four S4 segments contribute to a global conformational change to induce inactivation, though specific roles of each segment remain unknown [55] [80]. Other studies have suggested that the interaction between Cavβ and the AID modifies VDI and CDI through a conformational change between the S6 of domain I and the linker between domain I and II so that the linker occludes the channel pore; indeed, the presence of Cavβ in the complex shifts voltage dependence of inactivation more negative and increases the rate of inactivation, though this is dependent on isoform [25, 28, 34, 40, 41]. Depending on which isoform of Cavβ is part of the complex, the different isoforms of the γ subunit also induce a hyperpolarizing shift in VDI [41]. A recent study argued that the linker between domain I and II does not occlude the pore; rather inactivation is based on a displacement of the AID and the S6 of domain I towards the pore axis, initiating closure [67]. Though much is known about the major contributors to VDI and CDI, the molecular mechanisms by which LTCC inactivation is governed remains elusive.

1.2.3.4 L-type Calcium Channel Regulation by Facilitation

Changes in the stimulation frequency can regulate LTCC activity that either decreases or increases macroscopic calcium current through a mechanism known as facilitation [81-87]. This mechanism is critical to cardiac function because it regulates calcium influx at fast heart rates [34, 88]. Early studies demonstrated that in response to repetitive channel activation or a strong pre-pulse to positive potentials resulted in an increase in $I_{Ca,L}$ amplitude [85, 86]. The conclusion was this was governed in a voltage-dependent manner; however, increase in current due to short-pulse trains was lost when

calcium was replaced with barium [87]. Facilitation was also blocked by BAPTA, a fast calcium chelator, but was unaffected by EGTA, a slower calcium buffer, which indicated that the mechanism of facilitation is calcium-dependent and localized to the calcium channel [34, 82, 84]. It was then established that facilitation was mediated by CaM and CaMKII (Calmodulin Kinase II) [34, 81, 82, 84]. Recent studies have shown that inhibiting CaM or CaMKII results in blocking CDF; CaMKIIδ-knock out mouse displayed reduced CDF [34, 88]. It is known that the IQ motif is required for CDF to occur [89]. The proposed phosphorylation sites for CaMKII on the α_1 subunit are S1512 and S1570, though alanine mutations of these sites do not completely abolish CDF [90]. T500 on Cavβ is also a phosphorylation site for CaMKII, but deletion of this site did not affect CDF at all [91]. It has also been suggested that CDF is dependent on channel clustering [58]. When channels couple together to form a cluster, the entire population of channels within the cluster activate together to amplify influx during high-frequency stimulation, thereby potentially demonstrating a CaMKII-independent mechanism of facilitation [58]. While much is known about this regulatory process, the molecular mechanisms by which the LTCC is facilitated remains elusive.

1.2.3.5 Modulation of the L-type Calcium Channel

During the fight-or-flight response, LTCC activity is enhanced by β-adrenergic receptor (β-AR) stimulation to increase contractility [25, 28, 92-95]. This form of regulation has been defined as LTCC modulation and is the most thoroughly studied LTCC regulatory mechanism [25, 28]. Voltage-clamp experiments first described that addition of adrenaline or norepinephrine resulted in increased inward I_{Ca} and increased conductance

that translated to increased plateau height and duration of the action potential [94, 95]. Later studies demonstrated these effects were mediated by cAMP and of cAMP-dependent protein kinase; direct injection of cAMP or the catalytic subunit of cAMP-dependent protein kinase yielded I_{Ca} identical to I_{Ca} treated with adrenaline or norepinephrine [94, 96-100]. While cAMP can be increased due to activation of multiple receptors, LTCC modulation occurs specifically through the signaling downstream of β-AR stimulation [101]. cAMP localized to the t-tubule and caveole compartments of the cardiomyocyte has been shown to be the critical microdomain for β-AR stimulation, compared to cAMP in the cytosolic compartments [101, 102]. It has now known that the pathway includes the following cascade: β-AR stimulation, activation of adenylyl cyclase, increase in cAMP, activation of PKA and phosphorylation of the LTCC [103]. Upon activation of β-ARs, $I_{Ca,L}$ increases significantly, voltage dependent activation is shifted to hyperpolarized potentials, and CDI is enhanced; the overall result is a gain of LTCC function [103].

Studies in Chinese hamster ovary cells first revealed that modulation of the LTCC required the activation of the cAMP-dependent protein kinase A (PKA; [28, 104, 105]. Phosphorylation of LTCC by PKA results in a two- to four-fold increase in $I_{Ca,L}$ in the cell, and was long thought to be the main mechanism of LTCC modulation [28, 31, 106-109]. Ser1928, Ser1700, and Thr1704 on α_{1C} and Ser459, Ser478, and Ser479 on Cavβ were all eligible to be the critical site or sites needed for LTCC modulation; however, single mutations of each site did not eliminate LTCC modulation [91, 110, 111]. When all of the serines and threonines were mutated at the same time *in vivo*, treatment with isoproterenol still induced LTCC modulation [112]. However, recent studies demonstrate that alanine

substitutions at Ser1700 and Thr1704 in transgenic mice markedly decreased basal and modulated $I_{Ca,L}$ [107, 108, 113].

LTCCs can undergo proteolytic cleavage at the distal C-terminus (dCT), resulting in increased channel activity [114]. The C-terminus of LTCC contains Ser1928, suggesting that the dCT was the major substrate of PKA-mediated regulation [114]. Expressing a truncated channel and the dCT in non-muscle cells demonstrated that the dCT is still bound to the channel non-covalently and serves as an auto-inhibitor to the channel [114]. Within the C-terminus of the LTCC lies a modified-leucine zipper that interacts with A-kinase anchoring protein-15 (AKAP15), a scaffolding protein that anchors PKA to the LTCC [31, 108]. The interaction between the dCT, AKAP15, and PKA is essential for modulation; disruption of the interaction ablates LTCC response to activation of cAMP via forskolin [108, 114, 115]. In the absence of dCT, the effects of modulation by PKA were more prominent [116]. However, disruption of the substrate recognition site within the C-terminus for proteolytic cleave by calpain-like proteases did not affect LTCC modulation [112]. The importance of phosphorylation of the LTCC in regards to modulation remains inconclusive due to inconsistent results from both cell lines and animal models; this suggests that modulation may require key protein-protein interactions in order to enhance LTCC activity [31, 109].

$Ca_V\beta$ has been shown to be a critical component of modulation for the LTCC [31, 40, 41, 109]. It was originally thought that the main role of $Ca_V\beta$ was to traffic channels to the membrane and modulated LTCC activity through phosphorylation [25, 28, 40, 41, 91]. However, disruption of the phosphorylation sites did not affect modulation [91]. A study in transgenic mice where the interaction with the AID of LTCC and $Ca_V\beta$ was disrupted

demonstrated that the AID-Cavβ interaction was essential for modulation, not trafficking; without Cavβ, channels did not respond to β-adrenergic stimulation [117]. When flexibility is introduced to the domain I-II linker that connects the AID to the pore, current parallels channels that cannot bind Cavβ, further suggesting that the coupling between Cavβ and the AID is crucial for modulation [118]. Cavβ also tightly binds to a 700 kDa protein termed "ahnak" [103, 119]. When bound to Cavβ, Ahnak represses $I_{Ca,L}$; repression is relieved by PKA phosphorylation [103, 119]. However, transgenic mice that were Ahnak-deficient showed intact β-AR responsiveness, demonstrating Ahnak is not critical to LTCC modulation [120]. Cavβ also bind to RGK proteins, which serve as endogenous inhibitors of the LTCC and potential targets of PKA phosphorylation [17, 103]. This will be further discussed in the next section, as well as explored through the studies described in this dissertation.

Another proposed mechanism of LTCC modulation is channel clustering [31, 59]. Functional channels that reside in the transverse tubules of a cardiomyocyte can form clusters to enhance calcium influx [58, 59]. In response to β-AR stimulation, cAMP levels increase in the transverse tubule microdomain, and channels cluster together to form 'super-clusters' that have enhanced physical interactions between LTCC C-termini and amplification of calcium influx to the level of modulated channels [59]. This could be due to a 'reserve' population of channels that could be mobilized specifically in response to β-AR stimulation to form the 'super-clusters' and enhance $I_{Ca,L}$ [59]. However, clustering does not necessarily explain the hyperpolarized shift in activation seen in modulated LTCCs. It is also unclear which element within the complex response to PKA phosphorylation to mediate the initial influx of calcium to trigger the physical interactions

between CaM on neighboring LTCCs [59]. Therefore, clustering may be a supportive component to enhanced $I_{Ca,L}$, it does not appear to be the underlying mechanism for modulation. Though many studies have focused on β-AR stimulation and its regulation of the LTCC, a conclusive mechanism for modulation remains undetermined [31].

1.2.4 Role of the L-type Calcium Channel in Cardiac Pathophysiology

Because of the central role that LTCC and $I_{Ca,L}$ plays in normal cardiac function, disruption of either structure or function of the LTCC contributes to electrical and mechanical dysfunction within the cardiomyocyte [45]. Alterations in channel function contribute to numerous cardiovascular diseases; understanding how the LTCC is modified in various pathological states will potentially uncover new therapeutic targets and agents to treat these diseases [121].

1.2.4.1 Arrhythmias

Cardiac arrhythmias are generally categorized into two major groups: enhanced/abnormal impulse generation (also known as focal activity) and conductance disturbances (also known as reentry) [122, 123]. Enhanced focal activity promotes the spontaneous generation of action potentials, due to disease conditions, such as in heart failure (HF), that cause the membrane to rest at more depolarized potentials [122]. The most common causes of enhanced focal activity are: early afterdepolarizations (EADs) that occur before full repolarization of the action potential and delayed afterdepolarizations (DADs) that occur after full repolarization [122]. Reentry occurs when a group of cells or fibers not activated during an initial wave of depolarization recover excitability and

activate while the rest of the tissue is in the refractory period, creating reciprocating tachycardia [123]. Arrhythmias can also occur due to mutations within calcium-handling proteins that cause dysfunctional calcium channels, transports, or related proteins [122]. In this section, arrhythmias specifically associate with the LTCC will be discussed.

1.2.4.2 Early After Depolarizations

EADs instigate local focal activity by depolarizing neighboring tissue that then promotes ventricular tachyarrhythmias associated with HF and long QT syndrome (LQTS) [122, 123]. These events typically occur during bradycardia under conditions of reduced repolarization reserve, either due to significantly decreased outward current or enhanced inward currents [61, 63, 122, 123]. One major contributor to EAD production is reactivation of the LTCC during phase 2 or phase 3 of the action potential, leading to excessive prolongation of the action potential [122]. Other ionic currents contribute to EAD formation, but inward current such as $I_{Ca,L}$ is required for EADs to propagate [63]. LTCCs can reactivate when steady-state activation and inactivation overlap, known as the window current, between -40 and 0 mV [62, 63, 124, 125]. In many cardiac pathological conditions that are at high risk for ventricular tachycardia or ventricular fibrillation (ex. activation of CaMKII, Timothy Syndrome, Long QT Syndrome), the rate of $I_{Ca,L}$ inactivation can be slowed significantly, thereby generating an increase in late inward depolarizing current [61-63]. This creates a pool of LTCCs that never inactivate [61-63]. Three possibilities to treat EADs include: 1) shift $I_{Ca,L}$ steady-state activation in the depolarizing direction by < 5 mV; 2) shifting steady-state inactivation in the hyperpolarzing direction by <5 mV; or 3) reducing the non-inactivating component [62]. The crucial aspect is to adjust the kinetics

of $I_{Ca,L}$ to reduce window current without reducing peak $I_{Ca,L}$; this is a major downfall to traditional treatments like verapamil or nifedipine [62]. Indeed, reducing peak $I_{Ca,L}$ is not needed to suppress EAD formation, but rather only decreasing the late, arrhythomogenic component of $I_{Ca,L}$ [62, 63]. This way, excitation contraction coupling and overall contractility is unaffected. One drug of promise that seems to decrease the late $I_{Ca,L}$ without affecting peak $I_{Ca,L}$ is roscovitine, cyclin-dependent kinase inhibitor that is part of a new class of drug known as 'gate modifiers' [62, 63, 126-130].

1.2.4.3 Timothy Syndrome

Genetic mutations in the C-terminus of LTCC, either G402S or G406R, revealed a novel arrhythmia syndrome that was termed Timothy Syndrome (TS; [131, 132]. Because LTCC is expressed in multiple tissues, this syndrome disrupts multiple organ systems [131, 132]. In the original 1992 study, children affected by the mutation displayed varying severity in symptoms, such as 60% of patients had autism, 50% had cavities in their teeth, and 36% suffered from hypoglycemia [131]. However, 100% of patients had QT prolongation, 71% had ventricular tachyarrhythmia and 94% had bradycardia; arrhythmias were the deadliest for these children, with 12 of 17 children dying due to arrhythmic episodes [131]. The mutations in the channel causes almost complete loss of inactivation, thereby delaying repolarization of the action potential, prolonging QT interval, and increasing the risk of spontaneous, abnormal secondary depolarizations, arrhythmias and sudden death [131-133]. A single mutation of G406R induces the classical TS by disrupting voltage dependent inactivation [121]. When both mutations are present, TS is more severe and exhibits long QT syndrome [121]. Both mutations also contribute to

disrupting calcium-dependent inactivation, with G406R causing more serious disruption [134]. Therapies available include: i) verapamil, a calcium channel blocker, decreases the number of ventricular fibrillation episodes but does not shorten QT interval and is not handled well by many TS patients [126, 135]; ii) mexiletine is a class IB antiarrhythmic drug used to shorten QT interval, but does not demonstrate any significant effect on LTCC [126, 136]; iii) Nifedipine, a dihydropyridine calcium channel antagonist, normalized VDI kinetics, but can alter calcium transients that could affect activation of the slow-activating potassium current [63, 126, 127, 137, 138]; iv) Roscovitine is a cyclin-dependent kinase inhibitor that dampens $I_{Ca,L}$ amplitude, slows activation, enhances inactivation, and normalizes the calcium influx during an action potential, but has been found to block voltage-gated potassium channels, including HERG [126-130]. Though the underlying mechanism of TS still remains unknown, much has been discovered about the role of calcium channel function in regards to other cardiac pathology, such as Long QT syndrome; this has provided new technologies and avenues for potential therapeutics that not only applies to TS but also arrhythmias in general [126].

1.2.4.4 Brugada Syndrome

Brugada Syndrome is characterized by elevation of the ST segment of the ECG, followed by a negative T wave [139, 140]. While this syndrome is typically associated with mutations within the $Na_V1.5$ complex, Brugada Syndrome 3 and 4 are caused by mutations in α_{1C} (A39V, G490R, E1115K, R1880Q, V2014I, D2130N, E1829_Q1833, C1873Y, and E850del), $Ca_V\beta$ (S481L), and $\alpha_2\delta$ (S709N, D550Y, Q917H) of the LTCC, respectively [139, 141, 142]. Patients that have either of these specific types of Brugada Syndrome

display shortened QT intervals in addition to elevation of ST and a negative T wave [141]. This is because all of these mutations result in a significant decrease in $I_{Ca,L}$ [141, 142]. For A39V, current was decreased due to dysfunctional channel trafficking to the membrane; G490R displayed normal trafficking so may affect open probability of the channels within the membrane [141]. E1115K reduced single channel conductance without changing gating [142, 143]. V2014I dampened peak current density and shifted half-inactivation voltage to more negative potentials [142]. E1829_Q1833 yielded almost complete suppression of $I_{Ca,L}$ [142, 143]. For $Ca_V\beta$, S481L is located near the binding domain for $Ca_V\beta$- α_{1C}, thereby potentially interfering with that association in order to lead to a decrease in $I_{Ca,L}$ [142]. The changes in calcium channel surface expression or activity remain unknown for mutations in the $\alpha_2\delta$ subunit [142, 143]. Available treatments for Brugada Syndrome include implantable cardioverter-defibrillators and ventricular fibrillation suppression drugs, such as quinidine, denopamine, or cilostazol, and ventricular ablation; however, the multiple side effects that accompany any form of treatment demonstrate the need for refined treatment [144].

1.2.4.5 Heart Failure

Heart failure (HF) is a leading cause of mortality, and is defined as any abnormality in cardiac structure or function that results in the failure of the heart to meet the metabolic demands of the body [1, 2, 5, 122]. Heart failure with reduced ejection fraction, or systolic heart failure, is caused by reduced contractility due to alterations in cellular calcium handling [5, 122, 145]. $I_{Ca,L}$ remains unchanged or decreases in HF, potentially due to internalization of channels [52]. However, $I_{Ca,L}$ mainly contributes to the progression of

HF through two key mechanisms: cardiac hypertrophy and chronic β-AR stimulation [5, 45, 52, 145-147].

1.2.4.5.1 Cardiac Hypertrophy

Increases in calcium influx under pathological conditions trigger activation of pathological hypertrophy and HF [52, 145-147]. Intracellular calcium binding to CaM activates calcineurin, a serine-threonine protein phosphatase that mediates nuclear factor of activated T cells (NFAT) and myocyte enhancer factor 2 (MEF2) [146, 147]. Dephosphorylation of NFAT and MEF2 by calcineurin causes activation of transcription of hypertrophic response genes [146]. The source of calcium to activate calcineurin is thought to be the LTCC [52, 145, 148]. Early studies first hypothesized this when overexpression of either LTCC or $Ca_V\beta$ resulted in significant cardiac hypertrophy and heart failure in a range of a few weeks to a few months [12, 146, 149]. Indeed, calcium channel antagonists prevented cardiac hypertrophy [146, 150, 151]. It was therefore hypothesized that the LTCC provided the 'hypertrophic' calcium necessary to induce hypertrophy [146, 148]. It was then discovered that LTCCs that reside specifically in the microdomain of caveolin-3 provide the calcium required to induce activation of the calcineurin-NFAT pathway [52]. However, a follow-up study by the same group could not replicate these findings in a pressure-overload induced heart failure mouse model [152]. This indicated that cardiac hypertrophy was not solely due to the activation of calcineurin/NFAT [152, 153].

Another major calcium-dependent hypertrophic signaling pathway is the calcium-calmodulin-CaMKII-HDAC pathway [147, 153-155]. Activation of CaMKII has been seen

in experimental models of hypertrophy as well as patients with heart failure; CaMKII is activated by the binding of calcium to CaM [153, 154]. Under pathological conditions, CaMKII activity is upregulated and contributes to defective excitation-contraction coupling and excitation transcription coupling in mechanisms that favor pathological hypertrophy, such as activation of MEF2 [147, 154]. Indeed, transgenic mice overexpressing specific isoforms of CaMKII resulted in hypertrophy and HF; mice depleted of other isoforms of CaMKII demonstrated resistance to pathological remodeling [154]. One source of activation of CaMKII is the LTCC [153]. Several studies have demonstrated that increased $I_{Ca,L}$ in response to β-AR stimulation facilitates CaMKII activity [119, 153, 154]. Increased influx through caveolae LTCC has also been shown to induce activation of CaMKII [153]. Classical treatment of heart failure with reduced ejection fraction has included positive inotropic agents in order to increase cardiac performance; however, agents that increase $I_{Ca,L}$ induce long-term maladaptive effects, partly due to CaMKII-induced cardiac remodeling [5]. Understanding the role of microdomain-specific signaling in regards to the LTCC, CaMKII, and calcineurin could provide selective inhibitory targets that can better improve systolic function without instigating pathological remodeling [5, 153].

1.2.4.5.2 Loss of β-Adrenergic Receptor Stimulation

In order to increase contractility, a failing heart is under persistent adrenergic activation [156]. In heart failure, the LTCC becomes less responsive to PKA phosphorylation resulting in reduced contractility and a diminished fight-or-flight response [103]. Chronic stimulation of β-ARs promotes LTCC internalization and

hyperphosphorylation of the LTCC, thereby increasing the availability and open probability of the channels, but limits the response to β-AR agonists [103, 157, 158]. The increase in function leads to an increase in calcium influx, which in turn promotes the hypertrophic signaling pathways described above [5, 103, 119, 147, 153, 154]. Heart failure also promotes disruption of transverse tubule structure, thereby disrupting LTCC regulation [103, 159, 160]. Dislocation of LTCCs from transverse tubules disrupts highly localized regulation of the LTCC by β-ARs [103, 159, 160]. Because of all these major effects on the LTCC in regards to chronic β-AR stimulation, the hypothesis is that the LTCC plays a central role in the altered calcium handling seen in HF [157]. Current therapies for HF include β-blockers in order to prevent further structural and functional damage to the heart; however, these drugs do not address the critical issue of diminished contractility [156]. These treatments also can only serve a small population of patients suffering from HF, depending on their stage of HF and the presence of comorbidities [156]. A potentially successful treatment for HF would be a positive inotrope that increases $I_{Ca,L}$ downstream of β-ARs in a domain-specific manner so as not to activate hypertrophic pathways but increases cardiac performance [5, 153].

1.3 Rad

1.3.1 RGK Proteins

RGK proteins are a subfamily of small Ras-related G proteins that bind to $Ca_V\beta$. In over-expression systems, all tested RGK proteins profoundly inhibit all Ca_V1 and Ca_V2 channels [17, 20]. There are four members: Rad, Gem, Rem, and Rem2 [20]. Rad (Ras associated with diabetes) was the founding member of the family, first identified to be

overexpressed in skeletal and cardiac muscle of patients with type II diabetes [161]. Gem was the next member of the family identified in human peripheral blood T cells as a mitogen-induced gene and hypothesized to participate in receptor-mediated signal transduction [162]. Rem was then identified based on cloning using a degenerate PCR strategy based on structural similarity to Rad and Gem, and found to be expressed in skeletal and cardiac muscle, lung and kidney [163]. Rem2 was the last member to be discovered in neuronal tissue [164]. The common structure of all RGK proteins includes: conserved Rad-related core domain, series of nonconservative amino acid substitutions within regions involved in guanine nucleotide binding and hydrolysis, conserved polybasic C-terminal extension, and a large N-terminal extension relative to other Ras family proteins [17]. The C-terminus extension of RGK proteins lacks the CAAX (Cysteine, Aliphatic, Aliphatic, X is any amino acid) prenylation motif that is common to many Ras superfamily proteins, and directs the proteins to anchor to the membrane; instead, the C-terminus contains basic and hydrophic residues to target the plasma membrane [20]. RGK proteins have been implicated in numerous functions in different cell types, including cell shape remodeling, apoptosis of cardiomyocytes, synapse development, and neuronal proliferation [20]. This section and the remainder of the chapter will focus on Rad, and the physiological significance of Rad within the LTCC complex and overall cardiac function.

1.3.2 Structure of Rad

Rad is expressed in excitable and non-excitable tissues, and exists as a monomer, containing five α-helices (A1-A5) and one large β-sheet, comprised of two extended anti-parallel β-strands (B2, B3) and five extended parallel β-strands (B3, B1, B4-B6) [20, 165-172]. There are also three loop regions: switch I (residues 116-124), switch II (residues

147-153), and loop A3-B5 [165]. Unlike other small GTPases in the Ras family, the crystal structures of switch I and II in Rad are disordered, suggesting conformational flexibility within these regions; however, it must be noted that these structures do not include the N- and C-terminal extensions [165, 173]. This flexibility potentially allows optimal shape complementarity between Rad and the GK domain of $Ca_V\beta$; the residues on Rad required for $Ca_V\beta$ association are Arg208 and His237 [166, 174]. The C-terminus of Rad contains crucial binding sites for localization and function; CaM binds to the C-terminus of Rad in the region of residues 278-297 in a calcium dependent manner [175]. CaM, along with 14-3-3 proteins, contribute to the localization of Rad [176]. 14-3-3 proteins are involved in various signaling pathways, and associate with Rad in a phosphorylation-dependent manner, specifically at Ser39 and Ser301[166, 176]. The C-terminus of Rad also includes a region that can bind to negatively charged phospholipids in the plasma membrane, such as PI(3,4,5)P_3 and PI (4,5)P_2; when the plasma membrane is depleted of PI (4,5)P_2, Rad was unable to target to the plasma membrane [92, 177]. Rad also serves as a substrate for multiple kinases, including PKA (Ser272, Ser301), PKC, CaMKII (Ser273, Ser299) and casein kinase II that could serve as critical modulators of Rad function [92, 166, 175].

1.3.3 Function of Rad

When first identified in type II diabetic patients, Rad was hypothesized to be an inhibitory Ras GTPase that increased activity as a compensatory response in muscle when patients became insulin resistant [161]. Rad was then overexpressed in skeletal muscle and adipocyte cell lines to assess the contribution of Rad to insulin-mediated signaling and found to be a negative regulator of glucose uptake [178]. β-tropomyosin was also shown to interact with Rad, with associations enhanced after an increase in calcium influx; this

suggested that Rad was involved in skeletal muscle motor function and cytoskeletal organization [178, 179]. Following this study, Gem was reported to act as an inhibitor of high voltage-activated calcium channels through a direction interaction with the β-subunit [16]. This prompted the investigation of the role of Rad in regards to calcium channel inhibition in HEK cells; coexpression of wild-type Rad with LTCC and $Ca_V\beta_{2a}$ resulted in complete inhibition of detectable ionic current through direct interaction with $Ca_V\beta$ [17]. Inhibition of $I_{Ca,L}$ by Rad also required the expression of the C-terminal tail [17]. This finding was accompanied by multiple studies of human heart failure: one study demonstrated that a nonsynonymous single-nucleotide polymorphism within the Rad gene (Rad^{Q66P}) was found in patients with congestive heart failure [180]; myocardium collected from end-stage heart failure patients displayed significantly decreased protein levels of Rad [23, 181]. Because of these studies, Rad was hypothesized to play a central role in cellular calcium homeostasis.

Loss of function of Rad, either through overexpression of a dominant suppressive mutant of Rad (S105N) or via RNAi-mediated knockdown, yielded an increase in $I_{Ca,L}$, calcium transients, and contractility; these results were accompanied by action potential prolongation, QT prolongation and ventricular arrhythmias [182]. However, this mutant may not represent a dominant-negative protein; biochemical studies of Rad S105N reported this mutant may be a non-native protein that fails to bind nucleotide or exhibit only partial occupancy of the nucleotide, despite the site being equivalent to the known dominant negative mutation in Ras (S17N)[173]. The pathology seen in response to increased $I_{Ca,L}$ from the suppression of Rad could have been due to activated CaMKII; $Rad^{-/-}$ mice exhibited phosphorylated CaMKII, and increased heart growth in response to pressure

overload [181]. However, that particular study did not report the effects of Rad deletion on myocardial function; indeed, the same group also reported Rad was a critical negative regulator of vascular lesion formation [181]. Assessment of the effect of $Rad^{-/-}$ on cardiac function demonstrated significantly elevated systolic function in response to enhanced calcium handling and increased calcium current; interestingly, $I_{Ca,L}$, calcium handling and cardiac function that phenocopied β-AR stimulation [21, 23]. This was supported by the report of a large, sustained decrease in Rad in neonatal cardiac myocytes that were exposed to the adrenergic agonist phenylephrine [181]. However, Rad had also been reported to selectively negate β-AR signaling in regards to $I_{Ca,L}$; Rad knockdown to 30% of normal expression did not block the increase in current in response to isoproterenol [183]. Taken together, these varying results presented a complex cardiac phenotype that could include noncardiac influences, thereby making interpretation of the mechanism by which Rad regulates the LTCC confusing.

Impaired calcium handling within cardiomyocytes contributes to the loss of contractility in heart failure [6, 51, 147]. Current positive inotropes can be used acutely, but trigger pathological signaling when used long-term [5]. Because Rad protein expression is decreased in patients with heart failure, the small GTPase emerged as a potential therapeutic target to increase positive inotropy [21, 23, 181]. Indeed, $Rad^{-/-}$ displayed elevated cardiac function and preserved cardiac output with aging [22]. Under conditions of acute myocardial infarction, $Rad^{-/-}$ reduced mortality, contractile dysfunction, and scar development independent of preserving tissue viability, possibly by mediating an inflammatory response within the heart [184]. However, Rad deficiency promotes cardiac fibrosis through a lack of inhibition on expression of connective tissue growth factor [181].

It therefore remains unclear as to whether the down regulation of Rad in the context of heart failure is more of a pathological or compensatory response.

1.4 Working Hypothesis

It is well established that Rad is critical to regulation of the LTCC [166]. However, the resulting cardiac phenotype in $Rad^{-/-}$ models is puzzling due to the potential contributions of Rad deletion in noncardiac cell types obscuring the positive inotropic effects on the heart. Another level of complexity is the contradicting effects of β-AR stimulation on LTCC function with and without Rad present in the complex; these studies support Rad playing a critical role in PKA-mediated modulation of the LTCC but the mechanism remains unclear. Rad also seems to play a critical role in the cardiac response to heart failure, but the underlying mechanism to which this role belongs, pathological or compensatory, has yet to be determined.

The main objective of this dissertation is test the hypothesis that the deletion of Rad solely from cardiomyocytes provides a safe, stable target to increase positive inotropy downstream of β-AR signaling. Myocardial-specific deletion of Rad increases $I_{Ca,L}$ in a manner that parallels LTCC modulation that enhances calcium cycling and systolic function without promoting pathological remodeling or progression to heart failure (**Chapter 3**). Chronic, modulated $I_{Ca,L}$ as a result of Rad deletion is also seen in sinoatrial nodal cardiomyocytes, thereby promoting elevated sinus heart rate (**Chapter 4**). Inactivation of the LTCC in the absence of Rad in a manner that mirrors LTCC modulation (**Chapter 5**). LTCC regulation by Rad is governed by the C-terminus of Rad (**Chapter 6**). The positive inotropic effect of Rad deletion serves to protect and partially rescue

calcium handling and contractile function under conditions of pressure-overload induced heart failure (**Chapter 7**). Taken together, the results of this dissertation support the hypothesis that Rad serves as a major component of PKA-mediated LTCC modulation, and represents a promising therapeutic target for heart failure with reduced ejection fraction.

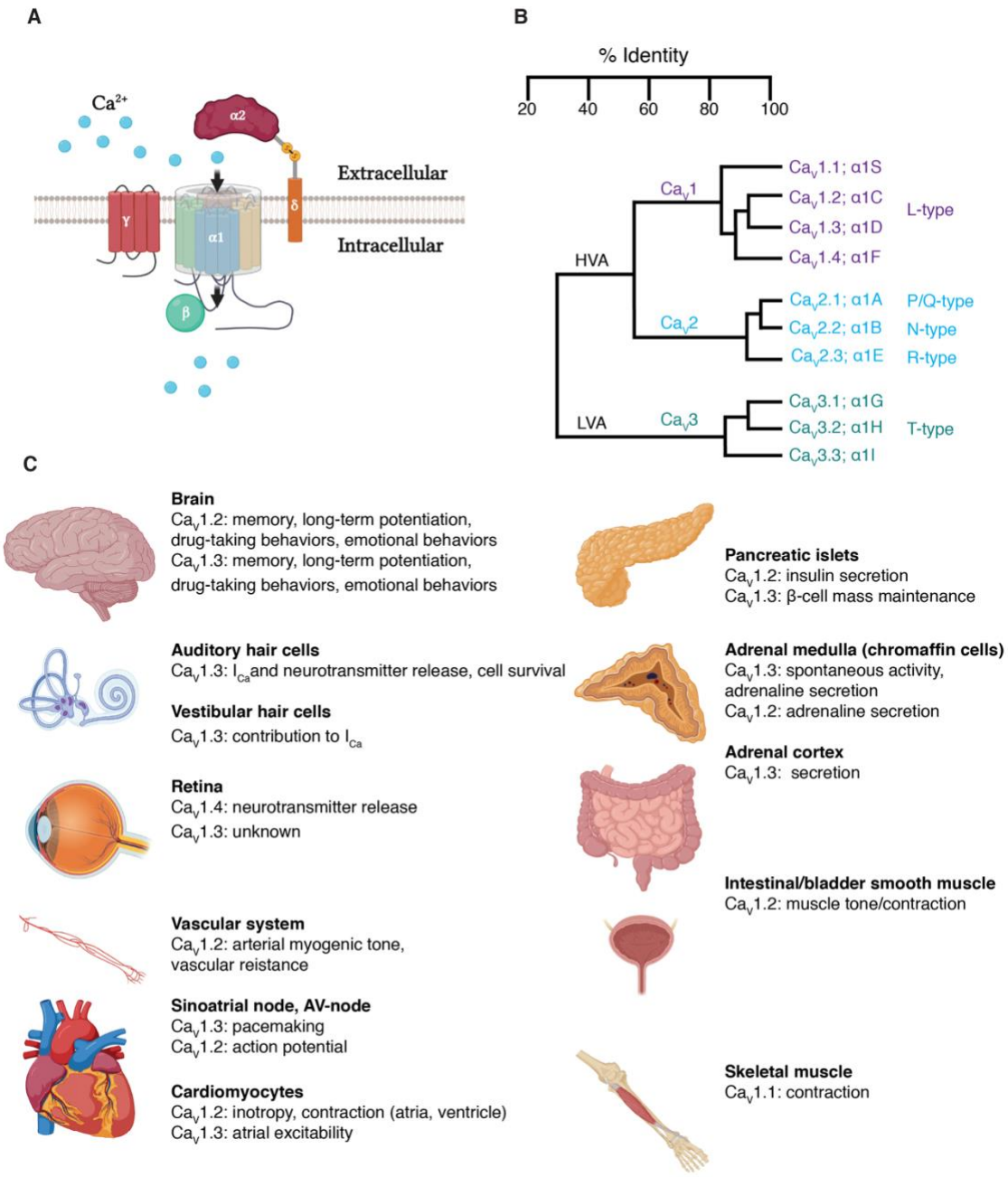

Figure 1.1 L-type Calcium Channel Complex.

A) Structure of the voltage gated calcium channel: the pore-forming subunit α1, the extracellular α2 subunit connected to the transmembrane δ subunit via a disulfide bridge, the intracellular β subunit and the transmembrane subunit γ. Modified from Ninomiya et. al 2020 [43]. **B)** A dendrogram of the three subfamilies for calcium channel genes showing the percent identity between the different cloned calcium channels. Modified from Hille, 1984 [27]. **C)** Tissue expression of the different LTCC isoforms. Modified from Zamponi et. al 2015 [30].

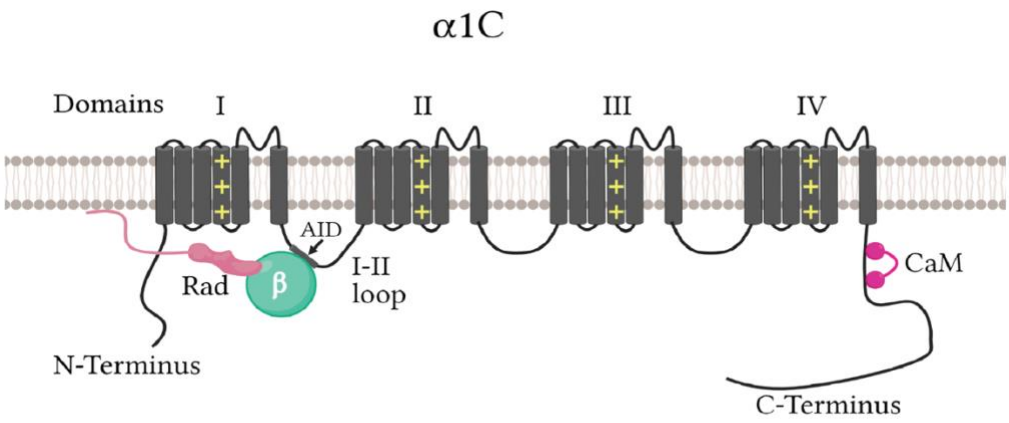

Figure 1.2 L-type Calcium Channel pore-forming subunit α_{1C}.
Schematic of α_{1C} subunit topology showing β subunit binding to AID motif, calmodulin (CaM) associating with the C-terminus of α_{1C}, and Rad interacting with both the β subunit and the plasma membrane. Modified from Papa et. al 2021 [118].

CHAPTER 2. MATERIALS AND METHODS

2.1 Animal Model

All experimental procedures and protocols were approved by the Animal Care and Use Committee of the University of Kentucky and conformed to the National Institute of Health "Guide for the Care and Use of Laboratory Animals."

Transgenic animals were generated on a C57BL/6J background in the Transgenic Animal and Genome Editing Core at Cincinnati Children's Hospital Medical Center. The conditional RRAD allele was made via a sequential insertion strategy using CRISPR-Cas9 technology, in which exons 2 and 3 were flanked by Cre recombinase-dependent loxP (flox: fl) recognition sequences (**see Chapter 3, Figure 3.1A**). The sgRNA's were engineered to contain either HindIII (5′) or EcoRI (3′) restriction sites, with offspring screened by genomic PCR analysis, and loxP insertion confirmed by Sanger sequencing. These mice ($RAD^{fl/fl}$) were then crossed (or not, as controls) with mice expressing a tamoxifen-inducible Cre recombinase (MerCreMer) under α-myosin heavy chain promoter [185] to produce $RAD^{fl/fl\text{-}MHC}$ animals. RAD deficiency was induced by a single intraperitoneal injection in control ($RAD^{fl/fl}$) and experimental mice with tamoxifen dissolved in sunflower seed oil (40 mg/kg body weight). All mice received tamoxifen and were used ≥2 weeks after tamoxifen treatment unless otherwise stated. $Rad^{fl/fl}$-MHC after receiving tamoxifen are abbreviated 'cRadKO,' and control mice expressing endogenous Rad are abbreviated, CTRL. This single tamoxifen injection protocol minimizes cardiomyopathological effects observed with multiday administration of tamoxifen [186]. Male and female mice were used; the age of the mice was 2-8 months, except for the long-

term follow up study in chapter 3. The age of the oldest mice used for study in chapter 3 were limited to 18 months, but the cellular studies were from mice <12 months of age. cRadKO was used for study in chapters 3-5, and 7. For telemetry studies in chapter 4, recordings were made before and after tamoxifen treatment in the same mice. For chapter 5, β1- and β2-adrenergic receptor double knock-out mice were from The Jackson Laboratory, JAX stock #003810 [187]. These mice were bred onto our $RAD^{fl/fl\text{-}MHC}$ animals to produce the triple knock out after administration of tamoxifen. For chapter 6, CRISPR/Cas9 gene engineering techniques were used to sequentially introduce a 3xFlag epitope tag to the N-terminus of the endogenous mouse *Rrad* gene (to generate 3xFlag-Rad mice), and then CRISPR/Cas9 was used to introduce a stop codon at A277 into the endogenous Flag-tagged *Rrad* gene to generate a second Flag-RadA277X mouse (generating a C-terminal truncation). See **Chapter 6, Figure 6.1** for schematic.

2.2 TAC

Transverse aortic constriction was performed essentially as described previously [188]. Briefly, mice were sedated in an isoflurane sedation box (induction 3% and maintenance 1.5%) and anesthetized to a surgical plane with an i.p. dose of ketamine (50 mg/kg) and xylazine (2.5 mg/kg). Anesthetized mice were intubated, and a midline cervical incision was made to expose the trachea and carotid arteries. A blunt 20-gauge needle was inserted into the trachea and connected to a volume-cycled rodent ventilator on supplemental oxygen at a rate of 1 L/min and respiratory rate of 140 bpm/min. Aortic constriction was performed by tying a 7–0 nylon suture ligature against a 27- gauge needle, which was promptly removed to yield a constriction of 0.4 mm in diameter. Pressure

gradients were determined by in vivo hemodynamics, and mice with gradients 30 mmHg were used.

2.3 Immunoblotting

Hearts freshly excised from $RAD^{fl/fl}$ (CTRL) and $RAD^{\Delta/\Delta}$ (cRadKO) were flash frozen, and tissue was pulverized using Freezer Mill (6775, SPEX SamplePrep) before sonication in cell lysis buffer containing (in mmol/liter), 50 Hepes, pH 7.5, 150 NaCl, 0.5% Triton X-100, 1 EDTA, 1 EGTA, 10 NaF, 2.5 $NaVO_4$, complete Protease Inhibitor Mixture (Roche 11697498001-1 tablet per 50 ml), phosphatase inhibitor mixture 2 (Sigma, P5726, ×100 solution), and phosphatase inhibitor mixture 3 (Sigma, P0044, ×100 solution) (500 µl of each inhibitor mixture). Lysates were centrifuged at 14,000 rpm and protein concentrations of supernatants were measured. Lysates were prepared in 4× SDS-PAGE loading buffer with 40.0 µg of total protein per lane resolved on 8, 15, or 4–20% SDS-PAGE gels and transferred to nitrocellulose/PVDF membranes. Immunoblotting was performed with: calsequestrin (1:3000, Abcam); RAD (1:2000, Everest Biotech); Cav1.2 (1:1000, Alomone); CaMKIId (1:1000, Santa Cruz Biotechnology); pCaMKII (1:1000, Santa Cruz Biotechnology); SERCA2a (1:1000, Badrilla); phospholamban phosphoserine 16 (1:1000, Badrilla); phosphor-threonine 17 (1:1000, Badrilla), and total PLN (1:1000, Invitrogen) antibodies, CTGF (1:1000, Santa Cruz Biotech) and GAPDH (1:1000, Cell Signaling Technology). Proteins were detected using SuperSignal enhanced chemiluminescence (Pierce), and immunoblots were developed and quantified using the Bio-Rad ChemiDoc MP Imaging System. The total protein loaded was quantified by

staining the membranes with Coomassie staining after the detection of the desired proteins or using stain-free gels (Bio-Rad).

2.4 Quantification of myofibril protein phosphorylation

Myofibrils were prepared from frozen mouse ventricular tissue homogenized in relaxing solution containing protease and phosphatase inhibitors (PhosSTOP and cOmplete ULTRA Tablets, Roche Applied Science). Samples were skinned for 15 min using 1% Triton X-100, centrifuged at 10,000 × g for 5 min, and resuspended in fresh relax. Samples were reduced using 2-mercaptoethanol in Laemmli buffer and boiled for 5 min. 5 μg of the solubilized myofibrils were loaded and electrophoretically separated using 4–20% Tris glycine minigels at 160 V for 70 min. Gels were fixed and stained with Pro-Q diamond phosphoprotein stain (Invitrogen) per the manufacturer's protocol. The same gels were then stained with Coomassie Blue for total protein expression. Densitometry of bands in Pro-Q and Coomassie-stained gels was performed using ImageJ software (National Institutes of Health). The degree of phosphorylation of a given protein was determined by the ratio of the Pro-Q signal to the protein contented loaded.

2.5 Ventricular myocyte isolation

Isolated ventricular cardiomyocytes were prepared as previously described [19]. Prior to heart excision mice were anesthetized with ketamine + xylazine (90 + 10 mg/kg intraperitoneal). Hearts were excised from adult $RAD^{fl/fl}$ (CTRL) and $RAD^{\Delta/\Delta}$ (cRadKO) and immediately perfused on a Langendorff apparatus with a high-potassium Tyrode buffer and then digested with 5 to 7 mg of liberase (Roche Applied Science). After digestion, atria

were removed and ventricular myocytes were mechanically dispersed. Calcium concentrations were gradually restored to physiological levels in a stepwise fashion, and only healthy quiescent ventricular myocytes were used for electrophysiological analysis or calcium imaging within 12 h.

2.6 Electrophysiological recordings

$I_{Ca,L}$ was recorded in the whole-cell configuration of the patch clamp technique as previously described [19]. All recordings were performed at room temperature (20 to 22 °C). The pipette solution consisted of (in mmol/liter) 125 Cs-methanosulfonate, 15 TEA-Cl, 1 $MgCl_2$, 10 EGTA, and 5 Hepes, 5 MgATP, 5 phosphocreatine, pH 7.2. Bath solution contained (in mmol/liter) 140 NaCl, 5.4 KCl, 1.2 KH_2PO_4, 5 Hepes, 5.55 glucose, 1 $MgCl_2$, 1.8 $CaCl_2$, pH 7.4. Once a cell was successfully patched, zero sodium bath solution was introduced into the chamber (mmol/liter) 150 N-methyl-D-glucamine, 2.5 $CaCl_2$, 1 $MgCl_2$, 10 glucose, 10 Hepes, 4-amino-pyridine, pH 7.2. Recordings of isoproterenol response were recorded in zero sodium bath solution containing 300 nM isoproterenol. Activation voltage dependence parameters were obtained by first transforming the peak current/voltage relationship to a conductance transform by fitting the ascending phase (typically V_{test} +15 to +40 mV) to a linear regression to obtain a reversal potential. Using G = I/V the conductance as a function of voltage transform was then fitted to a Boltzmann distribution of the form $G(V) = G_{max}/(1 + \exp(V_{1/2}/k))$, where G_{max} is the maximal conductance and $V_{1/2}$ is the activation midpoint. For steady-state availability curve, we pre-pulsed cells to Vpre ranging from −40 to +10 mV in 5-mV increments and recorded a V_{test} to 0 mV. Peak currents were plotted as a function of Vpre, and a Boltzmann

distribution was fitted to the resulting curve. Recordings of barium response were recorded in zero sodium bath solution containing 2.5 mmol/L $BaCl_2$. Recordings of Isoproterenol response were recorded in zero sodium bath solution containing 300 nM isoproterenol. Traces were normalized to peak $I_{Ca,L}$, and then mean amplitude was measured at 30 ms and 150 ms after peak. Remaining current was then calculated by subtracting the mean amplitude from 1. AP recordings were performed in the physiological Tyrodes bath solution as used for the other recordings. For AP recordings, the pipette solution contained (in mmol/L) 115 K-glutamate, 45 KCl, 3 Mg-ATP, and 10 HEPES, pH 7.21 (KOH). All AP recordings were performed at room temperature (20° to 22°C).

2.7 Calcium Transients

Calcium transients were recorded from ventricular cardiomyocytes loaded with cell permeable fura2-AM (Invitrogen) at 1.0 Hz to determine transient amplitude, upstroke velocity, and rate of decay. Sarcomere dynamics were simultaneously recorded by acquiring an optical signal of visible striations of the cardiomyocyte. All measurements were made following >2 min of conditioning of 1-Hz field stimuli to induce steady-state. Transients were recorded at 1 Hz. All Ca^{2+} transient/sarcomere dynamic data were analyzed using IonOptix IonWizard 6.3. Background fluorescence (Fbackground) for F_{380} and F_{340} were determined from cell-free regions. Data are expressed as $F_{340/380}$ and were corrected for Fbackground.

Calcium transients were also recorded from ventricular cardiomyocytes loaded with cell permeable fluo4-AM (Invitrogen) at 1.0 Hz to determine the transient rate of decay. All measurements were made following >5 min of conditioning of 1-Hz field stimuli to

induce steady-state. Using confocal microscopy, a line scan was taken of an individual cardiomyocyte. Transient decays from line scans were then fitted with a single exponential to determine the rate of decay.

2.8 Single Cell Database Analysis

Fastq files from single-cell RNA-sequencing (scRNA-seq) analysis of isolated mouse sinus atrial node (SAN) tissue, as reported by Linscheid and colleagues [189], were retrieved from NCBI Gene Expression Omnibus (accession number GSE130710, sample H4). Cell Ranger 3.1 pipeline (10X Genomics, USA) was used for read alignment using the mouse mm10 release 93 reference genome modified to include pre-mRNA. Cell calls were made using default parameters for Cell Ranger. Unique molecular identifier counts for all partitions identified as cells were greater than 2150. The re-analyze function in Cell Ranger was used to eliminate cell clusters enriched in mitochondrial reads as described on the 10x website (https://kb.10xgenomics.com). Only one cluster was eliminated because of enrichment in mitochondrial genes (the topmost differentially expressed genes were mitochondrial genes indicating that these RNAseq reactions were from dead cells). The remaining 5,472 cells used for analysis. K means clustering was used to define clusters. In Loupe Cell Browser, cells containing RRAD were selected. For cell type determination, we used the genes that were found by Linscheid et al to be the most differentially expressed in each cell type [189]. To be defined as a specific cell type cluster, the cluster had to have the following genes as their most deferentially expressed genes: sinus node myocytes: *Myh6, Ctnna3, Ryr2, Rbm20, Dmd, Ttn,* and *Tbx5*; fibroblasts: *Col1a1, Fbn1, Ddr2, Lama2, Lamc1, Pcsk6, Gpc6, Mecom, Rbms3*, and 4930578G10Rik; macrophages: *Maf,*

F13a1, Cd163, C3ar1, P2yr6, Mrc1, Mgl2, Adgre1, and *Dab2*; vascular endothelial: *Ptprb, Icam1, Vwf, Ldb2, Pecam1 and Cdh13*; adipocytes: *Ucp1, Cidea, Prdm16, Pparg, Lep, Ghr, Slc1a5, Pde3b, Sorbs1, Acsl1, and Adopr2*; endocardial: *Npr3, Cdh13, Engm Hmcn1 and Gmds* and epicardial cells: *CTRL1, Rbfox1, Kcnd2, Grip1, Plxna4 and Syne2*.

2.9 Quantitative Proteomics Database Analysis

The mass spectrometry proteomics data was downloaded from the ProteomeXchange Consortium via the PRIDE repository (https://www.ebi.ac.uk/pride/). Dataset for mouse SAN cells (PXD008736) include 6 samples with 12 fractions per sample performed in technical duplicate. Raw MS data were analyzed using MaxQuant v1.6.8.0 (Max-Planck Institute of Biochemistry, Department of Proteomics and Signal Transduction, Munich, Germany). Peptide search was performed using the UniProt reference proteome for *Mus musculus* (Proteome ID UP000000589). False-discovery rate (FDR) was set to 1% for peptide, protein, and side decoy identification with base FDR calculated on delta score. Unmodified, unique and razor peptides were used for protein quantification to address high amino acid sequence similarity between paralogous proteins. All other parameters were kept at default. For positive protein identification the minimum number of peptides was 2. Fixed and variable modifications included in the analysis were carbamidomethylation, methionine oxidation, and N-terminal acetylation with a maximum allowed number of 5 modifications per peptide. To ensure that sensitivity was adequate and that the cells isolated were SAN, we quantified the intensity of Catenin Alpha3 (CTNNA3) and Hyperpolarization-activated cyclic nucleotide gated channel 4 (HCN4) proteins, and

eliminated any samples that did not exhibit a significant quantity for each of these proteins. The remaining samples were used to quantify Rad protein.

2.10 RNA In Situ Hybridization

The in situ hybridization experiment was done using RNAscope® [190] (Advanced Cell Diagnostics). Hearts were fixed with 10% neutral buffered formalin for 16-32 hours at room temperature (RT). Washed the tissue in 100% ethanol and embedded in paraffin. Prepared 5µM paraffin sections on a charge slide in RNAase free condition. Sections were cut from the right atrial wall/appendage bounded by inferior and superior vena cava. RNAscope Multiplex Fluorescent Detection Reagent V2 kit (ACD, Cat. No. 323110) was used to probe Rrad and Hcn4 on the section as per the manufacturer's protocol. A custom designed probe for Rrad was generated (Mm-Rrad-O1, 885451). The Rrad probe recognized sequence corresponding to transcript downstream of the flox site shown to be reduced in heart lysate by qRT-PCR [19, 191]. HCN4 probe was from the ACD catalog (Mm-Hcn4-C2, 421271-C2).

2.11 Quantitative RT-PCR

Mice were anesthetized with ketamine and xylazine and hearts were quickly excised, after which the apex of the left ventricle was removed and snap frozen in liquid nitrogen. Frozen tissue was then homogenized, and RNA was isolated using the RNAqueous kit (Life Technologies) and quantified using a Nanodrop (ThermoScientific). cDNA was generated from 500 ng of RNA, which was then amplified via RT-PCR using TaqMan probes from Life Technologies: gapdh (Mm99999915_g1), nppa

(Mm01255747_g1), rcan1 (Mm01213406_m1), cacna1c (Mm01188822_m1), cacna1d (Mm01209927_g1), and ctgf (Mm01192933_g1). Threshold values (C_T) for nppa, rrad, and rcan1 were normalized by subtraction from gapdh, and WT (CTRL) was then subtracted from cRadKO ($\Delta\Delta C_T$) and fold-changes were calculated as $2^{-\Delta\Delta CT}$.

2.12 Histology

Mice were anesthetized with ketamine and xylazine and hearts were perfused with PBS followed by 10% formalin in PBS. Fixed hearts were halved along the short axis with papillary muscle visible, and both basal and apical regions were sectioned at 5-μm sections. Picosirius red staining (Direct red 80, Sirius red, Sigma 365548; icric acid, Sigma P6744; in acetic acid) for 1 h at room temperature was used to assess fibrosis (collagen). Sections were 100% ethanol treated and cleared with xylene. Bright field images were captured with polarized light and analyzed with FIJI (ImageJ2).

2.13 Echocardiography

Transthoracic echocardiography was performed using the Visual Sonics 770 imaging system equipped with a 30-MHz probe. Mice underwent transthoracic echocardiography, under light anesthesia (inhaled Isoflurane, 1–2%), with heart rate (350–500 beats per minute) and core temperature (37 °C) continuously monitored. The heart was visualized in 2-dimensional form from modified parasternal long axis, short axis, and apical views. The left ventricular dimensions and calculated left ventricular EF were measured from the short axis M-mode display. All measurements were obtained in triplicate and averaged. The

sonographer was blinded to animal genotype, and data analysis was performed with animal genotype blinded.

For the pharmacological stress echocardiogram, a single intraperitoneal injection of isoproterenol (ISO, 30 mg/kg, USP) was given immediately after baseline echocardiography measurements were recorded. Heart rate was monitored, within 5 min of increased heart rate the drug effect was confirmed, and echocardiography measures were repeated.

2.14 Radiotelemetry

For chapter 3, $RAD^{fl/fl}$-αMHC-CreERT2 mice were chronically instrumented in the left common carotid artery with a radiotelemetry probe (HD-X11, Data Sciences International; St. Paul, MN). Recordings commenced 2 weeks after surgical implantation of probes. Blood pressure was recorded continuously for 1 week prior to tamoxifen administration and then continuously for 2 weeks after tamoxifen.

For chapter 4, mice were anesthetized with isoflurane, and telemetry transmitter units (PhysioTel ETA-F10; Data Sciences International) were implanted in the peritoneal cavity under aseptic conditions. The two ECG leads were secured near the apex of the heart and the right acromion. Mice were housed singly and allowed to recover for at least 2 weeks prior to the start of baseline recordings. ECG data was analyzed for RR interval and PR interval using Ponemah software (Data Sciences International). For intrinsic heart rate atropine (1mg/kg) + propranolol (1mg/kg) was administered ip during the sleep phase. For heart rate variability we used Ponemah Software Platform (Data Sciences International) to

calculated SD of HR from normal to normal intervals for data collected from 3 runs of 1-3 minute continuous periods without noise events before and after ISO; for the air jet we limited the analysis to cover the ~5 minutes of sporadic agitation of mice by air jets. Traces were manually examined to verify absence of noise events.

2.15 Surface ECG

Mice were anaesthetized using 2% isoflurane and supplemented with O_2 at 1.5 L/min. Mice were placed in prone position on a Mouse Monitor S (Indus Instruments) and recorded according to the manufacturer's recommended settings for 5 min under the default filter set. ECGs were recorded for leads I, II, III and aVL for each animal and analyzed. For intrinsic heart rate, atropine (1 mg/kg) + propranolol (1 mg/kg) were administered IP.

2.16 Open Behavioral Assessment

Each subject was placed in its own 2x2 box and tracked using the EthoVision 12 software (Cincinnati, OH USA) for 15 min. Animals were assessed a month after surgery and again a month after tamoxifen treatment (two months post-surgery). Time duration (heat map), track visualization and distance traveled were collected.

2.17 Statistical Analysis

For statistical analyses performed on all cellular observations the mouse is the primary unit of analysis. Cellular mean ± S.E. values are represented in the figures. The

within-mouse averages of the cellular observations were used for analysis to perform the analysis on the level of the experimental units in the mice. The factors of mouse type and isoproterenol treatment (2 × 2 factorial design) were analyzed using 2-way ANOVA with multiple comparisons (specific test noted in figure legend). In the studies of responses across multiple time points, a repeated-measures ANOVA was performed. Post hoc t tests were performed to compare particular groups of interest. In the analyses involving the difference of means between CTRL and cRadKO mice under the assumption of normality of response variable, 2-sample t tests were used, and paired t tests were used before and after isoproterenol treatment comparisons. For ECG telemetry, Students paired t-test was used for baseline versus post-tamoxifen. In the analyses involving the difference of means between CTRL TAC and cRadKO mice, 2-sample *t* tests were used with Welch's correction, and paired *t* tests were used before and after isoproterenol treatment comparisons. Survival curves were compared using a Gehan-Breslow-Wilcoxon test for difference. $p < 0.05$ was considered statistically significant. All statistical analyses were performed using GraphPad Prism 9 (San Diego, CA).

CHAPTER 3. MYOCARDIAL-RESTRICTED ABLATION OF THE GTPASE RAD RESULTS IN A PRO-ADAPTIVE HEART RESPONSE IN MICE

3.1 Preface

The work of chapter 3 has been published [24]. The entirety of the published paper is presented. The nomenclature for cRadKO is labeled $RAD^{\Delta/\Delta}$ and CTRL is labeled $RAD^{fl/fl}$ in this chapter for consistency with what has been published. The results and methods attributed to others are presented for clarity and flow are *italicized*. The figure numbering of the chapter has been edited from the published work for consistency within the dissertation.

3.2 Introduction

There is an unfulfilled need to identify inotropic agents for the heart [5]. However, long-term use of inotropic agents is associated with adverse outcomes in patients [9, 10] that may be related to Ca^{2+}-homeostasis- or protein kinase A-induced maladaptive remodeling [192, 193]. The L-type Ca^{2+} channel complex (LTCC) provides trigger Ca^{2+} for Ca^{2+}-induced Ca^{2+}-release and serves as an upstream control point for modulating the inotropic response. The LTCC complex contains a pore-forming α-subunit ($Ca_V1.2$ in the ventricular myocardium) and auxiliary subunits including $Ca_V\beta2$, α2δ, and calmodulin [194]. In addition to established contributions to channel trafficking and gating, $Ca_V\beta$ subunits mediate RGK (Rem, Rad, Rem2, and Gem/Kir) GTPase inhibition of LTCC function in muscle, neuronal, and endocrine cells [16-18, 195-197]. RAD (Ras associated with diabetes) GTPase, was originally identified as a gene up-regulated in the skeletal muscle of a subset of patients with type 2 diabetics [161], and is the founding member of

the RGK subfamily of Ras-related small GTPases [166]. In heterologous expression systems, RAD shares the common RGK protein property of binding $Ca_V\beta$ subunits and profoundly inhibiting Ca_V1/Ca_V2 channel trafficking and activity, with exogenous RAD overexpression potently inhibiting $I_{Ca,L}$ in adult and embryonic ventricular myocytes [16-20]. *In vivo*, RAD deficiency promotes positive inotropic effects [21, 23]. In contrast, genetic deletion of the Rem GTPase displays no evidence for inotropic effects secondary to only modest increases of $I_{Ca,L}$ [19]. RAD is abundantly expressed in the heart, and our findings, as well as others showed that RAD protein levels fall in patients with end-stage nonischemic heart failure (heart failure with reduced ejection fraction, HFrEF) [23], and in a mouse model of cardiac hypertrophy [181], suggesting that RAD down-regulation may be an integral signaling component in myocardial adaptation.

A growing literature indicates that RAD serves as an endogenous inhibitor of myocardial LTCC activity and attenuates β-AR signaling [21, 22, 183]. Whole body RAD deletion ($gRAD^{-/-}$) results in progressive structural changes to the heart wall and increased myocyte size [22], increased up-regulation of the canonical fetal gene program associated with cardiac hypertrophy [22], and cardiac fibrosis [198]. In keeping with these molecular changes, RAD-deficient mice are reported to be more susceptible to cardiac hypertrophy [181]. These results are in agreement with earlier studies of genetically modified mouse models designed to augment trigger Ca^{2+}. Pore-forming $Ca_V1.2$ transgenic mice exhibit increased $I_{Ca,L}$ and develop heart failure within about 8 months [12]. $Ca_V\beta2$ overexpressing mice show a more rapid progression to pathological cardiac hypertrophy and death [149]. The conclusion from these early studies is that increased $I_{Ca,L}$ promotes pathological cardiac hypertrophy.

RAD protein is expressed in myocardial and nonheart tissues including, but not limited to, vascular smooth muscle [171] and in cells in the bone marrow [172]. Thus the complex cardiac phenotype observed in gRAD$^{-/-}$ mice may include noncardiac influences on cardiac remodeling that are superimposed over direct positive inotropic effect arising from increased trigger Ca^{2+}-current in the myocardium. The purpose of this study is address the key question: are pro-adaptive, positive-inotropic effects of RAD-deletion obscured by the loss of RAD in noncardiac cell types? A key hypothesis maintains that RAD deletion, by targeting LTCC downstream of β-AR signaling provides a gain of systolic function. Therefore, we engineered an inducible, myocardial-restricted RAD knockout mouse (RAD$^{\Delta/\Delta}$). Our results show that RAD$^{\Delta/\Delta}$ mice have enhanced heart function into senescence without evidence for structural remodeling. These major new findings challenge the dogmatic assumption that increased myocardial Ca^{2+} necessarily promotes pathology, and suggests that the heart pathology observed in gRAD$^{-/-}$ mice are the result of noncardiac influences of RAD loss.

3.3 Results

3.3.1 Development of conditional cardiac-restricted RAD-deficient transgenic mice

Standard gene targeting of RRAD in the mouse results in a complex phenotype, including cardiac remodeling [22] and fibrosis [198], with increased cardiac output [21]. To examine the role of RAD signaling selectively in cardiomyocytes, we used conditional gene targeting with the Cre-loxP system. To achieve cardiomyocyte-specific deletion, CRISPR/Cas9 techniques were used to genetically target RRAD, introducing loxP (flox: fl)

*recombination sites flanking exons 3 and 4 (RAD$^{fl/fl}$; **Figure 3.1A**). These exons encode a large portion of the RAD GTPase core that directs both guanine nucleotide binding and hydrolysis, and the C-terminal membrane targeting motif required for LTCC regulation [199] such that any transcribed mRNA that is translated following recombination would produce a truncated protein lacking biological activity. Successful introduction of loxP sites was confirmed by genomic PCR (**Figure 3.1B**). To permit cardiomyocyte-specific RAD deletion, RAD$^{fl/fl}$ mice were crossed with a mouse line expressing a tamoxifen-inducible Cre recombinase under control of the α-myosin heavy chain promoter (αMHC-CreERT2) [185]. RAD is abundantly expressed in the heart and other tissues [17, 161, 171, 172, 200], and administration of tamoxifen to RAD$^{fl/fl\text{-}MHC}$ mice (**Figure 3.1A**) resulted in RAD deletion from the myocardium (RAD$^{\Delta/\Delta}$) but not the spleen (**Figure 3.1C**). Disruption of RAD expression in the heart was confirmed by qRT-PCR (**Figure 3.1D**). RAD$^{fl/fl}$ without αMHC-CreERT2 (RAD$^{fl/fl}$) mice served as littermate controls, with RAD expression unaffected following tamoxifen challenge (**Figure 3.1C,D**). Unless stated, all RAD$^{\Delta/\Delta}$ and RAD$^{fl/fl}$ mice were subjected to analysis >2 weeks following tamoxifen exposure.*

3.3.2 Cardiac-restriced RAD-deficient mice (*RAD$^{\Delta/\Delta}$*) show improved function with no changes in heart dimensions

*Global constitutive RAD knockout mice (gRAD$^{-/-}$) showed increased $I_{Ca,L}$ [21] along with hypertrophic fetal gene program expression, structural remodeling [181], and fibrosis [198]. By contrast, ANF and RCAN1, markers of the fetal gene program, were not altered in RAD$^{\Delta/\Delta}$ (**Figure 3.2A**). There was also no difference in the ratio of heart to body*

*weight (**Figure 3.2B**) and RAD$^{\Delta/\Delta}$ shows no significant difference in fibrosis compared with RAD$^{fl/fl}$ (**Figure 3.2C,D**). This is in stark contrast to gRAD$^{-/-}$ hearts, in which RAD deficiency has been found to increase connective tissue growth factor (CTGF) expression, leading to greater extracellular matrix production and basal cardiac fibrosis [198]. Importantly, cardiomyocyte-restricted RAD deletion failed to increase CTGF expression (**Figure 3.2E,F**). Global RADKO mice experience hypertension [184], and this may be a significant driver of the cardiac remodeling observed in these mice, as gRAD$^{-/-}$ hearts have likely undergone adaptive alterations secondary to pressure overload. Importantly, RAD$^{\Delta/\Delta}$ showed no change in aortic pressure (**Figure 3.2G**). Taken together, these data demonstrate that myocardial-restricted RAD deficiency improves cardiac output without instigating structural remodeling.*

*To test the effect of myocardial-restricted RAD deficiency on heart function we longitudinally followed RAD$^{\Delta/\Delta}$ mice from induced knockout in early adulthood for an additional 15 months (**Figure 3.3A**). Ejection fraction (EF) significantly increased 7 days after tamoxifen administration and remained increased continuously for 15 months (**Figure 3.3B**). There was no difference in heart chamber size (**Figure 3.3C**) or in heart wall thickness (**Figure 3.3D,E**). Cardiomyocyte-restricted RAD deletion effects on in vivo heart function were not different between males and females (**Figure 3.3F-H**). EF has a shallow dependence on heart rate (HR) that is preserved in RAD$^{\Delta/\Delta}$. Regression analysis supports elevated EF in RAD$^{\Delta/\Delta}$ across the range of HR measured (**Figure 3.3I**).*

3.3.3 *RAD*$^{\Delta/\Delta}$ modification of voltage-gated calcium current, $I_{Ca,L}$

A straightforward explanation for enhanced heart function would be increased $I_{Ca,L}$ in RAD$^{\Delta/\Delta}$. Previous studies of whole body, constitutive RAD knockout showed that LTCC conductance increased, voltage dependence shifted negatively, and the predicted I_{CaL} window increased [21]; however, constitutive global RAD knockout hearts displayed structural remodeling. Thus, it is possible that changes in gRAD$^{-/-}$ $I_{Ca,L}$ were secondary to myocardial remodeling. To interrogate the contribution of RAD in structurally unaltered hearts, we measured $I_{Ca,L}$ in cardiomyocytes from mature RAD$^{\Delta/\Delta}$ hearts. **Figure 3.4A** shows representative families of $I_{Ca,L}$ traces from RAD$^{fl/fl}$ and RAD$^{\Delta/\Delta}$ for evaluating current/voltage (I(V)) relationships, and **Figure 3.4B** shows representative current traces generated by the steady-state availability voltage protocol. These representative traces highlight the increased current density and accelerated kinetics of RAD$^{\Delta/\Delta}$. The I(V) curves for $I_{Ca,L}$ show that RAD loss results in a greater current density compared with RAD$^{fl/fl}$ myocytes (**Figure 3.4C**). RAD deficiency results in greater maximal conductance (**Figure 3.4D,E**; maximal conductance: RAD$^{\Delta/\Delta}$ = 254 ± 19 pS/pF, n = 15; RAD$^{fl/fl}$ = 144 ± 12 pS/pF, n = 18; $p < 10^{-4}$). The normalized conductance voltage curves superimposed on the steady-state inactivation curves (**Figure 3.4F**) highlight the selective shift of steady-state activation with RAD ablation; activation midpoint is shifted toward more negative membrane potential (**Figure 3.4F,G**; RAD$^{\Delta/\Delta}$ = −18.3 ± 1.0 mV, n = 15; RAD$^{fl/fl}$ = −8.1 ± 1.9 mV, n = 18; $p < 10^{-4}$). Steady-state availability shows no significant difference of midpoint between RAD$^{fl/fl}$ and RAD$^{\Delta/\Delta}$ (RAD$^{\Delta/\Delta}$ = −24.2 ± 1.0 mV, n = 9; RAD$^{fl/fl}$ = −22.1 ± 1.7 mV, n = 11; p = 0.11). There is no sexual dimorphism in the effect of RAD deletion on $I_{Ca,L}$ (data not shown). The increase in $I_{Ca,L}$ could stem from an increase in Cav1.2. To

test this, we performed qRT-PCR for $Ca_V1.2$ from $RAD^{fl/fl}$ and $RAD^{\Delta/\Delta}$ hearts and found $Ca_V1.2$ mRNA did not change (**Figure 3.4H**). $Ca_V1.2$ protein levels from $RAD^{\Delta/\Delta}$ hearts was also not significantly different from that of $RAD^{fl/fl}$ (**Figure 3.4I**). Taken together these data show that myocardial-restricted RAD deficiency is sufficient to increase $I_{Ca,L}$ by modulating LTCC function.

$RAD^{\Delta/\Delta}$ $I_{Ca,L}$ decay is biphasic with a prominent fast and slow decay phase compared with monophasic decaying $RAD^{fl/fl}$ (**Figure 3.4A**; **Supplemental Figure 3.11**). At −5 mV the fast and slow decaying amplitudes of $RAD^{\Delta/\Delta}$ $I_{Ca,L}$ are roughly similar (**Supplemental Figure 3.11**); the slow-decay component is significantly slower than $RAD^{fl/fl}$ decay. The fast $I_{Ca,L}$ decay is >10-fold faster than the monotonic $I_{Ca,L}$ time constant observed in $RAD^{fl/fl}$ (**Supplemental Figure 3.11**). In summary, myocardial RAD-reduction results in larger, but faster decaying $I_{Ca,L}$.

3.3.4 *$RAD^{\Delta/\Delta}$* enhances cellular calcium homeostasis

$I_{Ca,L}$ provides trigger Ca^{2+} for myocardial Ca^{2+}-induced Ca^{2+} release. Whole-cell cytosolic Ca^{2+} dynamics are significantly larger in amplitude for $RAD^{\Delta/\Delta}$ compared with $RAD^{fl/fl}$ (**Figure 3.5A,B**), and the upstroke velocity of the cytosolic Ca^{2+}-transient is accelerated in $RAD^{\Delta/\Delta}$ (**Figure 3.5C**). To assess Ca^{2+} re-uptake we measured the time constant of the Ca^{2+} transient decay (τ). The value of the mean τ of $RAD^{\Delta/\Delta}$ was faster than that for $RAD^{fl/fl}$ but did not reach statistical significance using ratiometric imaging of fura2 in cardiomyocytes (**Figure 3.5D**). We augmented ratiometric imaging with a separate series of experiments using fluo4 for high speed 2-dimensional cytosol-restricted Ca^{2+} dynamics. A benefit of fluo4 imaging is the elimination of contaminating, slower

nuclear Ca^{2+} signals. Two-dimensional cytosolic Ca^{2+} decay was statistically significantly faster in $RAD^{\Delta/\Delta}$ than $RAD^{fl/fl}$ (**Figure 3.5E**; $RAD^{\Delta/\Delta}$ = 0.07 ± 0.003, n = 67, $RAD^{fl/fl}$ = 0.10 ± 0.005, n = 69; $p < 10^{-4}$). To probe mechanisms of re-uptake we assessed SERCA2a protein levels (**Figure 3.5F**). $RAD^{\Delta/\Delta}$ hearts expressed elevated SERCA2a protein levels ($p < 0.05$) but unchanged phospholamban (PLN) protein levels (see below). Taken together these data suggest that faster $I_{Ca,L}$ trigger (**Figure 3.4**) and increased SERCA2a expression conspire to contribute to accelerate Ca^{2+} transient dynamics following RAD knockout.

Sarcomere dynamics is an important determinant of myocardial function [201]. We therefore measured sarcomere length and dynamics (**Figure 3.6A**) simultaneously with calcium transients. Elevated calcium dynamics (**Figure 3.5**) accompanying RAD deficiency coincided with unchanged resting sarcomere length (**Figure 3.6A,B**), increased fractional shortening (**Figure 3.6C**; $RAD^{\Delta/\Delta}$ = 16.1 ± 0.9, n = 24, $RAD^{fl/fl}$ = 9.9 ± 1.0, n = 15; $p < 10^{-4}$), and the rate at which the cell shortened (**Figure 3.6D**; $RAD^{\Delta/\Delta}$ = −4.8 ± 0.4, n = 24; $RAD^{fl/fl}$ = −2.8 ± 0.3, n = 15; p = 0.0002). Overall, these results suggest an increase in contractility in $RAD^{\Delta/\Delta}$ compared with $RAD^{fl/fl}$, consistent with cellular dynamics driving improved heart function with $RAD^{\Delta/\Delta}$.

Davis et al. [202] introduced a predictive model of cardiac growth based on integrated tension measured from mean twitch tensions or sarcomere shortening. A negative score of this tension-integral model predicts dilated cardiomyopathy; a positive score trends toward hypertrophic remodeling. Using this model, we calculated the index score for our $RAD^{\Delta/\Delta}$ model to predict the direction and intensity of hypertrophy. The $RAD^{\Delta/\Delta}$ tension index score is +0.03 relative to $RAD^{fl/fl}$ (**Figure 3.6E**), predicting only a modest tendency toward concentric hypertrophy. This provides novel evidence that

increasing trigger calcium does not necessarily promote significant cardiac hypertrophy and pathological remodeling.

3.3.5 Basal $I_{Ca,L}$ in *RAD*$^{\Delta/\Delta}$ cardiomyocytes reflects a modulated $I_{Ca,L}$

The increase of $I_{Ca,L}$ in response to β-adrenergic stimulation is atop a constellation of effectors that enhances cardiac output in the fight or flight response. We therefore next tested the effect of acute isoproterenol (ISO) treatment on $I_{Ca,L}$ and calcium dynamics. RAD$^{fl/fl}$ ventricular cardiomyocyte $I_{Ca,L}$ conductance was significantly increased (**Figure 3.7A,Bi**, **Supplemental Figure 3.12**); however, ISO had no detectable effect on RAD$^{\Delta/\Delta}$ $I_{Ca,L}$ (**Figure 3.7A,Bii**, Fig. S2) resulting in ISO-treated RAD$^{fl/fl}$ conductance rising to a level that was indistinguishable from that of unstimulated RAD$^{\Delta/\Delta}$ cardiomyocytes (**Supplemental Figure 3.12**). Comparison of the voltage-dependence of activation of $I_{Ca,L}$ reveals that the acute ISO effect in RAD$^{fl/fl}$, whereas shifted negative, remained more positive than that for RAD$^{\Delta/\Delta}$ (**Figure 3.7D,E**, **Supplemental Figure 3.12**). Acute ISO had no detectable effect on $I_{Ca,L}$ kinetics (data not shown). Two summary conclusions are apparent: 1) RAD$^{\Delta/\Delta}$ $I_{Ca,L}$ is maximally modulated; and 2) RAD$^{fl/fl}$–modulated $I_{Ca,L}$ remains at a more positive activation midpoint potential than that for RAD$^{\Delta/\Delta}$. We conclude that basal RAD$^{\Delta/\Delta}$ phenocopies β-AR–modulated RAD$^{fl/fl}$ $I_{Ca,L}$.

3.3.6 *RAD*$^{\Delta/\Delta}$ basal heart function is elevated *in vivo*, yet retains a partial ISO response

Given that RAD deficiency results in $I_{Ca,L}$ resembling β-AR augmentation we next performed an echocardiography ISO stress test in RAD$^{fl/fl}$ and RAD$^{\Delta/\Delta}$ mice at 1 and 12

*months after tamoxifen administration. Acute in vivo ISO resulted in a significant gain of EF in RAD$^{fl/fl}$ and in RAD$^{\Delta/\Delta}$ mice at 1-month post-tamoxifen treatment (**Figure 3.8**). The ISO effect was preserved at 1 year (16-month-old mice). We conclude that myocardial-restricted RAD deletion provides stable inotropic support, without globally disrupting myocardial β-AR responsiveness.*

3.3.7 *RAD$^{\Delta/\Delta}$* retains β-adrenergic receptor modulation of calcium and sarcomere dynamics

To explore the source of ISO responsiveness in RAD knockout cardiomyocytes we next interrogated Ca^{2+} and sarcomere dynamical response to ISO. Acute ISO enhanced calcium dynamics in RAD$^{\Delta/\Delta}$ and RAD$^{fl/fl}$ ventricular cardiomyocytes (**Figure 3.9A**). For cytosolic Ca^{2+} handling, RAD$^{fl/fl}$ ISO response demonstrated an increase in amplitude, a faster upstroke velocity, and a faster rate of calcium reuptake compared with basal conditions, as expected (**Figure 3.9B-D**, **Supplemental Figure 3.13**). RAD$^{\Delta/\Delta}$ ISO response also demonstrated an increase in amplitude, faster upstroke velocity, and a faster rate of Ca^{2+}-reuptake. Compared with RAD$^{fl/fl}$ with ISO, RAD$^{\Delta/\Delta}$ with ISO had a relatively larger amplitude (RAD$^{\Delta/\Delta}$ = 2.6 ± 0.1, n = 49; RAD$^{fl/fl}$ = 2.0 ± 0.2, n = 37; p = 0.008), faster upstroke velocity (RAD$^{\Delta/\Delta}$ = 63 ± 3.0, n = 49; RAD$^{fl/fl}$ = 47 ± 5.0, n = 37; p = 0.009), and faster rate of calcium reuptake (RAD$^{\Delta/\Delta}$ = 0.11 ± 0.003, n = 49; RAD$^{fl/fl}$ = 0.13 ± 0.006, n = 38; p = 0.05; **Supplemental Figure 3.13**). To further test for active β-AR signaling in RAD$^{\Delta/\Delta}$ we assessed PLN-serine 16 phosphorylation status. At baseline, PLN Ser-16^{P} and Thr-17^{P} relative to total PLN protein were not different between RAD$^{\Delta/\Delta}$ and RAD$^{fl/fl}$ (**Figure 3.9E**). Acute ISO stimulation significantly increase phosphorylation of

PLN–Ser-16^{P} protein from RAD$^{\Delta/\Delta}$ hearts (**Figure 3.9F**) providing a basis for accelerated Ca^{2+}-reuptake.

To test for preservation of acute β-AR signaling to contractile function we measured sarcomere dynamics in response to isoproterenol (**Figure 3.10A**). Fractional shortening (**Figure 3.10B**, **Supplemental Figure 3.14**) and sarcomere relaxation was accelerated in RAD$^{\Delta/\Delta}$ (**Figure 3.10C**, **Supplemental Figure 3.14**). Acute ISO elevated the tension-integral index in RAD$^{fl/fl}$ approaching the level observed for RAD$^{\Delta/\Delta}$ (**Figure 3.10D,E**). To further investigate contractile mechanisms underlying the response to ISO, we assessed the phosphorylation status of sarcomeric proteins that modulate contractility [203, 204]. Acute ISO significantly increased phosphorylation of cMyBPC and TnI (**Figure 3.10F**). These data support the conclusion that RAD$^{\Delta/\Delta}$ does not exhibit de-sensitized myocardial β-AR signaling. The reduction of RAD imposes a chronic modulated $I_{Ca,L}$ while preserving β-AR modulation of critical targets, such as sarcoplasmic reticulum Ca^{2+}-reuptake and contractile apparatus proteins.

3.4 Discussion

There is need for inotropic agents; however, targeting excitation-contraction coupling has been met with failure [205]. Consistent with this literature, early findings with constitutive global RAD$^{-/-}$ (gRAD$^{-/-}$) suggested that elevated trigger Ca^{2+} led to increased cardiac hypertrophy [181]. The importance of the present study is the finding that cardiomyocyte-restricted RAD deletion results in a salutary cardiac phenotype, devoid of the wall remodeling observed in gRAD$^{-/-}$ mouse studies. Here, we successfully achieved conditional cardiomyocyte selective RAD deletion. Through functional measurements and

biochemical analysis, we demonstrate that: 1) RAD is expressed in cardiomyocytes of the heart and myocardial RAD deficiency promotes chronic enhanced heart function without structural remodeling or fibrosis. 2) Cardiomyocyte-specific RAD deletion leads to enhanced basal $I_{Ca,L}$ resembling β-AR modulated $I_{Ca,L}$. 3) Myocardial physiological function (Ca^{2+} handling and sarcomere dynamics) remain β-AR responsive. Moreover, RAD protein is reduced in nonischemic heart failure patients [23] suggesting that regulation of RAD contributes to a compensatory response.

There are two dogmatic paradigms that our present results challenge: first, that increases of calcium dynamics necessarily promote pathogenic cardiac hypertrophy; and second, that absence of RAD exacerbates pathological cardiac remodeling [19, 198]. Each of these are discussed below.

3.4.1 Increased calcium does not necessarily promote cardiac hypertrophy

A major finding of this study is that myocardial RAD deletion, with increased $I_{Ca,L}$, did not demonstrate structural remodeling (**Figure 3.3**). Previous studies have reported a connection between calcium influx through the LTCC and adverse growth of the heart wall [52, 148, 149]. Increasing $I_{Ca,L}$ through overexpression of the pore subunit α_{1C} or the β2 subunit of the LTCC led to cardiac hypertrophy, and eventual heart failure growth [12]. An $I_{Ca,L}$ phenotypic difference with these over-expression models and $RAD^{\Delta/\Delta}$ is in the kinetics of $I_{Ca,L}$. $RAD^{\Delta/\Delta}$ demonstrates a biphasic decay of current with fast and slow components (**Figure 3.4**, **Supplemental Figure 3.11**). The time course of $I_{Ca,L}$ is reminiscent of calcium-dependent fast inactivation contributed by the calcium load of the sarcoplasmic reticulum [206]. Fast decay in $RAD^{\Delta/\Delta}$ $I_{Ca,L}$ attributed to a large calcium

release from the SR might serve as a regulatory negative feedback mechanism to limit total LTCC Ca^{2+} flux, and in turn might not necessarily activate pathways to initiate pathological hypertrophy. Thus, even if dynamical total Ca^{2+} influx was increased in the intact myocardium, there may not be obligatory hypertrophic signaling by LTCC [152].

Over-expression of SERCA2a preserves myocardial function under conditions that otherwise would be expected to produce failure [207-210]. $RAD^{\Delta/\Delta}$ hearts display increased SERCA2a expression without a detectable change in PLN phosphorylation (**Figure 3.5,3.9**), resulting in a change in the ratio of SERCA2a to PLN that is consistent with overall faster Ca^{2+} transient decay dynamics. This favorable alteration toward less regulated SERCA2a complexes in our model has also demonstrated cardiac protection in high-intensity exercise models [207] and PLN-null mice [145], as well as in phase 1 and phase 2 trials of patients suffering from advanced heart failure [209, 210]. To summarize, we observe contemporaneous mechanistic changes in $RAD^{\Delta/\Delta}$ myocardium that plausibly sum to a stable gain of heart function including: increased, faster-decaying trigger Ca^{2+} and increased SERCA2a.

Davis et al. [202] proposed a tension-integral index model that distinguishes between hypertrophic and dilated cardiac remodeling. A key insight of the tension-integral index study was that the tension-integral predicted myocardial structural changes, but there were poor correlations to changes in calcium handling indices [202]. The $RAD^{\Delta/\Delta}$ approximates a WT tension-integral as a consequence of larger amplitude contractions offset by faster kinetics. Regardless, the $RAD^{\Delta/\Delta}$ heart showed elevated EF. Thus, how $RAD^{\Delta/\Delta}$ accommodates the increased demands of chronic increased cardiac function will be an important area of follow-up studies.

In a similar vein to sarcomere dynamics, the faster kinetics of $I_{Ca,L}$ in $RAD^{\Delta/\Delta}$ could also potentially serve to attenuate arrhythmogenic potential. Mahajan et al. [50] proposed modifying $I_{Ca,L}$ kinetics as a superior way to prevent arrhythmias, rather than through inhibiting $I_{Ca,L}$ activation. This would allow early peak $I_{Ca,L}$ to initiate normal SR calcium release, and diminish the effects of late $I_{Ca,L}$ on repolarization. As encouraging as the present results are for suggesting myocardial RAD deletion as a therapeutic direction for cardioprotection, thorough analysis of arrhythmogenic potential will require further studies, including, but not limited to alternative model systems to the mouse.

The $RAD^{\Delta/\Delta}$ model also differs from other models of increased $I_{Ca,L}$ because responsiveness to β-adrenergic receptor (β-AR) stimulation is retained. A hallmark feature of HFrEF is insensitivity of β-AR to chronic stimulation [145] that ultimately limits the contractile reserve of the heart. $RAD^{\Delta/\Delta}$ hearts retain β-AR responsiveness at the level of the cell (**Figure 3.9,3.10**) and whole heart (**Figure 3.8**), and did not develop heart failure. $I_{Ca,L}$ did not change after treatment with isoproterenol in our $RAD^{\Delta/\Delta}$ model (**Figure 3.7**), similar to overexpression of the α_{1C} model [197]. $I_{Ca,L}$ was larger in $RAD^{\Delta/\Delta}$ than in $RAD^{fl/fl}$ stimulated with ISO. This suggests that RAD may play a critical role in the ability for the LTCC to be modulated by β-AR stimulation; when RAD is deleted, basal $I_{Ca,L}$ is larger than currently seen following typical modulation. Further studies are warranted to define the molecular role for RAD in β-adrenergic Ca^{2+} current modulation. Finally, enhancing Ca^{2+} dynamics via targeting of β-AR signaling by G-protein coupling receptor kinase [211] or Raf kinase inhibition [212] also provides protection against pressure overload induced heart failure. In summary, increasing

Ca^{2+} dynamics in a manner that bypasses chronic β-AR activity is a potentially attractive target of therapeutic strategies for heart failure therapy.

3.4.2 Myocardial-restricted RAD deletion differs from whole body RAD deletion

Key differences exist between $RAD^{\Delta/\Delta}$ and the whole body deletion of RAD leading to the existing erroneous conclusion that RAD-reduction is pro-hypertrophic [181]. In the global RAD knockout model ($gRAD^{-/-}$), channel function and cellular calcium dynamics were similar to $RAD^{\Delta/\Delta}$, and in both models the myocardium retained responsiveness to β-AR stimulation [21]. However, myocardial RAD deficiency promotes enhanced heart function without structural remodeling or fibrosis. A major consideration is that $gRAD^{-/-}$ mice experience hypertension [184], whereas $RAD^{\Delta/\Delta}$ do not. This may result from loss of RAD in vascular smooth muscle [171, 213]; increased $I_{Ca,L}$ in vascular smooth muscle could lead to increased vascular resistance to progress toward hypertension. Regardless, $gRAD^{-/-}$ hearts have likely undergone adaptive signaling and therefore interpretation of studies of Ca^{2+} dynamics in $gRAD^{-/-}$ must consider the myriad of myocardial alterations secondary to pressure overload.

In summary, our findings suggest that increasing myocardial calcium handling does not necessarily promote pathological remodeling, in fact, by imposing a chronic modulated $I_{Ca,L}$ phenotype in the basal state we show that heart function increases stably into senescence. These findings are consistent with the notion that decreased RAD in heart failure patients [23, 181] contributes to a compensatory response. There is a major unmet need for treatments targeting inotropy [5]. We conclude that myocardial RAD deletion

might provide a potential new therapeutic target for positive inotropy without introducing damaging effects to the heart.

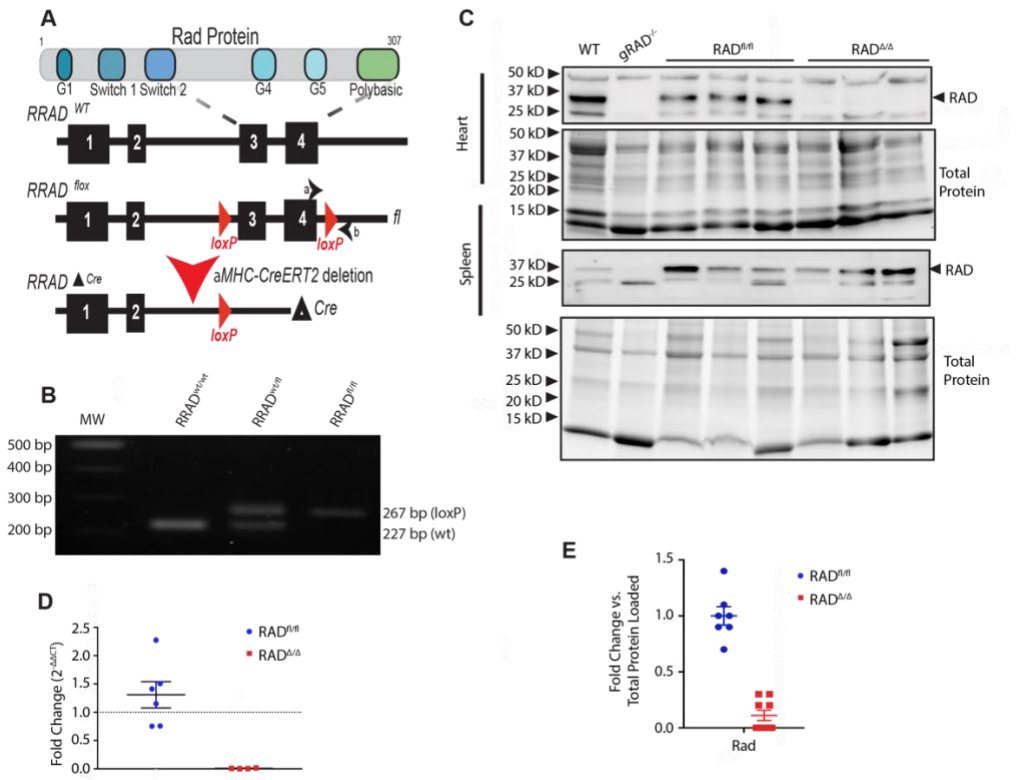

Figure 3.1 Myocardial deletion of Rad.

A) Graphic representation of the *RRAD* conditional targeting strategy. Flanking exons 3 and 4 of *RRAD* with loxP sites generated the floxed allele (*fl*). Cre-mediated recombination of the loxP sites results in the cKO allele (Δ). The approximate locations of the PCR primers used for genotyping (*a* and *b*) are shown. **B)** Genotyping PCR of tail genomic DNA yielded the following genotypes: $RRAD^{wt}$ (*lane 1*), $RRAD^{wt/fl}$ (*lane 2*), and $RRAD^{fl/fl}$ (*lane 3*). Amplicons were generated by primers *a* and *b* as shown in **A)**. **C)** Western blot analysis for RAD in protein lysates from wildtype (WT), global RAD knockout (gRADKO), $RAD^{fl/fl}$ and $RAD^{\Delta/\Delta}$ (2 weeks post-tamoxifen treatment) from total heart (*top panel*) and spleen (*bottom panel*). Note that RAD expression is retained in the spleen of $RAD^{\Delta/\Delta}$ mice following tamoxifen treatment. **D)** qRT-PCR analysis in mRNA samples from $RAD^{fl/fl}$ and $RAD^{\Delta/\Delta}$ hearts. *MW*, 100 bp DNA ladder. **E)** Quantification by Western blotting of RAD levels in the heart 4 weeks post-tamoxifen treatment (n = 7); ***p = 0.001.

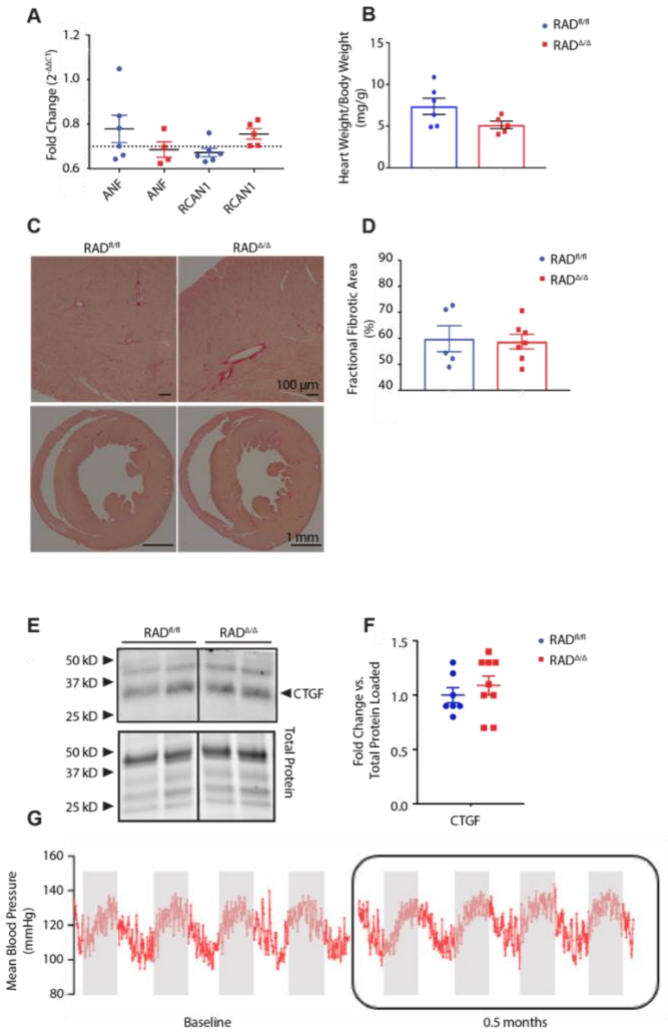

Figure 3.2 Cardiomyocyte-restricted Rad deletion does not induce markers of myocardial pathology.

A) qRT-PCR for ANF and RCAN1 mRNA expression levels. Rad$^{fl/fl}$ (n=6) and Rad$^{\Delta/\Delta}$ (n=5) as shown. **B)** Heart weight was not significantly different between Rad $^{\Delta/\Delta}$and Rad$^{fl/fl}$. **C**) Representative pictures of picroSirius Red staining with fibrosis quantification in **D**). Rad$^{fl/fl}$ (n=5) and Rad$^{\Delta/\Delta}$ (n=7) as shown. **E)** Western blot analysis with quantification in **F)** demonstrates no difference in CTGF expression. Lanes run on the same gel, but noncontiguous lanes are marked by the black line. Rad$^{fl/fl}$ (n=7) and Rad$^{\Delta/\Delta}$ (n=9). **p=0.008. **G)** Aortic pressure recordings, 4 continuous days from baseline (prior to tamoxifen), and from same mice 2 weeks after tamoxifen administration (Rad$^{\Delta/\Delta}$). Data are average of 3 mice. Data were fitted to a sine wave with fixed cycle length of 24h. Active (night-time) and resting (daytime) blood pressures were 129±2 mmHg (baseline), 132±5 mmHg (0.5 months); and 118±2 mmHg (baseline), 122±6 (0.5 months), respectively.

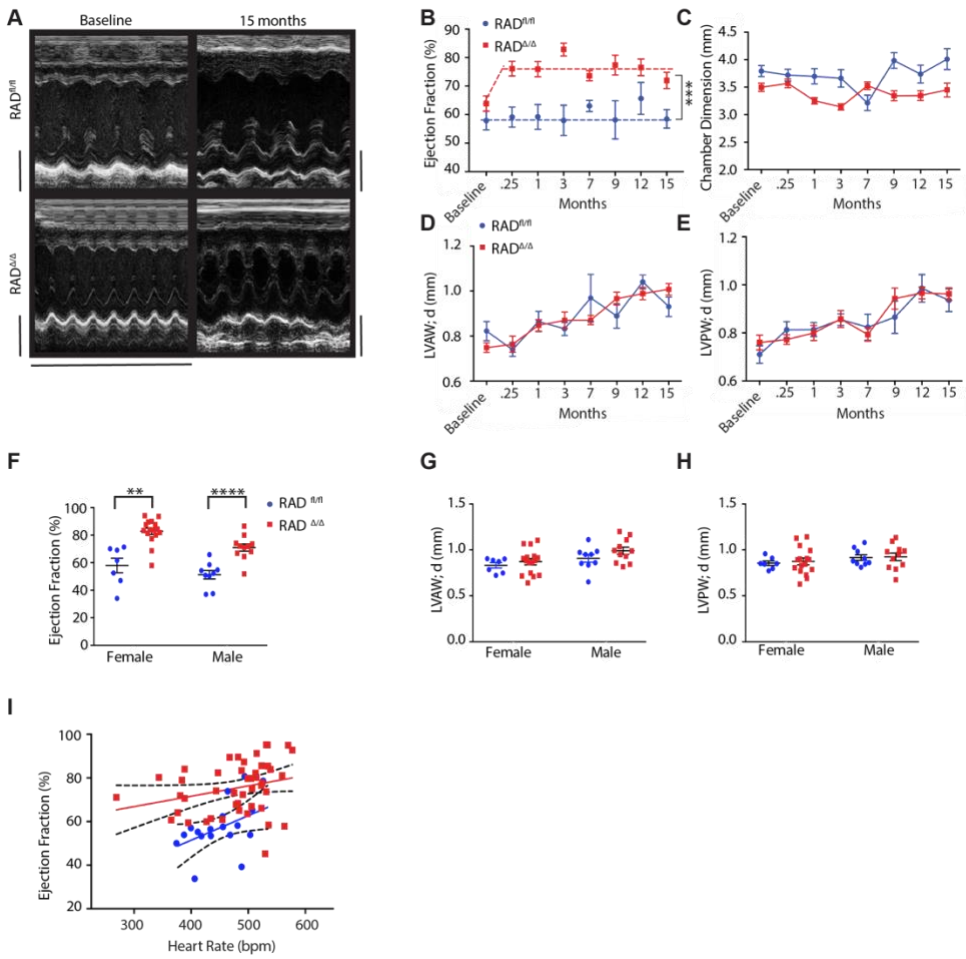

Figure 3.3 Figure 3.3. Myocardial Rad deletion results in a rapid, stable gain of cardiac function without pathological structural remodeling in vivo.

A) Representative M-mode short-axis echocardiography of female mice 1- week through 15-months following tamoxifen injection. *Scale bars* of depth: $RAD^{fl/fl}$ baseline = 0.69 mm; $RAD^{fl/fl}$ 15 months = 0.67 mm; $RAD^{\Delta/\Delta}$ baseline = 0.69 mm; $RAD^{\Delta/\Delta}$ 15 months = 0.76 mm; all images have a duration of 1 s. **B)** ejection fraction; **C)** left ventricular inner dimension; **D)** left ventricular anterior and **E)** posterior wall thickness. Dimensions (**C-E**) are shown in diastole. $RAD^{fl/fl}$ (n=7) and $RAD^{\Delta/\Delta}$ (n=17); by genetic modification, p = 0.0002; F = 20; by time p = 0.04; F = 2; by gene x time, p = 0.04; F = 2). **F-H**) Echocardiography of male and female mice 3 months after tamoxifen treatment. **F)** Ejection fraction. Sidak's multiple comparison test showed $RAD^{\Delta/\Delta}$ increased in EF ($p < 10^{-3}$ males, $p < 10^{-4}$ females; by genetic modification, $p < 10^{-4}$; F = 49; by sex, $p < 0.01$; F = 8; no interaction). $RAD^{fl/fl}$ 2-way ANOVA shows female gender contributed 8% to variance suggesting more sensitivity than males to $RAD^{\Delta/\Delta}$ ($p < 0.06$). **G)** Anterior wall thickness and **H)** Posterior wall thickness was not difference by $RAD^{\Delta/\Delta}$ or by male *versus* female. **I)** Linear regression of EF as a function of HR shows HR differences do not account for elevated EF in $RAD^{\Delta/\Delta}$. The *dashed lines* show 95% confidence limits. The slope is not different between $RAD^{\Delta/\Delta}$ and $RAD^{fl/fl}$; elevation of EF is significantly different ($p < 10^{-4}$). **p=0.006, ****$p<10^{-4}$.

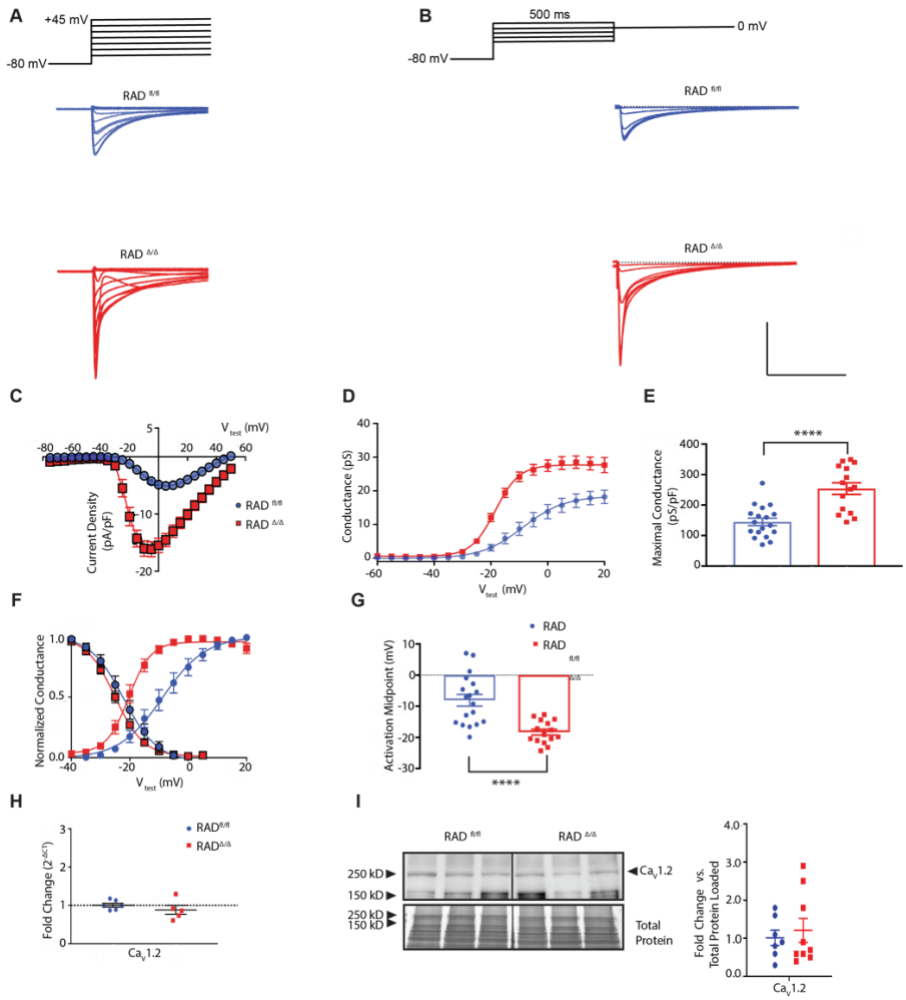

Figure 3.4 Myocardial Rad deletion results in increased calcium current ($I_{Ca,L}$).

A) Representative family of $I_{Ca,L}$ traces, V_{test} ranging from -75 to +45 mV in 10-mV increments, with voltage protocol schematic shown above. **B)** Representative family of $I_{Ca,L}$ traces, V_{test} ranging from -50 to 0 mV in 10-mV increments for determing steady-state availability, with voltage protocol schematic shown above. *Scale bars*: 500 pA and 200 ms. *Scale bars* common to panels **A)** and **B)**. **C)** Current voltage curve shows that $I_{Ca,L}$ density is increased in cardiomyocytes from $RAD^{\Delta/\Delta}$ compared to $RAD^{fl/fl}$. **D)** Conductance transform of the current/voltage curve demonstrates higher maximal conductance in $RAD^{\Delta/\Delta}$ compared with $RAD^{fl/fl}$ with quantification shown in **E)**. **F)** Conductance-voltage curve normalized to maximal conductance illustrates $RAD^{\Delta/\Delta}$ cardiomyocytes have shifted the activation midpoint. Smooth curves are Boltzmann distribution fitted to data. Steady-state availability was not different. Note that voltage for the availability curve is the value for the 500-ms pre-puls potential step (see schematic in **A**). **G)** Activation midpoint is significantly negative-shifted in $RAD^{\Delta/\Delta}$. Current data are from $RAD^{fl/fl}$ (N = 7 mice, n = 18 cells), $RAD^{\Delta/\Delta}$ (N = 7 mice, n = 17 cells). ****$p<10^{-4}$. **H)** Western blot analysis demonstrates no difference in $Ca_V1.2$ expression between $RAD^{fl/fl}$ and $RAD^{\Delta/\Delta}$. Lanes run on the same gel, but noncontiguous lanes are marked by the *black line*; total protein stained with Coomassie Blue and quantification are shown on the *right*. Western blot data from $RAD^{fl/fl}$ (7 mice) and $RAD^{\Delta/\Delta}$ (9 mice).

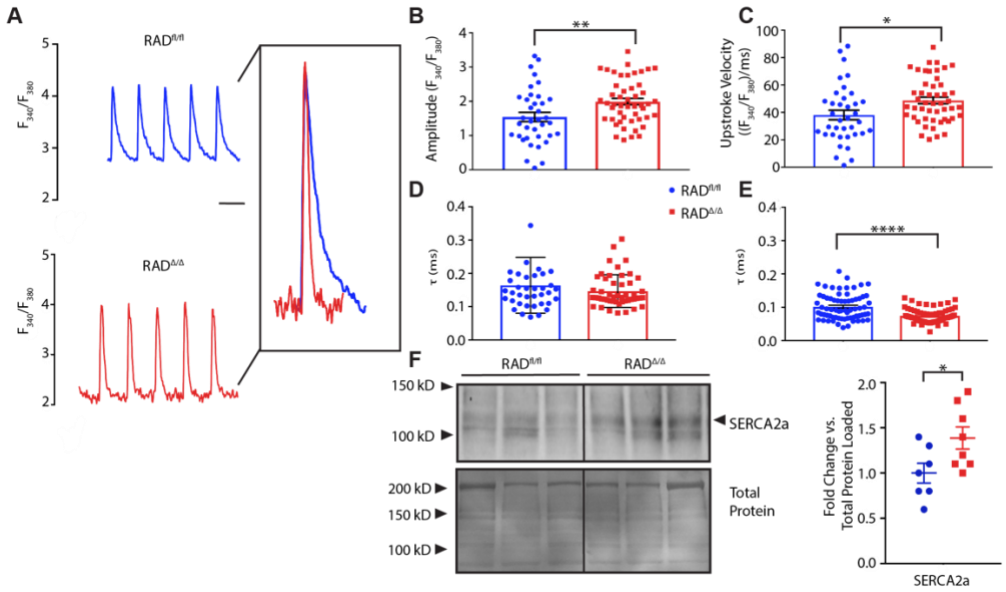

Figure 3.5 Rad$^{\Delta/\Delta}$ enhances cellular calcium handling.

A) Representative calcium transients from isolated ventricular cardiomyocytes loaded with fura2-AM, RAD$^{fl/fl}$ (*top*) and RAD$^{\Delta/\Delta}$ (*bottom*) paced at 1 Hz. **B)** Amplitude of the transients from RAD$^{\Delta/\Delta}$ are higher than in RAD$^{fl/fl}$. **C)** The velocity at which calcium enters the cytosol (upstroke of the transient) is faster in RAD$^{\Delta/\Delta}$ than in RAD$^{fl/fl}$. **D, E**) Calcium transient decay is faster in RAD$^{\Delta/\Delta}$ than in RAD$^{fl/fl}$. Measurements in **E)** used fluo4 AM and high speed 2- dimensional imaging. Measurements in **A-D)** used fura2 AM, RAD$^{fl/fl}$ (N = 10 mice, n = 38), RAD$^{\Delta/\Delta}$ (N = 8 mice, n = 49). For **E)** RAD$^{fl/fl}$ (N = 10 mice, n = 69), RAD$^{\Delta/\Delta}$ (N = 8 mice, n = 67). **F)** Western blot analysis demonstrates increased expression of SERCA2a, quantification is shown on the right (p = 0.035). Lanes run on the same gel, but noncontiguous lane marked by the black line. Below, total protein stained with Coomassie Blue. RAD$^{fl/fl}$ (7 mice) and RAD$^{\Delta/\Delta}$ (8 mice). *p=0.014, **p=0.008, ****p<10^{-4}

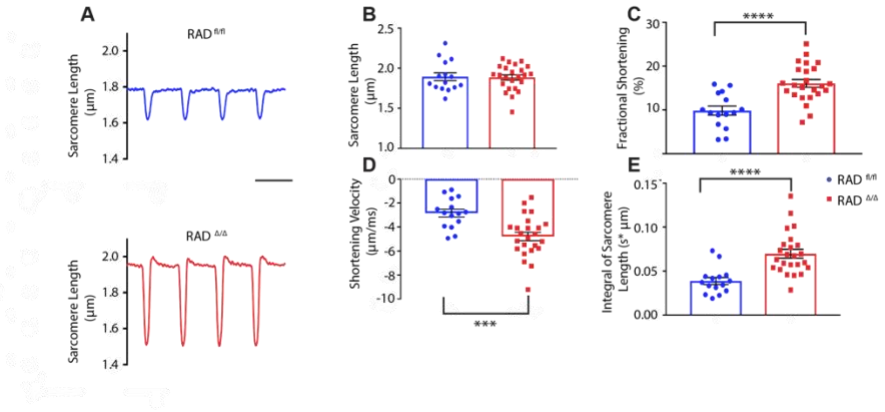

Figure 3.6 RAD$^{\Delta/\Delta}$ enhances sarcomere shortening and increases the tension-integral.

A) Representative sarcomere traces of RAD$^{fl/fl}$ and RAD$^{\Delta/\Delta}$ paced at 1 Hz. **B)** Diastolic sarcomere length was not different between RAD$^{fl/fl}$ and RAD$^{\Delta/\Delta}$. **C)** Sarcomere fractional shortening was higher in RAD$^{\Delta/\Delta}$ than in RAD$^{fl/fl}$. **D)** The velocity of shortening was faster in Rad$^{\Delta/\Delta}$ than in Rad$^{fl/fl}$. **E)** Integral of sarcomere length is larger for RAD$^{\Delta/\Delta}$ than in RAD$^{fl/fl}$. RAD$^{fl/fl}$ (N = 7 mice, n = 15 cells) and Rad$^{\Delta/\Delta}$ (N = 8 mice, n = 24 cells). ***$p<0.001$; ****$p<10^{-4}$

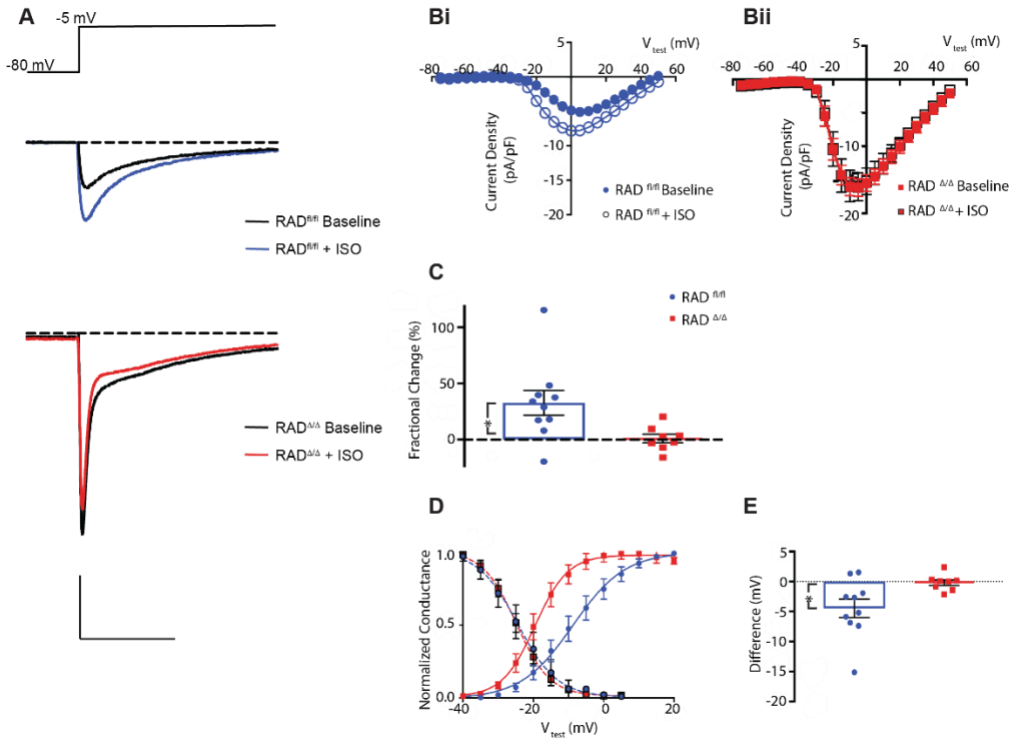

Figure 3.7 ISO does not alter RAD$^{\Delta/\Delta}$ $I_{Ca,L}$.

A) Representative $I_{Ca,L}$ traces at V_{test} of -5 mV before (*black line*) and after treatment with ISO (*colored line*; *blue* for RAD$^{fl/fl}$ and *red* for Rad$^{\Delta/\Delta}$). Scale bars: 500 pA and 200 ms. **B)** Current voltage curves superimposing basal and acute 1μM ISO treatment for RAD$^{fl/fl}$ (B,i) and RAD$^{\Delta/\Delta}$ (B,ii). **C)** Fractional change of maximal conductance between baseline and ISO response of RAD$^{fl/fl}$ (mean = 32.68%) and RAD$^{\Delta/\Delta}$ (mean = 0.84%). **D)** Conductance-voltage curve normalized to maximal conductance for ISO treated cells demonstrates RAD$^{\Delta/\Delta}$ cardiomyocytes have negative shifted activation midpoint relative to RAD$^{fl/fl}$ in ISO. Smooth curves are Boltzmann distribution fitted to data. Steady-state availability was not different. **E)** Difference between activation midpoints between baseline and ISO response of RAD$^{fl/fl}$ (mean = - 4.47) and RAD$^{\Delta/\Delta}$ (mean = -0.19). RAD$^{fl/fl}$ (N = 4 mice) and RAD$^{\Delta/\Delta}$ (N = 4 mice). *p =0.02

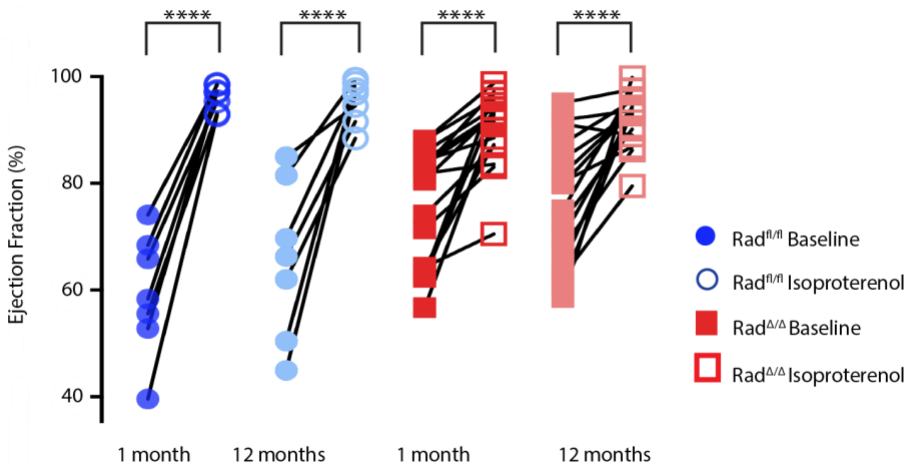

Figure 3.8 β-AR-mediated responsiveness retained following Rad deletion *in vivo*

Mice scanned at baseline (filled symbol) and after injection of isoproterenol (open symbol with connecting line). Ejection fraction increased with addition of isoproterenol in both $RAD^{fl/fl}$ and $RAD^{\Delta/\Delta}$. This response was retained 1 month and 12 months after induction of knock out. Data displayed from $RAD^{fl/fl}$ (N = 7) and $RAD^{\Delta/\Delta}$ (N = 17) using Student paired *t* test, ****$p < 0.0001$.

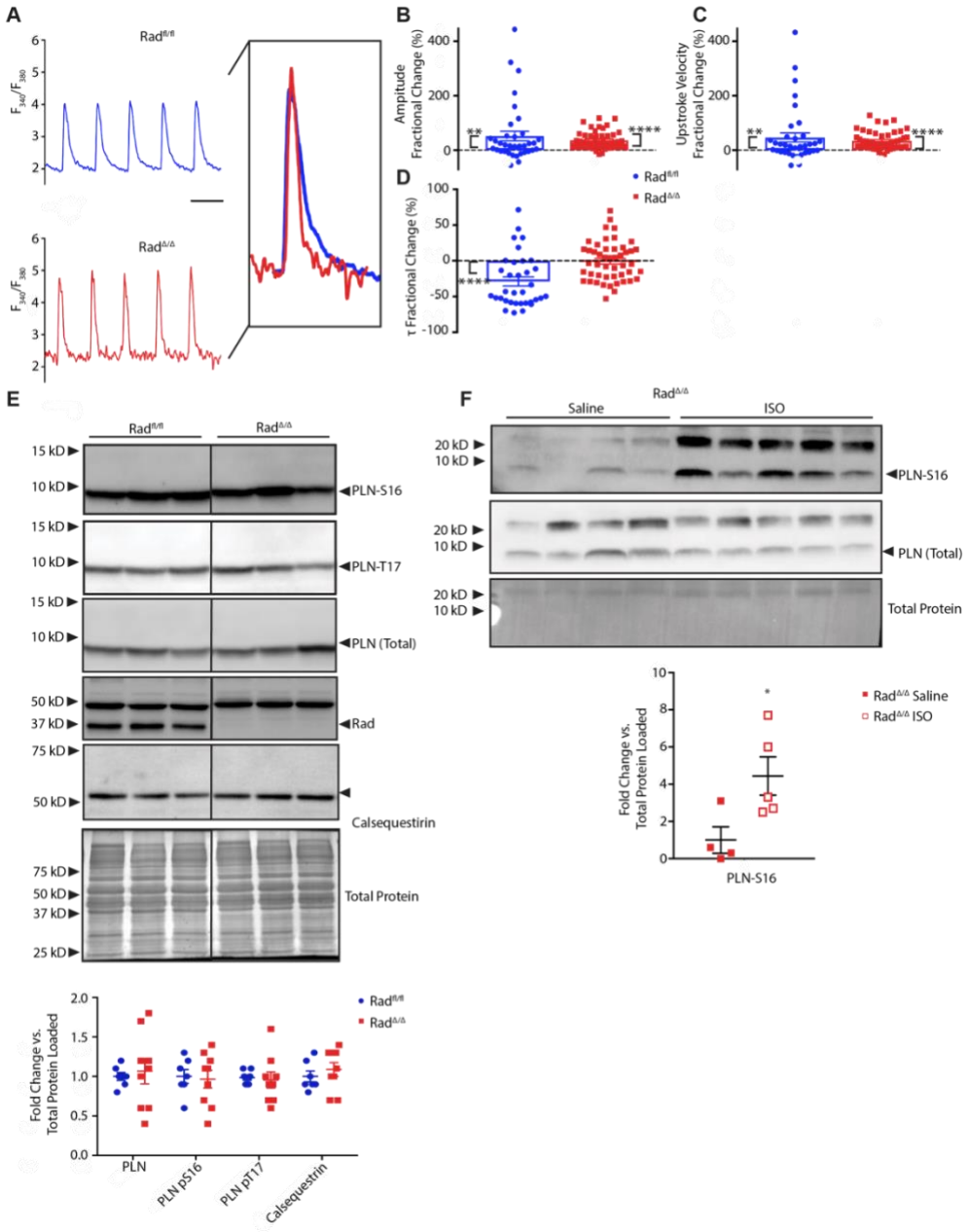

Figure 3.9 Cardiomyocyte cytosolic Ca^{2+} handling responds to β-AR-mediated activation in $RAD^{\Delta/\Delta}$.

A) Representative calcium transients from $RAD^{fl/fl}$ and $RAD^{\Delta/\Delta}$ cardiomyocytes paced at 1 Hz in 1μM ISO. **B)** Fractional change (ISO/baseline) of Ca^{2+} transient amplitude. **C)** Upstroke velocity, and **D)** Rate of decay. $RAD^{fl/fl}$ (N = 10 mice, n = 38 cells), $RAD^{\Delta/\Delta}$ (N = 8 mice, n = 49 cells) are shown. **E)** Western blot analysis of total and phosphorylated PLN, RAD, and calsequestrin (15% SDS-PAGE). Lower panel, quantification shows no significant effect of myocardial Rad deletion. $RAD^{fl/fl}$ (N = 6 mice) and $RAD^{\Delta/\Delta}$ (N = 9 mice) are shown. **F)** Acute ISO increased PLN $Ser16^{P}$ in $RAD^{\Delta/\Delta}$ (4-20% SDS-PAGE). $RAD^{\Delta/\Delta}$ (N = 5 mice) is shown. For all panels: *$p<0.05$; **$p = 0.005$.; ****$p<10^{-4}$

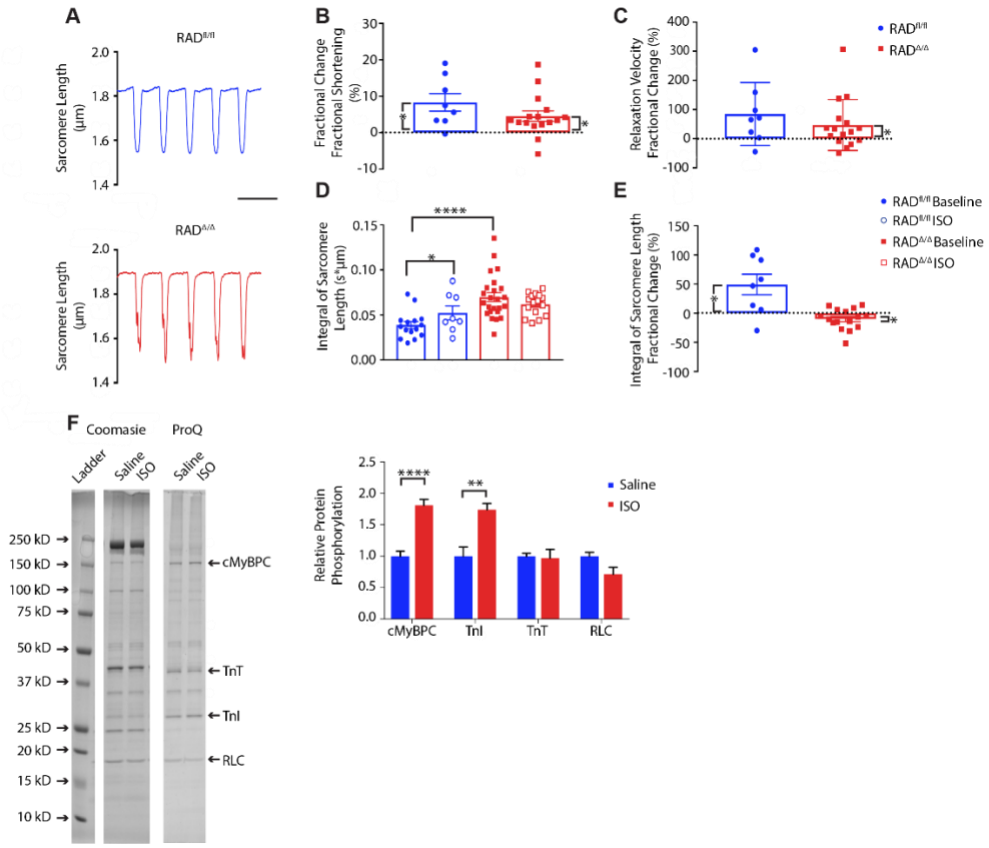

Figure 3.10 Sarcomere dynamics and proteins respond to β-AR-mediated activation in RAD$^{\Delta/\Delta}$.

A) Representative sarcomere traces of RAD$^{fl/fl}$ and RAD$^{\Delta/\Delta}$ paced at 1 Hz after treatment with 1µM ISO. **B)** Fractional change (ISO/baseline) in fractional shortening, and **C)** relaxation velocity. ISO significantly increases shortening and relaxation velocity in RAD$^{\Delta/\Delta}$. **D)** Integral of sarcomere length is larger in RAD$^{\Delta/\Delta}$ than in RAD$^{fl/fl}$. **E)** ISO treatment increased tension-integral index in RAD$^{fl/fl}$ but not in RAD$^{\Delta/\Delta}$. RAD$^{fl/fl}$ (N = 3 mice, n = 8 cells) and RAD$^{\Delta/\Delta}$ (N = 5 mice, n = 16 cells) are shown. **F)** Coomassie stain and ProQ phosphostain analysis demonstrating increased phosphorylation of proteins from RAD$^{\Delta/\Delta}$ hearts after treatment with ISO of cMyBPC and TnI, quantification to the right. Saline, N = 6 mice; and ISO, N = 6 mice were used. For all panels: *p=0.01, **p=0.0002, ****p<10^{-4}

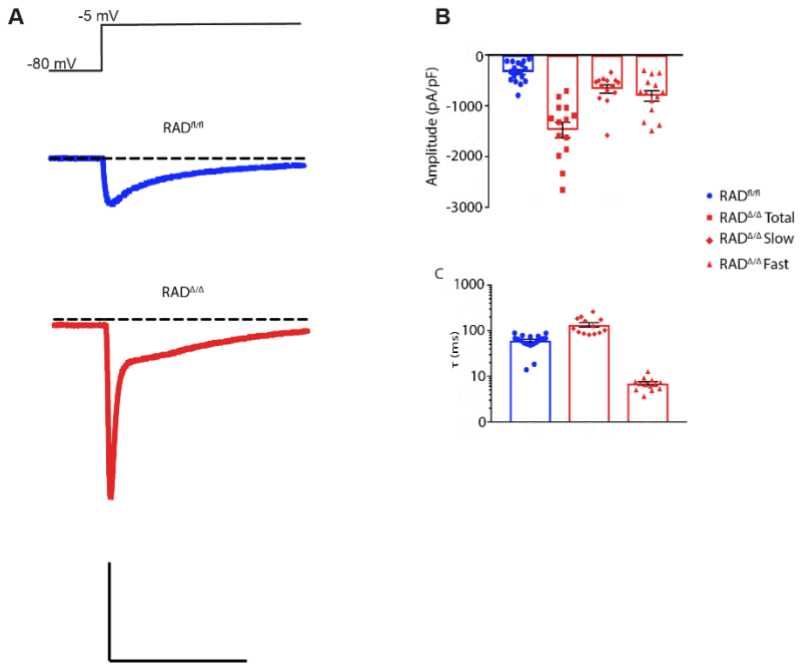

Supplemental Figure 3.11 Myocardial Rad deletion results in increased calcium current ($I_{Ca,L}$).

A) Representative $I_{Ca,L}$ traces for V_{test} at -5 mV, with voltage protocol shown above. **B)** and **C)** Amplitufe and rate of decay were measured using a fitted exponential function on current traces. $RAD^{fl/fl}$ was measured using a single exponential function. $RAD^{\Delta/\Delta}$ required the sum of two exponential functions. **B)** Total amplitude was larger in $RAD^{\Delta/\Delta}$ than in $RAD^{fl/fl}$ at -5 mV. **C)** Rate of decay (t) was faster $RAD^{\Delta/\Delta}$ than in $RAD^{fl/fl}$, both in the fast and slow phases at -5 mV. Data displayed from $RAD^{fl/fl}$ (7 mice, 18 cells) and $RAD^{\Delta/\Delta}$ (7 mice, 17 cells). ***p=0.0004, ****p<0.0001

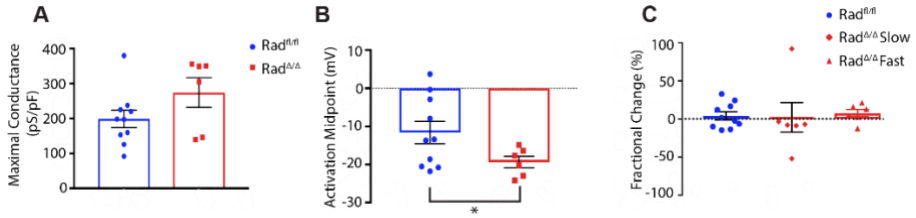

Supplemental Figure 3.12 RAD$^{\Delta/\Delta}$ $I_{Ca,L}$ response after β-adrenergic receptor stimulation.

A) No difference in maximal conductance in RAD$^{\Delta/\Delta}$ compared to RAD$^{fl/fl}$ ($p = 0.161$). **B)** Activation midpoint is also significantly negative-shifted in RAD$^{\Delta/\Delta}$. Rate of decay of current was measured using a fitted exponential function on current traces. RAD$^{fl/fl}$ was measured using a fitted exponential function. RAD$^{\Delta/\Delta}$ had two different phases, and was fitted best using two exponential functions. **C)** Fractional change in tau, in RAD$^{fl/fl}$ at -5 mV (mean = 4%) and RAD$^{\Delta/\Delta}$ (mean: slow = 2%; fast = 7%). Data displayed from RAD$^{fl/fl}$ (10 mice, n = 38) and RAD$^{\Delta/\Delta}$ (8 mice, n = 49). *$p = 0.04$.

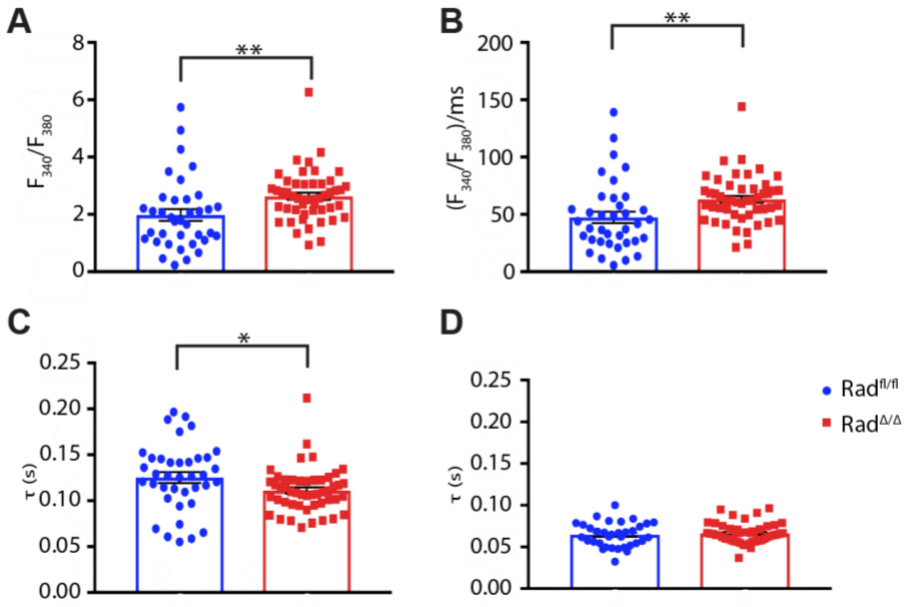

Supplemental Figure 3.13 RAD$^{\Delta/\Delta}$ cellular response after β-adrenergic receptor stimulation.

A) Amplitude of the transients from RAD$^{\Delta/\Delta}$ are higher than in RAD$^{fl/fl}$. **B)** The upstroke velocity is faster in RAD$^{\Delta/\Delta}$ than in RAD$^{fl/fl}$. **C)** and **D)** Rate of decay is faster in RAD$^{\Delta/\Delta}$ than in RAD$^{fl/fl}$. Measurements in **A-C)** used 5 mM Fura2 AM and measurements in **D)** used 5 mM Fluo4 AM ($p = 0.53$). Data displayed from RAD$^{fl/fl}$ (10 mice, n = 38) and RAD$^{\Delta/\Delta}$ (8 mice, n = 49). *$p = 0.04$, **$p = 0.008$

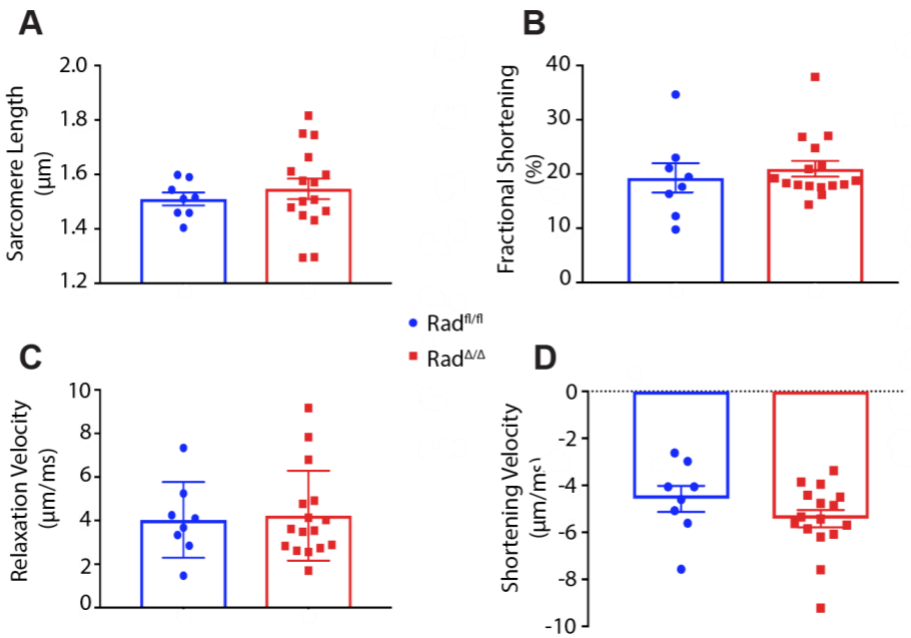

Supplemental Figure 3.14 No effect on sarcomere dynamics after treatment with ISO.

A) Diastolic sarcomere length was not different after ISO between $RAD^{fl/fl}$ and $RAD^{\Delta/\Delta}$. **B)** Percentage of fractional shortening was not different after ISO between $RAD^{fl/fl}$ and $RAD^{\Delta/\Delta}$. **C)** Relaxation velocity was no different after ISO between $RAD^{fl/fl}$ and $RAD^{\Delta/\Delta}$. **D)** Shortening velocity was not different after ISO between $RAD^{fl/fl}$ and $RAD^{\Delta/\Delta}$. Data displayed from $RAD^{fl/fl}$ (3 mice, 8 cells) and $RAD^{\Delta/\Delta}$ (5 mice, 16 cells).

CHAPTER 4. RAD-GTPASE CONTRIBUTES TO HEART RATE VIA L-TYPE CALCIUM CHANNEL REGULATION

4.1 Preface

The work of chapter 4 has been published [214] . The entirety of the published paper is presented. The results and methods attributed to others are presented for clarity and flow are *italicized*. The figure numbering of the chapter has been edited from the published work for consistency within the dissertation.

4.2 Introduction

Spontaneous electrical activity of the sinoatrial node (SAN) initiates cardiac rhythm and is a critical determinant of heart rate (HR). Cardiomyocytes of the SAN (SANcm) are highly specialized cells that generate automatic activity and form the cellular basis for cardiac pacemaking. SANcm exhibit a spontaneous diastolic depolarization. The early phase of diastolic depolarization is dominated by inward cationic funny current (If [215] carried by HCN4 [216]). The latter phase of diastolic depolarization is driven by voltage-gated L-type calcium channels (LTCC, with the main pore forming subunit, $Ca_V1.2$ or $Ca_V1.3$) [217] . To a large extent, I_f and the LTCC complex determine the 'membrane clock' that interacts with the calcium clock in the SAN [218, 219]. The inter-relation of the membrane clock and calcium clock is underscored by studies of the genetic model of loss of $Ca_V1.3$ impairing sarcoplasmic reticulum Ca^{2+}-release [220, 221], and by computational studies linking feedback loops among sarcoplasmic Ca^{2+}-release, NCX, and $I_{Ca,L}$ [222, 223]. The ability of $I_{Ca,L}$ to simultaneously contribute to membrane- and calcium-clocks

suggests that targeted regulation of the LTCC is a potentially powerful approach to control HR. Although cellular and molecular mechanisms that contribute to pacemaker activity are well established [224], bradyarrhythmia treatment options are limited mainly to electronic devices that are insensitive to autonomic nervous system regulation. Experimentally, nifedipine (an LTCC antagonist) has a negative chronotropic effect on the leading pacemaker site of the SAN [225]; similarly, genetic knockout of CaV1.3 induces bradycardia [226]. A fundamental premise of this study is that modulation of LTCC activity conferred by Rad provides a central nodal mechanism for sympathetic nervous system (SNS) control of SAN rhythm.

The LTCC is a heteromultimeric protein complex [194]. The pore-forming subunit of the LTCC in SANcm is carried by CaV1.3 [226-228] and CaV1.2 [217] channels. Key auxiliary subunits of the LTCC complex include $Ca_V\beta_2$, $\alpha_2\delta$, and CaM [194]. Recent work [117] highlights the importance of RGK proteins [166] as regulators of $I_{Ca,L}$ via association with the β subunits [17, 21, 24, 184]. Rad is a constituent of the LTCC complex in the myocardium [17, 92]. Sympathetic nervous system drive acts via β-AR signaling cascades, resulting in the activation of PKA which in turn modulates LTCC activity [229]. β-AR modulation is maintained in transgenic mouse models expressing mutant $Ca_V1.2$ and $Ca_V\beta$ that cannot be phosphorylated by PKA [91, 117], suggesting that a non-channel PKA target is central to channel modulation. Using proximity biotinylation to analyze β-adrenergic-dependent changes within the LTCC complex, Rad was recently shown to be depleted from the LTCC complex following acute β-AR stimulation. Rad depletion from the LTCC relieves the constitutive inhibition imposed by Rad association [17, 21, 24, 183]. In keeping with its presumptive role as an endogenous inhibitor of LTCC function, we

showed that LTCC activity is increased In Rad-null mice ($Rad^{-/-}$) with properties mirroring β-AR modulation of $I_{Ca,L}$ [21]. ECG telemetry showed that $Rad^{-/-}$ mice have a complex phenotype that includes differential vascular and inflammatory properties [184]. However, this model has multi-organ involvement [172, 184] and possible development-related effects that potentially confound analysis of heart rhythm modification originating from channel modulation in cardiomyocytes. To circumvent these effects, we recently developed an inducible myocardium-restricted Rad knockout (cRadKO) mouse [24]. Cardiomyocyte selective Rad deletion was shown to phenocopy β-AR modulated LTCC properties, increasing basal ventricular contractile function [24]. Using this same conditional KO model, we now test the hypothesis that myocardial Rad-knockout will modulate sinus heart rate. Here we show that cRadKO mice exhibit an elevated intrinsic heart rate, and elevated sleep phase heart rate. Mechanistically, Rad regulation of HR appears to be driven by modulated $I_{Ca,L}$ following Rad loss in SANcm. This work reveals Rad – LTCC interactions as a novel target for future therapeutics for symptomatic bradycardia.

4.3 Results

4.3.1 SANcm express Rad

In the cRadKO mouse model cre-recombinase is driven by a myosin heavy chain 6 promoter limiting expression to all cardiomyocytes (reference [185], and personal communication Jeff Molkentin). Following tamoxifen-mediated cre-recombination Rad protein levels are not detected from the whole hearts of cRadKO mice [24], suggesting cardiomyocyte-restricted expression of Rad in the heart. Similarly, single nucleus RNAseq

(snRNAseq) analysis of the mouse SAN showed that RRAD transcript is enriched ~10-fold in SAN cardiomyocytes (SANcm) compared to non-cardiomyocytes from the SAN region [189]. However, the SAN contains a heterogeneous mixture of cardiomyocytes [230]. *To assess Rad expression among SANcm, we re-examined a proteomics and snRNAseq dataset using tissue obtained from a segment of the right atrial wall, containing SAN and surrounding tissue [189]. t-distributed stochastic neighbor embedding (t-SNE) shows 203 (of 5,472) cells analyzed can be classified as SANcm (cardiomyocytes) based on the expression of Myh6, Ctnna3, RyR2, Rbm20, Dmd, Ttn, and Tbx5 [189, 231]. In addition to SANcm, clusters were classified as fibroblasts, epicardial, endocardial, macrophage, adipocyte, and an unidentified cluster [189]. Rad RNA was heterogeneously expressed in the SANcm cluster and enriched in a sub-population of SANcm. (**Figure 4.1A**). Within the SANcm cluster 38% of cells expressed RRAD transcript (77 of 203 cells). Re-analysis of scRNAseq data from van Eif and colleagues [231] also showed RRAD transcript in SANcm (data not shown). Analysis of the available proteomic database also support SAN expression of Rad protein. For context we also re-analyzed data for expression of HCN4, RyR2, and CaV1.2 (**Figure 4.1B**). To examine Rad expression in SANcm in CTRL mice we performed RNA in situ hybridization. HCN4+ cells prominently express Rad (**Figure 4.2, upper panels**). By contrast, cRadKO hearts show dramatically reduced Rad transcript (**Figure 4.2, middle panels**).* Consistent with our previously published study [24] , tamoxifen induction of the floxed-Rad gene results in loss of Rad from cardiomyocytes across the heart. Taken together, these new data suggest that Rad is expressed in SANcm; thus, the loss of Rad might impact SAN function.

4.3.2 L-type calcium current ($I_{Ca,L}$) in SANcm

Cells dispersed from the SAN region of cRadKO were morphologically indistinguishable from those of control mice (**Figure 4.3A**). Cells selected for recording beat spontaneously in physiological salt solution, were spindle shaped (**Figure 4.3A**). Cell capacitance was not different in cells from cRadKO mice (42±4pA/pF, n=17 and 42±4pA/pF, n=21 for CTRL and cRadKO, respectively; **Figure 4.3B**). SANcm from cRadKO mice showed larger current density (**Figure 4.3C**) with the peak of the peak $I_{Ca,L}$ occurring at +5mV for CTRL and 0mV for cRadKO (**Figure 4.3D**). A Boltzmann fit of the I(V) curves yielded maximal LTCC conductance showing a significant increase with Rad loss (4.8+0.8pS/pF, n=17, and 10+1.3pS/pF, n=21, p=0.0015 for CTRL and cRadKO, respectively, **Figure 4.3E**). The midpoint of current activation (V½) was -7.5±1.4mV for CTRL and -10.1±1.4 for cRadKO (**Figure 4.3F**). Steady state inactivation was not different between CTRL and cRadKO $I_{Ca,L}$ (data not shown). There was no significant difference in $I_{Ca,L}$ properties (current density, maximal conductance, or voltage dependence between females and males, **Supplemental Figure 4.8**). These data are consistent with alterations observed in $I_{Ca,L}$ from ventricular cardiomyocytes following Rad ablation [24], suggesting a major contribution of Rad to basal $I_{Ca,L}$ in SANcm.

A growing literature suggests that Rad, and other members of the RGK GTPase subfamily, play critical roles in calcium-channel modulation, serving as constitutive LTCC inhibitors, whose actions are regulated by protein phosphorylation [17, 92, 166]. In agreement with this model, we previously showed that Rad deletion results in ventricular $I_{Ca,L}$ that phenocopies the current in wild-type cardiomyocytes following acute β-AR

activation by isoproterenol (ISO) [24]. We next tested the effect of acute ISO on $I_{Ca,L}$ in SANcm from CTRL and cRadKO hearts. $I_{Ca,L}$ from CTRL SANcm was significantly increased (**Figure 4.4Ai**). Maximal conductance increased (+2.8±0.9pS/pF; **Figure 4.4Bi**) and the midpoint of activation shifted negative (-2.1±0.8mV; **Figure 4.4Ci**). By contrast, $I_{Ca,L}$ in SANcm from cRadKO hearts show no significant increase of conductance (-0.9±1.2pS/pF; **Figure 4.4Bii**) and no effect on activation midpoint (-0.2±0.6mV; **Figure 4.4Cii**). These results are consistent with our earlier findings from cardiac ventricular cardiomyocytes [21, 24], and support the working hypothesis that Rad functions as a key mediator of β-AR modulation of $I_{Ca,L}$.

4.3.3 RAD reduction increases intrinsic heart rate

Rad deletion instills a PKA modulated $I_{Ca,L}$ under otherwise unstimulated conditions in a cell autonomous fashion (**Figure 4.3**) [21, 23, 24]. $I_{Ca,L}$ contributes to the latter phase of the pacemaker depolarization in SANcm [224, 232-234] ; thus, modulated-like $I_{Ca,L}$ arising from Rad silencing predicts an elevated intrinsic SAN heart rate. To examine the effect of Rad loss on HR *in vivo*, $Rad^{fl/fl.MHC}$ mice were implanted with radiotelemetry units. Measurements were made at baseline and 3 weeks after tamoxifen administration to compare the impact of Rad loss on the same mice. *Combined β-AR-block (propranolol) and cholinergic antagonist (atropine) revealed intrinsic HR from ambulatory mice. Induced knockout of cardiomyocyte Rad resulted in a significant elevated intrinsic HR (**Figure 4.5A**). In females, intrinsic HR increased 153+19bpm between baseline and >3 weeks after tamoxifen (483±22bpm and 637±18bpm, for baseline and post-tamoxifen, respectively, **Figure 4.5B**). Male mice also showed significantly elevated*

intrinsic HR after tamoxifen (mean difference 63±12bpm; 502±8bpm and 565±11bpm, for baseline and post-tamoxifen, respectively, ***Figure 4.5C****).*

4.3.4 Rad-deletion effects on HR are greatest when Sympathetic Drive is Relatively Low

The autonomic nervous system (ANS) modulation of heart function is apparent as the diurnal variation of HR. Sympathetic nervous system (SNS) drive is mediated in cardiomyocytes via activation of β-ARs. ***Figure 4.6A*** *shows representative ECG traces during the sleep (day) and active phases (night) along with a 48h continuous recording of the moving average of HR at baseline and after Rad loss (****Figure 4.6B****). Sleep phase HR was significantly elevated with cRadKO (535±15bpm and 593±13bpm, baseline and cRadKO, respectively;* ***Figure 4.6C****) but the active phase HR was not different (652±8 and 671±10, baseline and post-tamoxifen, respectively;* ***Figure 4.6D****). Similar results were obtained for male mice (sleep phase, 511±11bpm and 598±11bpm; active phase, 647±9 and 671±13bpm, baseline and post-tamoxifen, respectively;* ***Figures 4.6E,F****). Diurnal variation remained, but the difference between active and sleeping phase HR diminished after Rad silencing.* Taken together these results are consistent with elevated $I_{Ca,L}$ in cRadKO SANcm driving more rapid sinus rhythm unmasked by reduced SNS drive during the sleep phase.

We observed no evidence of pathological effects on the heart into senescence with the knockout of Rad [22, 24]. Heart rate variability (HRV) reflects ANS input to the heart, and a decrease of HRV is associated with pathologies including progression to heart failure [235]. This coupled with a literature indicating that abnormal calcium homeostasis can

contribute to heart failure progression [236] motivated us to measure HRV. *Cardiac Rad deletion has no effect on HRV in either the active or sleep phases (mean differences before/after tamoxifen 2.2±4ms and 1.5±6ms, for sleep and active phase, respectively;* ***Figure 4.7A,B****).* In our recently published work we noted that despite tonic modulated $I_{Ca,L}$, the heart in cRadKO mice retains responsiveness to acute β-AR stimulation [24] consistent with the function of a healthy heart. To test for retention of autonomic nervous control of HR in cRadKO we measured the acute responses to a rapid air jet puff and exogenous ISO. *The rapid air jet activates the endogenous ANS 'fight or flight' response, whereas exogenous ISO acutely over-rides ANS control of HR. The air jet acutely increased HR +33±23bpm (593±13 to 623±24bpm; p=0.18), and HRV (39±6ms and 68±14ms, before and after air-jet, respectively;* ***Figure 4.7C****) whereas exogenous ISO increased HR +59±10bpm (674+11 to 733±8bpm, p<0.01), and reduced HRV (46±3ms and 18±2ms, for post-tam and ISO, respectively;* ***Figure 4.7D****).* Also, Poincare plots during the sleep and active phases also showed similar patterns in CTRL and cRadKO (**Figures 4.7E,F**).

4.4 Discussion

We showed previously that Rad-deficiency confers a β-AR –modulated phenotype on basal $I_{Ca,L}$ without structural or functional remodeling of the heart [23]. The main findings of this study are that in SANcm, the deletion of Rad results in elevated $I_{Ca,L}$ with properties approximating SNS modulated $I_{Ca,L}$. Second, the absence of Rad elevates intrinsic HR. Third, HR in ambulatory mice is unchanged during the active phase, but is significantly elevated during the sleep/resting phase. Early studies showed that modulated $I_{Ca,L}$ is a major contributor to an increased steepness of the diastolic depolarization of

SANcm [237]. Thus, these results support a key contribution of Rad – LTCC regulation of sinus rhythm in the heart (**Figure 4.9**).

SANcm have relatively low membrane capacitance and high input resistances; consequently, in theory, any relatively small inward cation flux, such as Ca^{2+} current, can accelerate pacemaker depolarizations [234, 238]. The contribution of $I_{Ca,L}$ to sinus rhythm was experimentally validated by demonstration of the slower HR of $Ca_V1.3$ knockout mice [226]. There has been some controversy in the field striving to attribute dominant mechanisms to pace-making. For example, some studies suggested that the sarcoplasmic reticulum Ca^{2+} clock shapes the spontaneous rate, but may not be a dominating factor [239]. Here we now show that $I_{Ca,L}$ modulation by Rad GTPase regulates the intrinsic SAN firing rate. Our findings do not challenge the primacy of the membrane versus Ca^{2+} clock; rather, the interdependence of the membrane and Ca^{2+} clock [224] underscores the critical impact of altered $I_{Ca,L}$ on SANcm autonomous firing. Perhaps most importantly, our work shows that Rad-LTCC regulation is a key molecular signaling node for SNS regulation of sinus rhythm.

4.4.1 Rad is a key contributor to SANcm $I_{Ca,L}$ modulation

SANcm express $I_{Ca,L}$ carried by pore forming $Ca_V1.2$ and $Ca_V1.3$ proteins. $Ca_V1.3$ contributes to pacemaker activity [226] and regulates the calcium clock in nodal cells [221]. $Ca_V1.2$ resides mainly in non-junctional plasma membrane where it is thought to mainly contribute to the membrane clock [240]. Our approaches do not allow us to dissect whether Rad has biased influence on $Ca_V1.2$ or $Ca_V1.3$. Liu et al showed that $Ca_V1.2$ and $Ca_V1.3$ indistinguishably respond to PKA to increase $I_{Ca,L}$ [92]. There are 3 independent

lines of evidence to support the contention that Rad functions in cardiomyocytes to regulate $I_{Ca,L}$ modulation. First, our early studies of global, constitutive Rad-KO mice showed Rad deletion phenocopies acute stimulation of the heart [23], and in this model $I_{Ca,L}$ was modulated at baseline [21]. Second, in the inducible, cardiac-restricted RadKO (cRadKO, as in the present study), ventricular $I_{Ca,L}$ was modulated at baseline [24]. Third, proximity proteomics evaluation in transgenic mice showed that following acute ISO stimulation, Rad association was reduced with LTCC proteins $Ca_V\beta2$ and $Ca_V1.2$ [92]. Taken together with the present findings, we conclude that Rad interacts with LTCC; thus, dynamical regulation by PKA of the LTCC heteromultimeric complex is an important contributor to SNS elevation of HR. In native myocardium the signal for Rad-LTCC rearrangements is likely in response to the β-AR –PKA signaling axis. The Rad knockout model provides an extreme, whereby the absence of Rad would represent a maximally depleted $Ca_V1.2$ microenvironment, relieving any Rad-dependent inhibition with respect to LTCC function.

There is an imperfect correspondence between intrinsic HR and $I_{Ca,L}$ by biological sex in cRadKO (**Supplementary Figure 4.8, Figure 4.3, 4.6**). Intrinsic HR response in cRadKO is greater in females than males, but there is not a significant difference in $I_{Ca,L}$ by sex. This finding raises new questions, principally, 'What male-specific factors contribute to lower intrinsic HR in the absence of Rad?' This doesn't necessarily mean that Rad influences other ion channels or Ca-clock components in a sex-specific manner; rather, this line of reasoning suggests that there are sex-specific intrinsic HR regulatory mechanisms, exclusive of Rad-LTCC signaling. For example, our early work showing Rad – $I_{Ca,L}$ regulation established absence of effects on T-type calcium channel current [17]. Nevertheless, while Rad might directly influence other channels, to date the only known

channel interaction partners with Rad are Cavβ subunits [166] and the C-terminus of the L-type channel [241]. There are a large number of signaling systems that sum to setting intrinsic HR [242] any one of which possibly can be altered in a sex specific fashion. The important conclusion is that regardless of sex, a common effect of Rad-deletion is increase $I_{Ca,L}$ along with intrinsic HR.

4.4.2 Relationship among SANcm heterogeneity, Rad expression, and SAN function

In rabbits, peripheral pieces of SAN tissue from regions bordering the crista terminalis have faster firing rates than the central pacemaker site, and pieces bordering the left atrium were quiescent [243]. The leading pacemaker site is not, however, a fixed location. During autonomic nervous system signaling different firing rates are driven by different cells in the SAN[244] and depending on external stimuli subsidiary areas can be activated [245]. Cell-cell coupling creates complex behavior [246]. For this reason, it is important to interpret cellular studies in context of tissue-level, or as in the present case *in vivo* studies of SAN function. Our finding that 38% of SANcm express enriched Rad transcript suggests an additional, new mechanism of heterogeneity that should be tested in future studies. It follows that the SANcm sub-types that do not express Rad may not possess adaptability to speed heart rate via a modulated $I_{Ca,L}$ mechanism, or that other RGK GTPases may play yet to be investigated regulatory roles. Conversely, Rad-expressing SANcm theoretically have the ability to increase rate and shape the ultimate overall SAN rate because the fastest firing SANcm should determine rate, which is consistent with the elevated HR in cRadKO mice. Future studies employing sophisticated in situ single cell

mapping might help resolve whether Rad-$I_{Ca,L}$ contributes to anatomical pacemaker shifts during sympathetic nervous system activation.

Modifiers of sinus rhythm may extend beyond regulation of HR per se, to secondary impacts on heart failure evidenced as promising effects of ivabradine in heart failure patients [247]. Moreover, β-AR blockers have been employed as a first line of HF treatment [248]. In the present study we show Rad reduction increases HR, and we previously showed Rad reduction increases cardiac inotropy without pathological consequences [21-24]. Thus, the suggestion that Rad knockout provides beneficial effects in the setting of HF is paradoxical to HR slowing effects of ivabradine and β-AR blockers; however, Rad reduction would directly treat loss of cardiac inotropy in failing heart, and thus we maintain is worthy of further study.

4.4.3 Diurnal impact and ANS drive with Rad reduction

Rad deletion elevates intrinsic HR consistent with the SANcm origin of the increased sinus rhythm. ANS net input is the sum of SNS drive and parasympathetic input, and the level of ANS drive is regulated by the baroreflex. With elevated HR, hence elevated cardiac output in cRadKO, it follows there should be compensatory reduced SNS drive. More direct measures of sympathetic nerve activity and circulating catecholamines are necessary to examine this issue, yet are highly invasive and can be difficult to interpret secondary to agitation of animals. For example, blood cannot be drawn from conscious mice without provoking a fight or flight response. Anesthesia can be used, but dramatically depresses measurements of circulating catecholamines (for example, compare [249] to [250]). To summarize, our data support the notion that we are not ‘knocking-out’ SNS input to the

cRadKO heart, rather we suggest that modulated $I_{Ca,L}$ in cRadKO dominant pacemaker cell may usurp the reflexive requirement for added SNS to balance net autonomic drive. In this way, Rad reduction strategies might aid aging related [251, 252] symptomatic bradycardia which has been attributed to depressed SANcm excitability, possibly secondary to declines of $Ca_V1.2$ protein [225].

4.5 Limitations

Heterogeneity of function at the cellular level is not fully explored here. We did not measure spontaneous AP nor spontaneous firing frequencies. Many of the dispersed SAN cells displayed irregular automatic beating or quiescence. A range of spontaneous activity from fast, regular activity to irregular to quiescence has been noted in dispersed SANcm [253]. Heterogeneity among SANcm is also demonstrated in single nucleus[189] and tbx3+ cell-sorted transcriptomics studies [231]. It is also possible that differential dispersed cell activity might arise from differential cellular damage artifact during enzymatic dispersal. We also did not consider Rad-deletion effects on non-LTCC targets. I_f is a major contributor to sinus heart rate [215, 218, 219], and while there is no evidence for Rad interactions in the cardiomyocyte beyond protein interactions of with LTCC-component proteins, we cannot completely rule out other interactions with Rad. Studies here are limited to the mouse. In future studies it will be important to test the impact of Rad reduction on human or other large mammalian SANcm retained in *ex vivo* tissue preparations.

4.6 Conclusions

In summary, we have demonstrated that $I_{Ca,L}$ contributes to sinus rate by a mechanism including Rad-regulated control of LTCC [24, 92]. We previously showed that Rad- ablation promotes a beneficial elevation in Ca^{2+} dynamics, stimulating heart ventricular function [23], albeit without any apparent pathological consequence [24]. Taken together, Rad reduction within all cardiomyocyte types is a powerful potential therapeutic approach for increasing cardiac output as it simultaneously increases HR and stroke volume. Future novel therapeutics for symptomatic bradycardia targeting Rad – LTCC may elevate HR while retaining βAR responsiveness.

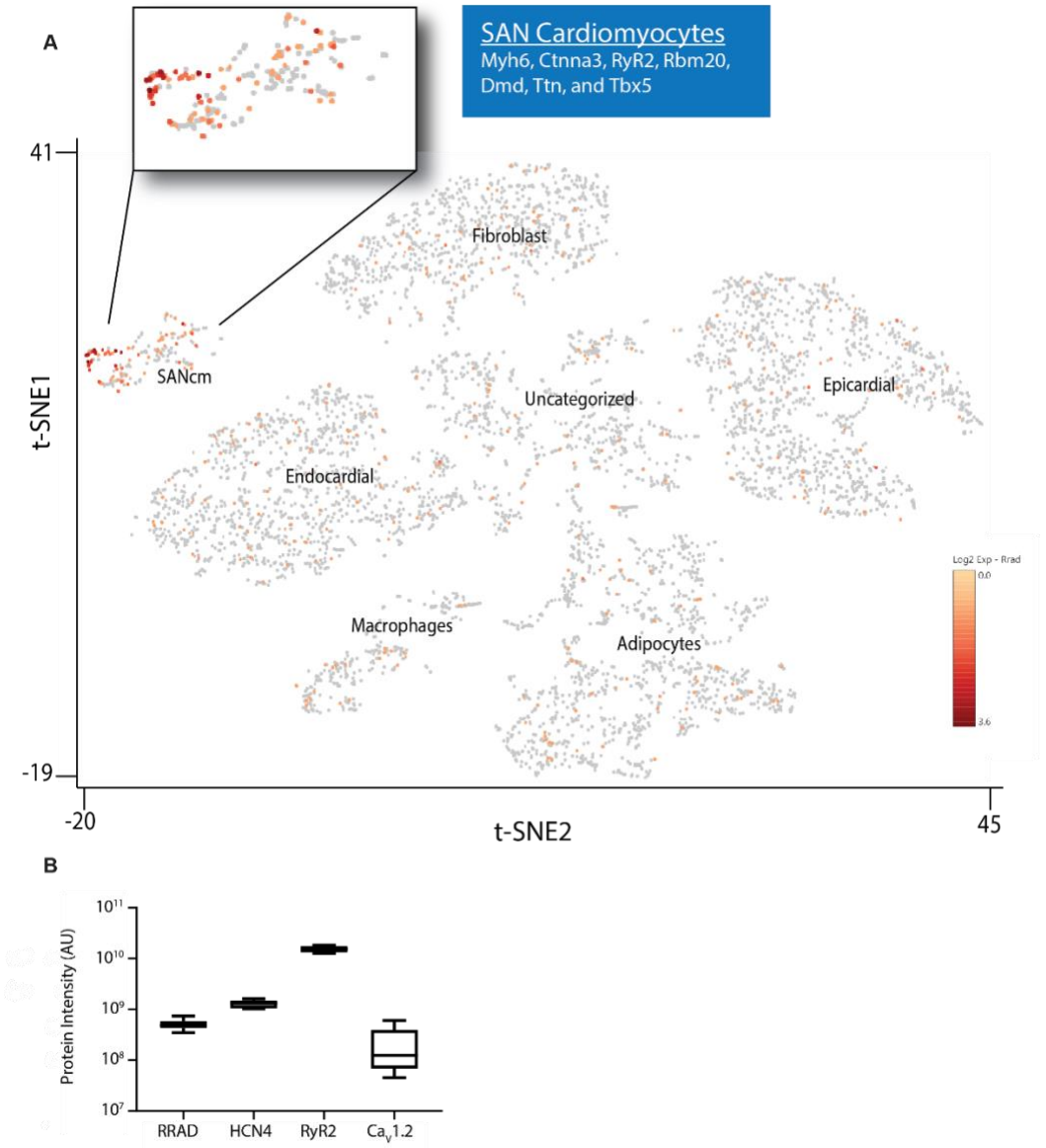

Figure 4.1 RRAD is expressed in SANcm.

A) Two-dimensional t-SNE (Stochastic Neighbor Embedding) plot outlines the major populations of the sinus node. Analysis of database from Linscheid et al. 2019. Each point represents a single nucleus. Cell populations are colored according to intensity of RRad expression, with an expanded view of the SANcm. **B)** Quantification of data mined from Linscheid et al. 2019, of the expression of Rad protein in relation to other proteins known to be expressed specifically in SANcm (HCN4) and cardiomyocytes in general (RyR2 and Cav1.2)**.**

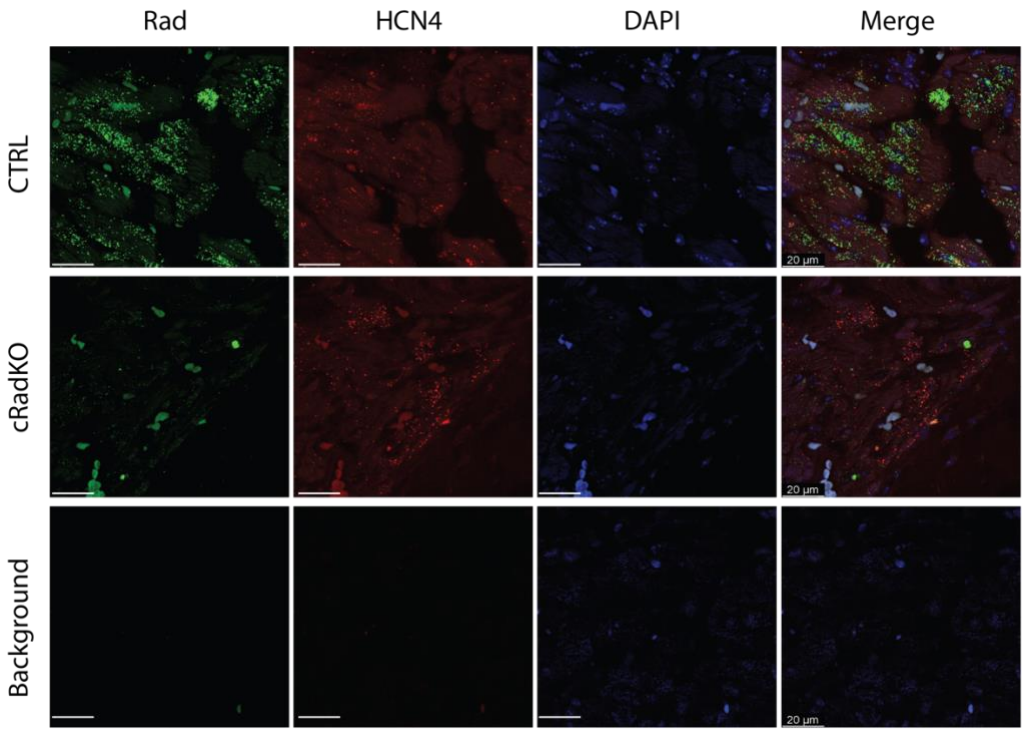

Figure 4.2 RAD is expressed in SANcm.

Representative images of single-molecule fluorescence in situ hybridization against Rad (green) and HCN4 (red) in CTRL (top images) and cRadKO (middle images) in SANcm. Lower panel, probe for bacterium DapB gene serves as a background control (bottom images). Heart tissue was collected >2 weeks after tamoxifen treatment. Tissue samples were stained with DAPI (blue). Images of channels merged displayed on the right. Representative of 3 CTRL and 3 cRadKO hearts. Scale bar: 20 mm.

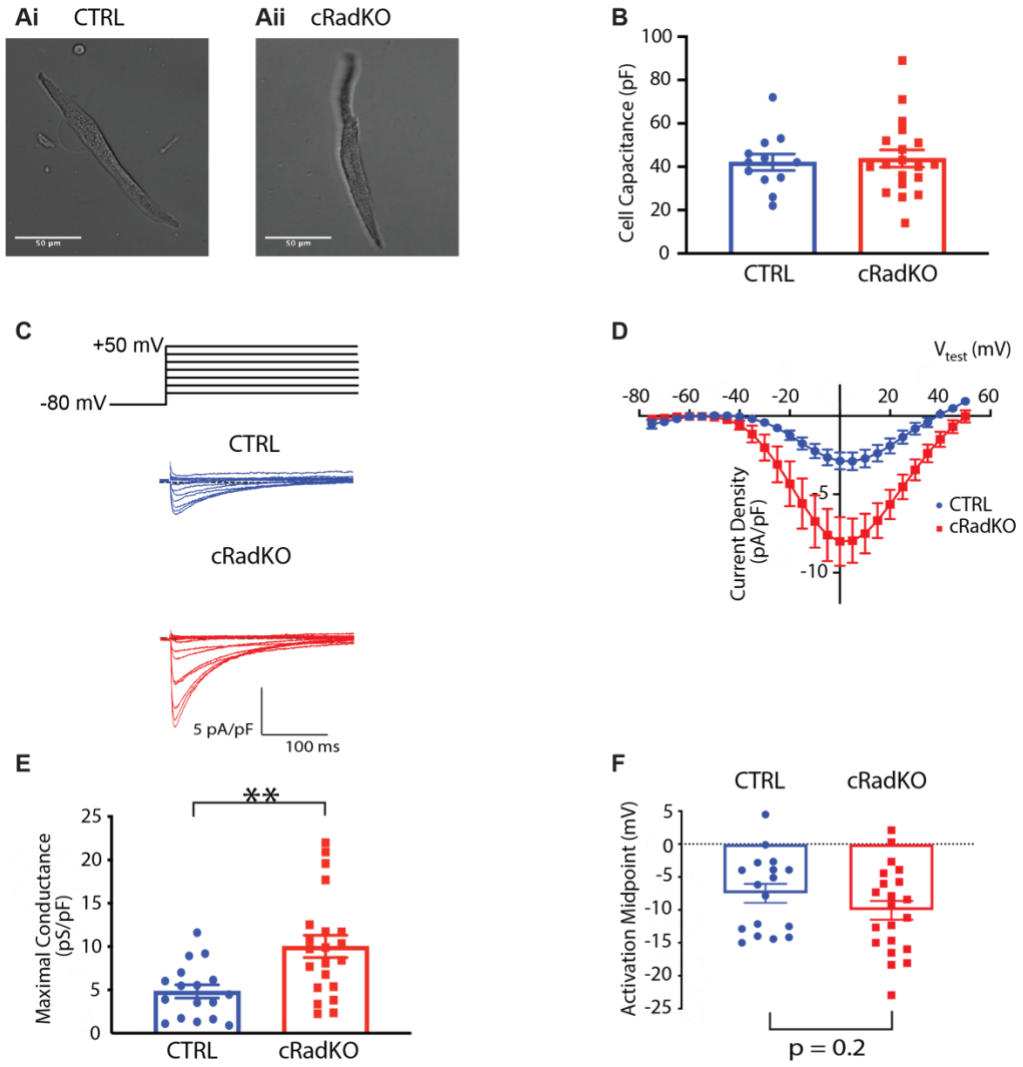

Figure 4.3 Rad reduction increases SANcm $I_{Ca,L}$.

A) Representative photomicrographs of SANcm selected for patching studies from CTRL **(Ai)** and cRadKO **(Aii)** hearts. **B)** Cell capacitance is not significantly different (p = 0.77). **C)** Family of $I_{Ca,L}$ for CTRL (blue) and cRadKO (red). Scale bars: 5 pA/pF, 100 ms**. D)** Current-voltage relationship for peak $I_{Ca,L}$ from CTRL and cRadKO SANcm. **E)** Maximal conductance is significantly increased (**p < 0.01) and **F)** activation midpoint trends toward a negative shift with Rad deletion (p=0.2). N = 8, n = 17 for CTRL; N = 9, n = 21 for cRadKO**.**

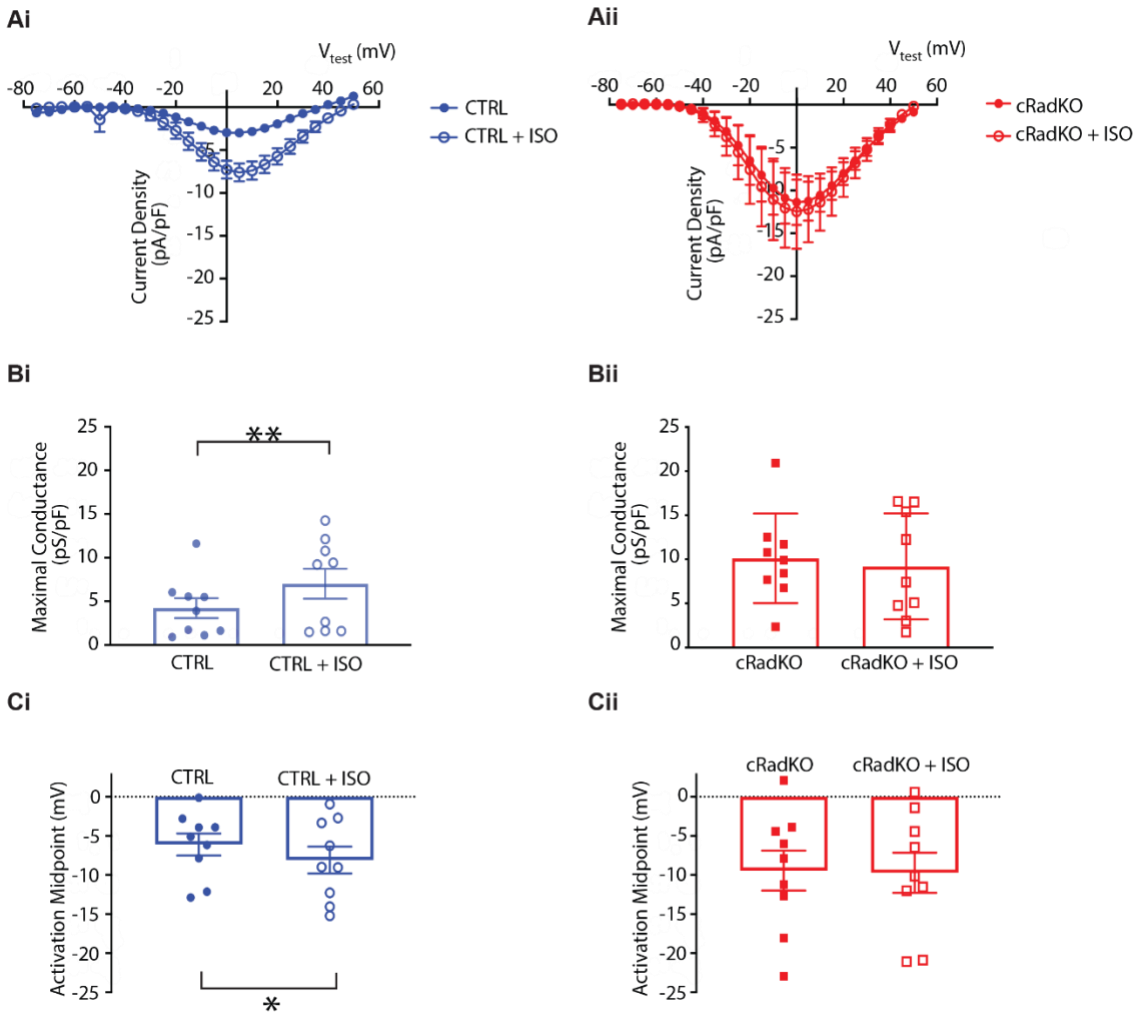

Figure 4.4 β-AR stimulation has no significant effect on cRadKO SANcm ICa,L.

A) Current-voltage relationships for CTRL **(Ai)** and cRadKO **(Aii)** for basal (closed symbols) and after 100 nM ISO (open symbols). **B)** Maximal conductance before and ISO for CTRL (**Bi,** **p =0.01) and cRadKO (**Bii,** p = 0.45). **C)** Activation midpoint before and ISO for CTRL (**Ci**, *p =0.05) and cRadKO (**Cii,** p = 0.68). N = 5, n = 9 for CTRL; N = 4, n = 9 for cRadKO.

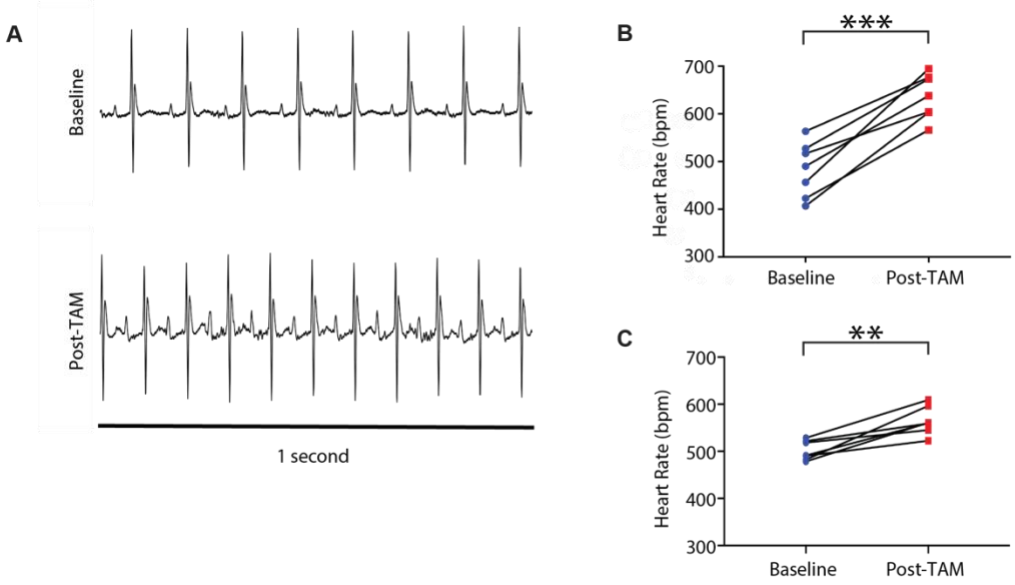

Figure 4.5 Intrinsic heart rate increases after Rad deletion.

A) Representative ECG signals during the sleep phase demonstrate an increase in intrinsic heart rate after tamoxifen treatment. **B,C)** Heart rate increases after tamoxifen treatment in **B)** females (***$p < 10^{-3}$, N=7 mice) and in **C)** males (**$p = 0.002$, N=7 mice).

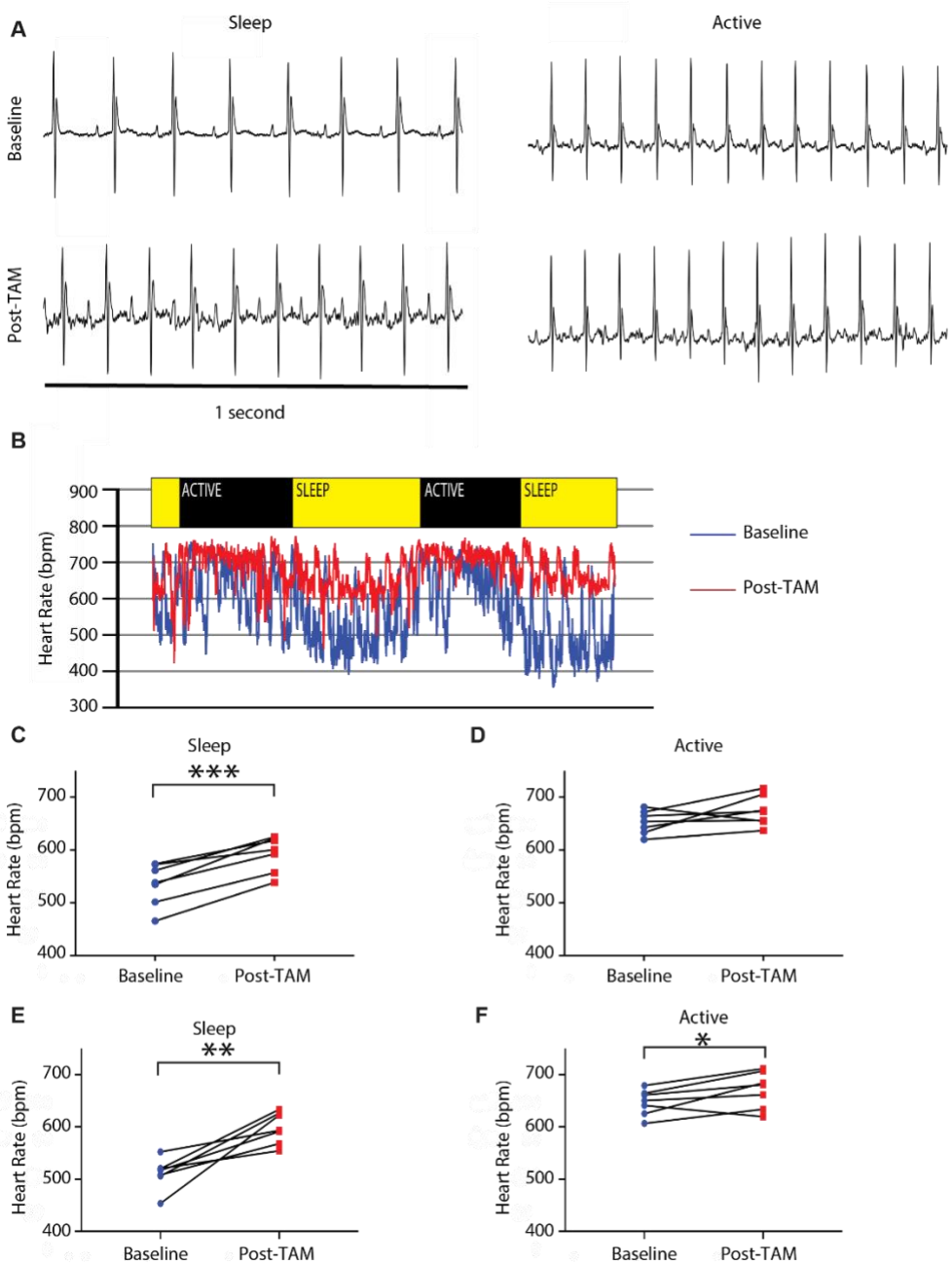

Figure 4.6 Rad deletion increases heart rate in the sleep phase.

A) Representative ECG signals demonstrate an increase in heart rate during sleep after tamoxifen treatment, but no change while active. **B)** Continuous recording of heart rate over 48 hours, before (Baseline) and after tamoxifen treatment (Post-TAM). **C)** Heart rate in the sleep phase increases after tamoxifen treatment in females (***$p < 10^{-3}$, N = 7 mice). **D)** No significant difference in heart rate during the active phase after tamoxifen treatment in females (p = 0.13). **E)** Heart rate during the sleep phase increases after tamoxifen treatment in males (**p = 0.0003, N = 7 mice). **F)** Heart rate in the active phase increases after tamoxifen treatment in males (*p = 0.05).

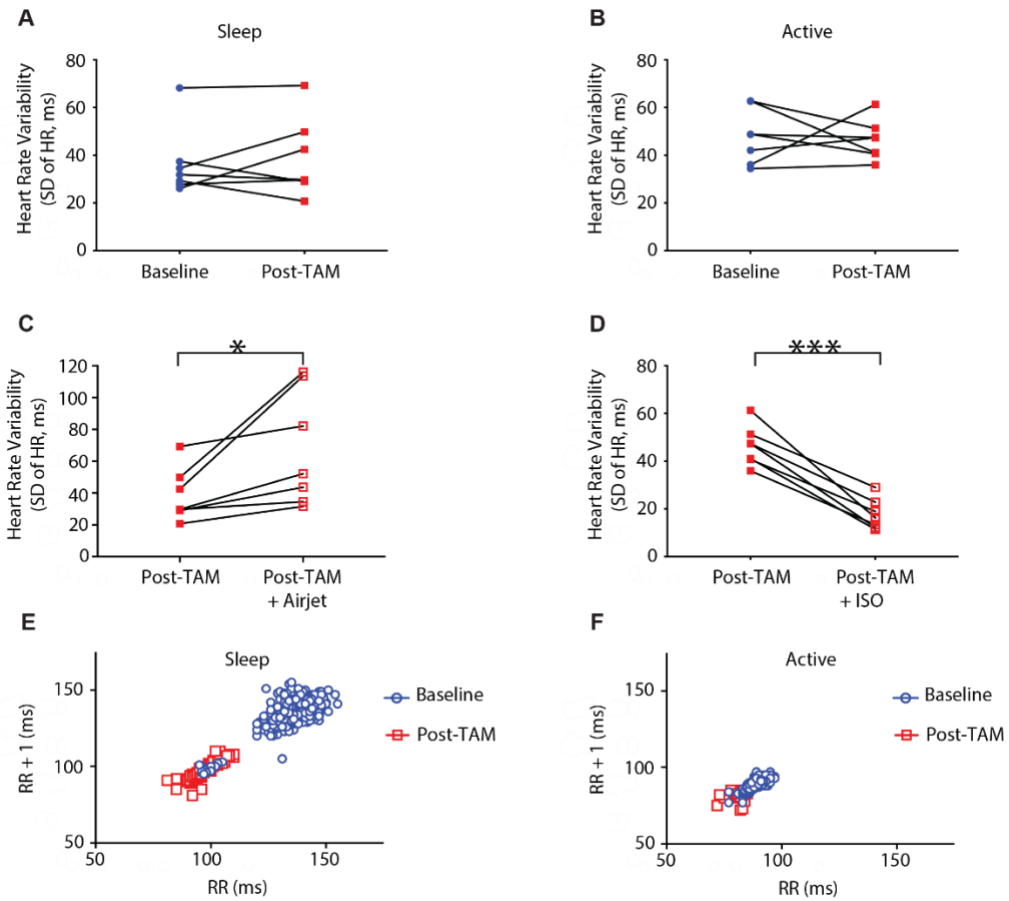

Figure 4.7 Rad deletion demonstrates preserved Heart Rate Variability (HRV).

A) HRV is not significantly different after tamoxifen treatment in the sleep phase ($p = 0.59$), or **B)** in the active phase ($p = 0.80$). **C)** HRV increases in Post-TAM after exposed to an airjet (*$p = 0.03$). **D)** HRV increases Post-TAM after an injection of isoproterenol (***$p < 10^{-3}$, N = 7 mice). **E), F)** Poincare plots in which the RR interval is plotted against the subsequent RR interval (RR + 1) in a representative mouse during the sleep phase **E)** and during the active phase **F).**

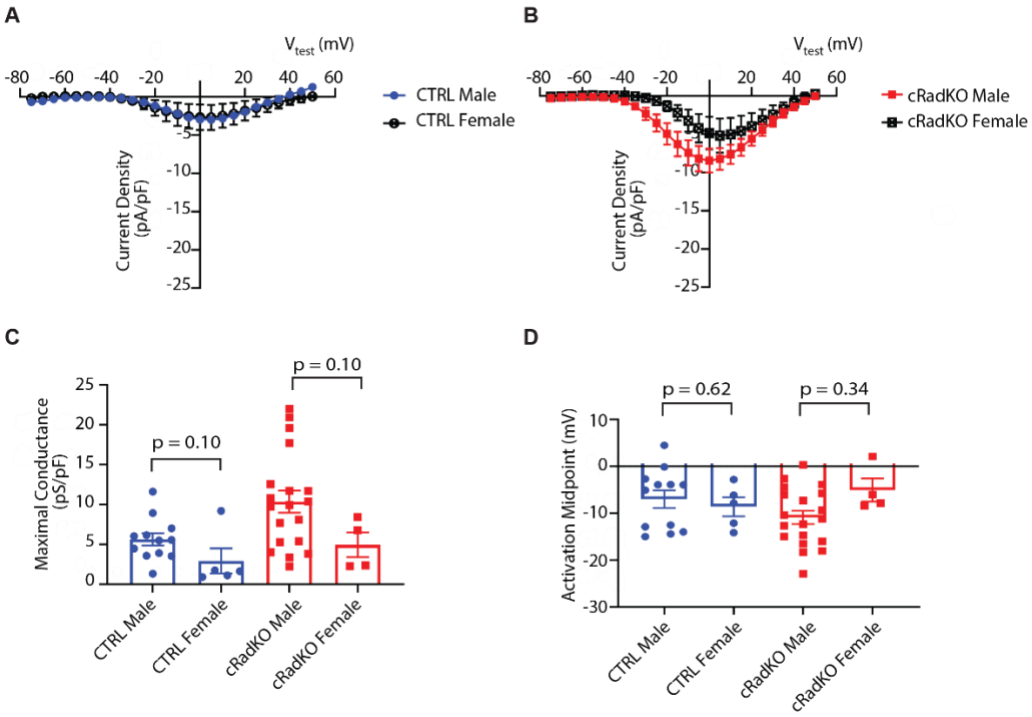

Supplemental Figure 4.8 No significant difference between males and females of $I_{Ca,L}$ in CTRL and cRadKO.

A) Current-voltage relationship for peak $I_{Ca,L}$ from CTRL males (blue circles) and females (black circles). **B)** Current-voltage relationship for peak $I_{Ca,L}$ from cRadKO males (red squares) and females (black squares). **C)** Maximal conductance for CTRL (males and females, p = 0.10) and cRadKO (males and females, p = 0.10). **D)** Activation for CTRL (males and females, p = 0.62) and cRadKO (males and females, p = 0.34). CTRL: Males: N = 6 mice, n = 12 cells; Females: N = 2 mice, n = 5 cells. cRadKO: Males: N = 8 mice, n = 19 cells; Females: N = 2 mice, n = 7 cells.

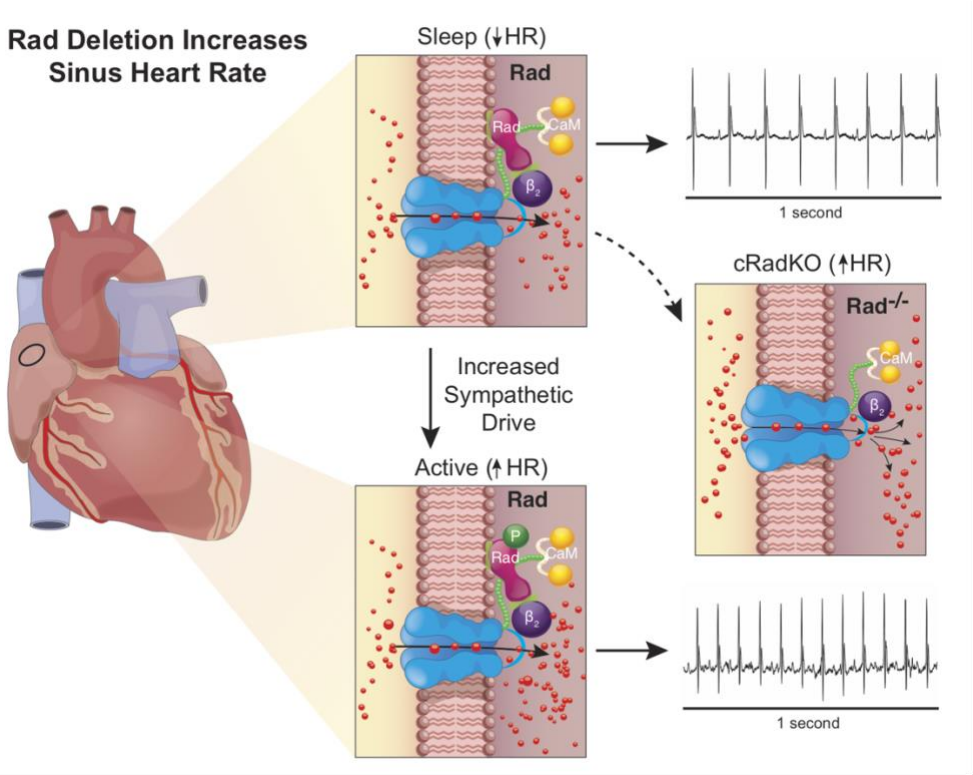

Figure 4.9 Rad Deletion Increases Sinus Heart Rate.
Rad deletion in sinoatrial cardioyocytes increases $I_{Ca,L}$ and increases heart rate consistent with β-adrenergic receptor modulated $I_{Ca,L}$ regulation. Heart rate during the sleep cycle is selectively elevated by Rad deletion. Rad-LTCC association may be a useful target for future therapeutics to treat symptomatic bradycardia.

CHAPTER 5. ENHANCED INACTIVATION BALANCES INCREASED PEAK L-TYPE CALCIUM CURRENT IN THE ABSENCE OF RAD

5.1 Preface

The work of chapter 5 has been submitted for review . The entirety of the paper is presented. The results and methods attributed to others are presented for clarity and flow are *italicized*. The figure numbering of the chapter has been edited from the submitted work for consistency within the dissertation.

5.2 Introduction

The L-type calcium channel (LTCC) is a heteromultimeric protein complex that governs the entry of calcium necessary to initiate a contraction, and the LTCC contributes to the cardiac action potential (AP) plateau phase [64]. Cardiomyocyte LTCC activity is tightly regulated to prevent calcium overload [254] and after-depolarizations of the AP [124, 125]. Decay kinetics of $I_{Ca,L}$ is a key point of control. Inactivation of the LTCC occurs by two distinct mechanisms: calcium dependent inactivation (CDI) and voltage dependent inactivation (VDI) [64, 65]. The early peak of L-type calcium current ($I_{Ca,L}$) triggers calcium induced calcium release (CICR) from the sarcoplasmic reticulum (SR) that is essential for excitation contraction coupling; calcium released from the SR, or entering through the channel itself, binds to calmodulin (CaM) prebound to the EF hand of the carboxyl-terminus of the main pore-forming subunit of the LTCC [255]. Ca^{2+}-CaM complexed within the LTCC causes a conformational change to induce CDI [68-71]. In addition, $I_{Ca,L}$ decay occurs by voltage dependent inactivation contemporaneously with the plateau phase of the AP [60, 74-76]. Under basal conditions, the decay of $I_{Ca,L}$ demonstrates

non-exponential decay with relatively early, fast and late, slow components [50, 61-63]. It is generally accepted that CDI contributes to the early, fast component and the late, slow component is dominated by VDI [60, 66]. Other studies claim that VDI contributes to both components but is dampened when calcium influx increases [60, 74-76].

The regulation of LTCC decay becomes particularly critical when the channel is modulated upon β-adrenergic receptor (β-AR) stimulation. During the fight-or-flight response, $I_{Ca,L}$ amplitude increases, voltage dependence of activation shifts to more negative potentials, and inactivation rates accelerate [60, 66, 256, 257]. Regulation of the LTCC by β-adrenergic receptor (β-AR) stimulation has been thoroughly investigated, yet complete understanding remains elusive, especially in regards to how inactivation is accelerated. Many studies claim that CDI is the major contributor to $I_{Ca,L}$ decay under modulated conditions because elevated calcium influx leads to more calcium interaction with CaM [60, 66]; however, increased $I_{Ca,L}$ due to overexpression of α1C, the pore-forming subunit of the LTCC, or of Ca_Vβ2a did not alter decay kinetics compared to the controls [12, 149]. Others argue that inactivation is accelerated due to interactions of the N-terminus and C-terminus with each other or other proteins [258-260]. Because β-adrenergic receptor (β-AR) stimulation initiates multiple molecular mechanisms, it is difficult to assess the main contributors to LTCC regulation [31].

In recent studies, Rad has emerged as a major contributor to LTCC modulation [23, 24, 92]. Rad is a member of the RGK subfamily of Ras-related small GTPases [166], and shares the common RGK protein property of profoundly inhibiting Ca_V1/ Ca_V2 channel activity. Overexpression of Rad in heterologous expression systems potently inhibits $I_{Ca,L}$ in adult and embryonic ventricular myocytes [16-20]. *In vivo*, Rad deficiency promotes

positive inotropy and is a critical determinant of current amplitude [24] and modulation [23, 92]. Our recent work showed that the absence of Rad from the channel complex results in increased LTCC activity that mirrors β-AR modulated $I_{Ca,L}$ and accelerates $I_{Ca,L}$ decay [21-24]. These findings were definitively supported utilizing proximity biotinylation to show that under conditions of β-AR stimulation, protein kinase A-mediated Rad phosphorylation alleviated constitutive inhibition caused by Rad association with the LTCC [92].

If Rad loss from the LTCC complex is essential for β-AR modulation of $I_{Ca,L}$, then the absence of Rad in myocardium could serve as a novel tool to investigate LTCC regulation under modulated conditions without interfering contributions of other signaling pathways normally activated under β-AR stimulation. Using a cardiomyocyte-restricted Rad deletion mouse model, we re-visit the hypothesis that modulation of the LTCC by β-AR stimulation is governed by the presence of Rad in the $Ca_V1.2$ macromolecular complex. Mechanistically, the absence of Rad yields increased inactivation to offset the increase in peak $I_{Ca,L}$. Here, we show that CDI and VDI are both accelerated in the absence of Rad. The combination of greater peak and accelerated kinetics conspires to prevent significant changes to action potential duration or QT interval, despite large peak $I_{Ca,L}$. The preservation of Rad knockout-instilled $I_{Ca,L}$ modulation in the absence of β-AR expression; thus showing that Rad imparts channel complex modulation independent of β-AR signaling. This work suggests Rad-LTCC interactions may be a novel target for future therapeutics to confer systolic advantage.

5.3 Results

5.3.1 cRadKO mirrors modulated LTCC

$I_{Ca,L}$ decay consists of an early, fast component and a late, slow component [50, 61-63, 65]. CDI is the dominant mechanism of inactivation of the fast component and under conditions of β-adrenergic stimulation [61, 68, 71, 74]; this idea, coupled with the emergent model that phosphorylated Rad is re-oriented from the LTCC during β-adrenergic stimulation to drive $I_{Ca,L}$ modulation [21, 23, 24, 92], predicts that Rad-deletion (in the basal state) should yield $I_{Ca,L}$ properties that are not different from wild-type (CTRL) following β-adrenergic modulation. We therefore compared the kinetics of $I_{Ca,L}$ in cardiomyocytes from CTRL after the addition of isoproterenol with basal $I_{Ca,L}$ in cardiomyocytes from cRadKO (**Figure 5.1**). For brevity, we will henceforth refer to CTRL $I_{Ca,L}$ and cRadKO $I_{Ca,L}$ as a stand-in for $I_{Ca,L}$ from CTRL or cRadKO ventricular cardiomyocytes. EGTA was used to allow a readout of the influence on global Ca^{2+}. $I_{Ca,L}$ traces from cRadKO and ISO-stimulated CTRL normalized to peak current demonstrates that basal cRadKO $I_{Ca,L}$ decay is not different from modulated CTRL (**Figure 5.1A**). Remaining early current (r_{30}) was not different between modulated CTRL $I_{Ca,L}$ and cRadKO $I_{Ca,L}$ **(Figure 5.1B; Supplemental Figure 5.10A** for 2-way ANOVA tabular results); similarly, there was no difference in the late component (r_{150}) [50, 63, 261, 262], at individual voltage steps (**Figure 5.1C, Supplemental Figure 5.10B** for 2-way ANOVA tabular results). cRadKO displayed larger current density at r_{30} (**Figure 5.1E**) and r_{150} (**Figure 5.1F**) compared to CTRL. Taken together, these results demonstrate that the kinetic signature of basal cRadKO approximates modulated $I_{Ca,L}$ kinetics.

5.3.2 Increased Ca^{2+} and Rad both contribute to CDI

If CDI is the dominant mechanism when the LTCC is modulated, then the source of calcium contributing to CDI could emanate from the sarcoplasmic reticulum, or from local calcium entering through the channel itself [263]. To evaluate global versus local Ca^{2+}, we investigated $I_{Ca,L}$ decay kinetics in the presence of either EGTA or BAPTA. These calcium buffers have similar steady-state binding affinities for calcium, but differ in binding rate constants [264]. EGTA buffers slower than BAPTA and allows investigation of the influence of global calcium on CDI; by contrast, the use of BAPTA limits CDI to local sources, mainly Ca^{2+} fluxing in the nanodomain of the channel [264, 265].

Figure 5.2 summarizes the analysis of r_{30} between cRadKO $I_{Ca,L}$ and CTRL $I_{Ca,L}$ under conditions reporting global Ca^{2+} (EGTA used as calcium buffer). Traces from cRadKO and CTRL $I_{Ca,L}$ demonstrate that cRadKO $I_{Ca,L}$ fast decay is greater than that for CTRL (**Figure 5.2A**). Across multiple voltage steps, there is less r_{30} in cRadKO $I_{Ca,L}$ than in CTRL $I_{Ca,L}$ (**Figure 5.2B, Supplemental Figure 5.10C** for 2-way ANOVA tabular results). Current density was larger in cRadKO compared to CTRL (**Figure 5.2C**). To assess whether remaining current depended on elevated current density, we plotted r_{30} as a function of current density (**Figure 5.2D**). CTRL trends towards a negative slope meaning that as current density increases, there is less remaining current, as expected for early, fast inactivation by CDI [60]. In contrast, cRadKO has a positive slope; as current density increases, there is more remaining current. This finding suggests a Ca^{2+}-independent contribution to the early, fast component of decay in a Rad-less LTCC.

We next assessed r_{30} in the presence of BAPTA to limit the pool of calcium local to the channel complex [264, 265] (**Figure 5.3**). Representative traces reveal an apparent smaller difference in decay between cRadKO and CTRL (**Figure 5.3A**). r30 across individual test potentials demonstrates no significant difference between cRadKO and CTRL $I_{Ca,L}$ (**Figure 5.3B, Supplemental Figure 5.10D** for 2-way ANOVA tabular results). In the presence of BAPTA, cRadKO maintains a larger current density compared to CTRL (**Figure 5.3C**). Local buffering by BAPTA eliminates the negative correlation of r30 with current density for CTRL $I_{Ca,L}$; however, the positive correlation of cRadKO r30 and current density remains in the presence of BAPTA (**Figure 5.3D, compare with Figure 5.2D**). Taken together these results suggest that the early, fast decay of $I_{Ca,L}$ in cRadKO is driven in part by SR released calcium, and in part by a Ca^{2+}-independent mechanism.

5.3.3 Rad does not alter the late component of LTCC decay

Late $I_{Ca,L}$ contributes to repolarization and SR calcium loading [50]; impaired inactivation of the late phase can result in AP duration prolongation and EADs [50, 61-63, 262]. We therefore analyzed $I_{Ca,L}$ r_{150} in cRadKO and CTRL in the presence of EGTA. Representative traces demonstrate no difference between cRadKO and CTRL $I_{Ca,L}$ (**Figure 5.2A, superimposed star**). There was no difference in r_{150} between the models at multiple test potentials (**Figure 5.4A, Supplemental Figure 5.10E** for 2-way ANOVA tabular results) but the interaction between voltage and CTRL versus cRadKO was significantly different, as shown by the crosses in **Figure 5.4A.** cRadKO, in comparison to CTRL, has larger current density at r_{150} (**Figure 5.4B**). A positive correlation is seen in both cRadKO

and CTRL when r_{150} is displayed as a function of current density (**Figure 5.4C**). In the presence of BAPTA, there was no difference in r_{150} (**see Figure 5.3A, superimposed star; Figure 5.4D, Supplemental Figure 5.10F** for 2-way ANOVA tabular results). Current density was not different for cRadKO compared to CTRL $I_{Ca,L}$ (**Figure 5.4E**). r_{150} plotted against current density demonstrated a positive correlation in both cRadKO and CTRL (**Figure 5.4F**). These data show that Rad deletion does not promote alterations to late $I_{Ca,L}$ kinetics.

The late, slow component of $I_{Ca,L}$ decay is thought to be dominated by voltage dependent inactivation (VDI) [60, 66, 74]. We therefore measured VDI in cRadKO by using barium as the charge carrier (**Figure 5.5**). Representative traces demonstrate faster decay in cRadKO compared to CTRL both at r_{30} and r_{150} (**Figure 5.5A**). There was less r_{30} in cRadKO (**Figure 5.5B,D; Supplemental Figure 5.11A** for 2-way ANOVA tabular results for B). At r_{150}, remaining current in cRadKO was not significantly less compared to CTRL (**Figure 5.5C,E; Supplemental Figure 5.11B** for 2-way ANOVA tabular results for C). A positive correlation is seen in cRadKO when either r_{30} or r_{150} are plotted as a function of current density (**Figure 5.5F,G**). This data, in concert with the regression plots from **Figures 5.2 and 5.3,** show that the absence of Rad enhances VDI. This suggests the presence of Rad contributes to dampening VDI.

5.3.4 Faster kinetics in cRadKO prevent alterations in cardiac electrophysiology

$I_{Ca,L}$ plays a critical role in regulating cardiac action potential duration; slight alterations to current density or inactivation of the LTCC can lead to electrical dysfunction, such as action potential prolongation, early after depolarizations, and

prolonged QT intervals [50, 61-63, 131, 132, 262]; Sympathetic stimulation via the β-AR signaling axis modulates trigger calcium, and shortens action potential duration [266]. Studies have shown that female mice exhibit prolonged action potential repolarization and longer QT intervals [267], making females more sensitive to reveal if Rad deletion has an effect on action potential duration and QT interval. We therefore measured action potentials from isolated ventricular cardiomyocytes, and used surface electrocardiogram (ECG) recordings to assess QT interval in female mice. Action potentials (AP) measured at 1 Hz from CTRL ventricular cardiomyocytes showed a pronounced inflection point positive to 0 mV (**Figure 5.6A, arrow**), rapid repolarization, and a slower repolarization phase negative to -50 mV (**Figure 5.6A**). cRadKO APs (**Figure 5.6A, red line**) demonstrated similar morphology to CTRL at baseline (**Figure 6A, blue line**) and after addition of isoproterenol [268] (**Figure 5.6B; cRadKO: black line, CTRL: green line).** Baseline AP amplitudes were not significantly different between models (**Figure 5.6C;** cRadKO: 127.4±1.0 mV, CTRL: 123.0±3.3 mV;). Comparing baseline action potential duration at 50% repolarization (APD_{50}) and at 80% repolarization (APD_{80}) demonstrates no significant difference between cRadKO and CTRL (**Figure 5.6D**: cRadKO: 6.5±0.98 ms, CTRL: 6.2±0.58 ms). At 80% repolarization (APD_{80}), cRadKO demonstrates faster repolarization than CTRL (**Figure 5.6E**, cRadKO: 17.1±1.5 ms, CTRL: 21.2±1.1 ms). CTRL action potential amplitude was not significantly different from cRadKO after ISO (**Figure 5.6F**). cRadKO APD_{50} was slightly shorter compared to baseline, but not significantly different from CTRL (**Figure 5.6G**; APD_{50} after ISO: cRadKO: 6.4±1.2 ms, CTRL: 6.0±0.71 ms). CTRL was longer at APD_{80} compared to baseline, but not

significantly different from cRadKO (**Figure 5.6H**; APD_{80} after ISO: cRadKO: 18.0±1.8 ms, CTRL: 23.4±2.0 ms**)**.

We next assessed *in vivo* electrical function. The increase in heart rate in response to sympathetic stimulation is the result of integrative mechanisms in both branches of the autonomic nervous system (ANS) [266], which could obscure a potential effect on QT interval due to a selective increase in $I_{Ca,L}$ in the absence of Rad. *We therefore measured the ECG under ANS block by treating the mice with atropine and propranolol* [269]. Baseline ECG measurements demonstrated no significant difference in QT or QTc (**Supplement Figure 5.12**). After administration of atropine and propranolol, representative surface ECG traces showed no apparent differences between CTRL and cRadKO (**Figure 5.6I**). Raw QT interval (**Figure 5.6J;** cRadKO: 40±6 ms, CTRL: 50±7 ms; p=0.35) and corrected QT interval (QTc) demonstrated no significant difference (**Figure 5.6K;** cRadKO: 33±5 ms, CTRL: 40±5 ms; p=0.41). This data, combined with the action potential measurements, support the idea that the faster kinetics balance the increase in peak $I_{Ca,L}$, thereby preventing significant alterations in cardiac electrophysiology.

5.3.5 cRadKO yields modulated kinetics of LTCC downstream of β-AR signaling

β_1-AR activation mediates positive chronotropic and inotropic responses of cardiomyocytes, and β_2-AR is thought to contribute to these processes more locally within cardiomyocytes [270]. To determine whether these receptors were contributing to the modulation effect of $I_{Ca,L}$ seen in cRadKO, we bred $RAD^{fl/fl\text{-}MHC\text{-}MCM}$ onto a β_1,β_2-AR

double knockout mouse [271] (dKO) to create an induced $RAD^{\Delta/\Delta}$,β_1,β_2-AR triple knock out mouse (tKO) after administration of tamoxifen. *Analysis of cardiac function through echocardiography demonstrated that ejection fraction was significantly different between CTRL and dKO after acute isoproterenol, demonstrating that β_1,β_2-AR response was disrupted (**Supplement Figure 5.12A;** CTRL: 93±1%, dKO: 60±3%; p<0.0001; data for CTRL+ISO echocardiography taken from our previously published dataset [24]; **Supplement Figure 5.13A**)*. Disruption of Rad expression in the heart in tKO was confirmed by qRT-PCR (**Supplement Figure 5.13B**). After the deletion of Rad, ejection fraction significantly increased in the tKO compared to dKO (**Figure 5.7A,B;** tKO: 72±2%, dKO: 51±4%; p<0.0001). Left ventricular inner dimensions decreased in the tKO (**Figure 5.7C;** tKO: 3.6±0.1 mm, dKO: 4.2±0.1 mm; p=0.003) without significant changes in the anterior or posterior walls (**Figure 5.7D,E;** For F: tKO: 0.88±0.1 mm, dKO: 0.80±0.1 mm; p=0.43; For G: tKO: 0.86±0.05 mm, dKO: 0.82±0.1 mm; p=0.52). Surface ECG showed no significant difference in raw QT interval (**Figure 5.7F,G;** tKO 39±4 ms, dKO 30±6 ms; p=0.19), corrected QT interval (QTc) (**Figure 5.7H;** tKO 31±4 ms, dKO 23±4 ms; p=0.14) or RR interval (**Figure 5.7I;** tKO 31±4 ms, dKO 23±4 ms; p=0.14) between dKO and tKO female mice. This data supports that the absence of Rad enhances cardiac function independent of β_1,β_2-AR signaling.

At the level of channel current, peak $I_{Ca,L}$ was significantly increased in tKO compared to dKO (**Figure 5.8A,B**). Rad deletion also resulted in a greater maximal conductance (**Figure 5.8C,D;** Gmax: tKO: 508±33 pS/pF, dKO: 230±32 pS/pF; p<0.0001) and a negative shift in activation midpoint (**Figure 5.8E;** tKO: -13.1±2.4 mV,

dKO: -6.12±1.7 mV; p=0.04). Analysis of kinetics demonstrated a trend of less remaining current in the tKO at r_{30} (**Figure 5.8F,G,I,**) and no difference at r_{150} (**Figure 5.8F,H,J)**. The interaction of voltage and dKO versus tKO was significantly different both at r_{30} and r_{150} (**crosses in Figure 5.8G,H**). Taken together, these results support the hypothesis that the deletion of Rad increases peak $I_{Ca,L}$ that mirrors modulated LTCCs without stimulation of β_1,β_2-AR signaling.

5.4 Discussion

The main findings of this study are that in the absence of Rad, increased peak L-type calcium current ($I_{Ca,L}$) is balanced by accelerated calcium dependent inactivation (CDI) and voltage dependent inactivation (VDI) (**Figure 5.9**). Accelerated LTCC kinetics prevent significant action potential and QT interval prolongation. In fact, APD_{80} is shorter in cRadKO (**Figure 5.6**). The loss of Rad from the L-type calcium channel (LTCC) complex results in modulated $I_{Ca,L}$ independent of β-adrenergic receptor (β-AR) signaling. To our knowledge, the cardiomyocyte-restricted Rad deletion model is the only known model to increase $I_{Ca,L}$ without disrupting calcium homeostasis, and without promoting pathological signaling [12, 149]. Therefore, myocardial Rad-LTCC interaction is a potential therapeutic target for positive inotropy while preserving β-AR signaling cascades beyond the LTCC.

5.4.1 Rad contributes to regulation of LTCC inactivation

A major implication of this study is the presence of Rad slows inactivation of the LTCC. The deletion of Rad accelerated only the early, fast component of $I_{Ca,L}$ decay without significantly altering the late, proarrhythmogenic component [50, 61-63, 262] (**Figure 5.1-5.5**). Cav1.2 channels have been shown to form clusters through physical interactions of their C-terminal tails [57-59, 272]. Calcium binding to calmodulin (CaM) on the LTCC promotes the physical interactions between channels, allowing channels to have synchronous activity [58]. This process is thought to occur in response to β-AR stimulation in order to enhance calcium influx through calcium dependent facilitation (CDF), but also to accelerate inactivation through CDI to prevent the development of arrhythmogenic events [59]; hyperactivation of a few channels could dictate the activity of the entire cluster [57, 58]. Rad, as well as the other members of the RGK protein family, bind to CaM in a calcium dependent manner via a conserved binding site on their C-termini [166]. It has been well established that CDI occurs when calcium binds to CaM and causes a conformational change to induce LTCC inactivation [68-71]. With CaM playing a major role in CDI and channel clustering, and Rad binding to CaM, it is therefore possible that Rad contributes to channel clustering and calcium dependent inactivation. In the absence of Rad, more channels may cluster together, thereby promoting an increase in peak $I_{Ca,L}$ [24] and an acceleration of the fast component of $I_{Ca,L}$ decay (**Figure 5.1-5.3**). Future studies investigating clustering in the absence of Rad might give further insight into how the LTCC undergoes CDF and CDI.

5.4.2 Rad is a key contributor to LTCC Modulation

The activation of protein kinase A (PKA) downstream of β-AR stimulation results in an increase in $I_{Ca,L}$, an increase in channel open probability, and an increase in the number of functional channels [109, 256], also known as 'modulation' of the LTCC. Phosphorylation of $Ca_V1.2$ was long thought to be the underlying mechanism of modulation [31], but recent studies have proposed that the mechanism of modulation relies more on protein-protein interactions within the LTCC or on LTCC clustering [24, 31, 57-59, 92, 109, 272]. It was also recently shown that Rad is essential for cAMP-PKA regulation of $Ca_V1.2$ [92]. Our studies have demonstrated that Rad-LTCC interaction is a key molecular signaling axis for LTCC modulation both in the ventricle and in sinoatrial node cardiomyocytes [24, 214] (see Chapter 4), and that the absence of Rad from the complex yields modulation of the LTCC. Our current findings expand on this through kinetic analysis, demonstrating that CTRL $I_{Ca,L}$ stimulated with isoproterenol decayed in a manner that was indistinguishable from cRadKO $I_{Ca,L}$ (**Figure 5.1**). When treated with isoproterenol, channels may form "super-clusters" along the t-tubules to amplify Ca^{2+} influx [59] and modify kinetics. The absence of Rad could promote these "super-clusters" to form under basal conditions, which could in turn promote more calcium induced calcium release from the sarcoplasmic reticulum to feedback onto the clusters to then accelerate CDI. The "super-clusters" that form in response to sympathetic stimulation via the β-AR axis signaling modulates trigger calcium, which could shorten action potential duration [266]. At the tissue level, sympathetic drive reduces transmural dispersion of action potentials [273]. If $I_{Ca,L}$ is selectively increased, all else remaining

equal, the resulting ventricular action potential duration would prolong, appearing on the ECG as a longer QT interval [274]. In cRadKO cardiomyocytes, increased LTCC peak current is offset by faster kinetics; thus, raising the possibility that the net effect of Rad loss on cardiac electrophysiology for action potential duration and QT prolongation is nullified [21] (**Figure 5.6,5.9**).

An alternate idea stems from Findlay who proposed that modulation of LTCC from β-AR stimulation resulted in a switch from VDI to CDI. Under basal conditions, it was thought that CDI contributed to decay at more negative potentials, while VDI dominated as the membrane became more depolarized. Findlay and others showed that VDI has a biphasic decay, and that rapid VDI contributes to the fast component of $I_{Ca,L}$, not just CDI [60, 74-76, 275]. However, in the presence of isoprenaline, CDI dominated at all voltages, and VDI was suppressed. Findlay's prediction was that CDI would then have little contribution to the action potential under basal conditions, but could promote severe slowing of $I_{Ca,L}$ decay and therefore elongation of the action potential after β-AR stimulation [60]. Our results demonstrate that the absence of Rad accelerates VDI both in the fast and slow components of $I_{Ca,L}$ decay (**Figure 5.5**). This does not result in elongation of the action potential nor does it significantly prolong the QT interval (**Figure 5.6**). It is therefore possible that Rad contributes to LTCC regulation by allowing this switch between VDI and CDI. Under basal conditions, the presence of Rad regulates VDI; when β-ARs are activated, Rad phosphorylation causes dissociation from the LTCC [92] and CDI then becomes the dominant inactivation mechanism as channels cluster together and elevate intracellular calcium. The synchronous activity of these clusters then promotes accelerated CDI so that the increase in $I_{Ca,L}$ is offset so as not to significantly

alter action potentials. Further studies into how phosphorylation of Rad alters its location within the complex or its interactions with other proteins could help elucidate how Rad contributes to LTCC inactivation, especially under conditions of β-AR stimulation.

5.4.3 Rad regulation of LTCC is independent of β-adrenergic receptor signaling

Our work has demonstrated that Rad is a critical component in LTCC modulation by β-AR stimulation [21, 23, 24]. Indeed, cardiomyocyte-restricted Rad-deletion demonstrates the extreme by which the loss of Rad yields maximally modulated $I_{Ca,L}$ that translates from channel function up to enhanced, *in vivo* cardiac function. Data collected from the $\beta_1\beta_2$-AR x Rad-triple knockout demonstrate that the maximal modulation of $I_{Ca,L}$ is due to the absence of Rad from the LTCC, exclusive of activation of β-ARs (**Figure 5.7-5.9**). Others who have utilized β_1-AR knock out, β_2-AR knock out, or $\beta_1\beta_2$-AR double knock models have reported minimal impacts on basal cardiac function, suggesting that there are potentially other controls for critical physiological functions, such as cardiac rate and contractility, to compensate for the loss of these receptors [187, 270, 276-279]. In $\beta_1\beta_2$-AR double knockout neonatal myocytes, β_3-AR was shown to stimulate contraction after treatment with isoproterenol, though desensitization occurred more rapidly compared to β_1-AR or β_2-ARs [279]. It is therefore possible there is a minor contribution from other sources to how the heart responds to increased sympathetic drive. However, our data clearly demonstrates a significant increase in function both at the level of whole heart and at the level of the channel when Rad is deleted in the $\beta_1\beta_2$-AR double knock out without significant prolongation of the QT interval. We have previously shown that Rad deletion allows for systolic advantage without promoting

damaging effects that are normally associated with the chronic use of positive inotropes [21, 24]. Therefore, we suggest that Rad reduction could serve as a treatment for heart failure that enhances systolic function while preserving β-AR signaling pathways, and without increasing proarrhythmic late $I_{Ca,L}$ [50, 61-63].

5.5 Limitations

It is possible that differential dispersed cell activity might arise from cellular damage artifact during enzymatic dispersal. However, our findings in this study are similar to other reports of Rad deletion on cardiac function [17, 21, 24, 92]. These studies are limited to the mouse. Mice have a larger sarcoplasmic reticulum calcium content and greater SERCA activity compared to larger species [257, 268]. Repolarizing current is mostly carried by I_{to} and I_{Kur} in the mouse, while larger species express I_{Kr} and I_{Ks} [268]. Despite these differences, the cardiac fight-or-flight response is conserved across multiple species, and this study gives further insight into how LTCC activity is modulated.

5.6 Conclusions

In summary, we have demonstrated that modulation of the LTCC is governed by the presence of Rad in the $Ca_V1.2$ macromolecular complex. The absence of Rad yields an increase in peak $I_{Ca,L}$ that is offset by an increase in both VDI and CDI so that action potential and QT interval are not significantly prolonged. β-AR mediated modulation of the LTCC is governed by Rad. Taken together, Rad reduction within cardiomyocytes is a compelling potential therapeutic approach for increasing cardiac function without the

need for β-blockers, thereby improving quality and quantity of life for those that suffer from heart failure.

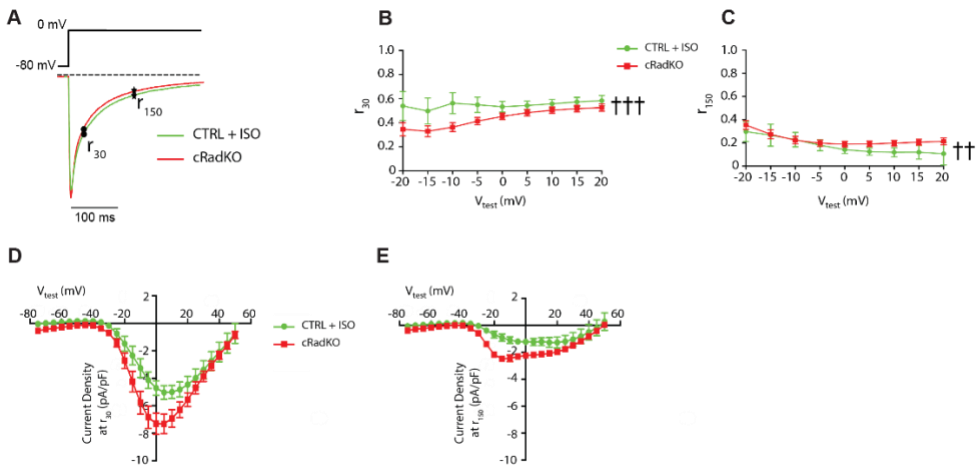

Figure 5.1 Rad deletion $I_{Ca,L}$ phenocopies modulated $I_{Ca,L}$.
A) Exemplar Ca^{2+} currents with 10 mM EGTA for CTRL with ISO (green) and cRadKO (no ISO, red), traces normalized to peak current at 0 mV Scale bar: 100 ms. Black dots indicate r_{30}, Black stars indicate r_{150}. Remaining current across voltage steps 30 ms after peak **B)** and 150 ms after peak **C) .** $I_{Ca,L}$ current density 30 ms **D)** and 150 ms **E)** after peak. Data in **(B,C)** analyzed by two-way ANOVA plus Šídák's multiple comparisons test (For B: voltage x CTRL v cRadKO: †††p = 0.0009; For C: voltage x CTRL v cRadKO: ††p = 0.007). N = 4 mice, n = 7 cells for CTRL; N = 10 mice, n = 23 cells for cRadKO.

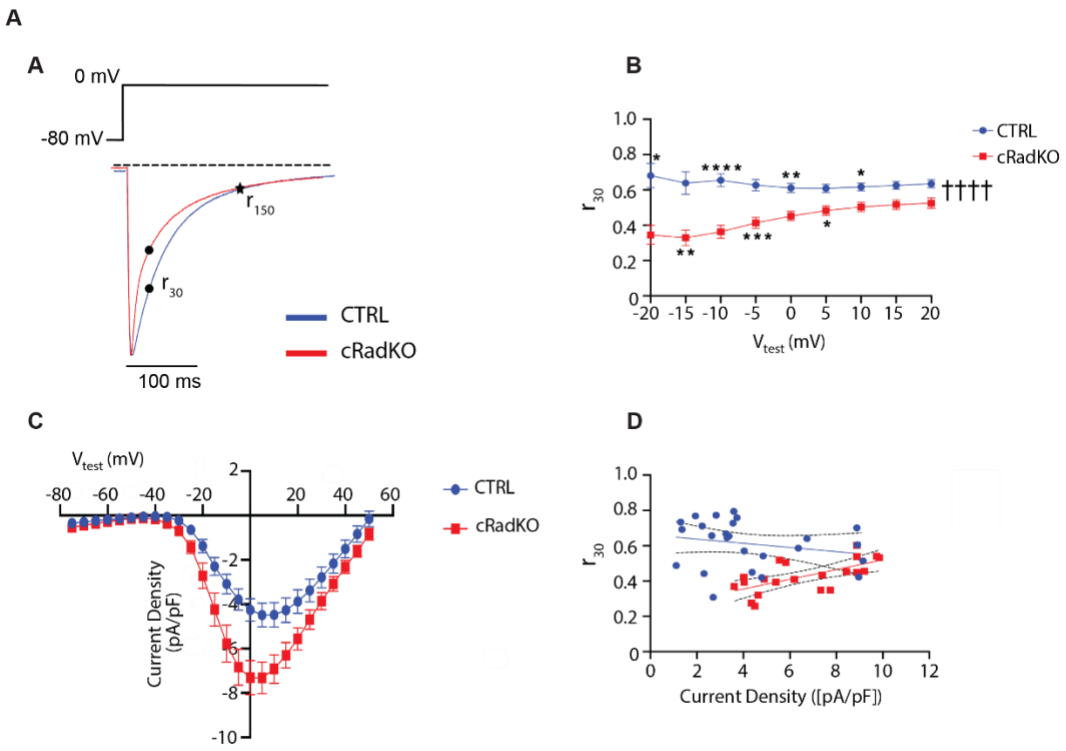

Figure 5.2 Rad deletion accelerates fast component of $I_{Ca,L}$ decay.
A) Exemplar Ca^{2+} currents with 10 mM EGTA for CTRL (blue) and cRadKO (red), traces normalized to peak current at 0 mV Scale bar: 100 ms. Black dots indicate r_{30}. **B)** Remaining current 30 ms after peak across voltage steps. **C)** $I_{Ca,L}$ current density 30 ms after peak. **D)** Regression plot of the absolute values of current density versus r_{30} (CTRL: slope = -0.01, deviation from zero: $p = 0.28$, $r^2 = 0.5$; cRadKO: slope = 0.03, deviation from zero: $p = 0.002$, $r^2 = 0.4$; dotted lines represent 95% confidence intervals). Data in (**B**) analyzed by two-way ANOVA plus Šídák's multiple comparisons test (For between CTRL and cRadKO: *$p < 0.05$, **$p < 0.01$, ***$p < 0.001$ and ****$p < 0.0001$, alternating asterisks for presentation clarity; For voltage x CTRL v cRadKO: ††††$p < 0.0001$). Data in (**D**) analyzed by simple linear regression. N = 10 mice, n = 25 cells for CTRL; N = 10 mice, n = 23 cells for cRadKO.

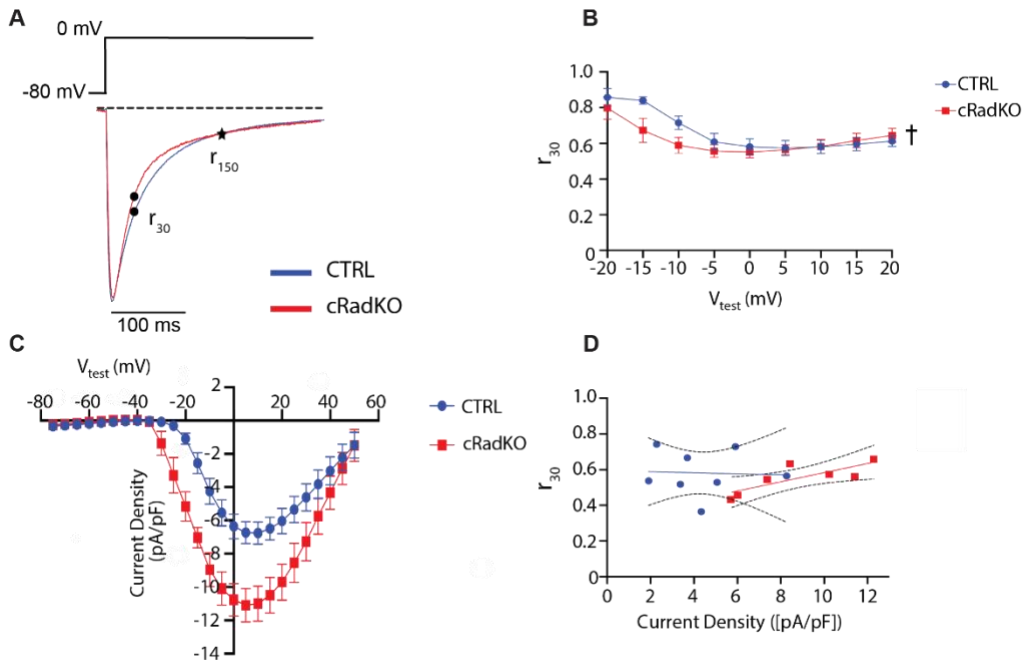

Figure 5.3 Rad regulation of ICa,L kinetics requires SR Ca^{2+} release.
A) Exemplar Ca^{2+} currents with 10 mM BAPTA for CTRL (blue) and cRadKO (red), traces normalized to peak current at 0 mV Scale bar: 100 ms. Black dots indicate r_{30}. **B)** Remaining current 30 ms after peak across voltage steps. **C)** $I_{Ca,L}$ current density 30 ms after peak. **D)** Regression plot of the absolute values of current density versus r_{30} (CTRL: slope = -0.003, deviation from zero: p = 0.91, r2 = 0.002; cRadKO: slope = 0.03, deviation from zero: p = 0.03, r2 = 0.6; dotted lines represent 95% confidence intervals). Data in (**B**) analyzed by two-way ANOVA plus Šídák's multiple comparisons test (For voltage x CTRL v cRadKO: †p = 0.03). Data in (**D**) analyzed by simple linear regression. N = 4 mice, n = 8 cells for CTRL; N = 4 mice, n = 7 cells for cRadKO.

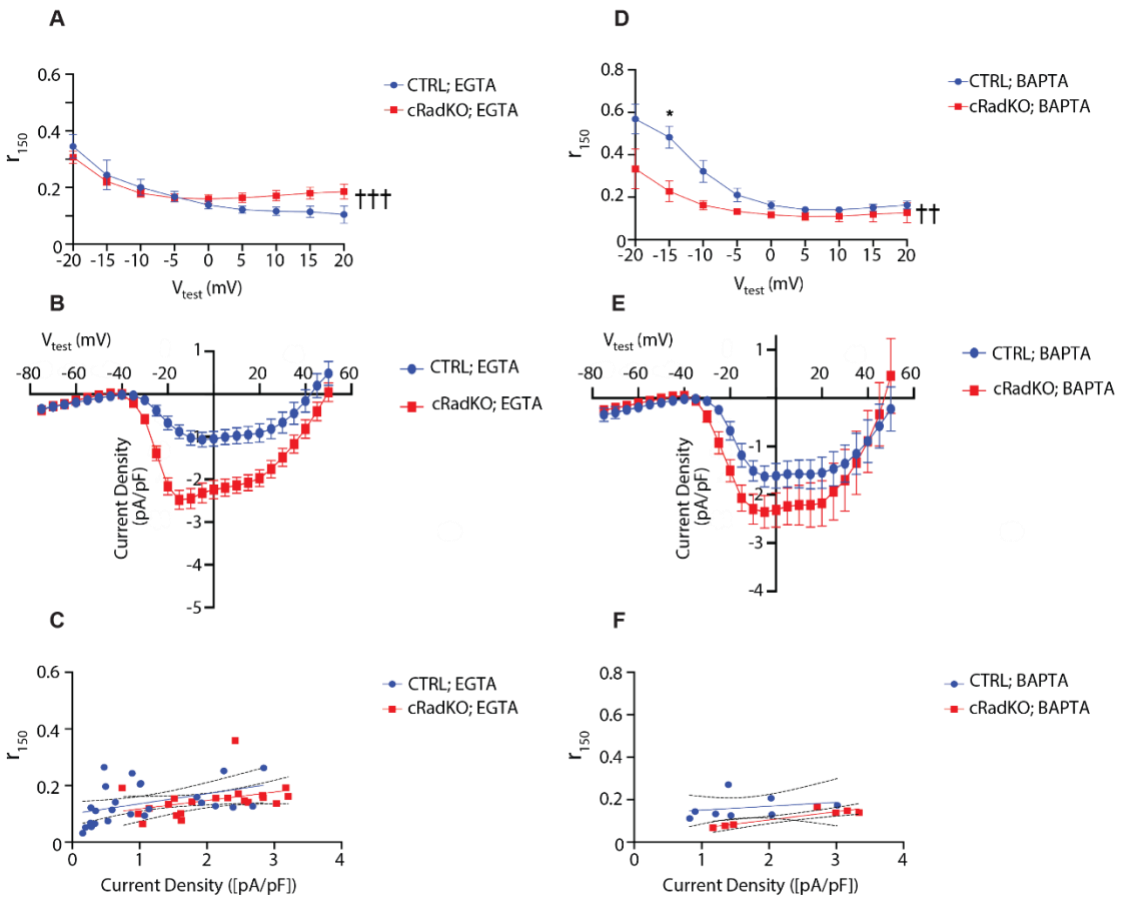

Figure 5.4 Rad does not alter slow component of $I_{Ca,L}$ decay.
A-C) Current measured with EGTA; **D-F)** Current measured with BAPTA; **A)** Remaining current 150 ms after peak across voltage steps. **B)** $I_{Ca,L}$ current density 150 ms after peak. **C)** Regression plot of the absolute values of current density versus r_{150} (CTRL: slope = 0.04, deviation from zero: p = 0.03, r^2 = 0.2; cRadKO: slope = 0.03, deviation from zero: p = 0.09, r^2 = 0.2; dotted lines represent 95% confidence intervals). N = 10 mice, n = 25 cells for CTRL; N = 10 mice, n = 23 cells for cRadKO. **D)** Remaining current 150 ms after peak across voltage steps. **E)** $I_{Ca,L}$ current density 150 ms after peak. **F)** Regression plot of the absolute values of current density versus r_{150} (CTRL: slope = 0.02, deviation from zero: p = 0.54, r^2 = 0.1; cRadKO: slope = 0.04, deviation from zero: p = 0.003, r^2 = 0.9; dotted lines represent 95% confidence intervals). N = 4 mice, n = 8 cells for CTRL; N = 4 mice, n = 7 cells for cRadKO. Data in (**A,D**) analyzed by two-way ANOVA plus Šídák's multiple comparisons test. (For A: For voltage x CTRL v cRadKO: †††p = 0.0009; For D: For between CTRL and cRadKO: *p = 0.03; For voltage x CTRL v cRadKO: ††p = 0.003. Data in (**C,F**) analyzed by simple linear regression.

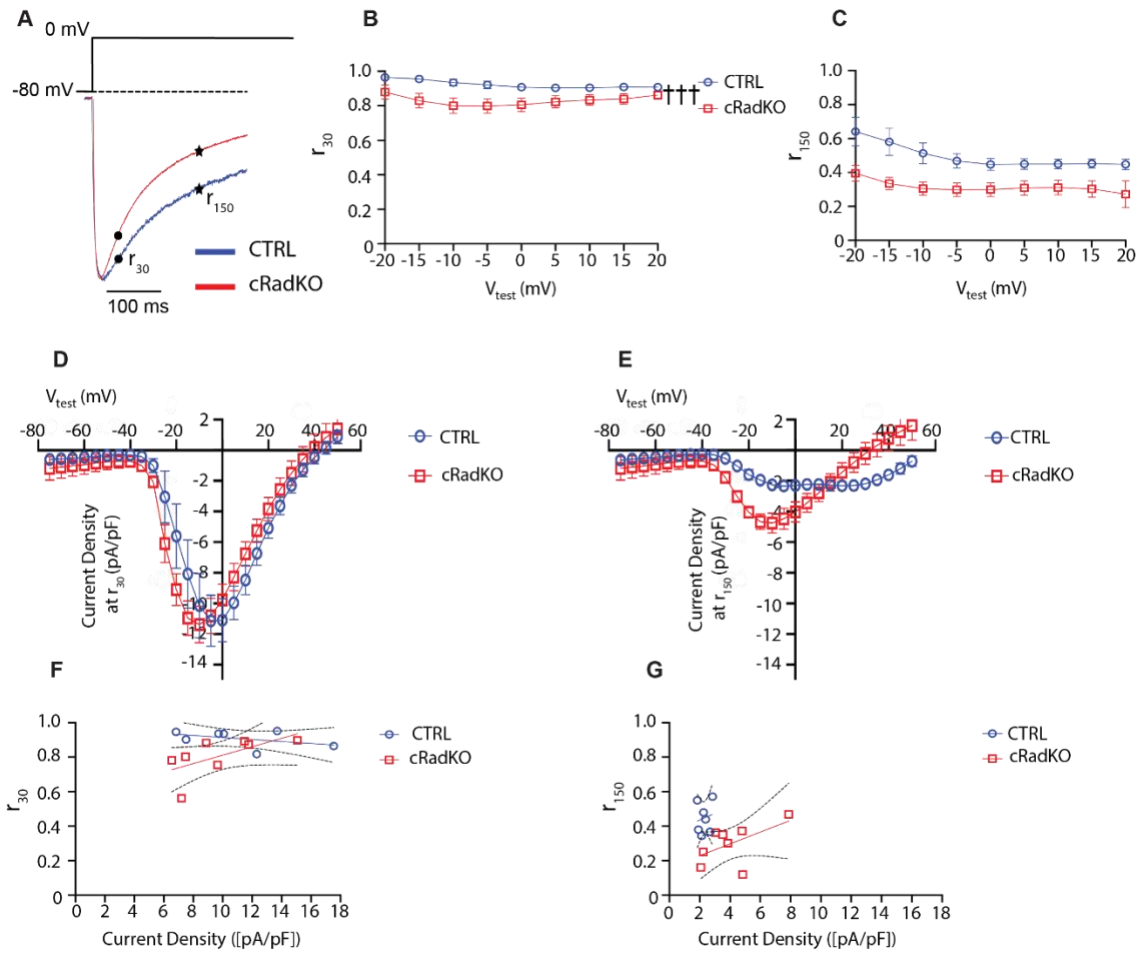

Figure 5.5 Rad deletion enhances VDI.
A) Exemplar Ba^{2+} currents with 10 mM EGTA for CTRL (blue) and cRadKO (red), traces normalized to peak current at 0 mV Scale bar: 100 ms. Black dots indicate r_{30}, Black stars indicate r_{150}. **B)** Remaining current 30 ms after peak across voltage steps. **C)** Remaining current 150 ms after peak across voltage steps. **D)** $I_{Ba,L}$ current density 30 ms after peak. **E)** $I_{Ba,L}$ current density 150 ms after peak. **F)** Regression plot of the absolute values of current density versus r_{30} (CTRL: slope = -0.006, deviation from zero: $p = 0.33$, $r^2 = 0.2$; cRadKO: slope = 0.02, deviation from zero: $p = 0.10$, $r^2 = 0.4$; dotted lines represent 95% confidence intervals). **G)** Regression plot of the absolute values of current density versus r_{150} (CTRL:slope = 0.04, deviation from zero: $p = 0.73$, $r^2 = 0.03$; cRadKO: slope = 0.03, deviation from zero: $p = 0.16$, $r^2 = 0.3$; dotted lines represent 95% confidence intervals). N = 3 mice, n = 7 cells for CTRL; N = 4 mice, n = 8 cells for cRadKO. Data in (**A,D**) analyzed by two-way ANOVA plus Šídák's multiple comparisons test (For A: For voltage x CTRL v cRadKO: †††$p = 0.0002$; For D: For voltage x CTRL v cRadKO: $p = 0.42$). Data in (**C,F**) analyzed by simple linear regression.

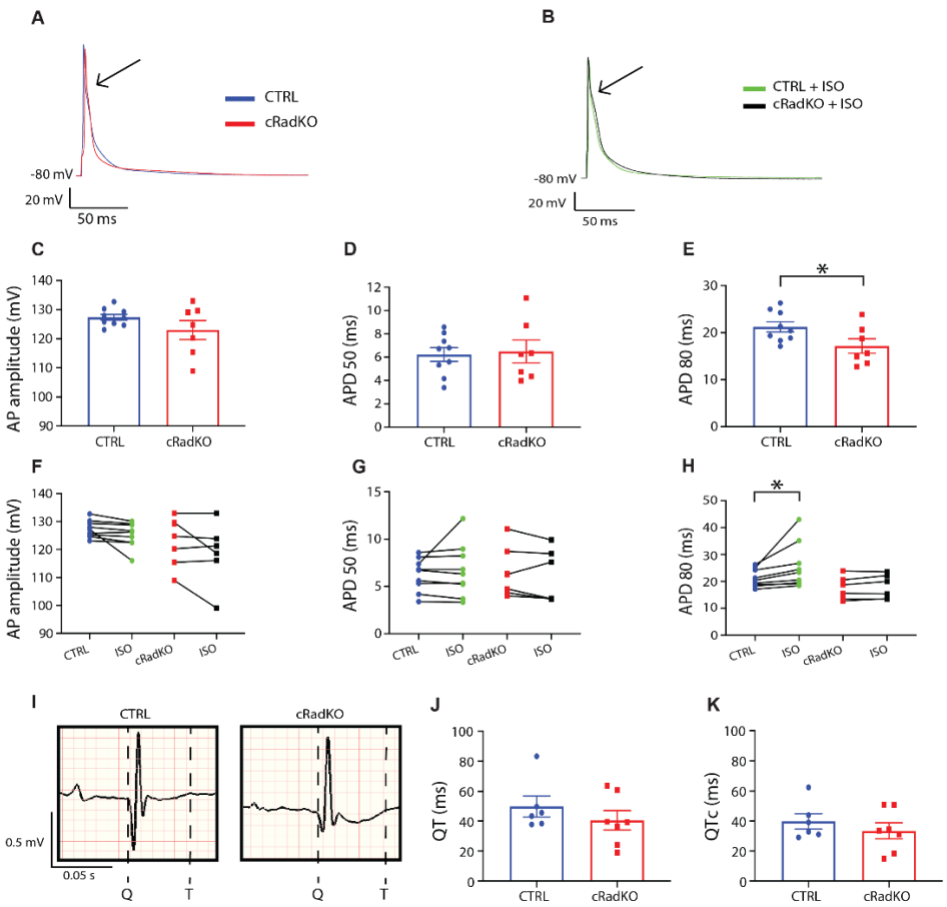

Figure 5.6 Rad deletion does not prolong action potential duration or QT interval.

Exemplar action potentials at **A)** baseline from CTRL (blue) and cRadKO (red), and after ISO **B)** from CTRL (green) and cRadKO (black); Scale bar: 20 mV, 50 ms; arrow indicating inflection point. **C)** Action potential ampltiude at baseline (p = 0.18) **D)** Action potential duration at 50% repolarization at baseline (p = 0.81). **E)** Action potential duration at 80% repolarization at baseline (*p = 0.04). N = 2 mice, n = 9 cells for CTRL; N = 2 mice, n = 7 cells for cRadKO. **F)** Action potential ampltiude after ISO (CTRL: p = 0.10, cRadKO: p = 0.20). **G)** Action potential duration at 50% repolarization after ISO (CTRL: p=0.45; cRadKO: p = 0.38). **H)** Action potential duration at 80% repolarization after ISO (CTRL: *p = 0.05; cRadKO: p=0.18). N = 2 mice, n = 9 cells for CTRL with ISO; N = 2 mice, n = 6 cells for cRadKO. **I)** Representative raw QT interval of intrinsic heart rate from surface ECG of CTRL and cRadKO, Scale bar: 0.5 mV, 50 ms. **J)** Raw QT interval (ms) is not significantly different (p = 0.35). **K)** Corrected QT interval (ms) is not significantly different (p = 0.41). CTRL: N = 6 mice; cRadKO: N = 7 mice. P values calculated using Student unpaired t-test comparing CTRL to cRadKO (**C-E,F-H, J-K**) and Student paired t-test comparing baseline to ISO (**F-H**). (**I-J**) measured after administration of atropine (1 mg/kg) and propranolol (1 mg/kg).

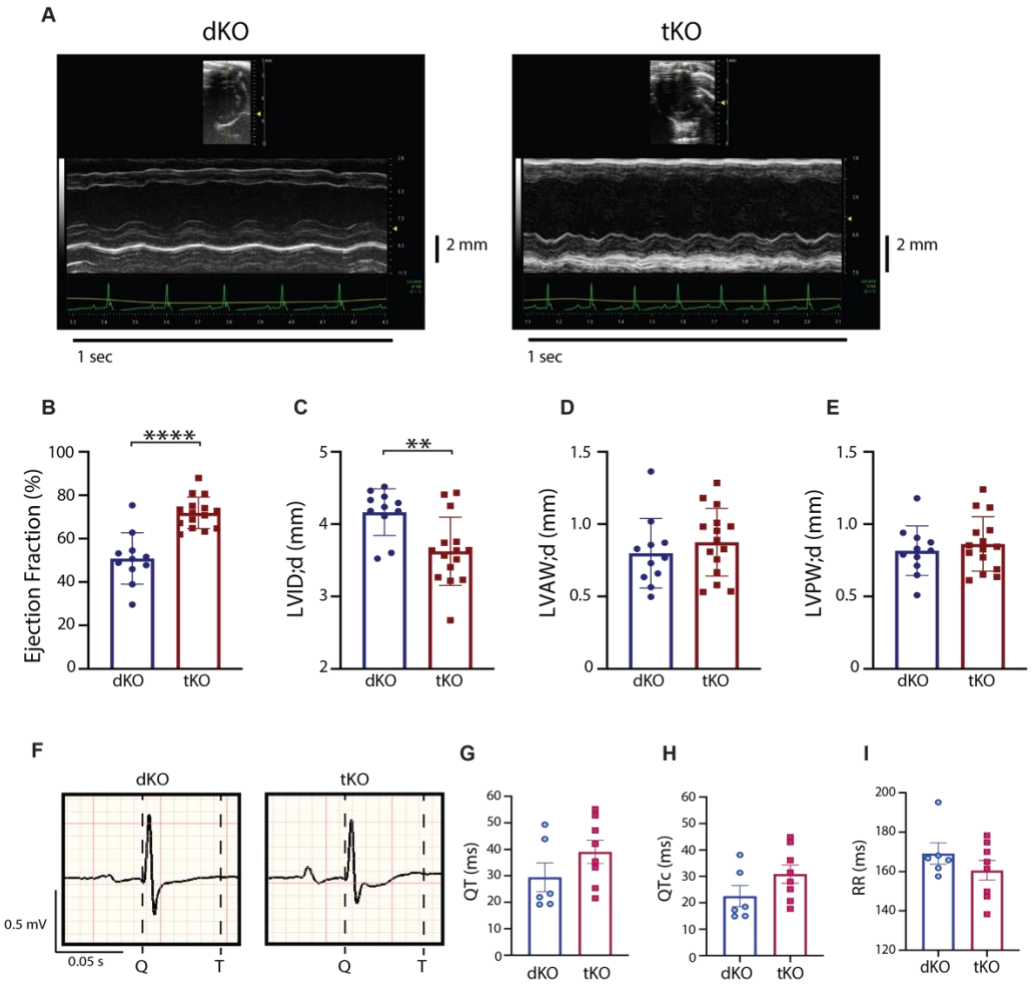

Figure 5.7 Rad deletion increases heart function exclusive of β1β2-Adrenergic Receptors.

A) Representative M-mode short axis echocardiography from dKO and tKO mice. Scale bars: 1 sec; 2 mm. **B)** Ejection fraction (****p<0.0001). **C)** Left ventricular inner dimensions (**p=0.003). **D)** Left ventricular anterior and **E)** Left ventricular posterior wall thickness (LVAW: p=0.43; LVPW: p=0.52). Dimensions (**C-E**) in diastole. dKO: N = 11 mice; tKO: N = 15 mice. **F)** Representative raw QT interval from surface ECG of dKO and tKO, Scale bar: 0.5 mV, 50 ms. **G)** Raw QT interval (ms) is not significantly different (p = 0.19). **H)** Corrected QT interval (ms) is not significantly different (p = 0.14). **I)** RR interval (ms) is not significantly different (p = 0.27). dKO: N = 6 mice; tKO: N = 8 mice. P values calculated using Student unpaired t-test for (**B-E, G-I**).

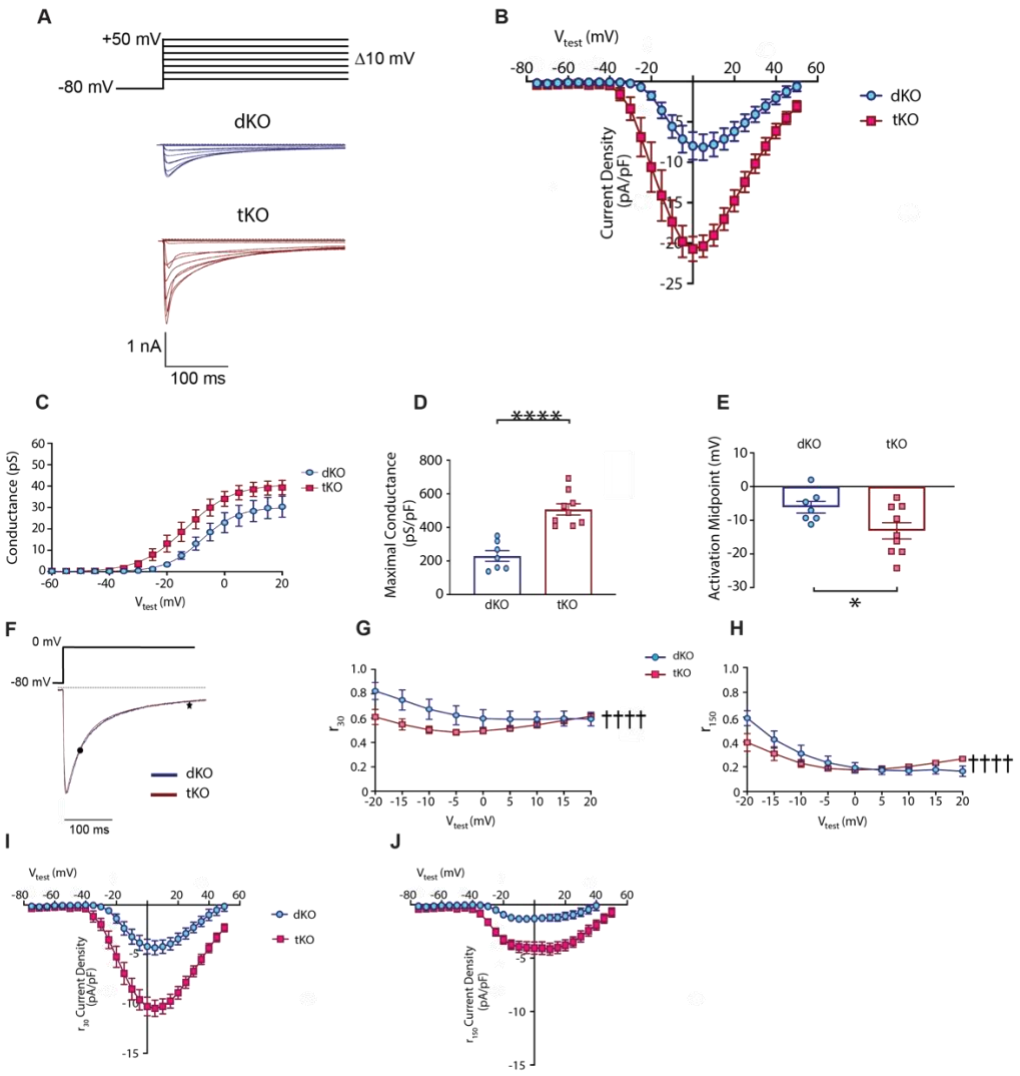

Figure 5.8 Rad deletion yields modulated $I_{Ca,L}$ in the absence of $\beta_1\beta_2$-Adrenergic Receptors.

A) Exemplar family of Ca^{2+} currents of dKO (dark blue) and tKO (dark red), Scale bar: 1 nA, 100 ms. **B)** Peak $I_{Ca,L}$ current density is larger in tKO compared to dKO. **C)** Conductance transform of current voltage curve demonstrates higher maximal conductance in tKO compared to dKO with quantification shown in **D)** (****$p < 0.0001$). **E)** Activation midpoint is significantly negative-shifted in tKO (*$p = 0.04$). **F)** Exemplar Ca^{2+} currents with EGTA for dKO (dark blue) and tKO (dark red), traces normalized to peak current at 0 mV Scale bar: 100 ms. Black dots indicate r_{30}, Black stars indicate r_{150}. Remaining current across voltage steps 30 ms after peak **G)** and 150 ms after peak **H)**. $I_{Ca,L}$ current density 30 ms **I)** and 150 ms **J)** after peak. dKO: N = 3 mice, n = 7 cells; tKO: N = 3 mice, n = 9 cells. P values calculated using Student unpaired t-test for (**D,E**). Data in (**G,H**) analyzed by two-way ANOVA plus Šídák's multiple comparisons test (For G: For voltage x CTRL v cRadKO: ††††$p < 0.0001$; For H: For voltage x CTRL v cRadKO: ††††$p < 0.0001$).

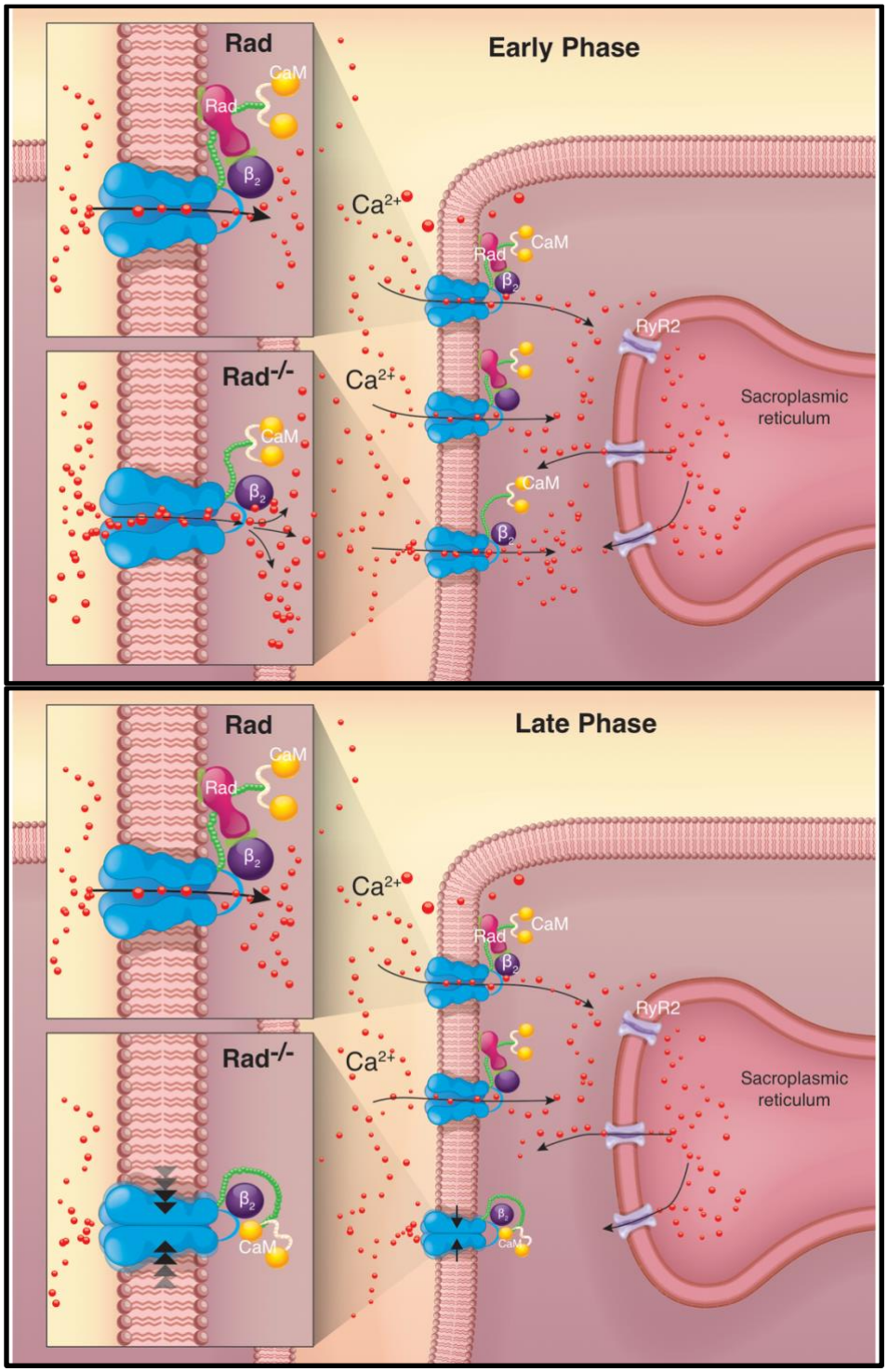

Figure 5.9 Rad modulates $I_{Ca,L}$ independent of $\beta_1\beta_2$-Adrenergic Signaling to Confer Systolic Advantage.

The absence of Rad results in modulated $I_{Ca,L}$ that enhances cardiac contraction (Early Phase) without promoting electrical dysfunction because of accelerated decay kinetics (Late Phase).

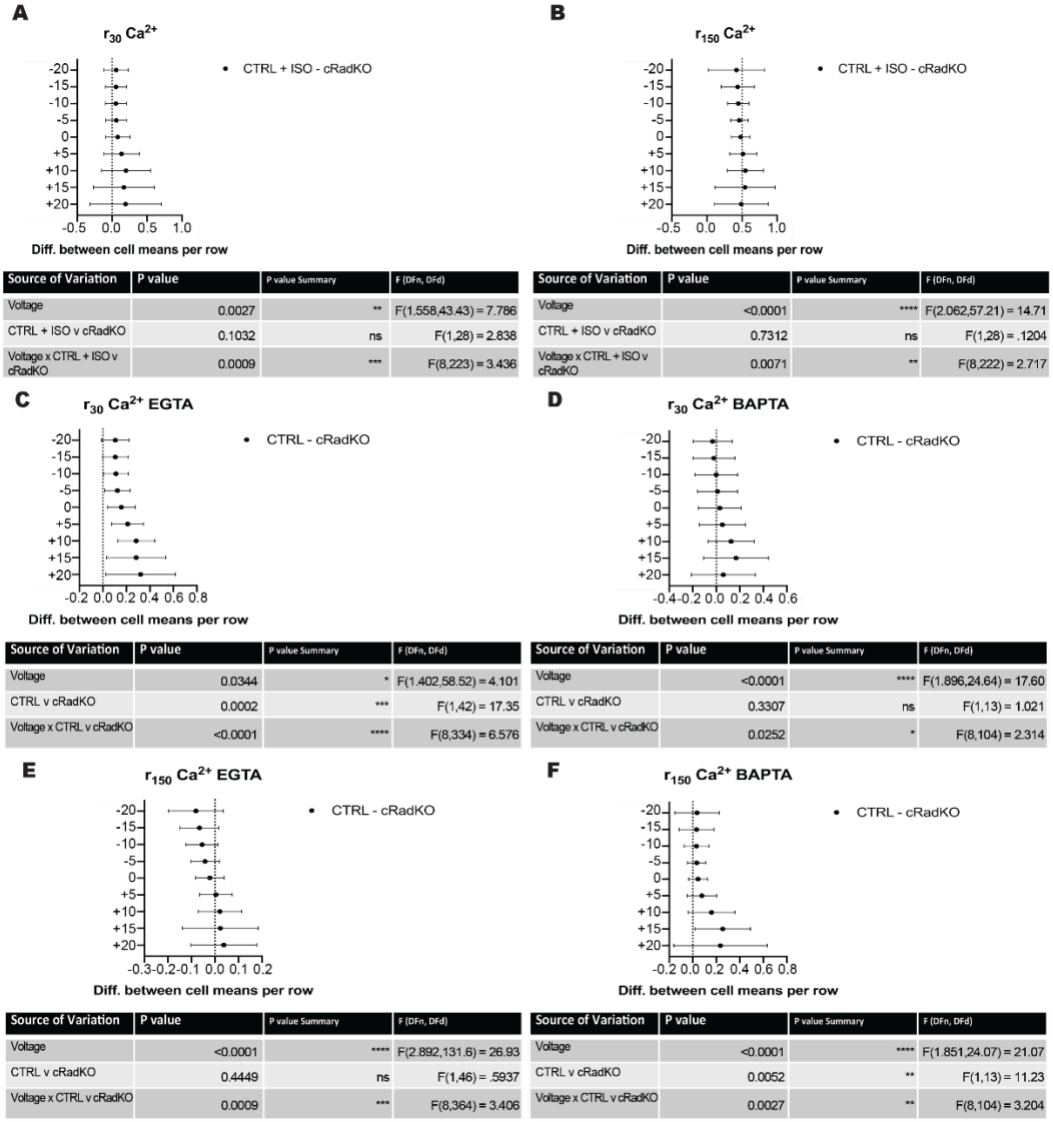

Source of Variation	P value	P value Summary	F (DFn, DFd)
Voltage	0.0027	**	F(1.558,43.43) = 7.786
CTRL + ISO v cRadKO	0.1032	ns	F(1,28) = 2.838
Voltage x CTRL + ISO v cRadKO	0.0009	***	F(8,223) = 3.436

Source of Variation	P value	P value Summary	F (DFn, DFd)
Voltage	<0.0001	****	F(2.062,57.21) = 14.71
CTRL + ISO v cRadKO	0.7312	ns	F(1,28) = .1204
Voltage x CTRL + ISO v cRadKO	0.0071	**	F(8,222) = 2.717

Source of Variation	P value	P value Summary	F (DFn, DFd)
Voltage	0.0344	*	F(1.402,58.52) = 4.101
CTRL v cRadKO	0.0002	***	F(1,42) = 17.35
Voltage x CTRL v cRadKO	<0.0001	****	F(8,334) = 6.576

Source of Variation	P value	P value Summary	F (DFn, DFd)
Voltage	<0.0001	****	F(1.896,24.64) = 17.60
CTRL v cRadKO	0.3307	ns	F(1,13) = 1.021
Voltage x CTRL v cRadKO	0.0252	*	F(8,104) = 2.314

Source of Variation	P value	P value Summary	F (DFn, DFd)
Voltage	<0.0001	****	F(2.892,131.6) = 26.93
CTRL v cRadKO	0.4449	ns	F(1,46) = .5937
Voltage x CTRL v cRadKO	0.0009	***	F(8,364) = 3.406

Source of Variation	P value	P value Summary	F (DFn, DFd)
Voltage	<0.0001	****	F(1.851,24.07) = 21.07
CTRL v cRadKO	0.0052	**	F(1,13) = 11.23
Voltage x CTRL v cRadKO	0.0027	**	F(8,104) = 3.204

Supplemental Figure 5.10 Two-way ANOVA 95% confidence intervals and tabular results.

A) 95% confidence intervals and tabular results for Figure 5.1B. **B)** 95% confidence intervals and tabular results for Figure 5.1C. **C)** 95% confidence intervals and tabular results for Figure 5.2B. **D)** 95% confidence intervals and tabular results for Figure 5.3B. **E)** 95% confidence intervals and tabular results for Figure 5.4A. **F)** 95% confidence intervals and tabular results for Figure 5.4D.

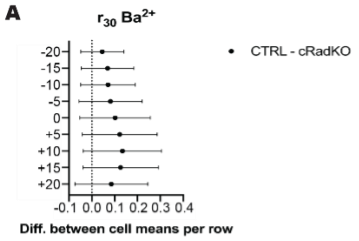

Source of Variation	P value	P value Summary	F (DFn, DFd)
Voltage	0.0011	**	F(2.352,30.58) = 7.807
CTRL v cRadKO	0.0388	*	F(1,13) = 5.279
Voltage x CTRL v cRadKO	0.0002	***	F(8,104) = 4.156

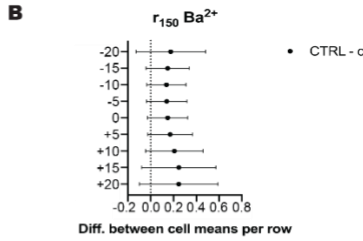

Source of Variation	P value	P value Summary	F (DFn, DFd)
Voltage	0.0055	**	F(2.266,29.46) = 5.880
CTRL v cRadKO	0.0081	**	F(1,13) = 9.756
Voltage x CTRL v cRadKO	0.4161	ns	F(8,104) = 1.033

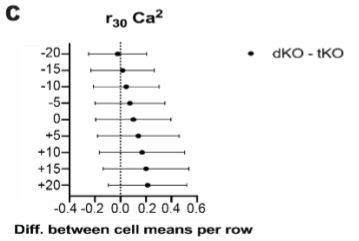

Source of Variation	P value	P value Summary	F (DFn, DFd)
Voltage	0.0047	**	F(1.256,17.58) =9.313
CTRL v cRadKO	0.1299	ns	F(1,14) = 2.589
Voltage x CTRL v cRadKO	<0.0001	****	F(8,112) = 5.205

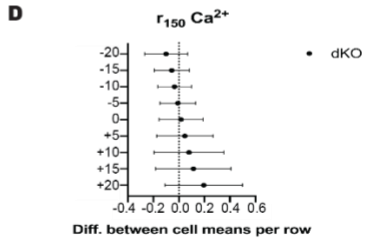

Source of Variation	P value	P value Summary	F (DFn, DFd)
Voltage	<0.0001	****	F(1.274,17.84) = 25.54
CTRL v cRadKO	0.5203	ns	F(1,14) = .4350
Voltage x CTRL v cRadKO	<0.0001	****	F(8,112) = 4.678

Supplemental Figure 5.11 Two-way ANOVA 95% confidence intervals and tabular results.

A) 95% confidence intervals and tabular results for Figure 5.5B. **B)** 95% confidence intervals and tabular results for Figure 5.5C. **C)** 95% confidence intervals and tabular results for Figure 5.8G. **D)** 95% confidence intervals and tabular results for Figure 5.8H.

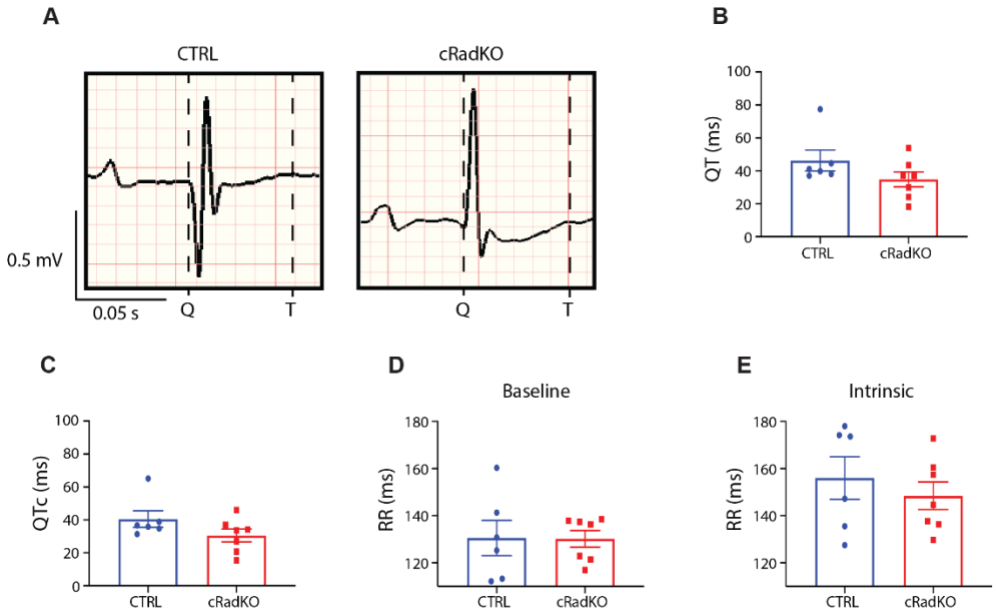

Supplemental Figure 5.12 Surface ECG Measurements.
A) Representative raw QT interval of baseline heart rate from surface ECG of CTRL and cRadKO, Scale bar: 0.5 mV, 50 ms. **B)** Raw QT interval (ms) is not significantly different (p = 0.16). **C)** Corrected QT interval (ms) is not significantly different (p = 0.14). **D)** Baseline RR interval (ms) is not significantly different (p = 0.97). **E)** Intrinsic RR interval (ms) is not significantly different (p = 0.48) CTRL: N = 6 mice; cRadKO: N = 7 mice. P values calculated using Student unpaired t-test for (**B-E**).

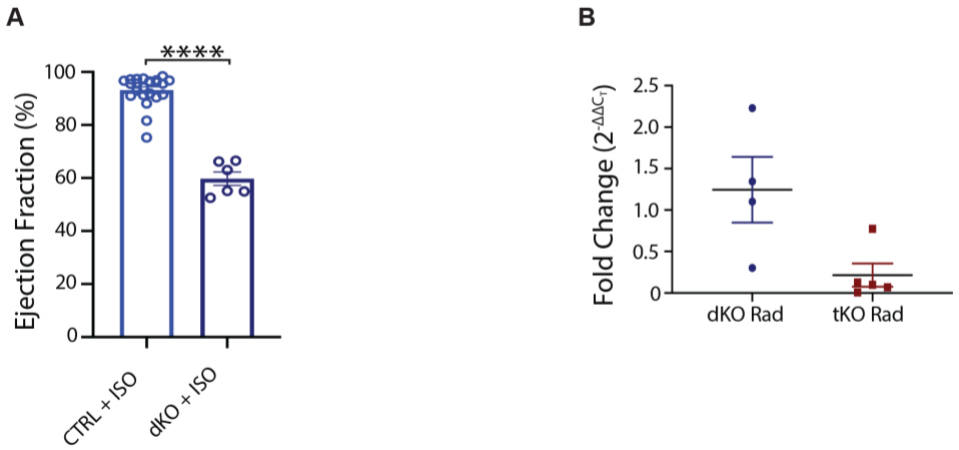

Supplemental Figure 5.13 Whole Heart measurements of dKO and tKO. **A)** Ejection fraction of CTRL (N = 23) and dKO (N = 6) after acute isoproterenol (30 mg/kg). Data for CTRL+ISO taken from published dataset in [24]. (****p<0.0001). **B)** qRT-PCR analysis of samples from dKO and tKO hearts.

CHAPTER 6. ALTERATIONS TO RAD STRUCTURE MODULATE LTCC GATING

6.1 Preface

The results and methods attributed to others are presented for clarity and flow are *italicized*.

6.2 Introduction

The L-type calcium channel (LTCC) is a critical signal transducer within cardiomyocytes that translates the electrical signal from an action potential into calcium release needed for a contraction [25]. Because of this essential role, the LTCC is tightly regulated to prevent calcium overload and electrical dysfunction [6, 124, 125]. Regulation of the LTCC is governed by auxiliary subunits within the complex, protein associations, and transiently interacting signaling molecules [25, 92, 280-282]. Cavβ, a key auxiliary subunit within the channel complex, contributes to channel trafficking and gating, and serves as a mediator of protein associations with the LTCC, including RGK proteins [16, 17, 195-197]. Studies in heterologous expression systems demonstrate all RGK proteins inhibit LTCC current ($I_{Ca,L}$) [16, 17, 161, 283-285]; data from these studies suggest that RGK proteins contribute to LTCC regulation through stabilization of voltage sensing, reduced channel open probability, and cell surface stabilization [199, 241, 286, 287].

Rad was the founding member of the RGK subfamily, first identified as a gene upregulated in skeletal muscle [161]. Similar to other RGK proteins, Rad binds to Cavβ and acts as an endogenous inhibitor of the LTCC [16-20]. Overexpression of Rad blocks LTCC calcium current ($I_{Ca,L}$); Rad deletion from the complex increases $I_{Ca,L}$, shifts

activation to hyperpolarized potentials, and enhances inactivation [16, 17, 19, 20, 166, 195] (see chapter 3,5). Rad also plays a central role in modulation of the LTCC by β-adrenergic stimulation [92, 118] (see chapter 3,5). These studies strongly implicate Rad as a key regulator of LTCC activity; however, the mechanism by which Rad governs channel function remains unknown [288].

Rad-mediated regulation of $I_{Ca,L}$ requires the presence of Rad's C-terminal tail, but does not necessarily require an interaction with $Ca_V\beta$ [196, 199]. Indeed, the absence of the C-terminus of Rad eliminates LTCC inhibition; replacement of the tail with an artificial membrane anchor restores $I_{Ca,L}$ blockade [199]. Because the C-terminus of Rad includes binding regions for key regulators of LTCC, such as 14-3-3, PKA, and calmodulin, it is possible that the C-terminus is the mediator of Rad regulation of the LTCC [55, 92, 175, 177, 241, 281, 289]. In order to assess the structural mechanisms by which Rad governs $I_{Ca,L}$ *in vivo*, two mouse models were developed: Rad-Flag and Rad-Flag A277X. Both models contain three copies of the Flag epitope tag attached to the N-terminus of Rad, with Rad-Flag A277X bearing a C-terminal truncation of the Flag-tagged Rad gene. In the absence of the C-terminus, cardiac function was enhanced and wall thickness increased. This was due to elevated $I_{Ca,L}$; in fact, $I_{Ca,L}$ in Rad-Flag A277X mirrored modulated $I_{Ca,L}$ and Rad deletion because current density was increased, voltage dependent activation shifted in a hyperpolarizing direction, and inactivation was accelerated [24, 103] (see chapter 3,5). This work confirms the requirement of the C-terminus of Rad for inhibition and modulation of the LTCC.

6.3 Results

Studies in heterologous expression systems report Rad mediated regulation of the LTCC requires the C-terminus of Rad [17, 92, 199, 280, 282]; however, this has not been tested *in vivo*. Therefore, *we developed two mouse models: a wild-type 3xFlag-Rad (**Figure 6.1**, **red**; abbreviated Rad-Flag) and 3xFlag-Rad^{A277X} (**Figure 6.1**, **blue**; abbreviated as Rad-Flag A277X) that bears a C-terminal truncation within the endogenous Flag-tagged Rad gene. The 3x indicates the three copies of Flag epitope introduced in frame to the amino terminus of endogenous wild-type Rrad gene*. This allows investigation of potential interactions and binding partners of Rad that are currently unknown while preserving the native protein stoichiometry; this also provides a background to compare how these interactions change when the C-terminus of Rad is truncated. Therefore, Rad-Flag is used as a control for Rad-Flag A277X. For comparison, the means of published WT and cRadKO are also included in graphs as black dotted lines.

6.3.1 Rad-Flag A277X increases cardiac function and wall thickness

Transgenic mouse models that alter components of the L-type calcium channel complex can promote pathological hypertrophy and death [12, 149, 290]. *It was therefore important to assess cardiac structure and function through echocardiography to determine if there were any adverse effects from knocking in 3X Flag-Rad (referred to as Rad-Flag) or truncating the C-terminus of Rad (Rad-Flag A277X). Surprisingly, we found that Rad-Flag hearts demonstrated a phenotype similar to dilated cardiomyopathy compared to published data for WT (**Figure 6.2**). Ejection fraction (EF) was significantly decreased in Rad-Flag while Rad-Flag A277X trended towards an increase in EF (**Figure 6.2A**). Left*

*ventricular inner dimensions were significantly smaller in Rad-Flag A277X compared to Rad-Flag (**Figure 6.2B**). Rad-Flag A277X exhibited significantly thicker walls in both the anterior wall and posterior wall compared to Rad-Flag (**Figure 6.2 C,D, respectively**).* This data suggests the absence of the C-terminus of Rad enhances cardiac function while also promoting cardiac hypertrophy.

6.3.2 Rad-Flag A277X enhances LTCC gating

A potential explanation for an increase in cardiac performance and wall thickness in Rad-Flag A277X could be due to increased L-type calcium current ($I_{Ca,L}$) density [12, 149]. I therefore measured $I_{Ca,L}$ from isolated ventricular cardiomyocytes from Rad-Flag and Rad-Flag A277X mice (**Figure 6.3**). **Figure 6.3A** shows representative families of $I_{Ca,L}$ traces from Rad-Flag (**teal**) and Rad-Flag A277X (**pink**) for evaluating current/voltage (I(V)) relationships. The I(V) curve for Rad-Flag A277X shows increased current density compared Rad-Flag (**Figure 6.3B**). Capacitance is significantly larger in Rad-Flag A277X than in Rad-Flag (**Figure 6.3C**). Rad-Flag A277X also demonstrated a larger maximal conductance compared to Rad-Flag (**Figure 6.3D**). The normalized conductance voltage curves superimposed on the steady-state inactivation curves (**Figure 6.3E**) highlight the negative shift in activation and inactivation in Rad-Flag A277X; activation midpoint was significantly shifted toward more negative membrane potential (**Figure 6.3F**). Analysis of the decay kinetics revealed Rad-Flag A277X enhances inactivation (**Figure 6.4**). Traces from Rad-Flag and Rad-Flag A277X $I_{Ca,L}$ demonstrated that Rad-Flag A277X $I_{Ca,L}$ decay is faster than that for Rad-Flag (**Figure 6.4A**). Across multiple voltage steps, there was less remaining current in the early component of decay (r_{30}) in Rad-Flag A277X $I_{Ca,L}$ than

in Rad-Flag $I_{Ca,L}$ (**Figure 6.4B, Figure 6.4F** for 2-way ANOVA tabular results). Current density of r_{30} was larger in Rad-Flag A277X compared to Rad-Flag (**Figure 6.4C**). Analysis of the late component of decay (r_{150}) revealed less remaining current in Rad-Flag A277X (**Figure 6.4D, Figure 6.4G** for 2-way ANOVA tabular results) with larger current density at r_{150} (**Figure 6.4E**). These data support that Rad regulates channel gating through interactions with its C-terminus; in the absence of the C-terminus, LTCC activity is enhanced.

6.4 Discussion

The major finding of this study is that the C-terminus of Rad is required for Rad-mediated regulation of the LTCC. By deleting the C-terminus of Rad, $I_{Ca,L}$ significantly increases and activates at more negative potentials; inactivation is also accelerated. These effects mirror LTCC modulation and when Rad is not present in the channel complex [24, 103]. These alterations in LTCC function further support that Rad plays a critical role in physiological modulation of the LTCC.

The mechanism by which Rad governs LTCC activity remains unclear [288]. As a regulator of $I_{Ca,L}$, Rad must govern I in a manner that alters one or multiple variables of the equation: $I = N_T \text{ X } p_f \text{ X } p_o \text{ x } I$ where I represents macroscopic calcium current of the cell, N_T is the total number of channels, p_f is the probability that a given channel is available to open, p_o is the probability the channel will open, and i is the unitary current through an open pore [282, 291, 292]. Voltage-dependence of activation of $Ca_V1.2$ is thought to be controlled by the interactions of multiple components within the channel complex, including the S4 and S6 segments of domain I of the α_1 subunit (IS4, IS6 respectively), the

AID (α-interacting domain), the I-II linker between domain I and II of the α_1 subunit, and $Ca_V\beta$ [55, 118, 293]. A recent study also implicated that Rad inhibits LTCC function through an interaction with $Ca_V\beta$ that alters the IS6-AID connection and is alleviated after PKA phosphorylation [55]. A hallmark feature of PKA-mediated LTCC modulation is a hyperpolarizing shift in activation [103]. Rad serves as a critical target of phosphorylation by PKA, and the absence of Rad from the complex results in modulated-like $I_{Ca,L}$ [92, 103] (see chapter 3,5). Studies in heterologous expression systems demonstrate the C-terminus of RGK proteins is critical to inhibition of the LTCC [17, 92, 280], and Rad-Flag A277X supports this *in vivo*. When the C-terminus of Rad is deleted, $I_{Ca,L}$ mirrors LTCC modulation: increase in $I_{Ca,L}$ current density, hyperpolarizing shift in activation, and accelerated inactivation [103]. Results from these studies support that the C-terminus of Rad is essential for Rad-mediated regulation of the LTCC.

The C-terminus of Rad includes a region that can bind to negatively charged phospholipids in the plasma membrane, such as PI(3,4,5)P_3 and PI (4,5)P_2 [92, 177]; when the plasma membrane is depleted of PI (4,5)P_2, Rad was unable to target to the plasma membrane [177]. It is therefore possible that Rad-Flag A277X mirrors Rad deletion because Rad is not present in the complex. The C-terminus of Rad also includes key sites of PKA phosphorylation that induce modulation of the LTCC [92]. It is therefore possible that Rad regulates the LTCC through interactions with the C-terminus of Rad, S4 and S6 segments of α_{1C}, and $Ca_V\beta$. Upon phosphorylation of one or multiple sites within the C-terminus of Rad, Rad is somehow removed from the LTCC that may allow $Ca_V\beta$ to stabilize the linker between IS6 and the AID, thereby promoting a higher P_o [92, 118].

Rad inhibition of LTCC can occur either through mechanisms dependent on binding to $Ca_V\beta$ or mechanisms independent of binding to $Ca_V\beta$ [281]; these independent mechanisms could be through calmodulin regulation since the C-terminus of Rad also contains a binding region for calmodulin [175, 281, 289]. CaM plays a critical role in LTCC inactivation and channel clustering and binds to Rad in a calcium-dependent manner [58, 59, 68-71, 166]. Clustered channels promote cooperative gating of neighboring channels and larger calcium influx, especially under conditions of β-adrenergic receptor stimulation [58, 59]. In the absence of the C-terminus of Rad, there is larger calcium influx (**Figure 6.3**) and enhanced inactivation, specifically the early component of inactivation that is dominated by CDI (**Figure 6.4**); the large increase in $I_{Ca,L}$ mirrors modulated $I_{Ca,L}$ that is not drastically different from a lack of Rad in the channel complex [24, 50, 61-63] (**Figure 6.3**; see chapter 3,5). A clear mechanism by which Rad regulates LTCC activity and modulation remains unknown; however, it is evident from these studies that P_f and P_o of the LTCC are mediated, in part, by multiple interactions between the C-terminus of Rad and other components of the LTCC.

A limitation to this study is the unexpected alterations in cardiac function and structure exhibited by the Rad-Flag mouse. Compared to multiple parameters published for healthy WT, Rad-Flag had decreased function and chamber dilation, indicating that inserting a Flag-tag on Rad somehow induced dilated cardiomyopathy [290] (**Figure 6.2**). In the presence of 3XFlag, Rad gains a net -12 charge. Because of the location of Rad within the complex, binding with $Ca_V\beta$ [92, 195, 280, 281], it is possible that the new net negative charge in Rad-Flag interacts with the positive charged S4 segments of the LTCC to stabilize them through a surface charge screening effect [294]. As a result, activation

midpoint is shifted more positive (**Figure 6.3**) and cardiac function is compromised (**Figure 6.2**). The changes in cardiac structure and function make it difficult to truly compare Rad-Flag to Rad-Flag A277X. However, even in this complex phenotype, it is evident that Rad is in close proximity to the LTCC and the absence of the C-terminus of Rad induces similar effects of Rad-deletion: large increase in calcium current density, a hyperpolarized shift in activation, and accelerated inactivation (**Figure 6.2,6.3**). Future studies utilizing a different knock-in strategy, such as a biotin ligase-based system like BioID, may be better suited to analyze the protein-protein interactions that are crucial for Rad-LTCC since recent published work demonstrates this model system does not affect cardiac function or structure [295].

In summary, these studies confirm that Rad-mediated regulation of the LTCC requires the C-terminus of Rad. Deletion of the C-terminus of Rad induced a modulated state of the LTCC, similar to a LTCC complex devoid of Rad, further supporting Rad as a critical component to LTCC modulation. Though the mechanism of Rad inhibition of the LTCC is unresolved [288], it is clear that the mechanism relies on the C-terminus of Rad.

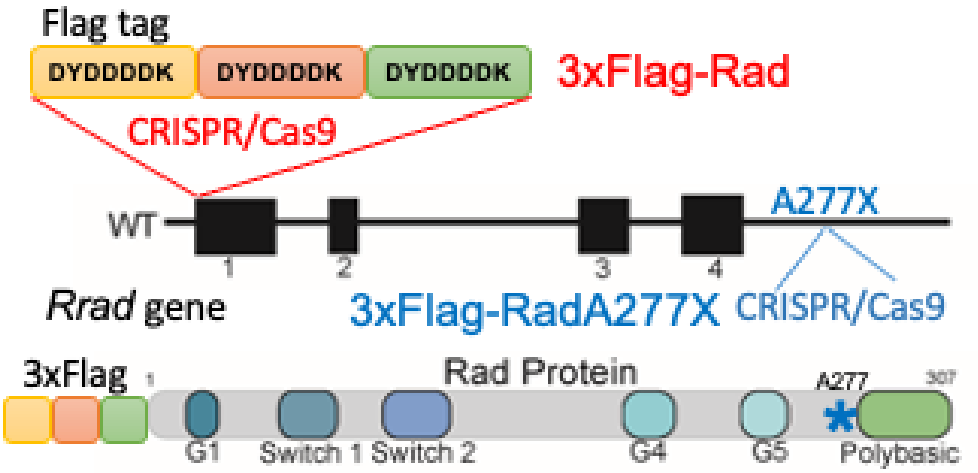

Figure 6.1 Schematic of Rad-Flag and Rad-Flag A277X transgenic mice. CRISPR/Cas9 gene engineering techniques were used to sequentially introduce 3xFlag epitope tag to the N-terminus of the endogenous mouse *Rrad* gene (to generate Rad-Flag mice). CRISPR/Cas9 was then used to introduce a stop codon at A277 into the endogenous Flag-tagged *Rrad* gene to generate a second mouse, Rad-Flag A277X (generating a C-terminal truncation).

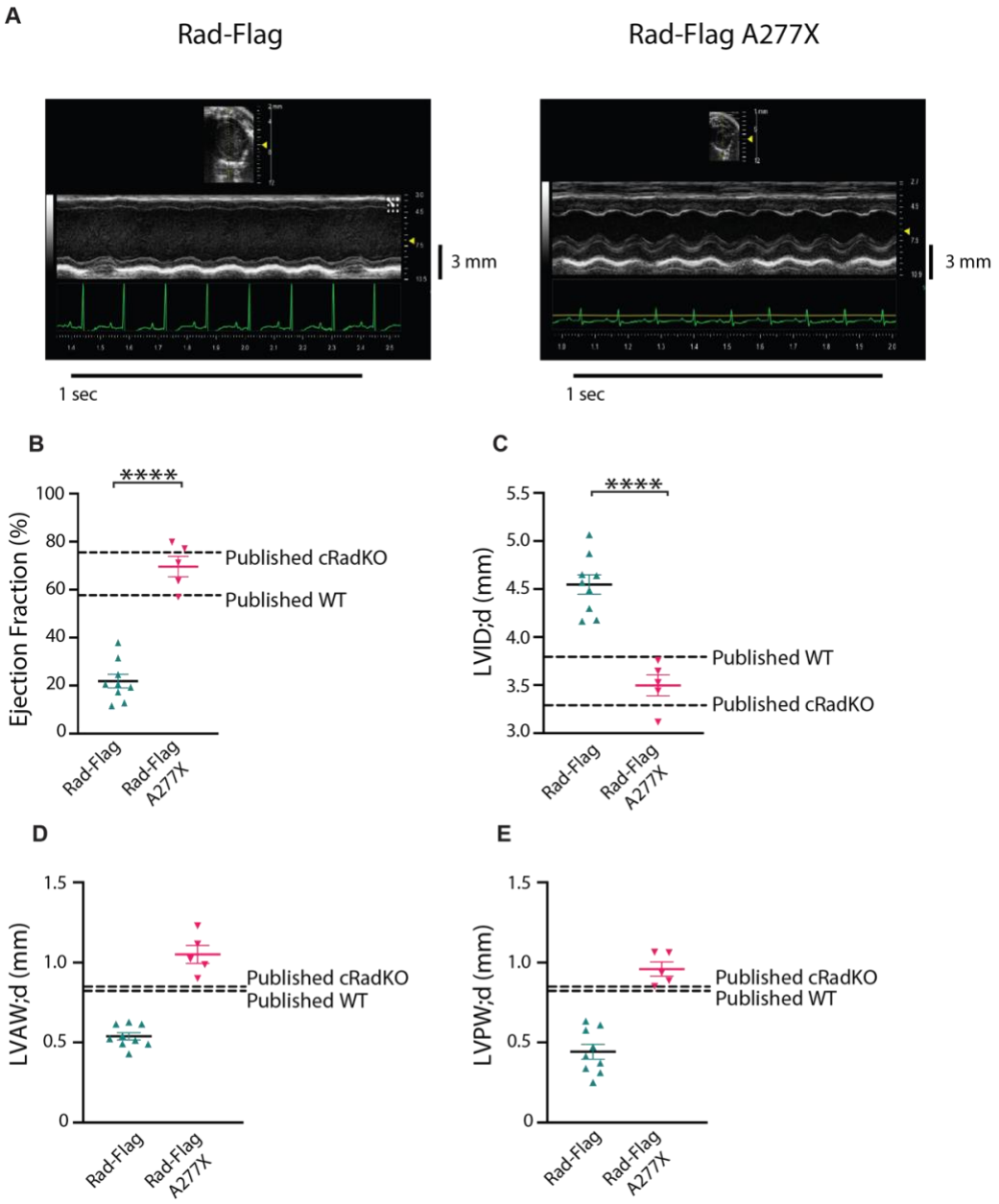

Figure 6.2 Rad-Flag A277X enhances cardiac function and increases wall thickness.

A) Representative M-mode short axis echocardiography from Rad-Flag and Rad-Flag A277X mice. Scale bars: 1 sec; 2 mm. **B)** Ejection fraction (****p < 0.0001). **C)** Left ventricular inner dimensions (****p < 0.0001). **D)** Left ventricular anterior and **E)** Left ventricular posterior wall thickness (LVAW: ****p < 0.0001; LVPW: ****p < 0.0001). Dimensions (**C-E**) in diastole. Dotted lines represent mean summary of published WT and published cRadKO (Ahern et. al 2019, [24]). Data displayed from female mice: Rad-Flag: N = 11 mice; Rad-Flag A277X: N = 15 mice. P values calculated using Student unpaired *t*-test for (**B-E**).

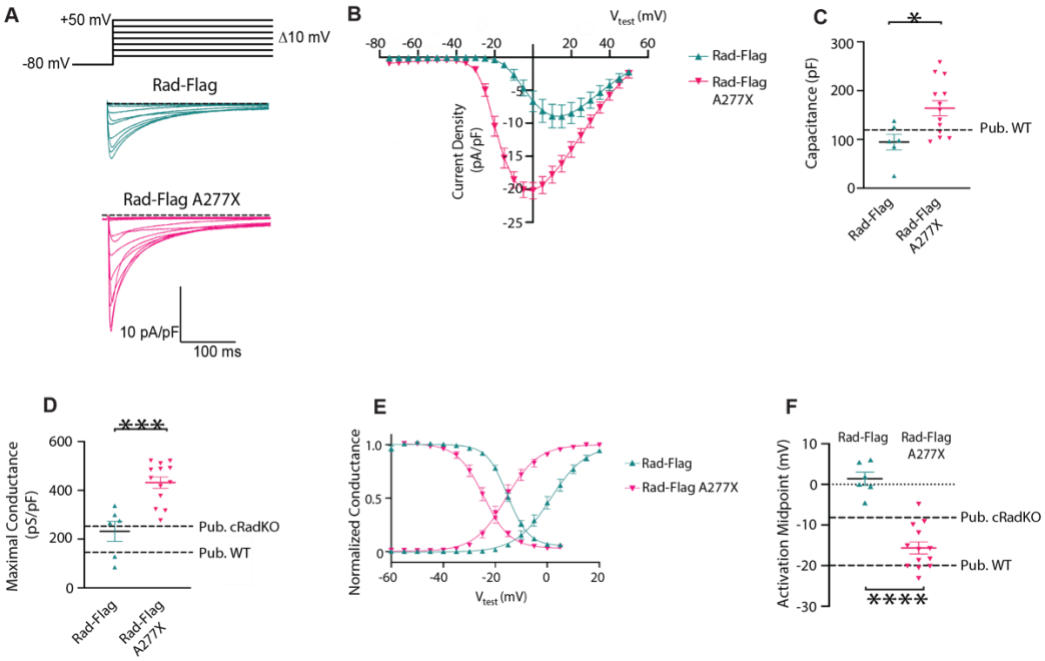

Figure 6.3 Rad-Flag A277X enhanced LTCC function

A) Representative family of $I_{Ca,L}$ currents from V_{test} ranging from -75 mV to +45 mV in 10 mV increments, with voltage protocol schematic shown above. Scale bars: 10 pA/pF, 100 ms. **B)** Current-voltage relationship for peak $I_{Ca,L}$ from Rad-Flag and Rad-Flag A277X ventricular cardiomyocytes. **C)** Cell capacitance is significantly larger in Rad-Flag A277X compared to Rad-Flag (*p = 0.01). **D)** Maximal conductance is significantly increased in Rad-Flag A277X compared to Rad-Flag (***p = 0.0003). **E)** Conductance-voltage curves normalized to maximal conductance in Rad-Flag and Rad-Flag A277X. Smooth curves are Boltzmann distribution fitted to data. **F)** Activation midpoint is significantly negative-shifted in Rad-Flag A277X compared to Rad-Flag (****p < 0.0001). Data for **C,D,F** analyzed by unpaired Student's *t*-test. Data displayed from female mice: Rad-Flag (N = 3 mice, n = 9 cells) and Rad-Flag A277X (N = 3 mice, n = 13 cells).

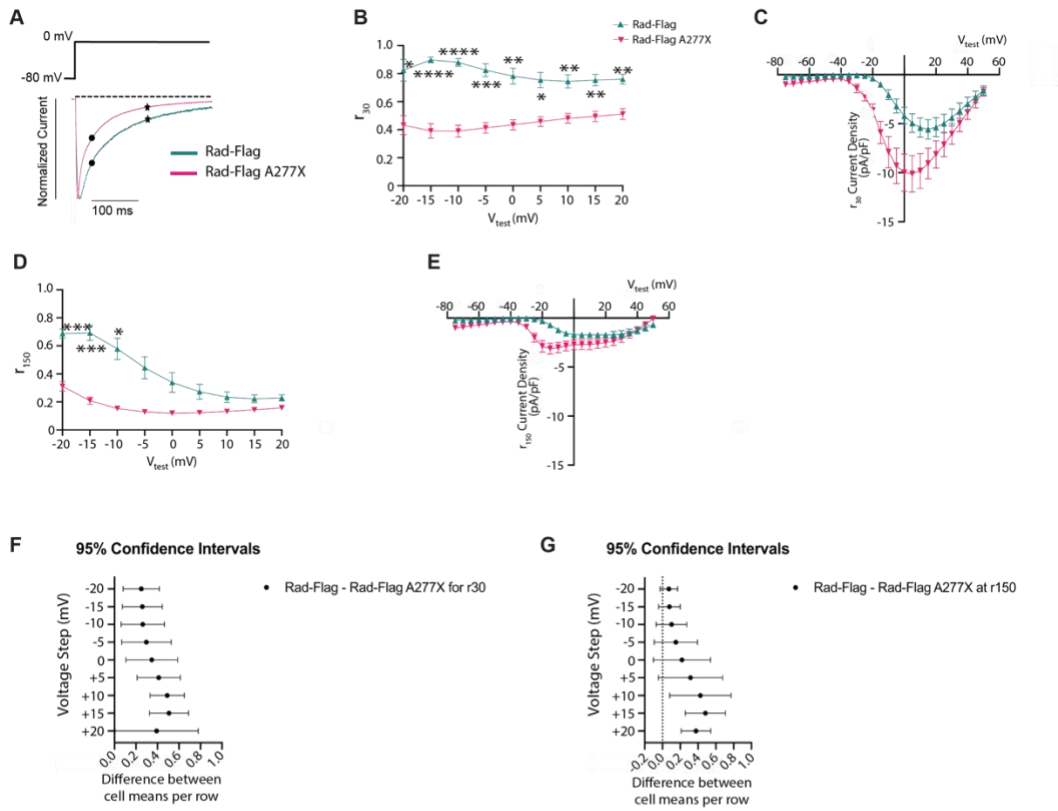

Source of Variation	P value	P value Summary	F (DFn, DFd)
Voltage	0.5597	ns	F(1.141,17.98) = .4044
Genotype	<0.0001	****	F(1,16) = 40.24
Voltage x Genotype	<0.0001	****	F(8,126) = 5.262

Source of Variation	P value	P value Summary	F (DFn, DFd)
Voltage	<0.0001	****	F(2.023,31.86) = 69.70
Genotype	<0.0001	****	F(1,16) = 48.42
Voltage x Genotype	<0.0001	****	F(8,126) = 31.10

Figure 6.4 Rad-Flag A277X enhanced inactivation.
A) Exemplar Ca^{2+} currents with EGTA for Rad-Flag (teal) and Rad-Flag A277X (pink), traces normalized to peak current at 0 mV Scale bar: 100 ms. Black dots indicate r_{30}, Black stars indicate r_{150}. **B)** Remaining current across voltage steps 30 ms after peak (*p < 0.05; **p < 0.009; ***p < 0.0002; ****p < 0.0001; p values alternated between above and below for clarity). **C)** $I_{Ca,L}$ current density 30 ms after peak. **D)** Remaining current across voltage steps 150 ms after peak (*p < 0.02; ***p < 0.0052; p values alternated between above and below for clarity). **E)** $I_{Ca,L}$ current density 150 ms after peak. Data for B,C analyzed by two-way ANOVA plus Šídák's multiple comparisons test with **F)** 95% confidence intervals and tabular results for Figure 6.3B and **G)** 95% confidence intervals and tabular results for Figure 6.3D. Data displayed from female mice: Rad-Flag: N = 3 mice, n = 6 cells; Rad-Flag A277X: N = 3 mice, n = 13 cells.

CHAPTER 7. MYOCARDIAL RAD DELETION PRESERVES CARDIAC FUNCTION IN PRESSURE-OVERLOAD INDUCED HEART FAILURE

7.1 Preface

The results and methods attributed to others are presented for clarity and flow are *italicized*.

7.2 Introduction

Heart failure (HF) is an emerging epidemic. About 50% of HF patients die within five years of their diagnosis [296]. Heart failure occurs when a substantial amount of functional myocardial cells is lost (or altered) in response to injury, leading to left ventricular systolic dysfunction [297]. In an effort to maintain adequate function, the heart initiates several compensatory mechanisms to improve contractility; however, these processes contribute to the progression of failure [297]. Leading therapeutics include positive inotropic agents, but these drugs induce pathological signaling when used chronically [5]. Therefore, an ideal goal would be to identify a novel target that could safely improve inotropy and cardiac function without promoting pathological signaling and remodeling.

The L-type calcium channel (LTCC) is a heteromultimeric protein complex that provides trigger calcium necessary to induce a contraction, and is an upstream regulator of modulating inotropy within cardiomyocytes. The LTCC complex is comprised of a pore-forming α-subunit (Cav1.2 in the myocardium), Cavβ2, α2δ, and calmodulin [194]. LTCC function is tightly regulated to prevent calcium overload and stimulation of multiple hypertrophic signaling pathways that promote heart failure [6, 12, 148, 149]. A key

regulator of LTCC activity is Rad (Ras associated with diabetes), a member of the RGK subfamily (Rem, Rad, Rem2, and Gem/Kir) of Ras-related small GTPases; Rad serves as an endogenous inhibitor of LTCC activity and is abundantly expressed in the heart [16-18, 195-198]. Rad deficiency yields an increase in $I_{Ca,L}$ that promotes enhanced cardiac function [21, 23, 24]; expression levels of Rad significantly decrease in patients suffering from heart failure with reduced ejection fraction [23] as well as in a mouse model of cardiac hypertrophy [181]. This suggests that Rad down-regulation may be a critical component in the signaling for ventricular remodeling.

Studies utilizing whole-body Rad knockout ($gRAD^{-/-}$) mice reported progressive structural remodeling, increased myocyte size, increased up-regulation of the fetal gene program associated with cardiac hypertrophy, and cardiac fibrosis [21, 198]. These results are in line with other mouse models that have dramatically increased $I_{Ca,L}$ as seen in the absence of Rad [12, 149]. However, our recent studies have shown that myocardial Rad deficiency increases $I_{Ca,L}$ to enhance cardiac function into senescence without evidence for structural remodeling or progression to heart failure [24]. This may be because Rad expression has been maintained in non-cardiac tissue, such as vascular smooth muscle [171] and in cells in the bone marrow [172], that could influence cardiac remodeling in response to increased positive inotropy. A key hypothesis is that decreased Rad contributes to a compensatory response under conditions of a failing heart [23, 181]. Given that myocardial Rad deletion improves systolic heart function without pathological remodeling, we hypothesized that myocardial Rad deletion will mitigate myocardial remodeling in advanced stages of heart failure. Utilizing our inducible, myocardial-restricted Rad knockout (cRadKO) mouse, we investigated the effect of Rad deletion in

response to pressure-overload induced heart failure by transverse aortic constriction (TAC). We assessed cardiac function and structure when Rad was depleted before TAC, when the induction of Rad deletion was initiated at time of surgery, and when Rad deletion was induced one-month post-TAC surgery. We found in all three paradigms that cRadKO had better survival and improved cardiac function compared to our CTRL. This was commensurate with enhanced trigger calcium and preserved excitation contraction coupling. These major new findings suggest Rad as a novel potential target to safely enhance positive inotropy to rescue cardiac function under failing conditions.

7.3 Results

7.3.1 cRadKO protects *in vivo* heart function from pressure-overload induced heart failure

cRadKO was induced 4 weeks prior to TAC and mice were followed for 3 months after surgery (**Figure 7.1A**). Survival was significantly improved in cRadKO mice subjected to TAC compared to CTRL mice (**Figure 7.1B**). *In vivo cardiac function was assessed by echocardiography before surgery and at time points shown in the timeline (**Figure 7.1A**). At 3-months post-surgery, cRadKO with TAC maintained an elevated ejection fraction compared to CTRL (**Figure 7.1C**; F**igure 7.2A** for 2-way ANOVA tabular results). There was no difference in heart chamber size in cRadKO with TAC compared to sham (**Figure 7.1D;** F**igure 7.2B** for 2-way ANOVA tabular results) or in heart wall thickness (**Figure 7.1E-F**; **Figure 7.2C,D** respectively for 2-way ANOVA tabular results); by contrast, CTRL with TAC demonstrated significant chamber dilatation. TAC*

*significantly elevated heart weight/body weight in CTRL but not in cRadKO, consistent with the echocardiography in vivo measures (**Figure 7.1G**; **Figure 7.2E** for 2-way ANOVA tabular results). TAC significantly increased fibrosis in CTRL and in cRadKO compared to CTRL Sham, but there was no difference in the degree of fibrosis with respect to knockout. (**Figure 7.3B,C**; **Figure 7.4A** for 1-way ANOVA tabular results). qRT-PCR of ANF displayed no significant difference in any of the groups (**Figure 7.3D**; **Figure 7.4B** for 1-way ANOVA tabular results).* Taken together these data suggest that Rad reduction confers a gain of systolic function that promotes survival and prevents structural remodeling.

7.3.2 cRadKO enhances *in vivo* heart function after pressure-overload

Current management of advanced heart failure is limited in improving quality of life, and ultimately does not prevent the progression of heart failure to advanced stages; however, HF patients demonstrate functional benefit to inotropic agents [298]. *Using ECG telemetry we previously observed tamoxifen increase of heart rate within 3 to 7 days. In the present experiment we administered tamoxifen at the time of surgery; consequently, myocardial Rad reduction is expected to occur by ~7days after surgery* (see timeline, **Figure 7.5A**). No mortality was observed in cRadKO after TAC, while 25% mortality was seen in our CTRL mice (**Figure 7.5B**). *Echocardiographic assessment of these mice at baseline (see timeline) demonstrated no significant difference between groups in function or structure, as expected (**Figure 7.5C-F; Figure 7.6A-D** for 2-way ANOVA tabular results). However, one month after surgery, cRadKO maintained normal function while CTRL mice declined significantly (**Figure 7.5C**). cRadKO mice also maintained normal*

*left ventricular inner dimensions while CTRL mice had enlarged inner dimensions (**Figure 7.5D**). cRadKO demonstrated thicker anterior and posterior walls compared to CTRL mice (**Figure 7.5E,F**). Three months after surgery, we measured heart weight/body weight from the surviving animals and found no significant difference between groups (**Figure 7.5G**).* This data supports that in the early stages of heart failure, Rad reduction preserves systolic function.

7.3.3 cRadKO maintains elevated calcium cycling after pressure-overload

The increase in left anterior wall and posterior wall thickness seen in cRadKO could be due to defective excitation-contraction coupling within cardiomyocytes [181, 299-303]. Therefore, we isolated cardiomyocytes from our CTRL and cRadKO TAC mice that were given tamoxifen at time of surgery and measured $I_{Ca,L}$ (**Figure 7.7;** see timeline, **Figure 7.7A**) and calcium handling (**Figure 7.9**; see timeline, **Figure 7.9A**). Representative $I_{Ca,L}$ traces in **Figure 7.7B,G** highlight increased current density and accelerated kinetics, respectively. The current/voltage (I(V)) curves for I_{CaL} show that cRadKO had a greater current density compared to CTRL (**Figure 7.7C**). Maximal conductance was greater for cRadKO (**Figure 7.7D**; maximal conductance: cRadKO = 450 ± 41 pS/pF, n=12; CTRL = 195 ± 25 pS/pF, n=8; ****p<0.0001) and the activation midpoint was shifted towards more negative membrane potential (**Figure 7.7E,F**; cRadKO = -10.3 ± 1.1 mV, n=12; CTRL = -3.2 ± 2.1 mV, n=8; *p=.01). Analysis of kinetics demonstrated less remaining current in cRadKO TAC compared to CTRL TAC in the early component (r_{30}) (**Figure 7.7G,H**; **Figure 7.8A** for 2-way ANOVA tabular results) and no difference in the late component (r_{150}) of decay (**Figure 7.7G,I**; **Figure 7.8B** for 2-way ANOVA tabular results).

Whole-cell cytosolic calcium dynamics were also significantly larger in amplitude in cRadKO compared to CTRL (**Figure 7.9B,C**; cRadKO = 2.2 ± 0.2 $F_{340/380}$, n=11; CTRL = 1.5 ± 0.2 $F_{340/380}$, n=21; *p=.03). Upstroke velocity of the calcium transient was also accelerated in cRadKO compared to CTRL (**Figure 7.9D**; cRadKO = 55.2 ± 5.1 ($F_{340/380}$)/ms, n=11; CTRL = 39.1 ± 4.8 ($F_{340/380}$)/ms, n=21; *p=.03). To assess cytosolic clearance of Ca^{2+}, we measured the time constant (τ) of the calcium transient decay, and found that it was faster in cRadKO compared to CTRL (**Figure 7.9E**; cRadKO = 0.16 ± 0.01 s, n=11; CTRL = 0.12 ± 0.01 s, n=21; *p=.02).

Under normal physiological heart rates, the contractility of failing myocytes is significantly less than normal [303, 304]; increasing the pacing rate of isolated myocytes decreases contractility while normal myocytes demonstrate an increase in contractility [303]. We therefore measured sarcomere dynamics from failing myocytes isolated from cRadKO and CTRL simultaneously with calcium transients (**Figure 7.10**). Elevated calcium dynamics accompanying Rad deletion coincided with unchanged resting sarcomere length (**Figure 7.10B,C**), unchanged fractional shortening (**Figure 7.10D**), and no change to the rate at which the cell shortened (**Figure 7.10E**). Using the model published by Davis et. al [202], we calculated the integrated tension and found the index score for cRadKO is +0.06 and CTRL is +0.05 (**Figure 7.10F**), indicating a modest trend toward concentric hypertrophy in response to pressure overload in both models. This is further supported by the increase in wall thickness we observed in both CTRL and cRadKO (**Figure 7.1,7.5**). Taken together, this data suggests that excitation-contraction coupling is not defective, but rather calcium homeostasis is enhanced to preserve systolic function.

7.3.4 Response to β-adrenergic receptor stimulation remains blunted in cRadKO after pressure-overload

A hallmark feature of heart failure is the down-regulation of β-adrenergic receptors, resulting in a blunted response in contractility [303, 305]. We therefore measured $I_{Ca,L}$ and calcium transients after the addition of isoproterenol to assess whether there was a β-adrenergic receptor response (**Figure 7.11,7.12**). Given that $I_{Ca,L}$ from cRadKO resembles β-adrenergic modulated $I_{Ca,L}$, we did not expect any response. As expected, we did not see any change in current density (**Figure 7.11Bii**), maximal conductance (**Figure 7.11C,D**) or activation midpoint (**Figure 7.11E,F**) in response to isoproterenol in cRadKO with TAC. Compared to CTRL, cRadKO had larger maximal conductance and trended towards a more negative activation midpoint (**Figure 7.11C,E**). For cytosolic calcium handling, there was no difference between cRadKO and CTRL in calcium transient amplitude, upstroke velocity or the rate of decay (**Figure 7.12B-E**). There was also no response to isoproterenol in either CTRL or cRadKO in amplitude or upstroke velocity (**Figure 7.12F,G**). The rate of decay accelerated in CTRL in response to isoproterenol, with no change in cRadKO (**Figure 7.12H**). Taken together, this data demonstrates that $I_{Ca,L}$ is maximally modulated in the absence of Rad, and responsiveness to β-adrenergic stimulation remains blunted in both CTRL TAC and cRadKO TAC.

7.3.5 cRadKO promotes recovery of function in advanced stages of pressure-overload

Increased positive inotropy due to Rad deletion preserved cardiac structure and function both before the onset of pressure-overload induced heart failure (**Figure 7.1-7.4**)

and in the early stages of onset (**Figure 7.5-7.12**). We therefore induced Rad deletion in mice one month after TAC surgery to assess more advanced heart failure (**Figure 7.13A**, timeline). Survival was assessed beginning at the time of surgery (**Figure 7.13B**). One month after Rad knockout (two months post-surgery) resulted in 71% survival in cRadKO TAC and 26% survival in CTRL TAC. Echocardiographic assessment showed enhanced ejection fraction after Rad deletion that was not significantly different from CTRL Sham (**Figure 7.13C**; **Figure 7.14A** for 2-way ANOVA tabular results). There was no significant difference in heart chamber size after Rad deletion compared to CTRL Sham, while CTRL TAC showed significant chamber dilatation (**Figure 7.13D**; **Figure 7.14B** for 2-way ANOVA tabular results). Left ventricular anterior wall thickness significantly increased after Rad deletion compared to CTRL Sham, while no difference was detected in left ventricular posterior wall (**Figure 7.13E,F**; **Figure 7.14C,D** for 2-way ANOVA tabular results). Taken together, these data suggest that the reduction of Rad in the presence of pressure-overload induced heart failure promotes increased cardiac function through a compensatory response.

7.3.6 cRadKO prevents progression of cardiac dysfunction in advanced stages of pressure-overload

Left ventricular ejection fraction can appear normal under conditions of left ventricular systolic function [306]. *To further assess left ventricular systolic function, we also used speckle-tracking echocardiography to evaluate global longitudinal strain and circumferential strain in CTRL TAC and cRadKO TAC compared to CTRL Sham (**Figure 7.15B,C**). One month after surgery, before the deletion of Rad, both TAC groups*

*demonstrated significantly lower longitudinal strain compared to Sham; however, after Rad deletion cRadKO TAC returned to the level of CTRL Sham and cRadKO Sham, while CTRL TAC remained lower (**Figure 7.15B; Figure 7.16A** for 1-way ANOVA tabular results). Analysis of circumferential strain resulted in a similar improvement in cRadKO TAC compared to CTRL Sham, while CTRL TAC remained low (**Figure 7.15C; Figure 7.16B** for 1-way ANOVA tabular results).* These data further support that the reduction of Rad improves left ventricular systolic function in the presence of pressure-overload induced heart failure.

Hearts that undergo hypertrophy without left ventricular dysfunction demonstrate an increase in heart weight/body weight and in wall thickness without changes to lung weight/body weight or left ventricular chamber size [307]. *We therefore measured heart weight/body weight and lung weight/body weight in CTRL TAC and cRadKO TAC compared to respective Sham groups (**Figure 7.15D-F**). CTRL TAC heart weight/body weight was significantly increased compared to CTRL Sham, as expected, while cRadKO TAC heart weight/body weight was not significantly increased compared to CTRL Sham (**Figure 7.15D; Figure 7.16C** for 1-way ANOVA tabular results). Lung weight/body weight was significantly increased in CTRL TAC, with no significant difference in cRadKO TAC, compared to CTRL Sham (**Figure 7.15E; Figure 7.16D** for 1-way ANOVA tabular results). Both of these measurements correlate with contractile function and heart failure [307]. Plotting this correlation for CTRL TAC, cRadKO TAC, and our Sham groups support this and reveal that cRadKO TAC develops hypertrophy without progressing towards failure (**Figure 7.15F**).* Many of the cRadKO TAC were in the same quadrant as

both Sham groups, demonstrating that Rad reduction promotes recovery from pressure-overload induced heart failure.

7.3.7 cRadKO improves quality of life in advanced stages of pressure-overload

Locomotor activity is significantly reduced in mice that suffer from congestive heart failure [308]. To determine if elevated cardiac function due to Rad loss improved behavior and quality of life, we subjected our mice to an open field test to assess locomotive behavior (**Figure 7.17**). Mice were assessed a month after surgery, and again one month after tamoxifen treatment (2 months post-surgery; see timeline in **Figure 7.17A**). cRadKO TAC mice spent more time walking around the cage, while CTRL TAC mice mostly resided in the corner in which they were placed (lower right corner; see heat map and track visualization, **Figure 7.17B,C** respectively). When compared to TAC mice before tamoxifen, cRadKO TAC mice covered similar distance within the cage while CTRL TAC mice covered significantly less distance (**Figure 7.17D**; **Figure 7.17E** for 1-way ANOVA tabular results). Taken together, our data supports the hypothesis that the deletion of Rad provides a positive inotropic boost that promotes survival and improves quality of life in advanced stages of heart failure.

7.4 Discussion

The main finding of this study is Rad depletion from the myocardium improves survival and preserves cardiac function against pressure-overload induced heart failure. This is demonstrated by reduced mortality, reduced lung congestion, elevated cardiac function, physiological hypertrophy, and improved strain in response to increased trigger

calcium and preserved excitation contraction coupling. In combination with previous studies that report reduced Rad protein in nonischemic heart failure patients [23, 181], our study demonstrates that regulation of Rad contributes to the compensatory response and by depleting Rad, cardiac function is preserved in heart failure. This suggests Rad should be considered as a potential therapeutic target to safely enhance positive inotropy without promoting further damage to the heart.

7.4.1 Myocardial-restricted Rad deletion preserves cardiac function in pressure-overload induced heart failure

Classical inotropes (such as dobutamine, dopamine, and PDE-inhibitors) have failed due to adverse outcomes when used long-term due to maladaptive cardiac remodeling in response to increased adrenergic activity [5, 192]. In theory, treatments that could enhance inotropy without stimulating adrenergic activity would be ideal in order to increase contractility without long-term consequences of adrenergic activation [5]. Indeed, it has been shown that antagonists of β_1-adrenergic receptors can reverse remodeling, improve left ventricular function and prolong survival [192]. Our current study, combined with our previous work with myocardial-restricted depletion of Rad, supports Rad as a unique target for a new generation of positive inotropes to achieve this ideal therapy. We have previously shown that depleting the myocardium of Rad serves as a positive inotrope without stimulating pathological remodeling into senescence; this was possible because calcium cycling was enhanced downstream of β-adrenergic signaling [24]. In conditions of pressure-overload, the reduction of Rad continues to enhance positive inotropy through increased trigger calcium and preserved excitation contraction coupling (**Figure 7.7,7.9**).

This translates to protection from pressure-overload induced heart failure (**Figure 7.1,7.3**) as well as the ability to rescue cardiac function and structure in advanced stages of pressure-overload induced heart failure (**Figure 7.5,7.13,7.15,7.17**). By increasing contractility independent of adrenergic activation, cRadKO preserves the compensatory phase so that function and structure remain in a healthy range (**Figure 7.15**) reminiscent of endurance training [309] rather than the canonical heart failure phenotypes. Our work is further supported by evidence of down-regulation of Rad protein seen in patients with nonischemic heart failure [23, 181]. As encouraging as the present results are for suggesting Rad as a therapeutic direction for cardioprotection, future studies should investigate the effects of Rad deletion in heart failure in larger animal species.

A major consideration in using positive inotropes as a treatment for heart failure is the energetic demands that these drugs incur. In normal cardiomyocytes, calcium activates both ATP-consumption and ATP-regeneration in order to maintain the redox state of NADH and $FADH_2$ [5]. However, under conditions of failure, calcium uptake into the mitochondria is disrupted and leads to oxidative stress [5, 310, 311]. This promotes arrhythmias, systolic dysfunction, and pathological remodeling [5, 311]. A theory to avoid this mismatch is to increase sarcoplasmic reticulum calcium content and release, supported by animal models and patients with improved left ventricular ejection fraction having significant upregulation of SERCA [312, 313]. We have previously shown that myocardial Rad deletion promotes upregulation of SERCA without a reciprocal upregulation of PLN in the presence of elevated systolic function and no pathological remodeling [24]. Data shown in chapter 2 and 3 also show no detectable arrhythmias or electrical dysfunction in cRadKO without heart failure; after pressure-overload, cRadKO still demonstrated

accelerated kinetics that resemble $I_{Ca,L}$ kinetics measured from healthy cRadKO myocytes (**Figure 7.7**). It is therefore possible that the deletion of Rad is preserving the balance of ATP-consumption and ATP-regeneration, allowing cardiac function to be protected in the presence of pressure-overload induced heart failure. Future studies should explore the role in which Rad contributes to energy production within the myocardium, and the mechanism by which the absence of Rad potentially improves mitochondrial function. This would give more insight into how positive inotropes could balance excitation contraction coupling and the energetic demands of the heart to provide better, more sustainable treatment [5].

7.4.2 Myocardial-restricted Rad deletion differs from whole-body knockout of Rad

In the TAC model the heart experiences an abrupt and chronic increase of afterload. Despite a large number of studies utilizing the TAC model for pressure overload hypertrophy the initial signaling effects that signal compensatory changes in the myocardium are poorly understood [192]. When Rad is deleted before surgery, cRadKO showed an increase of fibrosis (**Figure 7.3**), suggesting that while myocardial Rad deletion spares functional and myocardial architectural remodeling, the heart remains responsive to effectors activated in response to TAC surgery. In whole-body Rad knockout mice, CTGF is elevated and fibrosis spontaneously develops as early as ten weeks of age [198]; in contrast, myocardial Rad deletion did not demonstrate any spontaneous fibrosis or increased expression of CTGF [24], except under the stress of pressure-overload in our current study. Rad has also been associated with non-LTCC functions [21, 145, 211], thus, we cannot rule out contributions to transcriptional regulation or cell signaling outside the LTCC signalosome. Our finding that TAC induced fibrosis is present without detriment to

function following TAC also raises an interesting question – namely, the suggestion here is that cRadKO illuminates a possible distinction between fibrotic signaling and protection against loss of function as an association rather than a necessary cause-effect relationship, at least in certain cases. In summary, in sharp contrast to global Rad knockout studies, we now show that myocardial Rad deletion is beneficial for heart function in health in response to imposed chronic pressure overload.

In conclusion, our findings suggest that increasing positive inotropy through myocardial-restricted Rad deletion protects the cardiac function from pressure-overload induced heart failure by maintaining a compensated-like heart. Deleting Rad also rescues cardiac function in advanced stages of pressure-overload induced heart failure. There is a major unmet need for treatments targeting inotropy [5]; these results support Rad as a potential therapeutic approach for increasing cardiac output safely without promoting pathological remodeling.

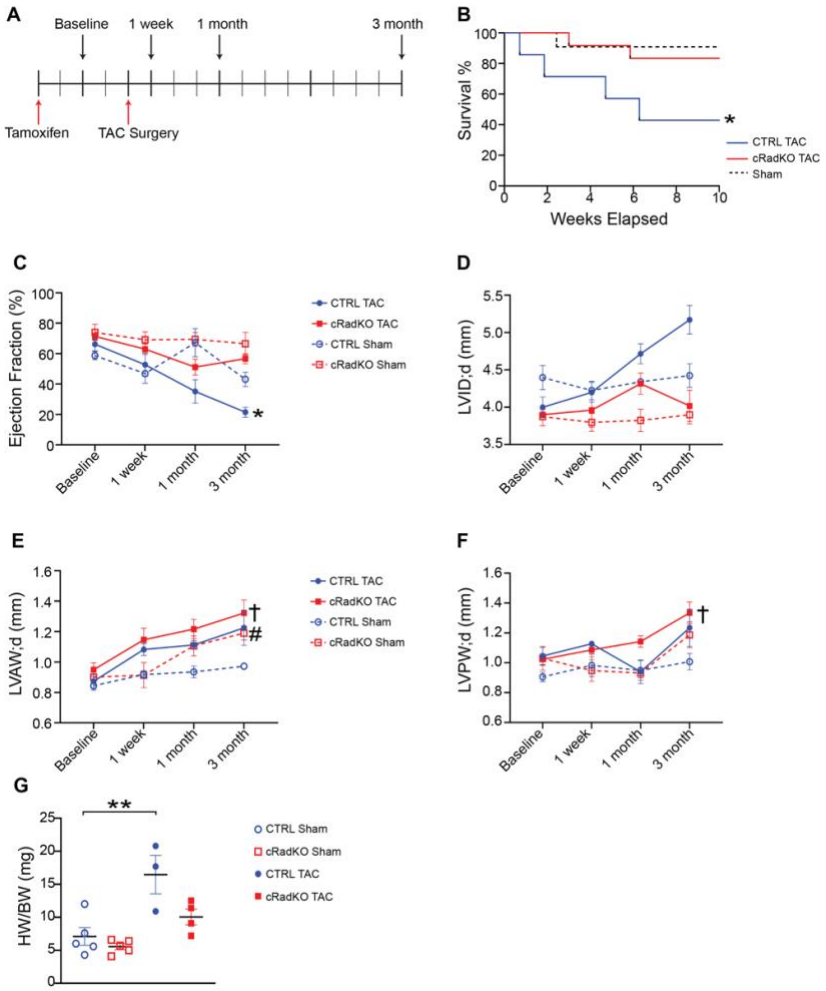

Figure 7.1 Loss of cardiomyocyte Rad before pressure overload prevents progression of cardiac dysfunction.

A) Experimental timeline. Red arrows indicate time of tamoxifen injection and TAC surgery. Black arrows above timeline indicate echocardiography time points following surgery. **B)** Kaplan-Meier survival plot of CTRL with TAC, cRadKO with TAC, and Sham. Between group differences in survival were tested by Gehan-Breslow-Wolcoxon test (*p = 0.03). **C-F)** Echocardiographic assessment of ejection fraction (**C**, *p = 0.05), left ventricular inner dimensions in diastole (**D**), and left ventricular wall thickness of anterior wall (**E**, ††p = 0.007, ##p = 0.009); posterior wall in diastole (**F**, †p = 0.01). Data in C-F analyzed by 2-way repeated measures ANOVA with Dunnett's multiple comparisons test. Data displayed from male mice; CTRL (Sham: N = 3; TAC: N = 3) and cRadKO (Sham: N = 6; TAC: N = 9). **G)** Heart-to-body weight ratio at 3 months post-TAC (**p = 0.002). Data from mice that did not survive not included. Data in G analyzed by 1-way ANOVA with Dunnett's multiple comparisons test. Data displayed from male mice; CTRL (Sham: N = 5; TAC: N = 3) and cRadKO (Sham: N = 5; TAC: N = 4). For all panels: *CTRL Sham v CTRL TAC; †CTRL Sham v cRadKO TAC; #CTRL Sham v cRadKO Sham.

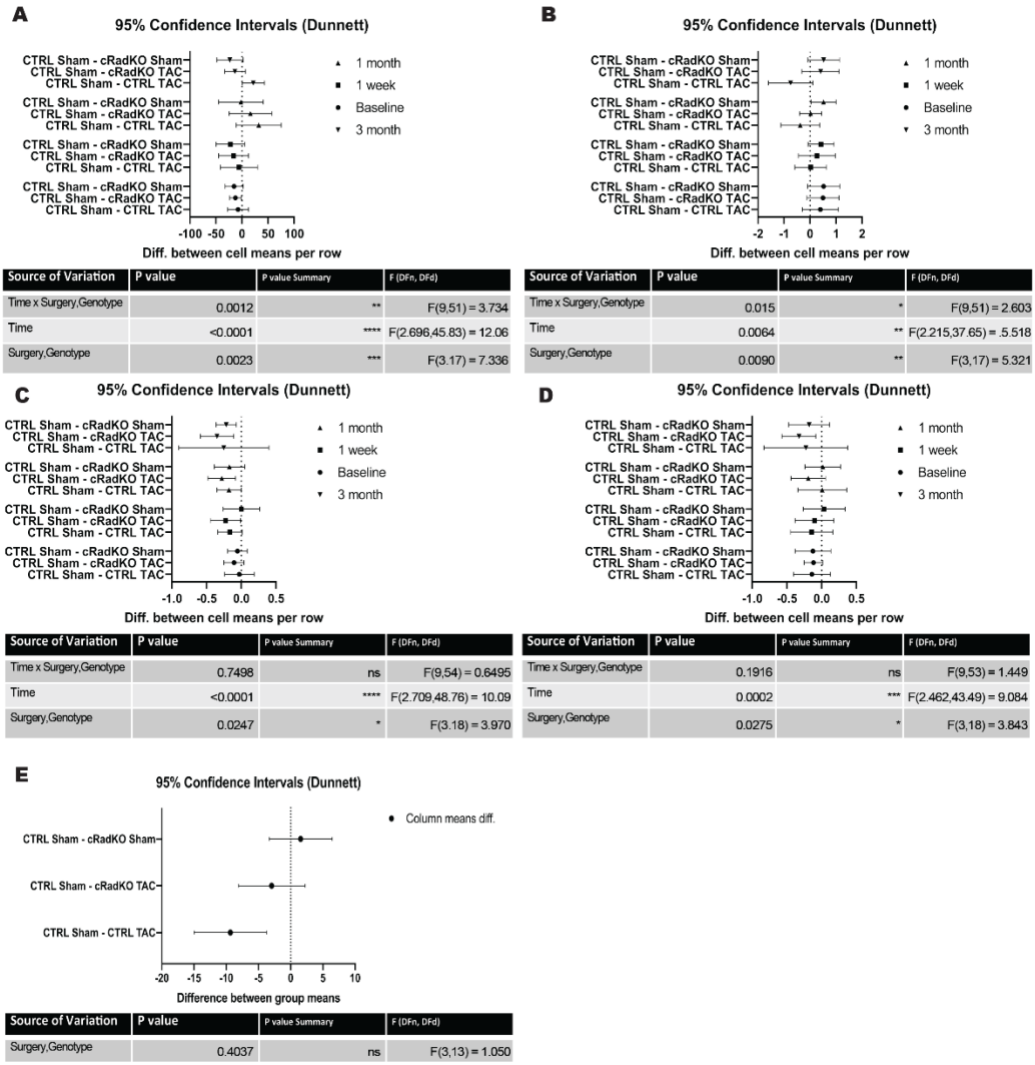

Source of Variation	P value	P value Summary	F (DFn, DFd)
Time x Surgery,Genotype	0.0012	**	F(9,51) = 3.734
Time	<0.0001	****	F(2.696,45.83) = 12.06
Surgery,Genotype	0.0023	***	F(3,17) = 7.336

Source of Variation	P value	P value Summary	F (DFn, DFd)
Time x Surgery,Genotype	0.015	*	F(9,51) = 2.603
Time	0.0064	**	F(2.215,37.65) = .5.518
Surgery,Genotype	0.0090	**	F(3,17) = 5.321

Source of Variation	P value	P value Summary	F (DFn, DFd)
Time x Surgery,Genotype	0.7498	ns	F(9,54) = 0.6495
Time	<0.0001	****	F(2.709,48.76) = 10.09
Surgery,Genotype	0.0247	*	F(3,18) = 3.970

Source of Variation	P value	P value Summary	F (DFn, DFd)
Time x Surgery,Genotype	0.1916	ns	F(9,53) = 1.449
Time	0.0002	***	F(2.462,43.49) = 9.084
Surgery,Genotype	0.0275	*	F(3,18) = 3.843

Source of Variation	P value	P value Summary	F (DFn, DFd)
Surgery,Genotype	0.4037	ns	F(3,13) = 1.050

Figure 7.2 ANOVA 95% confidence intervals and tabular results.
A) 95% confidence intervals and tabular results for two-way ANOVA for Figure 7.1C. **B)** 95% confidence intervals and tabular results for two-way ANOVA for Figure 7.1D. **C)** 95% confidence intervals and tabular results for two-way ANOVA for Figure 7.1E. **D)** 95% confidence intervals and tabular results for two-way ANOVA for Figure 7.1F. **E)** 95% confidence intervals and tabular results for one-way ANOVA for Figure 7.1G.

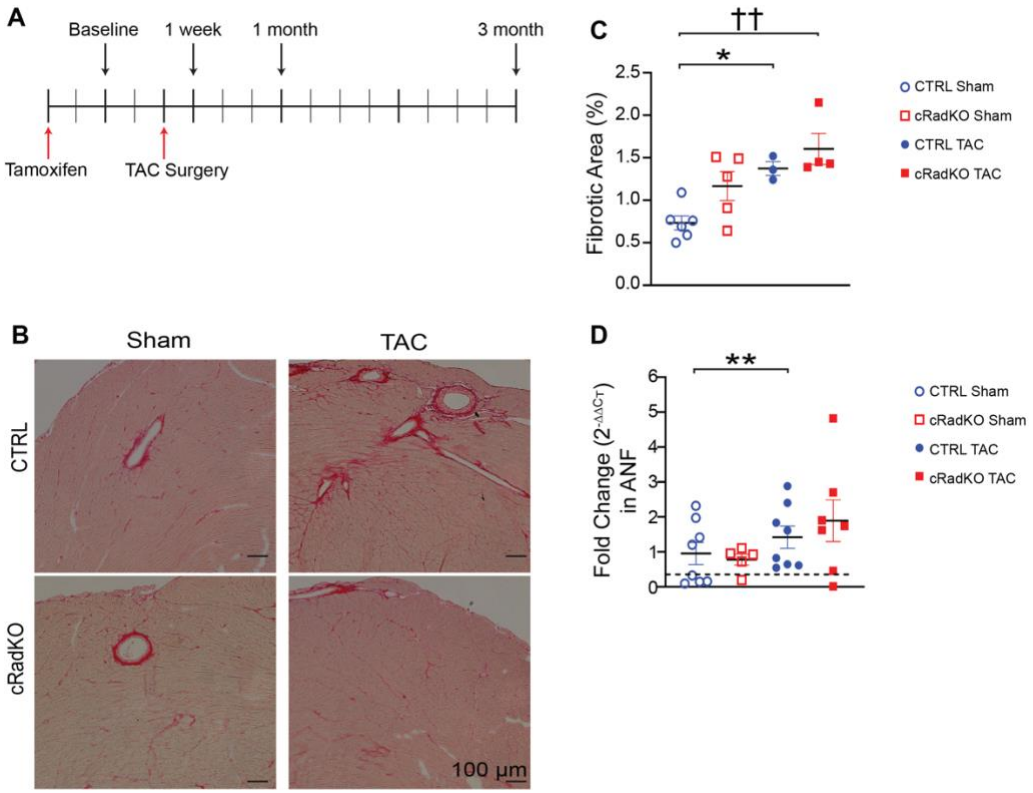

Figure 7.3 Loss of cardiomyocyte Rad before pressure overload does not protect all pathological signaling.
A) Experimental timeline. **B)** Representative pictures of picrosirius Red staining with fibrosis quantification in **C)** (*p = 0.02; ††p = 0.001); Scale bar: 100 µm. Data displayed from male mice; CTRL (Sham: N = 6; TAC: N = 3) and cRadKO (Sham: N = 4; TAC: N = 5). **D)** qRT-PCR for ANF mRNA expression levels. Data analyzed by one-way ANOVA plus Dunnett's multiple comparisons test. Data displayed from male mice; CTRL (Sham: N = 8; TAC: N = 8) and cRadKO (Sham: N = 5; TAC: N = 7). For all panels: *CTRL Sham v CTRL TAC; †CTRL Sham v cRadKO TAC; #CTRL Sham v cRadKO Sham.

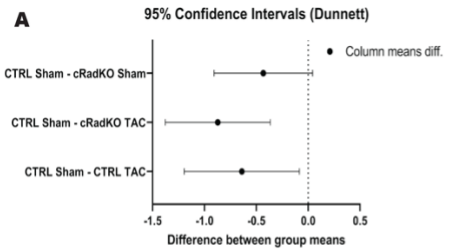

Source of Variation	P value	P value Summary	F (DFn, DFd)
Time x Surgery,Genotype	0.7498	ns	F(9,54) = 0.6495
Time	<0.0001	****	F(2.709,48.76) = 10.09
Surgery,Genotype	0.0247	*	F(3,18) = 3.970

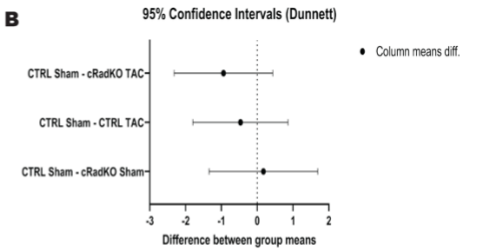

Source of Variation	P value	P value Summary	F (DFn, DFd)
Time x Surgery,Genotype	0.1916	ns	F(9,53) = 1.449
Time	0.0002	***	F(2.462,43.49) = 9.084
Surgery,Genotype	0.0275	*	F(3,18) = 3.843

Figure 7.4 One-way ANOVA 95% confidence intervals and tabular results. **A)** 95% confidence intervals and tabular results for two-way ANOVA for Figure 7.3C. **B)** 95% confidence intervals and tabular results for two-way ANOVA for Figure 7.3D.

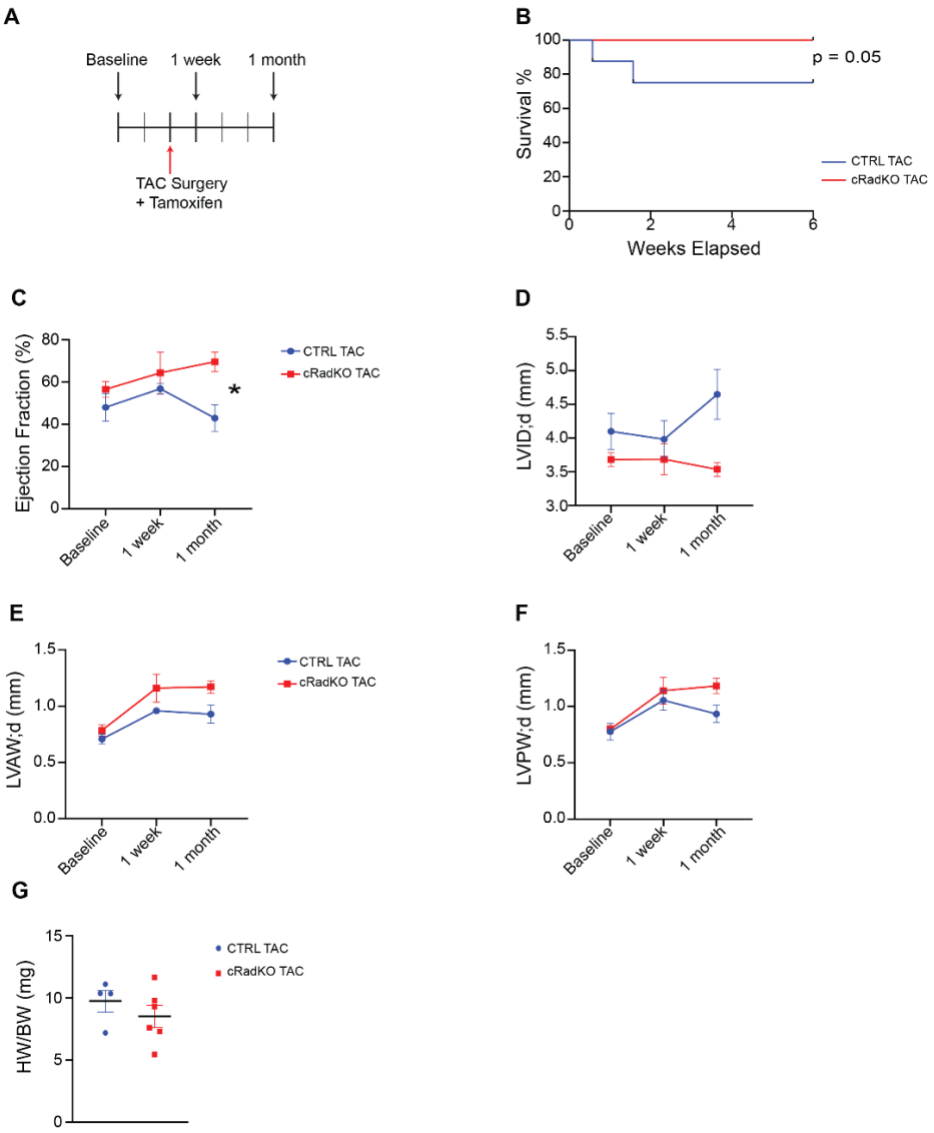

Figure 7.5 Loss of cardiomyocyte Rad before pressure overload promotes survival and enhances cardiac function.
A) Experimental timeline. Red arrows indicate time of tamoxifen injection and TAC surgery. Black arrows above timeline indicate echocardiography time points following surgery. **B)** Kaplan-Meier survival plot of CTRL with TAC and cRadKO with TAC. Between group differences in survival were tested by Gehan-Breslow-Wolcoxon test (p = 0.05). **C-F)** Echocardiographic assessment of ejection fraction (**C**, *p = 0.04), left ventricular inner dimensions in diastole (**D**), and left ventricular wall thickness of anterior wall (**E**); posterior wall in diastole (**F**). Data in C-F analyzed by 2-way repeated measures ANOVA with Šídák's multiple comparisons test. Data displayed from female mice; CTRL (N = 4) and cRadKO (N = 8). **G)** Heart-to-body weight ratio at 3 months post-TAC and post Rad deletion. Data from mice that did not survive not included. Data in G analyzed by Student's unpaired *t*-test with Welch's correction. Data displayed from female mice; CTRL (N = 4) and cRadKO (N = 6).

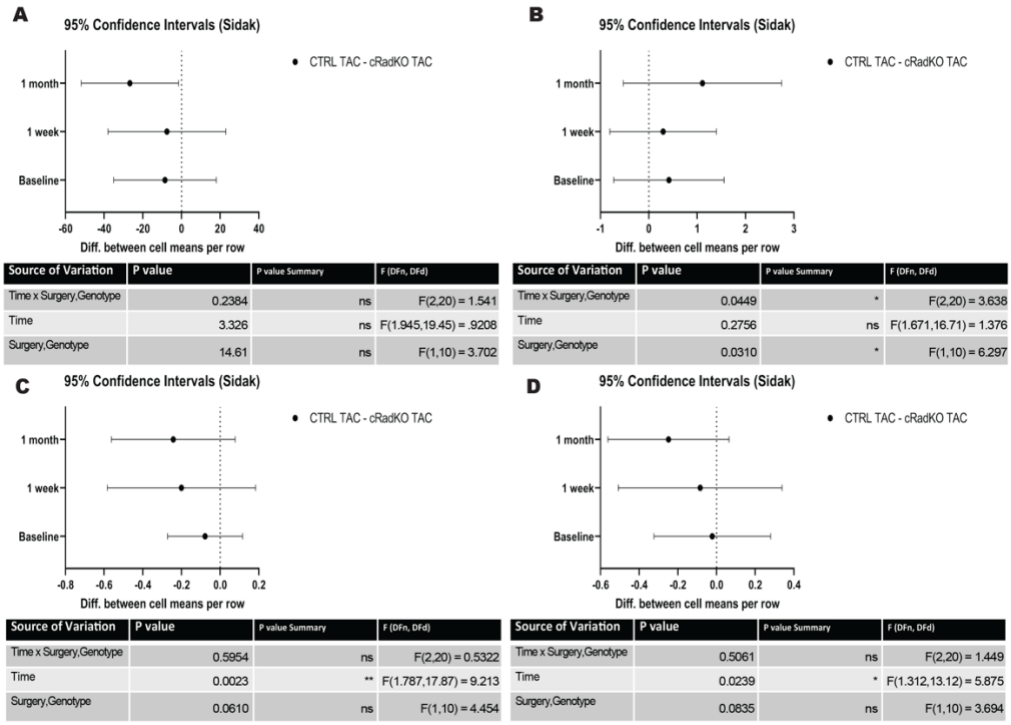

Source of Variation	P value	P value Summary	F (DFn, DFd)
Time x Surgery,Genotype	0.2384	ns	F(2,20) = 1.541
Time	3.326	ns	F(1.945,19.45) = .9208
Surgery,Genotype	14.61	ns	F(1,10) = 3.702

Source of Variation	P value	P value Summary	F (DFn, DFd)
Time x Surgery,Genotype	0.0449	*	F(2,20) = 3.638
Time	0.2756	ns	F(1.671,16.71) = 1.376
Surgery,Genotype	0.0310	*	F(1,10) = 6.297

Source of Variation	P value	P value Summary	F (DFn, DFd)
Time x Surgery,Genotype	0.5954	ns	F(2,20) = 0.5322
Time	0.0023	**	F(1.787,17.87) = 9.213
Surgery,Genotype	0.0610	ns	F(1,10) = 4.454

Source of Variation	P value	P value Summary	F (DFn, DFd)
Time x Surgery,Genotype	0.5061	ns	F(2,20) = 1.449
Time	0.0239	*	F(1.312,13.12) = 5.875
Surgery,Genotype	0.0835	ns	F(1,10) = 3.694

Figure 7.6 ANOVA 95% confidence intervals and tabular results.
A) 95% confidence intervals and tabular results for two-way ANOVA for Figure 7.5C. **B)** 95% confidence intervals and tabular results for two-way ANOVA for Figure 7.5D. **C)** 95% confidence intervals and tabular results for two-way ANOVA for Figure 7.5E. **D)** 95% confidence intervals and tabular results for two-way ANOVA for Figure 7.5F.

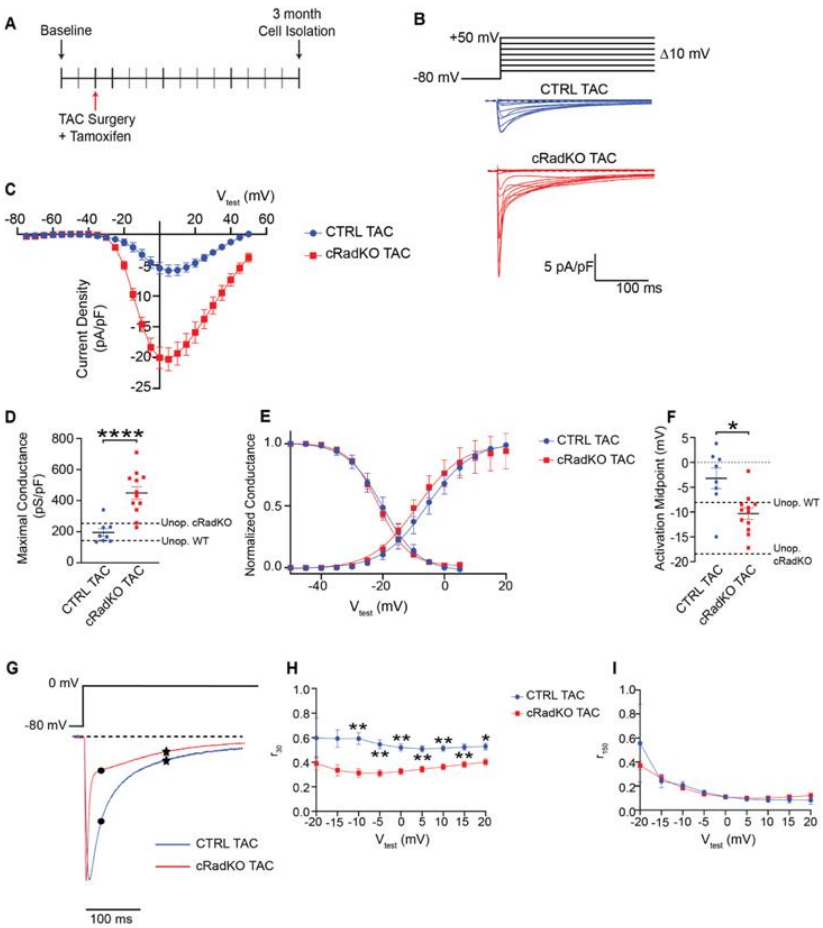

Figure 7.7 Loss of cardiomyocyte Rad increases ICa,L after pressure-overload.

A) Experimental timeline showing study design. **B)** Exemplar family of Ca^{2+} currents of CTRL TAC (blue) and cRadKO TAC (red) from V_{test} ranging from -75 to +50 mV in 10 mV increments (voltage protocol shown above); Scale bar: 5 pA/pF, 100 ms. **C)** Current-voltage relationship for peak $I_{Ca,L}$ current density from CTRL TAC and cRadKO TAC ventricular myocytes. **D)** Maximal conductance is significantly increased in cRadKO TAC compared to CTRL TAC (****$p < 0.0001$; dotted lines represent maximal conductance for published unoperated WT and cRadKO, included for reference). **E)** Conductance-voltage curves normalized to maximal conductance in CTRL TAC and cRadKO TAC. Smooth curves are Boltzmann distribution fitted to data. **F)** Activation midpoint is significantly negative-shifted in cRadKO TAC (*$p = 0.01$). **G)** Exemplar Ca^{2+} currents with EGTA for CTRL TAC (blue) and cRadKO TAC (red), traces normalized to peak current at 0 mV Scale bar: 100 ms. Black dots indicate r_{30}, Black stars indicate r_{150}. Remaining current across voltage steps 30 ms after peak **H)** and 150 ms after peak **I)**. P values calculated using Student unpaired t-test for (**D,F**). Data in (**H,I**) analyzed by two-way ANOVA plus Šídák's multiple comparisons test (**$p < 0.009$; *$p < 0.03$). Data displayed from female mice; CTRL (N = 4 mice, n = 8 cells) and cRadKO (N = 4 mice; n = 12 cells).

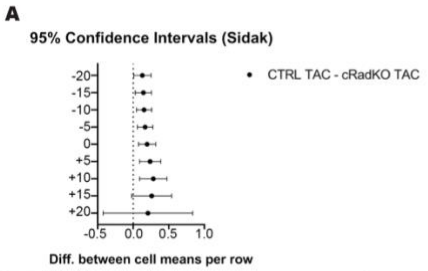

Source of Variation	P value	P value Summary	F (DFn, DFd)
Voltage x Surgery,Genotype	0.2464	ns	F(8,144) = 1.303
Voltage	0.3589	ns	F(1.400,25.20) = 0.987
Surgery,Genotype	0.0010	**	F(1,18) = 15.35

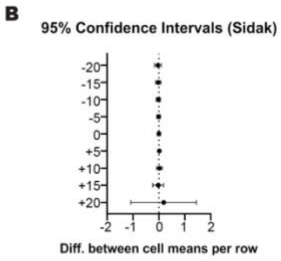

Source of Variation	P value	P value Summary	F (DFn, DFd)
Voltage x Surgery,Genotype	0.8127	ns	F(8,144) = .5555
Voltage	0.0135	*	F(1.067,19.20) = 7.180
Surgery,Genotype	0.7075	ns	F(1,18) = .1453

Figure 7.8 ANOVA 95% confidence intervals and tabular results.
A) 95% confidence intervals and tabular results for two-way ANOVA for Figure 7.7H. **B)** 95% confidence intervals and tabular results for two-way ANOVA for Figure 7.7I.

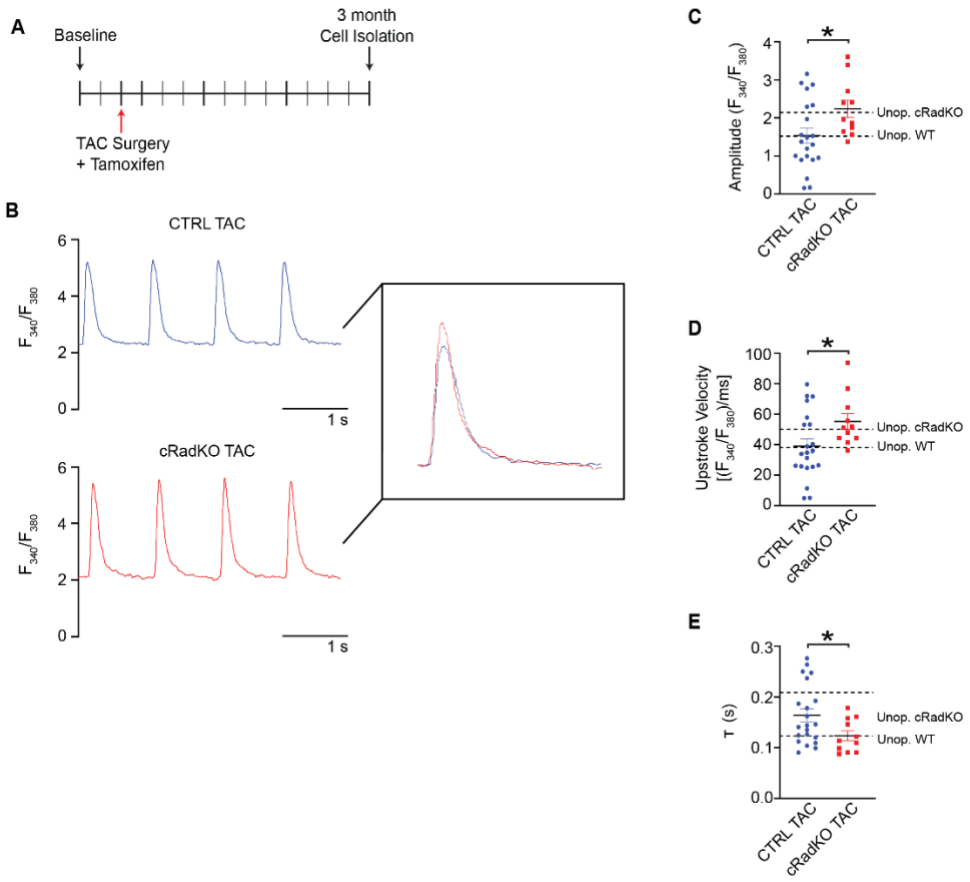

Figure 7.9 Loss of cardiomyocyte Rad enhances cellular calcium handling after pressure-overload.
A) Experimental timeline showing study design. **B)** Representative calcium transients from isolated ventricular cardiomyocytes loaded with fura2-AM, CTRL TAC (top, blue) and cRadKO TAC (bottom, red) paced at 1 Hz. Scale bar: 1 second. **C)** Amplitude of the calcium transients from cRadKO TAC are larger compared to CTRL TAC (*p = 0.03). **D)** The velocity at which calcium enters the cytosol (upstroke of the transient) is significantly faster in cRadKO TAC compared to CTRL TAC (*p = 0.03). **E)** Rate at which calcium leaves the cytosol (downstroke of the transient) is significantly faster in cRadKO TAC compared to CTRL TAC (*p = 0.02). P values calculated using Student unpaired *t*-test for (**C-E**). Data displayed from female mice; CTRL (N = 5 mice, n = 21 cells) and cRadKO (N = 3 mice; n = 11 cells).

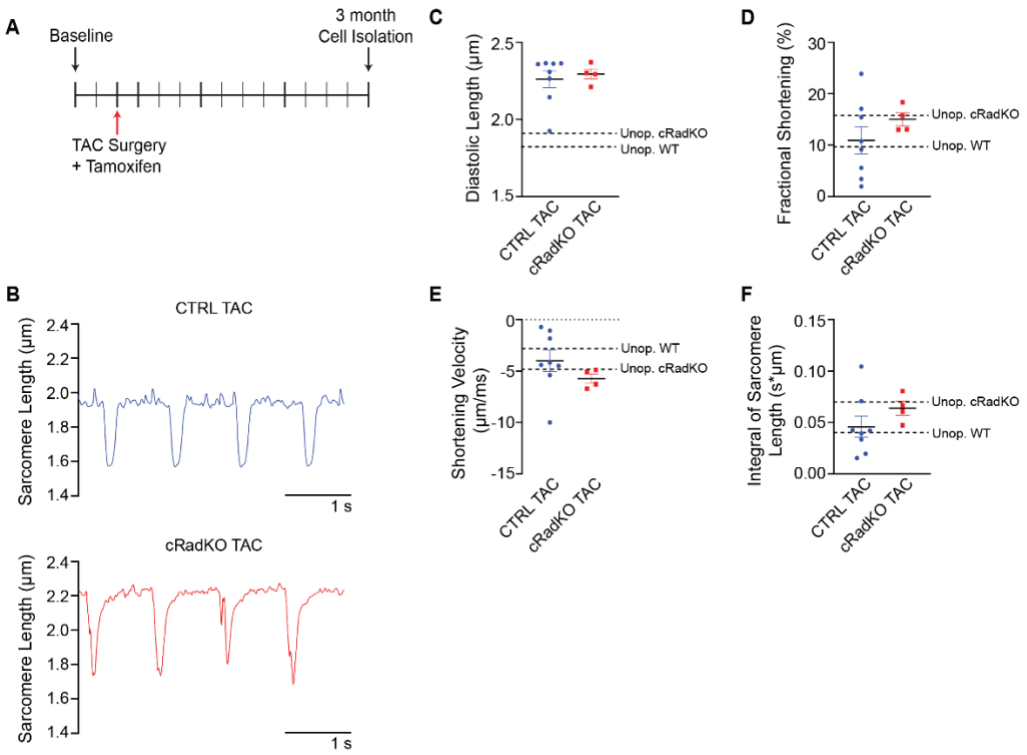

Figure 7.10 Loss of cardiomyocyte Rad does not alter sarcomere dynamics after pressure-overload.

A) Experimental timeline showing study design. **B)** Exemplar sarocomere length traces from isolated ventricular cardiomyocytes loaded with fura2-AM, CTRL TAC (top, blue) and cRadKO TAC (bottom, red) paced at 1 Hz. Scale bar: 1 second. **C)** Diastolic sarcomere length (dotted lines represent means of diastolic length for published unoperated WT and cRadKO, included for reference). **D)** Sarcomere fractional shortening (dotted lines represent means of diastolic length for published unoperated WT and cRadKO, included for reference). **E)** Sarcomere shortening velocity (dotted lines represent means of diastolic length for published unoperated WT and cRadKO, included for reference). **F)** Integral of sarcomere length (dotted lines represent means of diastolic length for published unoperated WT and cRadKO, included for reference). P values calculated using Student unpaired *t*-test for (**C-F**). Data displayed from female mice; CTRL (N = 5 mice, n = 8 cells) and cRadKO (N = 3 mice; n = 4 cells).

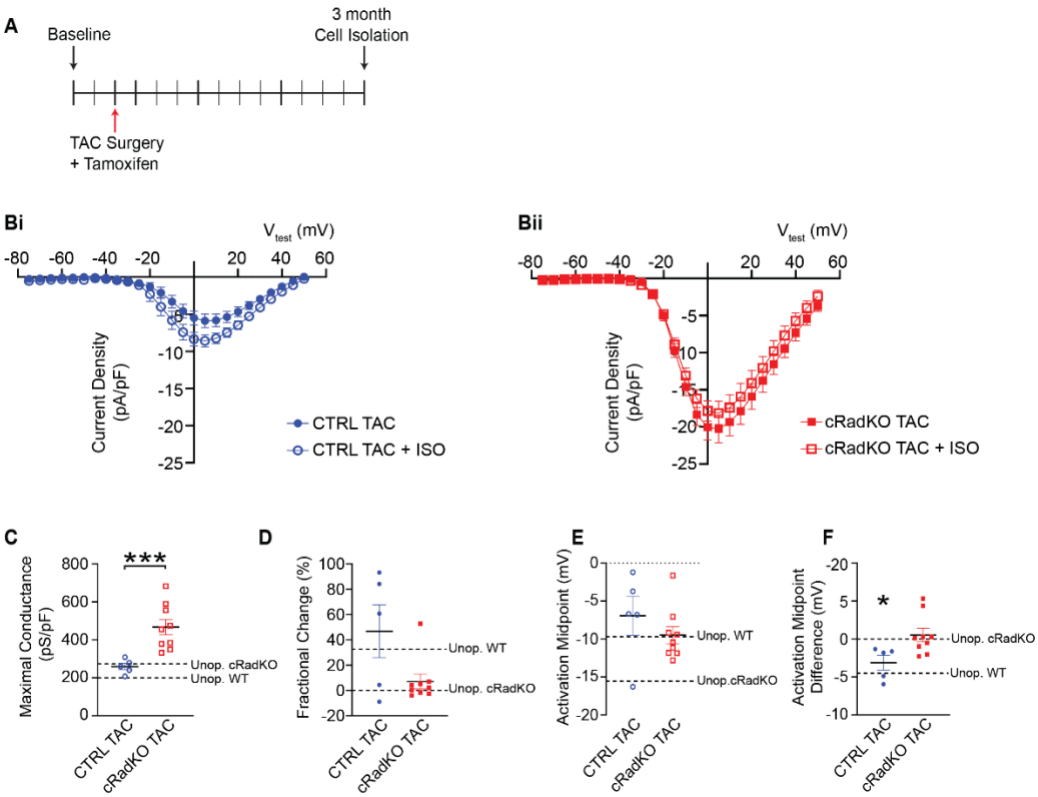

Figure 7.11 β-AR stimulation does not alter $I_{Ca,L}$ in Rad deletion after pressure-overload.

A) Experimental timeline showing study design. **Bi,ii)** Current-voltage relationship for peak $I_{Ca,L}$ current density from CTRL TAC (left, blue) and cRadKO TAC (right, red) from isolated ventricular myocytes after treatment with 300 nM isoproterenol (ISO). **C)** Maximal conductance is significantly increased in cRadKO TAC compared to CTRL TAC (***p = 0.0007; dotted lines represent maximal conductance for published unoperated WT + ISO and cRadKO + ISO, included for reference). **D)** Fractional change of maximal conductance between baseline and ISO response of CTRL TAC (mean = 47%) and cRadKO (mean = 7%). Neither group demonstrated a significant response, as measured by deviation from zero. **E)** Activation midpoint is not significantly negative-shifted in cRadKO TAC compared to CTRL TAC after treatment with ISO (dotted lines represent maximal conductance for published unoperated WT + ISO and cRadKO + ISO, included for reference). **F)** Difference in activation midpoint between baseline and ISO response of CTRL TAC (mean = -3.1 mV) and cRadKO (mean = 0.51 mV). CTRL TAC demonstrated a significant response, as measured by deviation from zero (*p = 0.03). P values calculated using Student unpaired *t*-test for (**C,E**) and one sample *t*-test for (**D,F**). Data displayed from female mice; CTRL (N = 3 mice, n = 5 cells) and cRadKO (N = 4 mice; n = 9 cells).

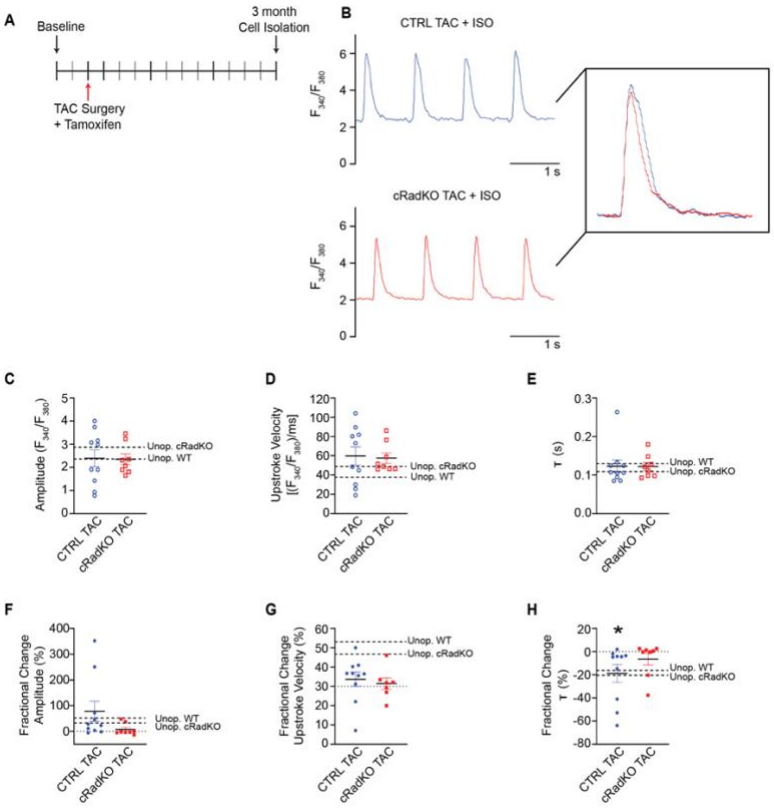

Figure 7.12 β-AR stimulation response in cellular calcium handling is blunted after pressure-overload.

A) Experimental timeline showing study design. **B)** Representative calcium transients from isolated ventricular cardiomyocytes loaded with fura2-AM, CTRL TAC (top, blue) and cRadKO TAC (bottom, red) after treatment with 1 µM isoproterenol (ISO), paced at 1 Hz. Scale bar: 1 second. **C)** Amplitude of the calcium transients from cRadKO TAC and CTRL TAC after treatment with ISO. **D)** The velocity at which calcium enters the cytosol (upstroke of the transient) in cRadKO TAC and CTRL TAC after treatment with ISO. **E)** Rate at which calcium leaves the cytosol (downstroke of the transient) in cRadKO TAC and CTRL TAC after treatment with ISO. **F)** Fractional change of amplitude between baseline and ISO response of CTRL TAC (mean = 78%) and cRadKO (mean = 7%). Neither group demonstrated a significant response, as measured by deviation from zero. **G)** Fractional change of upstroke velocity between baseline and ISO response of CTRL TAC (mean = 7%) and cRadKO (mean = 3%). Neither group demonstrated a significant response, as measured by deviation from zero. **H)** Fractional change of rate of decay between baseline and ISO response of CTRL TAC (mean = -19%) and cRadKO (mean = -6%). CTRL demonstrated a significant response, as measured by deviation from zero (*p = 0.04). P values calculated using Student unpaired *t*-test for (**C-E**) and one sample *t*-test for (**F-H**). Data displayed from female mice; CTRL (N = 4 mice, n = 10 cells) and cRadKO (N = 3 mice; n = 8 cells).

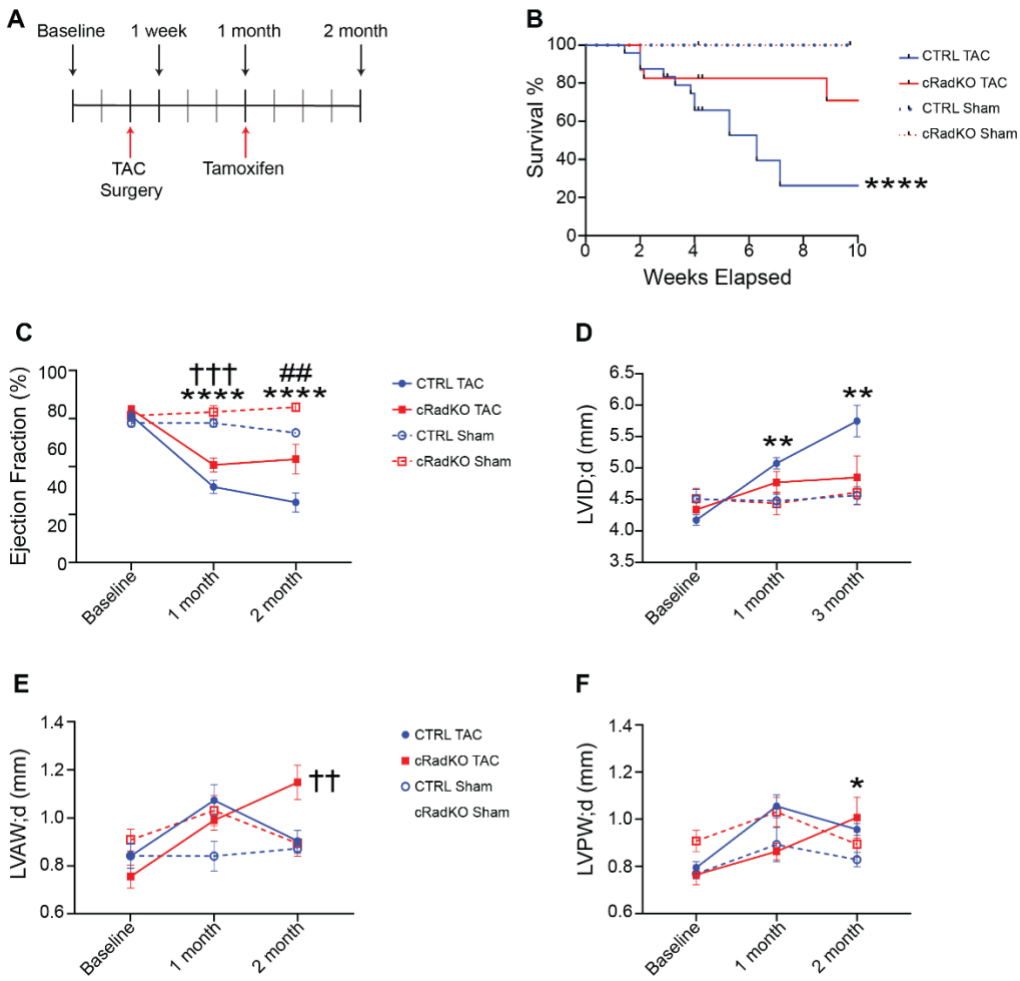

Figure 7.13 Loss of cardiomyocyte Rad after pressure overload prevents progression of cardiac dysfunction.

A) Experimental timeline. Red arrows indicate time of TAC surgery and time of tamoxifen injection 1-month post-surgery. Black arrows above timeline indicate echocardiography time points following surgery. **B)** Kaplan-Meier survival plot of CTRL with TAC, cRadKO with TAC, and Sham. Between group differences in survival were tested by Gehan-Breslow-Wolcoxon test (****$p < 0.0001$). **C-F)** Echocardiographic assessment of ejection fraction (**C**, ****$p < 0.0001$; †††$p = 0.0003$; ##$p = 0.002$), left ventricular inner dimensions in diastole (**D**, **$p = 0.003$), and left ventricular wall thickness of anterior wall (**E,** ††$p = 0.009$); posterior wall in diastole (**F**, *$p = 0.02$). Data in C-F analyzed by 2-way repeated measures ANOVA with Dunnett's multiple comparisons test. Data displayed from male mice; CTRL (Sham: N = 6; TAC: N = 10) and cRadKO (Sham: N = 7; TAC: N = 10). Data from mice that did not survive not included. For all panels: *CTRL Sham v CTRL TAC; †CTRL Sham v cRadKO TAC; #CTRL Sham v cRadKO Sham.

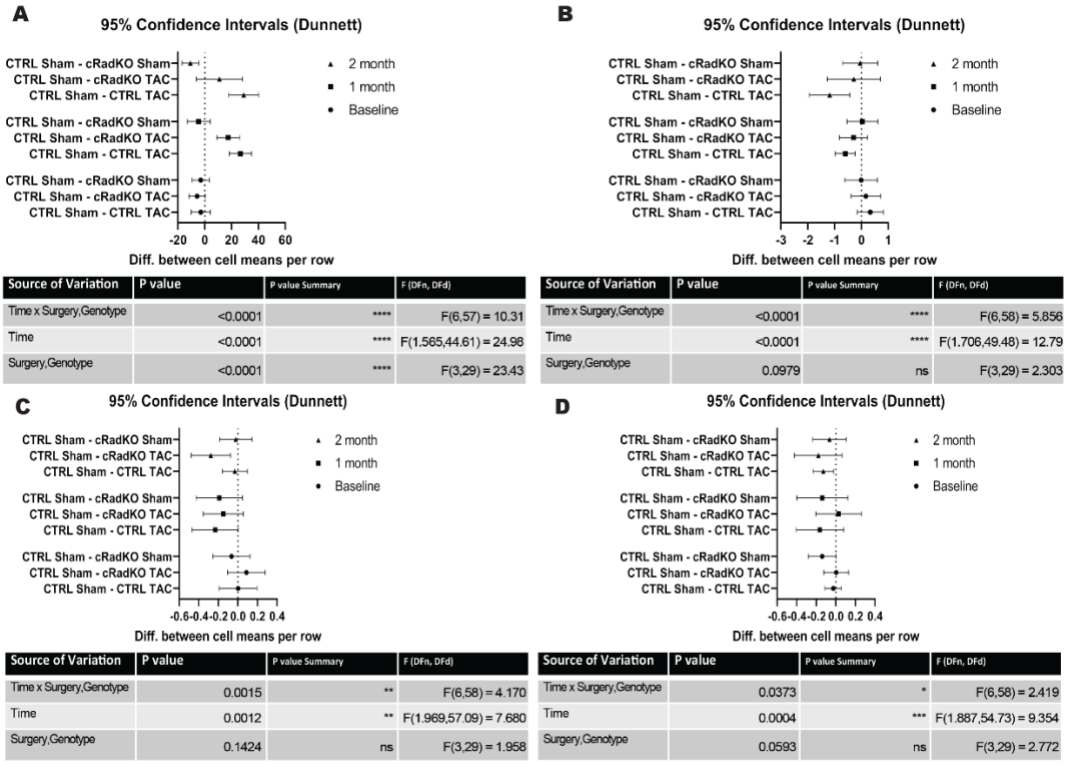

Source of Variation	P value	P value Summary	F (DFn, DFd)
Time x Surgery,Genotype	<0.0001	****	F(6,57) = 10.31
Time	<0.0001	****	F(1.565,44.61) = 24.98
Surgery,Genotype	<0.0001	****	F(3,29) = 23.43

Source of Variation	P value	P value Summary	F (DFn, DFd)
Time x Surgery,Genotype	<0.0001	****	F(6,58) = 5.856
Time	<0.0001	****	F(1.706,49.48) = 12.79
Surgery,Genotype	0.0979	ns	F(3,29) = 2.303

Source of Variation	P value	P value Summary	F (DFn, DFd)
Time x Surgery,Genotype	0.0015	**	F(6,58) = 4.170
Time	0.0012	**	F(1.969,57.09) = 7.680
Surgery,Genotype	0.1424	ns	F(3,29) = 1.958

Source of Variation	P value	P value Summary	F (DFn, DFd)
Time x Surgery,Genotype	0.0373	*	F(6,58) = 2.419
Time	0.0004	***	F(1.887,54.73) = 9.354
Surgery,Genotype	0.0593	ns	F(3,29) = 2.772

Figure 7.14 ANOVA 95% confidence intervals and tabular results.
A) 95% confidence intervals and tabular results for two-way ANOVA for Figure 7.13C. **B)** 95% confidence intervals and tabular results for two-way ANOVA for Figure 7.13D. **C)** 95% confidence intervals and tabular results for two-way ANOVA for Figure 7.13E. **D)** 95% confidence intervals and tabular results for two-way ANOVA for Figure 7.13F.

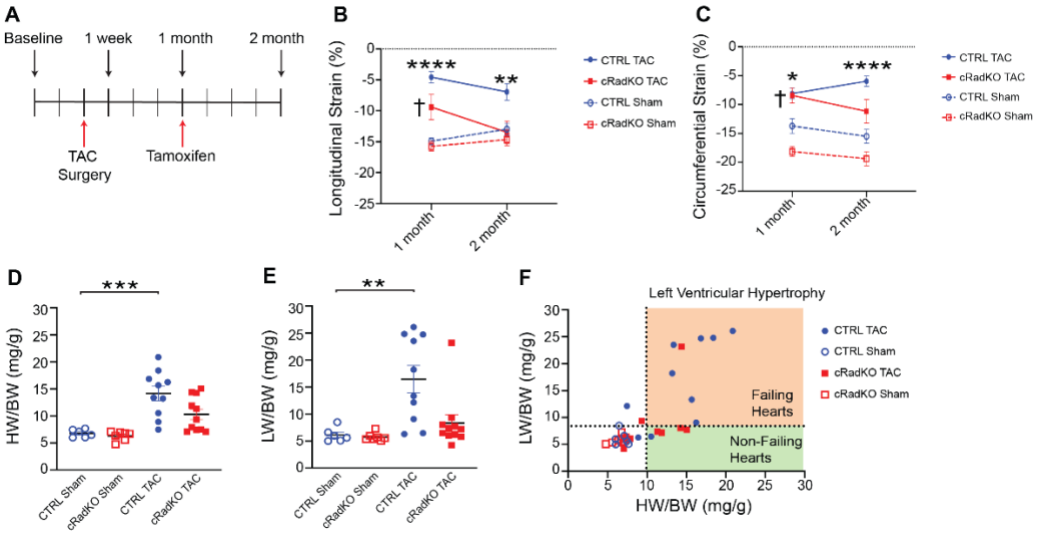

Figure 7.15 Loss of cardiomyocyte Rad after pressure overload prevents progression of cardiac dysfunction.

A) Experimental timeline. **B)** Pooled data for longitudinal strain. Rad deletion increased global longitudinal strain (****p < 0.0001; ††p = 0.0003; **p = 0.03). **C)** Pooled data for circumferential strain. Rad deletion enhanced circumferential strain (*p = 0.01; †p = 0.02; ****p < 0.0001). **D)** Heart weight to body weight ratio measured two-months post-surgery, one-month post Rad deletion (***p = 0.0002). **E)** Lung weight to body weight ratio measured two-months post-surgery, one-month post Rad deletion (**p = 0.002). **F)** Linear regression of lung weight body weight ratio as a function of heart weight body weight ratio. Orange region indicates hearts with left ventricular hypertrophy and in failure; green region represents hearts with left ventricular hypertrophy but not in failure. Data in (**B,C**) analyzed by two-way repeated measures ANOVA with Dunnett's multiple comparisons test. Data in (**D,E**) analyzed by one-way ANOVA with Dunnett's multiple comparisons test. Data displayed from male mice; CTRL (Sham: N = 6; TAC: N = 10) and cRadKO (Sham: N = 7; TAC: N = 11). Data from mice that did not survive not included. For all panels: *CTRL Sham v CTRL TAC; †CTRL Sham v cRadKO TAC; #CTRL Sham v cRadKO Sham.

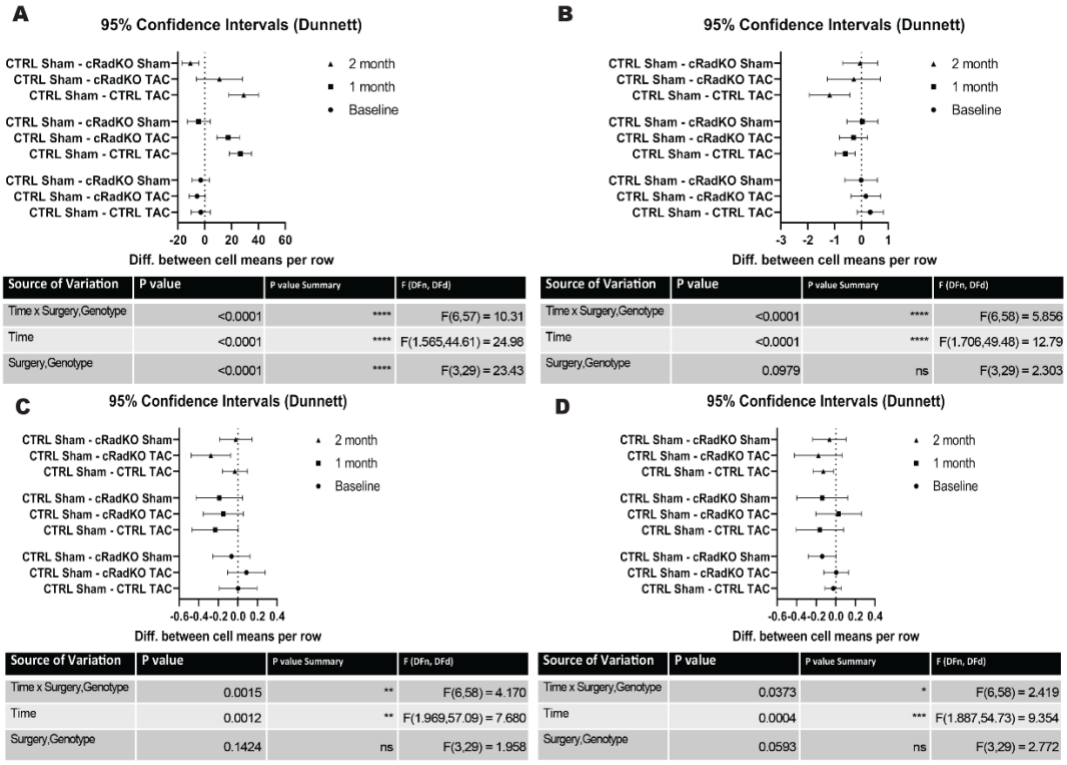

Source of Variation	P value	P value Summary	F (DFn, DFd)
Time x Surgery,Genotype	<0.0001	****	F(6,57) = 10.31
Time	<0.0001	****	F(1.565,44.61) = 24.98
Surgery,Genotype	<0.0001	****	F(3,29) = 23.43

Source of Variation	P value	P value Summary	F (DFn, DFd)
Time x Surgery,Genotype	<0.0001	****	F(6,58) = 5.856
Time	<0.0001	****	F(1.706,49.48) = 12.79
Surgery,Genotype	0.0979	ns	F(3,29) = 2.303

Source of Variation	P value	P value Summary	F (DFn, DFd)
Time x Surgery,Genotype	0.0015	**	F(6,58) = 4.170
Time	0.0012	**	F(1.969,57.09) = 7.680
Surgery,Genotype	0.1424	ns	F(3,29) = 1.958

Source of Variation	P value	P value Summary	F (DFn, DFd)
Time x Surgery,Genotype	0.0373	*	F(6,58) = 2.419
Time	0.0004	***	F(1.887,54.73) = 9.354
Surgery,Genotype	0.0593	ns	F(3,29) = 2.772

Figure 7.16 ANOVA 95% confidence intervals and tabular results.
A,B) 95% confidence intervals and tabular results for two-way ANOVA for Figure 7.15B,C respectively. **C,D)** 95% confidence intervals and tabular results for two-way ANOVA for Figure 7.13D,E respectively.

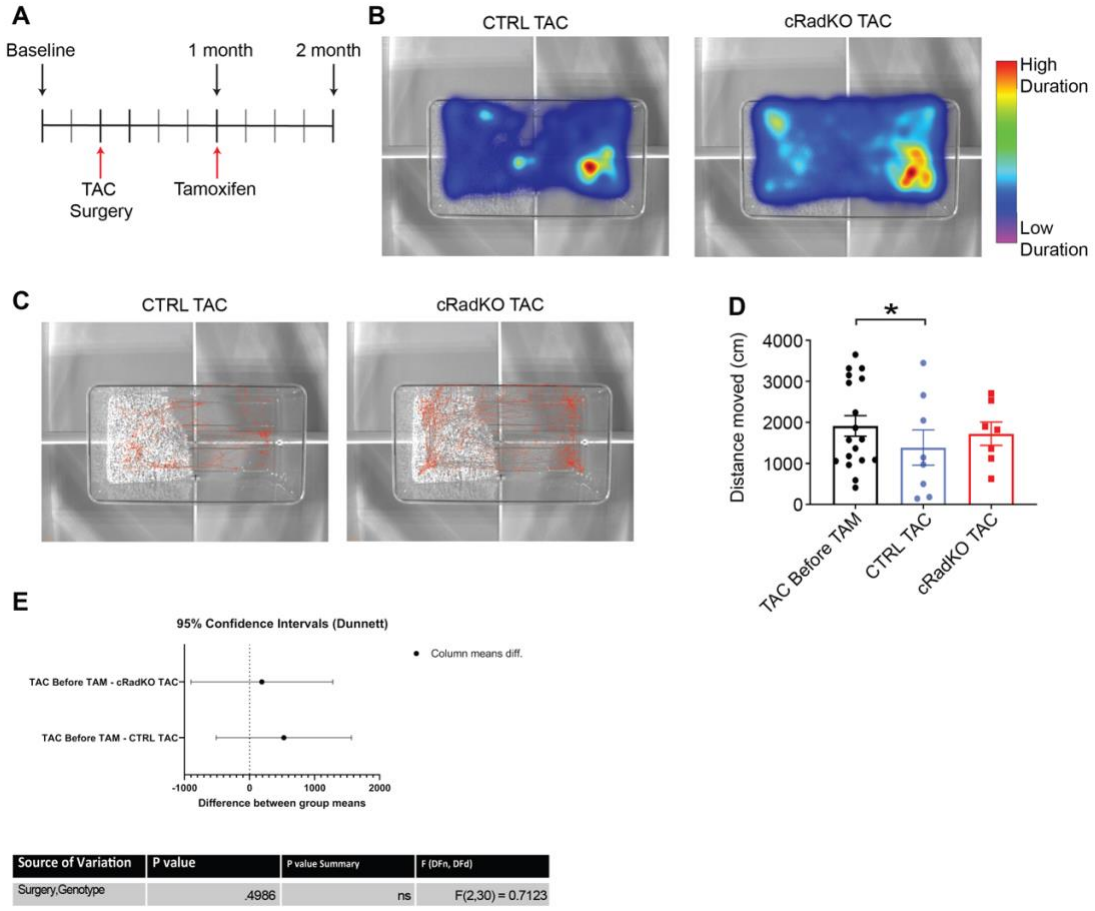

Source of Variation	P value	P value Summary	F (DFn, DFd)
Surgery,Genotype	.4986	ns	F(2,30) = 0.7123

Figure 7.17 Loss of cardiomyocyte Rad after pressure overload improves locomotive activity.

A) Experimental timeline. Black arrows indicate when behavior was measured (1 month after surgery, before tamoxifen injection, labeled as TAC Before TAC;2 months after surgery, 1 month after tamoxifen injection labeled as CTRL TAC or cRadKO TAC). **B)** Heat maps of activity in the open field, color is defined as the average time spent in seconds in a given location. Blue represents the least duration to Red, representing the highest duration. cRadKO TAC spent more time moving around within the open field compared to CTRL TAC. **C)** Representative 15 min. of tracks in the open field of CTRL TAC (left) and from cRadKO TAC (right). cRadKO TAC demonstrated more movement compared to CTRL TAC. **D)** Quantification of the distance covered within the open field. CTRL TAC mice covered significantly less distance compared to their one month time point (TAC Before TAM) while cRadKO covered similar distance (*p = 0.03). Data analyzed by one-way ANOVA plus Dunnett's multiple comparisons test, with 95% confidence intervals and tabular results in **E)**. Data displayed from male mice; TAC Before TAM (N = 15), CTRL TAC (N = 8), and cRadKO TAC (N = 7). For panel D: *TAC Before TAM v CTRL TAC; †TAC Before TAM v cRadKO TAC.

CHAPTER 8. DISCUSSION

A novel treatment for heart failure with reduced ejection fraction would be to improve contractility in a manner that preserves the fight-or-flight response within the heart. The main objective of this dissertation was to test the hypothesis that disrupting Rad inhibition of the L-Type calcium channel (LTCC) can stably enhance cardiac function by increasing LTCC calcium current ($I_{Ca,L}$) downstream of β-adrenergic receptor (β-AR) stimulation; this improves cardiac performance without inducing pathological remodeling and progression to heart failure. It is well established that the absence of Rad results in increased $I_{Ca,L}$ [17, 19-24, 288, 314]; however, the mechanism by which Rad inhibits the LTCC remains unclear [288]. The work of this dissertation contributes to the understanding of Rad-mediated LTCC inhibition by: 1) revealing the role of Rad in LTCC modulation, and 2) unmasking a potential new target to selectively enhance $I_{Ca,L}$ without promoting pathology. Each of these are discussed below.

8.1 Rad is a critical regulatory site for LTCC modulation

A major mechanism for modulating calcium cycling is sympathetic stimulation [6, 25, 28, 31, 92, 94, 95, 103]. cRadKO leads to enhanced basal $I_{Ca,L}$ resembling β-AR modulated $I_{Ca,L}$ (**Chapter 3, Chapter 4, Chapter 5).** The hallmark features of PKA-mediated LTCC modulation are: significant increase in $I_{Ca,L}$, hyperpolarized shift in voltage dependent activation, and increased rate of inactivation; all result in a gain of LTCC function [103]. In the absence of Rad, $I_{Ca,L}$ increases ~three fold compared to control (CTRL), voltage dependent activation is shifted to more negative potentials, and the rate of inactivation is accelerated in ventricular and sinoatrial cardiomyocytes (**Chapter 3, Figure 4; Chapter 4, Figure 3; Chapter 5, Figure 1-5**). The effect of Rad deletion on $I_{Ca,L}$ is not dependent on signaling from β-ARs, demonstrating no detectable response to isoproterenol (**Chapter 3, Figure 4; Chapter 4, Figure 3**) and increasing $I_{Ca,L}$ in the absence of β-ARs (**Chapter 5, Figure 7-9**). These results led to the conclusion that Rad may be absent from the LTCC in order for modulation to occur. Proximity proteomics evaluation in transgenic mice further contributed to this hypothesis, demonstrating that

following acute isoproterenol treatment, Rad association with the $Ca_V1.2$ and $Ca_V\beta$ was reduced [92]. Taken together, the results of this dissertation and that of recent publications establish Rad as the critical phosphorylation site by PKA to induce LTCC modulation [21-24, 92].

8.2 Rad governs $I_{Ca,L}$ by multiple mechanisms

Amplification of $I_{Ca,L}$ can be described by the classic equation: $I = N_T \times P_f \times P_o \times i$, where I represents macroscopic calcium current of the cell, N_T is the total number of channels, P_f is the probability that a given channel is available, P_o is the probability that the channel will be open, and i is the unitary current through an open pore [282, 291, 292]. Rad regulation of $I_{Ca,L}$ can occur by manipulating one or multiple variables of this equation to produce an increase in macroscopic current.

It is well established PKA phosphorylation increases $I_{Ca,L}$ by elevating P_f and P_o [315]. Indeed, single channel recordings of $Ca_V1.2$ depleted of Rad displayed almost no blank sweeps, and most sweeps exhibited either intermediate or high levels of opening [92]. The mechanism of voltage-dependent of activation of $Ca_V1.2$ remains unclear but has been proposed to include a number of critical elements: S4 and S6 segments of domain I of the α_1 subunit (IS4, IS6 respectively), the AID (α-interacting domain), the I-II linker between domain I and II of the α_1 subunit, and $Ca_V\beta$ [55, 118, 293]. $Ca_V\beta$ binding to $Ca_V1.2$ enhanced P_o and caused a hyperpolarizing shift in activation; this required a rigid linker between IS6 and the AID [92, 316]. It has been speculated that Rad interaction with $Ca_V\beta$ may structurally alter the IS6-AID linker as a way to lower P_o-gating, and thereby inhibit the LTCC [118]. The C-terminal tail of Rad is the domain that binds to $Ca_V\beta$ and is critical to Rad-mediated LTCC regulation [17]. Sites for PKA and CaMKII phosphorylation, binding for 14-3-3, binding for CaM, and association with plasma membrane all reside within the C-terminus of Rad [175, 177, 281]. These studies suggest that Rad-mediated inhibition of the LTCC, and therefore LTCC modulation, is regulated through its C-terminal tail. Indeed, the truncation of the C-terminus of Rad results in $I_{Ca,L}$ that is indistinguishable from cRadKO (**Chapter 6, Figures 6.2-6.4**), supporting the hypothesis that LTCC modulation relies on the C-terminus of Rad. This raises the possibility that upon

Rad phosphorylation, Rad is sequestered from the complex by 14-3-3 binding to sites both on the N- and C-terminal extensions, alleviating the association with $Ca_V\beta$ so that the IS6-AID linker can be stabilized to support high P_o gating [118, 166, 281].

Another emerging hypothesis of the mechanism enhancing P_f and P_o, and thereby LTCC modulation, is channel clustering. Calcium bound to CaM allows channels to form physical connections between the C-terminal tails of neighboring channels to induce clustering (~8 channels within an average cluster) [57-59]. The activity of the cluster would be driven by the channel(s) with the highest activity within the cluster [57]. These channels also inactivate more rapidly through calcium-dependent inactivation in order to prevent arrhythmogenesis; this causes coupling between channels to fade [58]. However, coupling persists longer than the current that evoked it, thereby acting as a type of 'molecular memory' that might serve to augment calcium influx in times of repetitive membrane depolarization, such as seen in calcium-dependent facilitation or an increase in action potential frequency [58]. Upon β-AR stimulation, channels can form 'super-clusters' (~32% increase in cluster size) that allow them to gate cooperatively [59]. These 'super-clusters' were localized to transverse tubules, same microdomain as the source of cAMP used for signaling downstream of β-AR stimulation [59, 101, 102]. Rad binds to CaM in a calcium dependent manner through a region located on the C-terminus of Rad [166]. With CaM playing a central role in calcium-dependent facilitation, calcium dependent inactivation, and clustering, it is possible that Rad inhibits LTCC P_F and P_o through binding to CaM and blocking cluster formation. Upon phosphorylation by PKC, Rad binding to CaM is reduced [317]. Therefore, the absence of Rad from the complex would result in a constant state of channel clustering that would display enhanced calcium influx and accelerated inactivation, as seen both in cRadKO and when the C-terminus of Rad is absent (Rad-Flag A277X) (**Chapter 3, Figure 3.4; Chapter 4, Figure 4.3; Chapter 5, Figure 5.1-5.5; Chapter 6, Figure 6.2-6.4**). The reduction of Rad binding could also cause a conformational change within the LTCC so that $Ca_V\beta$ could stabilize the IS6-AID linker. Future studies investigating channel clustering in the absence of Rad might shed light onto how the LTCC undergoes modulation, facilitation, and inactivation.

A potential explanation for enhanced $I_{Ca,L}$ seen in the absence of Rad is an increase in the total number of channels expressed in the plasma membrane. An initial hypothesis for RGK regulation of $Ca_V1.2$ channels was by regulating surface expression and limiting channel trafficking to the membrane [16, 176, 314, 318]. Indeed, in PC12 cells, Rad blocked surface expression of LTCCs by binding to $Ca_V\beta_3$ and sequestering the subunit to the nucleus so that α-subunits could not be trafficked to the membrane [176]. In a transgenic mouse model that expressed a dominant negative mutant of Rad (S105N), α_{1C} protein expression was significantly increased [182]. Based on these studies, the prediction would be that Rad governs channel activity by simply limiting channel formation and proper surface trafficking; therefore, in the absence of Rad, channel expression would increase. Interestingly, qRT-PCR for $Ca_V1.2$ mRNA was not significantly different between CTRL and cRadKO nor was $Ca_V1.2$ total protein expression different; however, this does not reveal whether protein was trafficked to the membrane (**Chapter 3, Figure 3.4**). Investigation of channel trafficking in cRadKO was not pursued in this dissertation; however, previous studies have demonstrated that RGK inhibition, including Rad, occurs at the cell surface rather than through altering α_1 surface expression or trafficking [20, 88, 183, 282, 319]. A recent study proposed that β-AR stimulation causes an increase in $Ca_V1.2$ surface expression by triggering rapid mobilization of $Ca_V1.2$-cargo-carrying endosomes to the sarcolemma surface; the hypothesis is that channel activity is augmented through insertion and recycling of $Ca_V1.2$ [320]. It is speculated that when Rad is phosphorylated, the dissociation of Rad from $Ca_V\beta$ releases the channel complex and permits trafficking to the surface [320]. Studies in heterologous expression systems support this hypothesis, demonstrating Rem decreased $Ca_V1.2$ surface density by 65%, though inhibition of Rem on $Ca_V1.2$ was not relieved after β-AR stimulation [282, 314]. Therefore, it is possible that the absence of Rad promotes modulation of the LTCC simply by permitting the insertion of a pool of channels normally lying in reserve for when β-ARs are activated.

Though the mechanisms of LTCC modulation and RGK-mediated inhibition have been studied extensively, a conclusive explanation remains elusive. It is possible that regulation by Rad is a combination of the mechanisms described above, or potentially dependent on protein-protein interactions with Rad and the LTCC that are currently unknown. Indeed, the role of Rad in LTCC modulation has just been established [24, 92].

Advances in microscopy techniques and technology, combined with new FRET biosensors may allow investigation of LTCC nanodomains, and specific protein-protein interactions to better understand how the presence and absence of Rad contributes to LTCC regulation [31].

8.3 Hypertrophic signaling is not exclusively dependent on elevated $I_{Ca,L}$

A central dogma of calcium cycling is increasing $I_{Ca,L}$ inevitably leads to myocyte hypertrophy [12, 148, 149, 321-329]. Indeed, overexpression of α_{1C} or $Ca_V\beta$ in transgenic mice yields enhanced $I_{Ca,L}$ followed by rapid progression to pathological hypertrophy, heart failure and death [12, 149, 327]. An early study of global Rad knockout also reported increased hypertrophy due to activated CaMKII, without any cardiac functional evaluations [181]; Crucial observations from these overexpression models that are important to note: the α_{1C} overexpression model exhibited minimal difference in left ventricular inner dimensions and in posterior wall thickness compared to non-transgenic controls [12]; $Ca_V\beta$ overexpression reported cardiac hypertrophy without functional assessment by echo, or indication of activation of CaMKII or calcineurin [330]. The global Rad knockout model reported hypertrophy based on hyperphosphorylation of CaMKII, but no cardiac functional evaluation [181]. Contrary to these studies, decreased LTCC activity also produces severe hypertrophy and remodeling due to calcineurin and CaMKII activation [290]. Cardiac-specific Rad deletion exhibited no significant changes in cardiac structure compared to CTRL under conditions of elevated $I_{Ca,L}$ and enhanced calcium handling (**Chapter 3, Figures 3.3-3.5; Chapter 5, Figures 5.7,5.8; Chapter 6, Figures 6.2-6.4**); there was also no indication of hyperphosphorylation of phospholamban by CaMKII, suggesting CaMKII was not activated in cRadKO (**Chapter 3, Figures 3.5,3.9**). These contradicting results indicate increased $I_{Ca,L}$ does not necessarily guarantee activation of hypertrophic signaling.

Cardiac growth can be predicted through a model based on integrated tension measured from mean twitch tensions or sarcomere shortening. A negative score in this model forecasts dilated cardiomyopathy, and a positive score indicates potential hypertrophic remodeling [202]. When developing the model, the study reported that

predicting heart remodeling solely on any singular calcium parameter was poor; the model had to include mechanical parameters in order to achieve accurate predictions [202]. Based on this model, cRadKO approached a WT tension-integral as a consequence of larger calcium transient amplitudes (**Chapter 3, Figures 3.5,3.6**). This could be due to enhanced $I_{Ca,L}$ kinetics (**Chapter 3, Figure 3.3; Chapter 5, Figures 5.2-5.5**) and/or due to increased expression of SERCA2a (**Chapter 3, Figure 3.5**). Activation of calcineurin requires a high and sustained calcium signal [146]; the acceleration of $I_{Ca,L}$ decay in cRadKO may be sufficient to prevent activation of calcineurin and hypertrophic signaling even though peak $I_{Ca,L}$ is increased. Even in conditions of pressure-overload induced heart failure, the integrated tension model predicted only modest concentric hypertrophy (**Chapter 7, Figure 7.10**), which is consistent with the slight increase in wall thickness observed in all three TAC paradigms of Rad deletion (**Chapter 7, Figures 7.1,7.5,7.13**). Elevated SERCA2a without a mirroring change in phospholamban, as seen in cRadKO, would also prevent a high and sustained calcium signal within the cytosol. This beneficial modification would allow enhanced calcium uptake without the need for phosphorylation of phospholamban; indeed, this type of regulation displays cardioprotection in conditions of high-intensity exercise and advanced heart failure [207-210]. Hypertrophic signaling activation therefore is not as straightforward as simply an increase in peak $I_{Ca,L}$; rather, enhanced calcium current may be a weak inducer or contributes to hypertrophic signaling secondary to chronic stimulation of β-ARs.

An intriguing finding of this work is that attaching an epitope tag, Flag, to Rad caused significant alterations to cardiac function and structure (**Chapter 6**). Many studies have utilized transgenic mouse models that express an epitope tag such as Flag to investigate LTCC gating properties and binding partners; however, none of these studies report functional assessments to demonstrate healthy cardiac function and structure [57-59, 92, 117, 118, 166, 331]. These types of genetic manipulations have the potential to trigger indirect, secondary effects on that confound the direct effects which could cause misinterpretations of the results [332]. An example of this were studies recently conducted investigating the role of junctophilin-2 (JPH-2) in formation and stabilization of transverse tubules. When all cardiomyocytes are depleted of JPH-2, there was a dramatic loss of transverse tubules and severe cardiac dysfunction; this led to the conclusion that JPH-2 was

critical for transverse tubule maturation and preserving cardiac function [333, 334]. However, loss of transverse tubules is a hallmark feature of pathological remodeling [335]. Therefore, the question remains of whether loss of JPH-2 promotes transverse tubule loss that then leads to heart failure, or heart failure promotes loss of transverse tubule, causing JPH-2 to decrease. Utilizing a genetic mosaic model to deplete either a low percentage or high percentage of JPH-2 within cardiomyocytes demonstrated that low percentage loss of JPH-2 yielded minimal transverse tubule disorganization and no disturbances to cardiac function; this was only seen in high percentage loss of JPH-2 [332]. This study demonstrated JPH-2 does not play as critical of a role in transverse tubule maturation as originally demonstrated [332]. This study combined with the results from Rad-Flag highlight how direct effects on cardiac gene manipulation may be misinterpreted due to confounding, secondary effects, such as heart failure conditions, especially when manipulating genes that affect the LTCC.

8.4 Enhanced $I_{Ca,L}$ does not necessarily promote electrical dysfunction

Experimental and theoretical studies have also identified $I_{Ca,L}$ as a critical component in arrhythmogenesis due to its central role in action potential duration; specifically, reactivation of $I_{Ca,L}$ in the late phase of decay induces early afterdepolarizations (EADs) that trigger fatal arrhythmias [50, 61-63]. Recent studies have demonstrated that reducing the non-inactivating component of $I_{Ca,L}$, known as the pedestal current, can reduce the formation of EADs without affecting excitation contraction coupling [50, 61]. This suggests a new class of drug action that act as 'gating modifiers' to promote subtle changes in the biophysical parameters of $I_{Ca,L}$ to reduce the late, arrhythmogenic component without affecting contractility or action potential duration [62]. A prototype drug that appears to achieve this is a drug called roscovitine [62, 126-130, 138]. The work of this dissertation supports Rad as another potential 'gating modifier.' The absence of Rad reduced the pedestal current (**Chapter 3, Figure 3.3**) and the late component of $I_{Ca,L}$ was not significantly different between cRadKO and CTRL (**Chapter 5, Figures 5.2-5.5**). Action potential duration and QT interval were not significantly different between cRadKO or CTRL (**Chapter 5, Figure 5.6**), demonstrating that Rad could be a safe 'gating modifier' drug target since this type of regulation can occur without activation of β-AR stimulation

(**Chapter 5, Figure 5.7,5.8**). In fact, this work establishes that the C-terminus of Rad could be the target for a small peptide inhibitor since Rad-Flag A277X also demonstrated accelerated inactivation without altering the late component of $I_{Ca,L}$ that paralleled cRadKO (**Chapter 6, Figure 6.2-6.4**).

Another key consideration is potential electrical dysfunction within the sinoatrial node. Alterations in sinus node function parallel autonomic imbalance in the ventricles; this imbalance is evident in heart failure and can result in sudden cardiac death due to a decrease in heart rate variability [336]. Treatment with β-AR blockers suggest lowering heart rate contributes to survival for patients with heart failure; higher heart rates promote arrhythmogenesis and decreased contractility [336]. Contrary to these studies, cRadKO exhibited higher intrinsic heart rate without evidence of arrhythmogenesis on the background of enhanced $I_{Ca,L}$ in sinoatrial cardiomyocytes, and increased contractility in the ventricle (SANcm; **Chapter 3, Figure 3.3; Chapter 4, Figure 4.4,4.5**). These paradoxical results suggest that modulated $I_{Ca,L}$ may promote balance of autonomic input without the required increase in sympathetic drive. Previous studies indicate there are mechanisms that increase and decrease sinus rate in order to preserve autonomic balance [336]. In fact, a recent study discovered SANcm undergo a nonfiring mode; the SANcm tissue network rhythm is set by the balance between firing and nonfiring cells [337]. Cells that are electrically coupled are in a phasic entrainment, and are grouped together either in a firing mode, or a nonfiring mode; a firing cell that interacts with a nonfiring cell is called tonic entrainment [337]. In tonic entrainment, cells that are in a nonfiring mode electronically draw the flow of cations from more depolarized, firing cells via gap junctions, thereby creating a bradycardic rhythm [337]. Under sympathetic stimulation, cells shift more towards a firing mode in order to accelerate rhythm [337]. In the absence of Rad, it is possible that more SANcm could transition to a firing mode, thereby accelerating HR and sinus rhythm without necessarily disrupting the balance of nonfiring versus firing cells in a pathological manner, as demonstrated by the lack of change in heart rate variability. Indeed, this further supports the role of Rad in not only LTCC regulation of β-AR stimulation, but whole heart regulation by sympathetic stimulation. Taken together, targeting Rad is a powerful potential therapeutic approach because the absence

of Rad enhances positive inotropy and positive chronotropy in a manner that follows β-AR stimulation while still preserving cardiac responsiveness to adrenergic activation.

8.5 Targeting Rad represents the ideal positive inotrope

Currently, the ideal, theoretical treatment for heart failure would restore calcium handling in a failing heart without activating adrenergic signaling [5]. Depleting the LTCC of Rad could serve as a therapeutic target in order to make this ideal treatment a reality. First, the absence of Rad enhances calcium handling under basal conditions in a manner that preserves β-AR signaling within the cell and at the organ level (**Chapter 3, Figures 3.8-3.10**). Enhanced cardiac function is dependent on the presence of Rad in the LTCC complex, rather than solely on activating the fight-or-flight response (**Chapter 5, Figures 5.7,5.8**), thereby providing a positive inotropic target downstream of adrenergic signaling. Unlike studies conducted in global Rad knockout models, cRadKO does not promote pathological signaling [181-183] (**Chapter 3, Figures 3.3-3.5**). In fact, Rad deletion before the onset of pressure-overload induced heart failure provides cardiac protection and preserves survival (**Chapter 7, Figure 7.1**). This protection remained even when Rad was depleted at the time or four weeks after the induction of pressure-overload (**Chapter 7, Figures 7.5,7.13-7.17**). Calcium handling was still enhanced in cRadKO despite the exposure to thoracic aortic constriction surgery (TAC) (**Chapter 7, Figures 7.7-7.10**), though responsiveness to adrenergic stimulation was no longer detectable (**Chapter 7, Figures 7.11,7.12**). These results fit with earlier studies that reported Rad protein is reduced in nonischemic heart failure patients, and support the hypothesis that Rad contributes to the cardiac compensation in response to heart failure [23, 181].

Cardiac protection through the depletion of Rad does not extend to all pathological signaling seen in heart failure. When Rad was deleted prior to surgery, fibrosis increased significantly compared to Sham, and was not different from CTRL that underwent surgery (**Chapter 7, Figure 7.3**). This is not surprising since others have reported that the absence of Rad elevated connective tissue growth factor (CTGF) expression and increased fibrosis; however, the difference between that study and cRadKO is that fibrosis was not seen under normal physiological conditions or in Sham, but only when the heart was exposed to stress

under pressure-overload [24, 198] (**Chapter 3, Figure 3.2**). However, in response to myocardial infarction (MI), global Rad knockout mice displayed less fibrosis development compared to WT [184]. This raises an interesting notion – namely, fibrotic signaling and protection of cardiac function may not necessarily have a cause-effect relationship [338], at least in certain cases. These exceptions may be dependent on the type of injury the heart experiences as well as the tissue in which Rad is expressed/depleted. In response to TAC, gRad$^{-/-}$ mice displayed increased collagen accumulation and elevated CTGF to promote fibrosis [198]. In response to MI, upregulation of inflammatory cytokines and fibrosis were both significantly reduced in gRad$^{-/-}$ compared to WT [184]. Because Rad is expressed in other tissues, it is possible that gRad$^{-/-}$ undergoes adaptive signaling in response to different injuries as part of the cardiac compensatory response. Further investigation is needed to better assess the contributions of Rad to heart function outside of cardiac tissue; this may provide insight into how the depletion of Rad in other tissues may aid in cardiac protection in specific injuries.

A major concern with positive inotropes is the energy demanded of the heart in order to maintain elevated function [5]. In failing hearts, energy metabolism undergoes remodeling that leads to a 30% reduction in concentration of ATP, and ultimately results in impaired contractile reserve [339]. Under healthy conditions, calcium activates both ATP-consumption and -regeneration [5, 310]. However, calcium uptake is impaired in the failing heart, thereby promoting a mismatch between ATP consumption and production [5, 311]. One mechanism to potentially alleviate this mismatch is increasing expression of SERCA2a [5, 207-210]. As stated above, cRadKO results in an increase in SERCA2a expression, which may aid in preventing hypertrophic signaling as well as a potential metabolic mismatch (**Chapter 3, Figure 3.5**). However, Rad has also been implicated in metabolism. Expression of Rad negatively correlates with resting metabolic rate in skeletal muscle [340]. In cancer cells, Rad inhibited glucose transporter translocation to the plasma membrane, which is the first rate-limiting step in glucose metabolism; knockdown of Rad enhanced glycolysis [341, 342]. Rad was also found to be a negative regulator of glucose uptake in cultured myotubes, adiopocytes, and ovarian cancer cells [178, 200]. From these studies and the drastic increase in cardiac function seen in cRadKO, it is very likely that Rad plays a significant role in cardiac metabolism. The specific role in which Rad mediates

these mechanisms remains unclear; however, this understanding is crucial in determining how beneficial Rad would be as a positive inotrope target.

8.6 Future directions

The work in this dissertation establishes Rad as a central regulator of LTCC activity and modulation. However, there are questions that remain unanswered that encourage further investigation of Rad.

It is clear that modulation the LTCC occurs when Rad is not present, or in close proximity of the channel complex. However, it remains unclear as to where Rad is localized upon phosphorylation; it is possible that Rad remains close to the complex because of associations with structural proteins within the LTCC-Ryanodine Receptor junction like JPH-2 or Speg [343]. It is also possible that Rad is sequestered to a different location within the cell, possibly to regulate another mechanism in response to β-AR stimulation [320]. Future experiments could utilize the Rad-Flag A277X model to determine localization within the LTCC or cytosol in response to modulation since results from this model resemble a modulated LTCC or Rad-depleted channel. This is especially important since Rad is potentially implicated in other critical mechanisms such as channel trafficking, channel recycling, and metabolism [178, 200, 320, 340-342]. This may also be better suited for a model system that allows the fusion of an epitope tag such as Flag that manages to preserve healthy cardiac structure and function; a recent study demonstrated biotin-ligase system, BioID, was better suited for studies investigating protein localization and protein-protein interactions compared to other knock-in transgenic models [295]. This study reported normal cardiac function and structure, though the target protein was JPH-2, not a protein with the LTCC complex [295]. The BioID strategy may provide clearer insights into Rad localization and important binding partners, especially in regards to baseline conditions versus after β-AR stimulation.

The confirmation that the C-terminus of Rad is critical for regulation of LTCC activity encourages new targets to focus on understand how Rad inhibits the LTCC. Critical binding sites for Cavβ, 14-3-3, CaM, and negatively charged phospholipids in the plasma membrane all reside in the C-terminus of Rad [17, 92, 166, 177, 281]. Mutations

in binding could help resolve the critical components needed for Rad-mediated inhibition of the LTCC. For example, disruption of binding between Rad-CaM may promote channel clustering without the need for adrenergic activation. It is currently unknown how channels cluster together in the absence of Rad; this should be explored both in cRadKO and Rad-Flag A277X. Then, understanding how Rad binding to CaM affects clustering could give further insight into how channels cluster together, both at baseline and under modulated conditions.

Phosphorylation sites for PKA and CaMKII are also found on the C-terminus of Rad [17, 92, 166, 177, 281]. Mutations of these regulatory sites within the C-terminus could provide insight into which are critical for modulation of the LTCC by Rad. For instance, mutations at the phosphorylation sites for PKA and/or CaMKII to create phospho-mimetics may help elucidate what protein-protein interactions are needed for higher P_o, and whether this is a $Ca_V\beta$-dependent or -independent mechanism [282]. Phospho-mimetics may also contribute to understanding of Rad localization within the complex or cytosol under modulated conditions, and whether 'super-clusters' of LTCCs form without stimulation of β-ARs. These studies would not only help understand modulation in the ventricle, but also the sinoatrial node.

The effects of the C-terminal deletion of Rad were not investigated in the sinoatrial node in this dissertation. Future studies should investigate whether Rad-Flag A277X displays the same $I_{Ca,L}$ phenotype and exhibits the same effect on heart rate and heart rate variability as cRadKO. The prediction would be that Rad-Flag A277X would be indistinguishable from cRadKO in regards to SANcm $I_{Ca,L}$, heart rate, and heart rate variability. This would be critical to know if Rad is to serve as a therapeutic target as groups begin to develop small peptide inhibitors specifically made to inhibit calcium channels by altering the C-termini of RGK proteins [282].

Another potentially intriguing pursuit of investigation would be to develop a N-terminal deletion of Rad, and assess how this affects LTCC activity. The functional significant of the N-terminus extension of Rad, or any RGK protein, remains unknown [20]. One study removed the N-terminus of Gem and reported reduced activity of the GTPase, but did not report any effects on LTCC function [344]. The N-terminus of Rad,

and all RGK proteins, contains a binding site for 14-3-3 [166]. This may be a crucial site for removal of Rad from the LTCC upon phosphorylation so that the IS6-AID linker can be stabilize higher P_o [118, 166, 281]. The N-terminus may also contain other key binding sites that have yet to be discovered that could help explain how Rad-mediated inhibition occurs.

8.7 Limitations

A major implication of the studies conducted in this dissertation support Rad as a potential therapeutic target for positive inotropy. However, these studies were limited to mouse models; mice have a larger sarcoplasmic reticulum calcium content and greater SERCA activity compared to larger species that may accommodate the drastic change in $I_{Ca,L}$ better than larger animals [257, 268]. Repolarizing currents are also mostly conducted via I_{to} and I_{Kur} in mice, while larger species express I_{Kr} and I_{Ks} which could alter action potentials and QT interval in larger species that is not accounted for in mice [268]. It therefore is crucial that cardiac-specific Rad deletion be explored in larger animals or in model systems that better emulate human cardiac function.

A critical factor that is unexplored in this dissertation is the effect of Rad deletion on other ion channels. While there is no current evidence to suggest that Rad interacts with other channel complexes besides the LTCC, interactions may still exist. It is also possible that other ion channels that are affected by intracellular calcium could experience secondary effects due to Rad deletion. Indeed, it is possible that calcium-activated potassium channels could be activated in cRadKO so that balance is maintained in the plateau phase of the action potential and QT interval is not prolonged. This knowledge would become especially important in understanding the fight-or-flight response since this mechanism is conserved across multiple species.

8.8 Conclusions

Based on the results of the studies in this dissertation and literature that has been published during the course of this work, I speculate that Rad governs $Ca_V1.2$ channel availability and open probability through multiple interactions within the C-terminus of

Rad; this inhibition is relieved under conditions of β-AR stimulation due to phosphorylation of Rad by PKA that allows different proteins to interact and deplete the LTCC of Rad. Because Rad serves as the critical modulator of LTCC in response to sympathetic drive, depleting the LTCC of Rad yields a chronically modulated channel. The resulting increase in peak $I_{Ca,L}$ stimulates a larger calcium induced calcium release from the sarcoplasmic reticulum to enhance contraction; this is balanced through enhanced inactivation so that hypertrophic signaling is not initiated, nor is the late, arrhythmogenic component of $I_{Ca,L}$ increased. Therefore, Rad deletion specifically from cardiomyocytes could serve as an ideal positive inotrope for heart failure treatment due to the novel mechanism to increase $I_{Ca,L}$ in a manner that preserves structure, function, and the fight-or-flight response within the heart.

APPENDIX

List of Abbreviations

AID	α-Interaction Domain
AKAP15	A-kinase anchoring protein-15
ANF	Atrial Natriuertic Factor
ANOVA	Analysis of Variance
ANS	Autonomic Nervous System
AP	Action Potential
APD	Action Potential Duration
β-AR	β-Adrenergic Receptor
BAPTA	1,2-bis(o-aminophenoxy)ethane-N,N,N′,N′-tetraacetic acid
BW	Body Weight
CaM	Calmodulin
CaMKII	Calmodulin Kinase II
cAMP	cyclic-AMP
CDF	Calcium Dependent Facilitation
CDI	Calcium Dependent Inactivaiton

CICR	Calcium Induced Calcium Release
cRadKO	Cardiac-specific Rad Knockout (also known as $Rad^{\Delta/\Delta}$)
CTGF	Connective Tissue Growth Factor
CTNNA3	Catenin Alpha3
CTRL	Control (also known as $Rad^{fl/fl}$)
DAD	Delayed Afterdepolarization
DHP	1,4-dihydropyridine
dKO	$\beta_1\beta_2$-Adrenergic Receptor Double Knockout
EAD	Early Afterdepolarization
ECG	Electrocardiogram
EF	Ejection Fraction
EGTA	Ethylene glycol-bis(β-aminoethyl ether)-N,N,N′,N′-tetraacetic acid
FDR	False Discovery Rate
GAPDH	Glyceraldehyde-3-phosphate Dehydrogenase
GK	Guanylate kinase
$gRAD^{-/-}$	Whole Body Rad Deletion
HCN4	Hyperpolarization-activated Cyclic Nucleotide Gated Channel 4
HDAC	Histone Deacetylase

HERG	human *Ether-à-go-go*-Related Gene Potassium Channel
HF	Heart Failure
HFrEF	Heart Failure with Reduced Ejection Fraction
HR	Heart Rate
HRV	Heart Rate Variability
HVA	High-voltage-activated
HW	Heart Weight
I	Macroscopic Current
i	Unitary Current Through an Open Pore
$I_{Ca,L}$	L-type Calcium Current
ISO	Isoproterenol
LTCC	L-type Calcium Channel
LQTS	Long QT Syndrome
LVA	Low-voltage-activated
LVAW	Left Ventricular Anterior Wall
LVID	Left Ventricular Inner Dimension
LVPW	Left Ventricular Posterior Wall
LW	Lung Weight

MEF2	Myocyte Enhancer Factor 2
MerCreMer	Tamoxifen-Inducible Cre Recombinase
MHC	α-Myosin Heavy Chain
MI	Myocardial Infarction
NCX	Na^+/Ca^{2+} Exchanger
NFAT	Nuclear Factor of Activated T Cells
N_T	Total Number of Channels
PCR	Polymerase Chain Reaction
PDE	Phosphodiesterase
P_f	Probability that a Given Channel is Available
PKA	Protein Kinase A
PKC	Protein Kinase C
PLN	Phospholamban
P_o	Probability that the Channel will be Open
qRT	Quantitative Real Time
QTc	Corrected QT Interval
RAD	Rad Associated with Diabetes
$Rad^{fl/fl}$	RAD with loxP sites flanking exons 3-4 (control group for $Rad^{\Delta/\Delta}$)

$Rad^{\Delta/\Delta}$	Inducible, Myocardial-Restricted RAD Knockout
Rad-Flag	Wild-Type 3xFlag-Rad
Rad-Flag A277X	3xFlag-Rad^{A277X}
RCAN1	Regulator of Calcineurin 1
RT	Room Temperature
RyR2	Ryanodine Receptor 2
r_{30}	Remaining Current 30 ms After Peak
r_{150}	Remaining Current 150 ms After Peak
SAN	Sinoatrial Node
SANcm	Sinoatrial Node Cardiomyocyte
scRNA-seq	Single-cell RNA-sequencing
SD	Standard Deviation
SEM	Standard Error of Mean
SERCA2a	Sarco/Endoplasmic Reticulum Calcium ATPase
SH3	SRC Homology 3
SNS	Sympathetic Nervous System
SR	Sarcoplasmic Reticulum
TAM	Tamoxifen

TAC	Transverse Aortic Constriction
tKO	$\beta_1\beta_2$-Adrenergic Receptor, Rad Triple Knockout
TS	Timothy Syndrome
t-SNE	t-distributed Stochastic Neighbor Embedding
VGCC	Voltage-Gated Calcium Channel
VDI	Voltage Dependent Inactivation
WT	Wild-type

REFERENCES

1. Mathers, C.D. and D. Loncar, *Projections of global mortality and burden of disease from 2002 to 2030.* PLoS medicine, 2006. **3**(11): p. e442.
2. Kamouh, A. and G.S. Francis, *Contemporary management and research directions in advanced heart failure: where are we going?* Congestive Heart Failure, 2011. **17**(5): p. 241-247.
3. Marks, A.R., *Calcium cycling proteins and heart failure: mechanisms and therapeutics.* The Journal of clinical investigation, 2013. **123**(1): p. 46-52.
4. Lompré, A.-M., et al., *Ca2+ cycling and new therapeutic approaches for heart failure.* Circulation, 2010. **121**(6): p. 822-830.
5. Maack, C., et al., *Treatments targeting inotropy: a position paper of the Committees on Translational Research and Acute Heart Failure of the Heart Failure Association of the European Society of Cardiology.* European heart journal, 2019. **40**(44): p. 3626-3644.
6. Bers, D.M., *Cardiac excitation–contraction coupling.* Nature, 2002. **415**(6868): p. 198-205.
7. Shannon, T.R. and W.Y. Lew, *Diastolic release of calcium from the sarcoplasmic reticulum: a potential target for treating triggered arrhythmias and heart failure*. 2009, American College of Cardiology Foundation Washington, DC.
8. Lefkowitz, R.J., H.A. Rockman, and W.J. Koch, *Catecholamines, cardiac beta-adrenergic receptors, and heart failure.* Circulation, 2000. **101**(14): p. 1634-7.
9. Mebazaa, A., et al., *Short-term survival by treatment among patients hospitalized with acute heart failure: the global ALARM-HF registry using propensity scoring methods.* Intensive care medicine, 2011. **37**(2): p. 290-301.
10. Tacon, C.L., J. McCaffrey, and A. Delaney, *Dobutamine for patients with severe heart failure: a systematic review and meta-analysis of randomised controlled trials.* Intensive care medicine, 2012. **38**(3): p. 359-367.
11. Port, J.D. and M.R. Bristow, *Altered beta-adrenergic receptor gene regulation and signaling in chronic heart failure.* Journal of molecular and cellular cardiology, 2001. **33**(5): p. 887-905.
12. Muth, J.N., et al., *Cardiac-specific Overexpression of the α1 Subunit of the L-type Voltage-dependent Ca2+ Channel in Transgenic Mice LOSS OF ISOPROTERENOL-INDUCED CONTRACTION.* Journal of Biological Chemistry, 1999. **274**(31): p. 21503-21506.
13. Bodi, I., et al., *The L-type calcium channel in the heart: the beat goes on.* The Journal of clinical investigation, 2005. **115**(12): p. 3306-3317.
14. Hullin, R., et al., *Cardiac L-type calcium channel β-subunits expressed in human heart have differential effects on single channel characteristics.* Journal of Biological Chemistry, 2003. **278**(24): p. 21623-21630.
15. Chien, A.J., et al., *Roles of a membrane-localized βsubunit in the formation and targeting of functional L-type Ca2+ channels.* Journal of Biological Chemistry, 1995. **270**(50): p. 30036-30044.
16. Béguin, P., et al., *Regulation of Ca 2+ channel expression at the cell surface by the small G-protein kir/Gem.* Nature, 2001. **411**(6838): p. 701.

17. Finlin, B.S., et al., *Regulation of voltage-gated calcium channel activity by the Rem and Rad GTPases.* Proceedings of the National Academy of Sciences, 2003. **100**(24): p. 14469-14474.
18. Gunton, J.E., et al., *Mice deficient in GEM GTPase show abnormal glucose homeostasis due to defects in beta-cell calcium handling.* PloS one, 2012. **7**(6): p. e39462.
19. Magyar, J., et al., *Rem-GTPase regulates cardiac myocyte L-type calcium current.* Channels, 2012. **6**(3): p. 166-173.
20. Yang, T. and H.M. Colecraft, *Regulation of voltage-dependent calcium channels by RGK proteins.* Biochimica et Biophysica Acta (BBA)-Biomembranes, 2013. **1828**(7): p. 1644-1654.
21. Manning, J.R., et al., *Rad GTPase deletion increases L-type calcium channel current leading to increased cardiac contraction.* Journal of the American Heart Association, 2013. **2**(6): p. e000459.
22. Manning, J.R., et al., *Loss of Rad-GTPase produces a novel adaptive cardiac phenotype resistant to systolic decline with aging.* American Journal of Physiology-Heart and Circulatory Physiology, 2015. **309**(8): p. H1336-H1345.
23. Levitan, B.M., et al., *Rad-deletion phenocopies tonic sympathetic stimulation of the heart.* Journal of cardiovascular translational research, 2016. **9**(5-6): p. 432-444.
24. Ahern, B.M., et al., *Myocardial-restricted ablation of the GTPase RAD results in a pro-adaptive heart response in mice.* Journal of Biological Chemistry, 2019. **294**(28): p. 10913-10927.
25. Catterall, W.A., *Voltage-gated calcium channels.* Cold Spring Harbor perspectives in biology, 2011. **3**(8): p. a003947.
26. Hille, B., *Ionic channels ofexcitable membranes.* Sinauer Asso, 1984.
27. Bertil, H. and H. Bertil, *Ion channels of excitable membranes.* Sunderland, Mass.: Sinauer Associates. 3rd Edition.–2007, 2001.
28. Catterall, W.A., *Structure and regulation of voltage-gated Ca2+ channels.* Annual review of cell and developmental biology, 2000. **16**(1): p. 521-555.
29. Dolphin, A.C., *A short history of voltage-gated calcium channels.* British journal of pharmacology, 2006. **147**(S1): p. S56-S62.
30. Zamponi, G.W., et al., *The physiology, pathology, and pharmacology of voltage-gated calcium channels and their future therapeutic potential.* Pharmacological reviews, 2015. **67**(4): p. 821-870.
31. Pallien, T. and E. Klussmann, *New aspects in cardiac L-type Ca2+ channel regulation.* Biochemical Society Transactions, 2020. **48**(1): p. 39-49.
32. Reuter, H., *Calcium channel modulation by neurotransmitters, enzymes and drugs.* Nature, 1983. **301**(5901): p. 569-574.
33. Hess, P., J.B. Lansman, and R.W. Tsien, *Different modes of Ca channel gating behaviour favoured by dihydropyridine Ca agonists and antagonists.* Nature, 1984. **311**(5986): p. 538-544.
34. Hofmann, F., et al., *L-type CaV1. 2 calcium channels: from in vitro findings to in vivo function.* Physiological reviews, 2014. **94**(1): p. 303-326.
35. Tanabe, T., et al., *Primary structure of the receptor for calcium channel blockers from skeletal muscle.* Nature, 1987. **328**(6128): p. 313-318.

36. Liao, P., et al., *Splicing for alternative structures of Cav1. 2 Ca2+ channels in cardiac and smooth muscles.* Cardiovascular research, 2005. **68**(2): p. 197-203.
37. Pantazis, A., et al., *Functional heterogeneity of the four voltage sensors of a human L-type calcium channel.* Proceedings of the National Academy of Sciences, 2014. **111**(51): p. 18381-18386.
38. Yang, J., et al., *Molecular determinants of Ca 2+ selectivity and ion permeation in L-type Ca 2+ channels.* Nature, 1993. **366**(6451): p. 158-161.
39. Stary, A., et al., *Structural model of the Cav1. 2 pore.* Channels, 2008. **2**(3): p. 210-215.
40. Buraei, Z. and J. Yang, *Structure and function of the β subunit of voltage-gated Ca2+ channels.* Biochimica Et Biophysica Acta (BBA)-Biomembranes, 2013. **1828**(7): p. 1530-1540.
41. Buraei, Z. and J. Yang, *The β subunit of voltage-gated Ca2+ channels.* Physiological reviews, 2010. **90**(4): p. 1461-1506.
42. Davies, A., et al., *Functional biology of the α2δ subunits of voltage-gated calcium channels.* Trends in pharmacological sciences, 2007. **28**(5): p. 220-228.
43. Ninomiya, W., et al., *Electroretinographic abnormalities associated with pregabalin: a case report.* Documenta Ophthalmologica, 2020: p. 1-9.
44. Harvey, R.D. and J.W. Hell, *CaV1. 2 signaling complexes in the heart.* Journal of molecular and cellular cardiology, 2013. **58**: p. 143-152.
45. Shaw, R.M. and H.M. Colecraft, *L-type calcium channel targeting and local signalling in cardiac myocytes.* Cardiovascular research, 2013. **98**(2): p. 177-186.
46. Feng, T., S. Kalyaanamoorthy, and K. Barakat, *L-type calcium channels: structure and functions.* Ion Channels in Health and Sickness, 2018. **77305**.
47. Zühlke, R.D., et al., *Calmodulin supports both inactivation and facilitation of L-type calcium channels.* Nature, 1999. **399**(6732): p. 159-62.
48. Mori, M.X., M.G. Erickson, and D.T. Yue, *Functional stoichiometry and local enrichment of calmodulin interacting with Ca2+ channels.* Science, 2004. **304**(5669): p. 432-435.
49. Ben-Johny, M. and D.T. Yue, *Calmodulin regulation (calmodulation) of voltage-gated calcium channels.* Journal of General Physiology, 2014. **143**(6): p. 679-692.
50. Mahajan, A., et al., *Modifying L-type calcium current kinetics: consequences for cardiac excitation and arrhythmia dynamics.* Biophysical journal, 2008. **94**(2): p. 411-423.
51. Bers, D.M. and T. Guo, *Calcium signaling in cardiac ventricular myocytes.* Annals of the New York Academy of Sciences, 2005. **1047**(1): p. 86-98.
52. Makarewich, C.A., et al., *A Caveolae-Targeted L-Type Ca2+ Channel Antagonist Inhibits Hypertrophic Signaling Without Reducing Cardiac ContractilityNovelty and Significance.* Circulation research, 2012. **110**(5): p. 669-674.
53. Calaghan, S. and E. White, *Caveolae modulate excitation–contraction coupling and β2-adrenergic signalling in adult rat ventricular myocytes.* Cardiovascular research, 2006. **69**(4): p. 816-824.
54. Zagotta, W.N., et al., *Shaker potassium channel gating. II: Transitions in the activation pathway.* The Journal of general physiology, 1994. **103**(2): p. 279-319.

55. Beyl, S., et al., *Upward movement of IS4 and IIIS4 is a rate-limiting stage in Ca v 1.2 activation.* Pflügers Archiv-European Journal of Physiology, 2016. **468**(11): p. 1895-1907.
56. Kudrnac, M., et al., *Coupled and independent contributions of residues in IS6 and IIS6 to activation gating of CaV1. 2.* Journal of Biological Chemistry, 2009. **284**(18): p. 12276-12284.
57. Dixon, R.E., et al., *Ca2+ signaling amplification by oligomerization of L-type Cav1. 2 channels.* Proceedings of the National Academy of Sciences, 2012. **109**(5): p. 1749-1754.
58. Dixon, R.E., et al., *Graded Ca2+/calmodulin-dependent coupling of voltage-gated CaV1. 2 channels.* Elife, 2015. **4**: p. e05608.
59. Ito, D.W., et al., *β-adrenergic-mediated dynamic augmentation of sarcolemmal CaV1. 2 clustering and co-operativity in ventricular myocytes.* The Journal of physiology, 2019. **597**(8): p. 2139-2162.
60. Findlay, I., *Physiological modulation of inactivation in L-type Ca2+ channels: one switch.* The Journal of physiology, 2004. **554**(2): p. 275-283.
61. Madhvani, R.V., et al., *Shaping a new Ca2+ conductance to suppress early afterdepolarizations in cardiac myocytes.* The Journal of physiology, 2011. **589**(24): p. 6081-6092.
62. Karagueuzian, H., et al., *Enhanced late Na and Ca currents as effective antiarrhythmic drug targets.* Frontiers in pharmacology, 2017. **8**: p. 36.
63. Madhvani, R.V., et al., *Targeting the late component of the cardiac L-type Ca2+ current to suppress early afterdepolarizations.* Journal of General Physiology, 2015. **145**(5): p. 395-404.
64. Breijo-Marquez, F.R., *Cardiac Arrhythmias: New Considerations*. 2012: BoD–Books on Demand.
65. Pelzer, D., S. Pelzer, and T.F. McDonald, *Properties and regulation of calcium channels in muscle cells*, in *Reviews of Physiology, Biochemistry and Pharmacology, Volume 114*. 1990, Springer. p. 107-207.
66. Morales, D., T. Hermosilla, and D. Varela, *Calcium-dependent inactivation controls cardiac L-type Ca2+ currents under β-adrenergic stimulation.* Journal of General Physiology, 2019. **151**(6): p. 786-797.
67. Korkosh, V.S., et al., *Atomic mechanisms of Timothy syndrome-associated mutations in calcium channel Cav1. 2.* Frontiers in physiology, 2019. **10**: p. 335.
68. Peterson, B.Z., C.D. DeMaria, and D.T. Yue, *Calmodulin is the Ca2+ sensor for Ca2+-dependent inactivation of L-type calcium channels.* Neuron, 1999. **22**(3): p. 549-558.
69. Tadross, M.R., I.E. Dick, and D.T. Yue, *Mechanism of local and global Ca2+ sensing by calmodulin in complex with a Ca2+ channel.* Cell, 2008. **133**(7): p. 1228-1240.
70. Alseikhan, B.A., et al., *Engineered calmodulins reveal the unexpected eminence of Ca2+ channel inactivation in controlling heart excitation.* Proceedings of the National Academy of Sciences, 2002. **99**(26): p. 17185-17190.
71. Zamponi, G.W., *Calmodulin lobotomized: novel insights into calcium regulation of voltage-gated calcium channels.* Neuron, 2003. **39**(6): p. 879-881.

72. Fallon, J.L., et al., *Structure of calmodulin bound to the hydrophobic IQ domain of the cardiac Cav1. 2 calcium channel.* Structure, 2005. **13**(12): p. 1881-1886.
73. Findeisen, F. and D.L. Minor, Jr., *Disruption of the IS6-AID Linker Affects Voltage-gated Calcium Channel Inactivation and Facilitation.* Journal of General Physiology, 2009. **133**(3): p. 327-343.
74. Findlay, I., *Voltage-dependent inactivation of l-type ca2+ Currents in Guinea-Pig Ventricular Myocytes.* The Journal of Physiology, 2002. **545**(2): p. 389-397.
75. Findlay, I., *β-adrenergic and muscarinic agonists modulate inactivation of l-type ca2+ Channel Currents in Guinea-Pig Ventricular Myocytes.* The Journal of physiology, 2002. **545**(2): p. 375-388.
76. Findlay, I., *β-Adrenergic stimulation modulates Ca2+-and voltage-dependent inactivation of L-type Ca2+ channel currents in guinea-pig ventricular myocytes.* The Journal of physiology, 2002. **541**(3): p. 741-751.
77. McDonald, T.F., et al., *Regulation and modulation of calcium channels in cardiac, skeletal, and smooth muscle cells.* Physiological reviews, 1994. **74**(2): p. 365-507.
78. McDonald, T.F., et al., *Voltage-dependent properties of macroscopic and elementary calcium channel currents in guinea pig ventricular myocytes.* Pflügers Archiv, 1986. **406**(5): p. 437-448.
79. McMorn, S., et al., *Comparison of ultra-slow, voltage-dependent inactivation of the cardiac L-type Ca2+ channel with Ca2+ or Ba2+ as the charge carrier in ferret ventricular myocytes.* Experimental Physiology: Translation and Integration, 1996. **81**(4): p. 565-575.
80. Spaetgens, R.L. and G.W. Zamponi, *Multiple structural domains contribute to voltage-dependent inactivation of rat brain α1E calcium channels.* Journal of Biological Chemistry, 1999. **274**(32): p. 22428-22436.
81. Anderson, M.E., et al., *Multifunctional Ca2+/calmodulin-dependent protein kinase mediates Ca (2+)-induced enhancement of the L-type Ca2+ current in rabbit ventricular myocytes.* Circulation Research, 1994. **75**(5): p. 854-861.
82. Yuan, W. and D.M. Bers, *Ca-dependent facilitation of cardiac Ca current is due to Ca-calmodulin-dependent protein kinase.* American Journal of Physiology-Heart and Circulatory Physiology, 1994. **267**(3): p. H982-H993.
83. Dzhura, I., et al., *Calmodulin kinase determines calcium-dependent facilitation of L-type calcium channels.* Nature cell biology, 2000. **2**(3): p. 173-177.
84. Saucerman, J.J. and D.M. Bers, *Calmodulin binding proteins provide domains of local Ca2+ signaling in cardiac myocytes.* Journal of molecular and cellular cardiology, 2012. **52**(2): p. 312-316.
85. Lee, K.S., *Potentiation of the calcium-channel currents of internally perfused mammalian heart cells by repetitive depolarization.* Proceedings of the National Academy of Sciences, 1987. **84**(11): p. 3941-3945.
86. Noble, S. and Y. Shimoni, *Voltage-dependent potentiation of the slow inward current in frog atrium.* The Journal of physiology, 1981. **310**(1): p. 77-95.
87. Fedida, D., D. Noble, and A. Spindler, *Mechanism of the use dependence of Ca2+ current in guinea-pig myocytes.* The Journal of physiology, 1988. **405**(1): p. 461-475.

88. Xu, L., et al., *Alterations of L-type calcium current and cardiac function in CaMKIIδ knockout mice.* Circulation research, 2010. **107**(3): p. 398-407.
89. Poomvanicha, M., et al., *Facilitation and Ca2+-dependent inactivation are modified by mutation of the Cav1. 2 channel IQ motif.* Journal of Biological Chemistry, 2011. **286**(30): p. 26702-26707.
90. Blaich, A., et al., *Facilitation of murine cardiac L-type Cav1. 2 channel is modulated by Calmodulin kinase II–dependent phosphorylation of S1512 and S1570.* Proceedings of the National Academy of Sciences, 2010. **107**(22): p. 10285-10289.
91. Brandmayr, J., et al., *Deletion of the C-terminal phosphorylation sites in the cardiac β-subunit does not affect the basic β-adrenergic response of the heart and the Cav1. 2 channel.* Journal of Biological Chemistry, 2012. **287**(27): p. 22584-22592.
92. Liu, G., et al., *Mechanism of adrenergic Ca V 1.2 stimulation revealed by proximity proteomics.* Nature, 2020: p. 1-6.
93. Kumari, N., H. Gaur, and A. Bhargava, *Cardiac voltage gated calcium channels and their regulation by β-adrenergic signaling.* Life sciences, 2017.
94. Reuter, H., *Localization of beta adrenergic receptors, and effects of noradrenaline and cyclic nucleotides on action potentials, ionic currents and tension in mammalian cardiac muscle.* The Journal of Physiology, 1974. **242**(2): p. 429-451.
95. Vassort, G., et al., *Effects of adrenaline on membrane inward currents during the cardiac action potential.* Pflügers Archiv, 1969. **309**(1): p. 70-81.
96. Morad, M., C. Sanders, and J. Weiss, *The inotropic actions of adrenaline on frog ventricular muscle: relaxing versus potentiating effects.* The Journal of physiology, 1981. **311**(1): p. 585-604.
97. Tsien, R., *Adrenaline-like effects of intracellular iontophoresis of cyclic AMP in cardiac Purkinje fibres.* Nature New Biology, 1973. **245**(143): p. 120-122.
98. Tsien, R., W. Giles, and P. Greengard, *Cyclic AMP mediates the effects of adrenaline on cardiac Purkinje fibres.* Nature New Biology, 1972. **240**(101): p. 181-183.
99. Trautwein, W., J. Taniguchi, and A. Noma, *The effect of intracellular cyclic nucleotides and calcium on the action potential and acetylcholine response of isolated cardiac cells.* Pflügers Archiv, 1982. **392**(4): p. 307-314.
100. Osterrieder, W., et al., *Injection of subunits of cyclic AMP-dependent protein kinase into cardiac myocytes modulates Ca 2+ current.* Nature, 1982. **298**(5874): p. 576-578.
101. Warrier, S., et al., *cAMP microdomains and L-type Ca2+ channel regulation in guinea-pig ventricular myocytes.* The Journal of physiology, 2007. **580**(3): p. 765-776.
102. Bhogal, N.K., A. Hasan, and J. Gorelik, *The development of compartmentation of cAMP signaling in cardiomyocytes: the role of T-tubules and caveolae microdomains.* Journal of cardiovascular development and disease, 2018. **5**(2): p. 25.

103. Kumari, N., H. Gaur, and A. Bhargava, *Cardiac voltage gated calcium channels and their regulation by β-adrenergic signaling.* Life sciences, 2018. **194**: p. 139-149.
104. Yoshida, A., et al., *Cyclic AMP-dependent phosphorylation and regulation of the cardiac dihydropyridine-sensitive Ca channel.* FEBS letters, 1992. **309**(3): p. 343-349.
105. Sculptoreanu, A., et al., *Voltage-dependent potentiation of the activity of cardiac L-type calcium channel alpha 1 subunits due to phosphorylation by cAMP-dependent protein kinase.* Proceedings of the National Academy of Sciences, 1993. **90**(21): p. 10135-10139.
106. Fuller, M.D., et al., *Molecular mechanism of calcium channel regulation in the fight-or-flight response.* Science signaling, 2010. **3**(141): p. ra70-ra70.
107. Fu, Y., et al., *Phosphorylation sites required for regulation of cardiac calcium channels in the fight-or-flight response.* Proceedings of the National Academy of Sciences, 2013. **110**(48): p. 19621-19626.
108. A Catterall, W., *Regulation of cardiac calcium channels in the fight-or-flight response.* Current molecular pharmacology, 2015. **8**(1): p. 12-21.
109. Ahern, B.M. and J. Satin, *The L-type calcium channel current modulation mechanism: the plot thickens and fogs.* The Journal of clinical investigation, 2019. **129**(2): p. 496-498.
110. Ganesan, A.N., et al., *β-adrenergic stimulation of L-type Ca2+ channels in cardiac myocytes requires the distal carboxyl terminus of α1C but not serine 1928.* Circulation research, 2006. **98**(2): p. e11-e18.
111. Yang, L., et al., *β-adrenergic regulation of the L-type Ca2+ channel does not require phosphorylation of α1C Ser1700.* Circulation research, 2013. **113**(7): p. 871-880.
112. Katchman, A., et al., *Proteolytic cleavage and PKA phosphorylation of α1C subunit are not required for adrenergic regulation of CaV1. 2 in the heart.* Proceedings of the National Academy of Sciences, 2017. **114**(34): p. 9194-9199.
113. Fu, Y., et al., *Basal and β-adrenergic regulation of the cardiac calcium channel CaV1. 2 requires phosphorylation of serine 1700.* Proceedings of the National Academy of Sciences, 2014. **111**(46): p. 16598-16603.
114. Hulme, J.T., et al., *Autoinhibitory control of the CaV1. 2 channel by its proteolytically processed distal C-terminal domain.* The Journal of physiology, 2006. **576**(1): p. 87-102.
115. Fu, Y., et al., *Deletion of the distal C terminus of CaV1. 2 channels leads to loss of β-adrenergic regulation and heart failure in vivo.* Journal of Biological Chemistry, 2011. **286**(14): p. 12617-12626.
116. Oz, S., et al., *Protein kinase A regulates C-terminally truncated CaV1. 2 in Xenopus oocytes: roles of N-and C-termini of the α1C subunit.* The Journal of physiology, 2017. **595**(10): p. 3181-3202.
117. Yang, L., et al., *Cardiac Ca V 1.2 channels require β subunits for β-adrenergic–mediated modulation but not trafficking.* The Journal of clinical investigation, 2019. **129**(2): p. 647-658.
118. Papa, A., et al., *Adrenergic CaV1. 2 activation via rad phosphorylation converges at α1C I-II Loop.* Circulation Research, 2021. **128**(1): p. 76-88.

119. Weiss, S., et al., *Regulation of cardiac L-type Ca2+ channel CaV1. 2 via the β-adrenergic-cAMP-protein kinase A pathway: old dogmas, advances, and new uncertainties.* Circulation research, 2013. **113**(5): p. 617-631.
120. Pankonien, I., et al., *Ahnak1 is a tuneable modulator of cardiac Ca (v) 1.2 calcium channel activity.* Journal of muscle research and cell motility, 2011. **32**(4-5): p. 281-290.
121. Hu, Z., M.C. Liang, and T.W. Soong, *Alternative splicing of L-type CaV1. 2 calcium channels: implications in cardiovascular diseases.* Genes, 2017. **8**(12): p. 344.
122. Landstrom, A.P., D. Dobrev, and X.H. Wehrens, *Calcium signaling and cardiac arrhythmias.* Circulation research, 2017. **120**(12): p. 1969-1993.
123. Zipes, D.P., *Mechanisms of clinical arrhythmias.* Journal of cardiovascular electrophysiology, 2003. **14**(8): p. 902-912.
124. January, C.T., J.M. Riddle, and J.J. Salata, *A model for early afterdepolarizations: induction with the Ca2+ channel agonist Bay K 8644.* Circ Res, 1988. **62**(3): p. 563-71.
125. January, C.T. and J.M. Riddle, *Early afterdepolarizations: mechanism of induction and block. A role for L-type Ca2+ current.* Circ Res, 1989. **64**(5): p. 977-90.
126. Han, D., et al., *Dysfunctional Cav1. 2 channel in Timothy syndrome, from cell to bedside.* Experimental Biology and Medicine, 2019. **244**(12): p. 960-971.
127. Sheng, X., et al., *Two mechanistically distinct effects of dihydropyridine nifedipine on CaV1. 2 L-type Ca2+ channels revealed by Timothy syndrome mutation.* European journal of pharmacology, 2012. **685**(1-3): p. 15-23.
128. Yarotskyy, V. and K. Elmslie, *Roscovitine, a cyclin-dependent kinase inhibitor, affects several gating mechanisms to inhibit cardiac L-type (Ca (V) 1.2) calcium channels.* British journal of pharmacology, 2007. **152**(3): p. 386-395.
129. Yarotskyy, V., et al., *The Timothy syndrome mutation of cardiac CaV1. 2 (L-type) channels: multiple altered gating mechanisms and pharmacological restoration of inactivation.* The Journal of physiology, 2009. **587**(3): p. 551-565.
130. Yazawa, M., et al., *Using induced pluripotent stem cells to investigate cardiac phenotypes in Timothy syndrome.* Nature, 2011. **471**(7337): p. 230-234.
131. Splawski, I., et al., *Cav1. 2 calcium channel dysfunction causes a multisystem disorder including arrhythmia and autism.* Cell, 2004. **119**(1): p. 19-31.
132. Splawski, I., et al., *Severe arrhythmia disorder caused by cardiac L-type calcium channel mutations.* Proceedings of the National Academy of Sciences, 2005. **102**(23): p. 8089-8096.
133. Lorenzon, N.M. and K.G. Beam, *Disease-causing mutations of calcium channels.* Channels, 2008. **2**(3): p. 163-179.
134. Dick, I.E., et al., *Arrhythmogenesis in Timothy Syndrome is associated with defects in Ca 2+-dependent inactivation.* Nature communications, 2016. **7**(1): p. 1-12.
135. Jacobs, A., et al., *Verapamil decreases ventricular tachyarrhythmias in a patient with Timothy syndrome (LQT8).* Heart Rhythm, 2006. **3**(8): p. 967-970.
136. Li, G. and L. Zhang, *The role of mexiletine in the management of long QT syndrome.* Journal of Electrocardiology, 2018. **51**(6): p. 1061-1065.

137. Nitta, J.-i., et al., *Subcellular mechanism for Ca (2+)-dependent enhancement of delayed rectifier K+ current in isolated membrane patches of guinea pig ventricular myocytes.* Circulation research, 1994. **74**(1): p. 96-104.
138. Tohse, N., *Calcium-sensitive delayed rectifier potassium current in guinea pig ventricular cells.* American Journal of Physiology-Heart and Circulatory Physiology, 1990. **258**(4): p. H1200-H1207.
139. Campuzano, O., R. Brugada, and A. Iglesias, *Genetics of Brugada syndrome.* Current opinion in cardiology, 2010. **25**(3): p. 210-215.
140. Antzelevitch, C., *Role of spatial dispersion of repolarization in inherited and acquired sudden cardiac death syndromes.* American Journal of Physiology-Heart and Circulatory Physiology, 2007. **293**(4): p. H2024-H2038.
141. Antzelevitch, C., et al., *Clinical perspective.* Circulation, 2007. **115**(4): p. 442-449.
142. Zhang, Q., et al., *Mutations in voltage-gated L-type calcium channel: implications in cardiac arrhythmia.* Channels, 2018. **12**(1): p. 201-218.
143. Burashnikov, E., et al., *Mutations in the cardiac L-type calcium channel associated with inherited J-wave syndromes and sudden cardiac death.* Heart Rhythm, 2010. **7**(12): p. 1872-1882.
144. Mizusawa, Y. and A.A. Wilde, *Brugada syndrome.* Circulation: Arrhythmia and Electrophysiology, 2012. **5**(3): p. 606-616.
145. Goldhaber, J.I. and M.A. Hamilton, *Role of inotropic agents in the treatment of heart failure.* Circulation, 2010. **121**(14): p. 1655-60.
146. Wilkins, B.J. and J.D. Molkentin, *Calcium–calcineurin signaling in the regulation of cardiac hypertrophy.* Biochemical and biophysical research communications, 2004. **322**(4): p. 1178-1191.
147. Bers, D.M., *Calcium cycling and signaling in cardiac myocytes.* Annu. Rev. Physiol., 2008. **70**: p. 23-49.
148. Gao, H., et al., *Ca2+ influx through L-type Ca2+ channels and transient receptor potential channels activates pathological hypertrophy signaling.* Journal of molecular and cellular cardiology, 2012. **53**(5): p. 657-667.
149. Chen, X., et al., *Calcium influx through Cav1. 2 is a proximal signal for pathological cardiomyocyte hypertrophy.* Journal of molecular and cellular cardiology, 2011. **50**(3): p. 460-470.
150. Shimada, T., et al., *Long acting calcium antagonist amlodipine prevents left ventricular remodeling after myocardial infarction in rats.* Cardiovascular research, 1998. **37**(3): p. 618-626.
151. Massart, P.-E., et al., *Carvedilol and lacidipine prevent cardiac hypertrophy and endothelin-1 gene overexpression after aortic banding.* Hypertension, 1999. **34**(6): p. 1197-1201.
152. Correll, R.N., et al., *Caveolae-localized L-type Ca2+ channels do not contribute to function or hypertrophic signalling in the mouse heart.* Cardiovascular research, 2017. **113**(7): p. 749-759.
153. Tanaka, S., Y. Fujio, and H. Nakayama, *Caveolae-specific CaMKII signaling in the regulation of voltage-dependent calcium channel and cardiac hypertrophy.* Frontiers in physiology, 2018. **9**: p. 1081.

154. Anderson, M.E., J.H. Brown, and D.M. Bers, *CaMKII in myocardial hypertrophy and heart failure.* J Mol Cell Cardiol, 2011. **51**(4): p. 468-73.
155. Ikeda, S., et al., *Blockade of L-type Ca 2+ channel attenuates doxorubicin-induced cardiomyopathy via suppression of CaMKII-NF-κB pathway.* Scientific reports, 2019. **9**(1): p. 1-14.
156. Bristow, M.R., *β-Adrenergic receptor blockade in chronic heart failure.* Circulation, 2000. **101**(5): p. 558-569.
157. Chen, X., et al., *L-type Ca2+ channel density and regulation are altered in failing human ventricular myocytes and recover after support with mechanical assist devices.* Circulation research, 2002. **91**(6): p. 517-524.
158. Yang, L., et al., *Loss of β-adrenergic–stimulated phosphorylation of CaV1. 2 channels on Ser1700 leads to heart failure.* Proceedings of the National Academy of Sciences, 2016. **113**(49): p. E7976-E7985.
159. Balijepalli, R.C., et al., *Localization of cardiac L-type Ca2+ channels to a caveolar macromolecular signaling complex is required for β2-adrenergic regulation.* Proceedings of the National Academy of Sciences, 2006. **103**(19): p. 7500-7505.
160. Hong, T.-T., et al., *BIN1 is reduced and Cav1. 2 trafficking is impaired in human failing cardiomyocytes.* Heart rhythm, 2012. **9**(5): p. 812-820.
161. Reynet, C. and C.R. Kahn, *Rad: a member of the Ras family overexpressed in muscle of type II diabetic humans.* Science, 1993. **262**(5138): p. 1441-1444.
162. Maguire, J., et al., *Gem: an induced, immediate early protein belonging to the Ras family.* Science, 1994. **265**(5169): p. 241-244.
163. Finlin, B.S. and D.A. Andres, *Rem is a new member of the Rad-and Gem/Kir Ras-related GTP-binding protein family repressed by lipopolysaccharide stimulation.* Journal of Biological Chemistry, 1997. **272**(35): p. 21982-21988.
164. FINLIN, B.S., et al., *Rem2, a new member of the Rem/Rad/Gem/Kir family of Ras-related GTPases.* Biochemical Journal, 2000. **347**(1): p. 223-231.
165. Yanuar, A., et al., *Crystal structure of human Rad GTPase of the RGK-family.* Genes to Cells, 2006. **11**(8): p. 961-968.
166. Correll, R.N., et al., *The RGK family of GTP-binding proteins: regulators of voltage-dependent calcium channels and cytoskeleton remodeling.* Cellular signalling, 2008. **20**(2): p. 292-300.
167. Szymanowska-Narloch, A., et al., *Molecular profiles of non-small cell lung cancers in cigarette smoking and never-smoking patients.* Advances in medical sciences, 2013. **58**(2): p. 196-206.
168. Sonna, L.A., et al., *Selected contribution: effect of acute heat shock on gene expression by human peripheral blood mononuclear cells.* Journal of Applied Physiology, 2002. **92**(5): p. 2208-2220.
169. Kannangai, R., et al., *Hepatic angiomyolipoma and hepatic stellate cells share a similar gene expression profile.* Human pathology, 2005. **36**(4): p. 341-347.
170. Hawke, T.J., et al., *Rad is temporally regulated within myogenic progenitor cells during skeletal muscle regeneration.* American Journal of Physiology-Cell Physiology, 2006. **290**(2): p. C379-C387.
171. Fu, M., et al., *Rad GTPase attenuates vascular lesion formation by inhibition of vascular smooth muscle cell migration.* Circulation, 2005. **111**(8): p. 1071-1077.

172. Withers, C.N., et al., *Rad GTPase is essential for the regulation of bone density and bone marrow adipose tissue in mice.* Bone, 2017. **103**: p. 270-280.
173. Sasson, Y., et al., *RGK family G-domain: GTP analog complex structures and nucleotide-binding properties.* Journal of molecular biology, 2011. **413**(2): p. 372-389.
174. Béguin, P., et al., *RGK small GTP-binding proteins interact with the nucleotide kinase domain of Ca2+-channel β-subunits via an uncommon effector binding domain.* Journal of Biological Chemistry, 2007. **282**(15): p. 11509-11520.
175. Moyers, J.S., et al., *Rad and Rad-related GTPases interact with calmodulin and calmodulin-dependent protein kinase II.* Journal of Biological Chemistry, 1997. **272**(18): p. 11832-11839.
176. Beguin, P., et al., *Nuclear sequestration of β-subunits by Rad and Rem is controlled by 14-3-3 and calmodulin and reveals a novel mechanism for Ca2+ channel regulation.* Journal of molecular biology, 2006. **355**(1): p. 34-46.
177. Do Heo, W., et al., *PI (3, 4, 5) P3 and PI (4, 5) P2 lipids target proteins with polybasic clusters to the plasma membrane.* Science, 2006. **314**(5804): p. 1458-1461.
178. Moyers, J.S., et al., *Overexpression of Rad inhibits glucose uptake in cultured muscle and fat cells.* Journal of Biological Chemistry, 1996. **271**(38): p. 23111-23116.
179. Zhu, J., et al., *Rad, a novel Ras-related GTPase, interacts with skeletal muscle β-tropomyosin.* Journal of Biological Chemistry, 1996. **271**(2): p. 768-773.
180. Lynch, R.A., et al., *Novel and nondetected human signaling protein polymorphisms.* Physiological genomics, 2002. **10**(3): p. 159-168.
181. Chang, L., et al., *Rad GTPase deficiency leads to cardiac hypertrophy.* Circulation, 2007. **116**(25): p. 2976-2983.
182. Yada, H., et al., *Dominant negative suppression of Rad leads to QT prolongation and causes ventricular arrhythmias via modulation of L-type Ca2+ channels in the heart.* Circulation research, 2007. **101**(1): p. 69-77.
183. Wang, G., et al., *Rad as a novel regulator of excitation–contraction coupling and β-adrenergic signaling in heart.* Circulation research, 2010. **106**(2): p. 317-327.
184. Manning, J.R., et al., *Rad GTPase Deletion Attenuates Post-Ischemic Cardiac Dysfunction and Remodeling.* JACC: Basic to Translational Science, 2018. **3**(1): p. 83-96.
185. Sohal, D.S., et al., *Temporally Regulated and Tissue-Specific Gene Manipulations in the Adult and Embryonic Heart Using a Tamoxifen-Inducible Cre Protein.* Circulation Research, 2001. **89**(1): p. 20-25.
186. Lexow, J., et al., *Cardiac fibrosis in mice expressing an inducible myocardial-specific Cre driver.* Disease models & mechanisms, 2013. **6**(6): p. 1470-1476.
187. Rohrer, D.K., et al., *Cardiovascular and metabolic alterations in mice lacking both β1-and β2-adrenergic receptors.* Journal of Biological Chemistry, 1999. **274**(24): p. 16701-16708.
188. Gold, J.I., et al., *Determining the absolute requirement of g protein–coupled receptor kinase 5 for pathological cardiac hypertrophy.* Circulation research, 2012. **111**(8): p. 1048-1053.

189. Linscheid, N., et al., *Quantitative proteomics and single-nucleus transcriptomics of the sinus node elucidates the foundation of cardiac pacemaking.* Nature communications, 2019. **10**(1): p. 1-19.
190. Wang, F., et al., *RNAscope: a novel in situ RNA analysis platform for formalin-fixed, paraffin-embedded tissues.* The Journal of molecular diagnostics, 2012. **14**(1): p. 22-29.
191. Ahern, B.M., et al., *Myocardial-restricted ablation of the GTPase RAD results in a pro-adaptive heart response in mice.* Journal of Biological Chemistry, 2019.
192. Bristow, M.R., *Treatment of chronic heart failure with β-adrenergic receptor antagonists: a convergence of receptor pharmacology and clinical cardiology.* Circulation research, 2011. **109**(10): p. 1176-1194.
193. Lohse, M.J., S. Engelhardt, and T. Eschenhagen, *What Is the Role of β-Adrenergic Signaling in Heart Failure?* Circulation Research, 2003. **93**(10): p. 896-906.
194. Satin, J., *Regulation of cardiac calcium channels*, in *Cardiac Electrophysiology: From Cell to Bedside*. 2014, Elsevier. p. 103-113.
195. Finlin, B.S., et al., *Analysis of the complex between Ca2+ channel β-subunit and the Rem GTPase.* Journal of Biological Chemistry, 2006. **281**(33): p. 23557-23566.
196. Puckerin, A.A., et al., *Engineering selectivity into RGK GTPase inhibition of voltage-dependent calcium channels.* Proceedings of the National Academy of Sciences, 2018. **115**(47): p. 12051-12056.
197. Puhl III, H.L., et al., *Ancient origins of RGK protein function: Modulation of voltage-gated calcium channels preceded the protostome and deuterostome split.* PloS one, 2014. **9**(7).
198. Zhang, J., et al., *Rad GTPase inhibits cardiac fibrosis through connective tissue growth factor.* Cardiovascular research, 2011. **91**(1): p. 90-98.
199. Correll, R.N., et al., *Plasma membrane targeting is essential for Rem-mediated Ca2+ channel inhibition.* Journal of Biological Chemistry, 2007. **282**(39): p. 28431-28440.
200. Wang, Y., et al., *Ras-induced epigenetic inactivation of the RRAD (Ras-related associated with diabetes) gene promotes glucose uptake in a human ovarian cancer model.* Journal of Biological Chemistry, 2014. **289**(20): p. 14225-14238.
201. Kobirumaki-Shimozawa, F., et al., *Nano-imaging of the beating mouse heart in vivo: Importance of sarcomere dynamics, as opposed to sarcomere length per se, in the regulation of cardiac function.* The Journal of general physiology, 2016. **147**(1): p. 53-62.
202. Davis, J., et al., *A tension-based model distinguishes hypertrophic versus dilated cardiomyopathy.* Cell, 2016. **165**(5): p. 1147-1159.
203. Gresham, K.S., et al., *Sarcomeric protein modification during adrenergic stress enhances cross-bridge kinetics and cardiac output.* Journal of applied physiology, 2017. **122**(3): p. 520-530.
204. Gresham, K.S. and J.E. Stelzer, *The contributions of cardiac myosin binding protein C and troponin I phosphorylation to β-adrenergic enhancement of in vivo cardiac function.* The Journal of physiology, 2016. **594**(3): p. 669-686.
205. Bertero, E. and C. Maack, *Metabolic remodelling in heart failure.* Nature Reviews Cardiology, 2018. **15**(8): p. 457-470.

206. Sipido, K.R., G. Callewaert, and E. Carmeliet, *Inhibition and rapid recovery of Ca2+ current during Ca2+ release from sarcoplasmic reticulum in guinea pig ventricular myocytes.* Circulation research, 1995. **76**(1): p. 102-109.
207. Bupha-Intr, T., J. Laosiripisan, and J. Wattanapermpool, *Moderate intensity of regular exercise improves cardiac SR Ca2+ uptake activity in ovariectomized rats.* Journal of Applied Physiology, 2009. **107**(4): p. 1105-1112.
208. Freeman, K., et al., *Alterations in cardiac adrenergic signaling and calcium cycling differentially affect the progression of cardiomyopathy.* The Journal of clinical investigation, 2001. **107**(8): p. 967-974.
209. Jaski, B.E., et al., *Calcium upregulation by percutaneous administration of gene therapy in cardiac disease (CUPID Trial), a first-in-human phase 1/2 clinical trial.* Journal of cardiac failure, 2009. **15**(3): p. 171-181.
210. Jessup, M., et al., *Calcium upregulation by percutaneous administration of gene therapy in cardiac disease (CUPID) a phase 2 trial of intracoronary gene therapy of sarcoplasmic reticulum Ca2+-ATPase in patients with advanced heart failure.* Circulation, 2011. **124**(3): p. 304-313.
211. Raake, P.W., et al., *Cardiac G-protein–coupled receptor kinase 2 ablation induces a novel Ca2+ handling phenotype resistant to adverse alterations and remodeling after myocardial infarction.* Circulation, 2012. **125**(17): p. 2108-2118.
212. Schmid, E., et al., *Cardiac RKIP induces a beneficial β-adrenoceptor–dependent positive inotropy.* Nature medicine, 2015. **21**(11): p. 1298-1306.
213. Wang, J.-N., et al., *Response gene to complement 32 promotes vascular lesion formation through stimulation of smooth muscle cell proliferation and migration.* Arteriosclerosis, thrombosis, and vascular biology, 2011. **31**(8): p. e19-e26.
214. Levitan, B.M., et al., *Rad-GTPase contributes to heart rate via L-type calcium channel regulation.* Journal of Molecular and Cellular Cardiology, 2021. **154**: p. 60-69.
215. DiFrancesco, D., et al., *Properties of the hyperpolarizing-activated current (if) in cells isolated from the rabbit sino-atrial node.* The Journal of physiology, 1986. **377**(1): p. 61-88.
216. Chandler, N., et al., *Molecular architecture of the human sinus node: insights into the function of the cardiac pacemaker.* Circulation, 2009. **119**: p. 1562-1575.
217. Bohn, G., et al., *Expression of T-and L-type calcium channel mRNA in murine sinoatrial node.* FEBS letters, 2000. **481**(1): p. 73-76.
218. Lyashkov, A.E., et al., *Calcium cycling protein density and functional importance to automaticity of isolated sinoatrial nodal cells are independent of cell size.* Circulation research, 2007. **100**(12): p. 1723-1731.
219. Vinogradova, T.M., et al., *Rhythmic ryanodine receptor Ca2+ releases during diastolic depolarization of sinoatrial pacemaker cells do not require membrane depolarization.* Circulation research, 2004. **94**(6): p. 802-809.
220. Torrente, A.G., et al., *L-type Cav1.3 channels regulate ryanodine receptor-dependent Ca2+ release during sino-atrial node pacemaker activity.* Cardiovasc Res, 2016. **109**(3): p. 451-61.
221. Torrente, A.G., et al., *L-type Cav1. 3 channels regulate ryanodine receptor-dependent Ca2+ release during sino-atrial node pacemaker activity.* Cardiovascular Research, 2016. **109**(3): p. 451-461.

222. Lyashkov, A.E., et al., *Positive Feedback Mechanisms among Local Ca Releases, NCX, and I(CaL) Ignite Pacemaker Action Potentials.* Biophys J, 2018. **114**(5): p. 1176-1189.
223. Lyashkov, A.E., et al., *Positive feedback mechanisms among local Ca releases, NCX, and ICaL ignite pacemaker action potentials.* Biophysical journal, 2018. **114**(5): p. 1176-1189.
224. Yaniv, Y., E.G. Lakatta, and V.A. Maltsev, *From two competing oscillators to one coupled-clock pacemaker cell system.* Frontiers in physiology, 2015. **6**: p. 28.
225. Jones, S.A., M.R. Boyett, and M.K. Lancaster, *Declining into failure: the age-dependent loss of the L-type calcium channel within the sinoatrial node.* Circulation, 2007. **115**(10): p. 1183-1190.
226. Mangoni, M.E., et al., *Functional role of L-type Cav1. 3 Ca2+ channels in cardiac pacemaker activity.* Proceedings of the National Academy of Sciences, 2003. **100**(9): p. 5543-5548.
227. Christel, C.J., et al., *Distinct localization and modulation of Cav1.2 and Cav1.3 L-type Ca2+ channels in mouse sinoatrial node.* The Journal of Physiology, 2012. **590**(24): p. 6327-6341.
228. Mangoni, M.E., et al., *Functional role of L-type Cav1.3 Ca2+ channels in cardiac pacemaker activity.* Proc Natl Acad Sci U S A, 2003. **100**(9): p. 5543-8.
229. Hartzell, H.C., et al., *Sympathetic regulation of cardiac calcium current is due exclusively to cAMP-dependent phosphorylation.* Nature, 1991. **351**(6327): p. 573-576.
230. Boyett, M.R., H. Honjo, and I. Kodama, *The sinoatrial node, a heterogeneous pacemaker structure.* Cardiovascular research, 2000. **47**(4): p. 658-687.
231. van Eif, V.W., et al., *Transcriptome analysis of mouse and human sinoatrial node cells reveals a conserved genetic program.* Development, 2019. **146**(8).
232. Protas, L., D. DiFrancesco, and R.B. Robinson, *L-type but not T-type calcium current changes during postnatal development in rabbit sinoatrial node.* American Journal of Physiology-Heart and Circulatory Physiology, 2001. **281**(3): p. H1252-H1259.
233. Mesirca, P., A.G. Torrente, and M.E. Mangoni, *Functional role of voltage gated Ca2+ channels in heart automaticity.* Frontiers in physiology, 2015. **6**: p. 19.
234. Verheijck, E.E., et al., *Contribution of L-type Ca2+ current to electrical activity in sinoatrial nodal myocytes of rabbits.* American Journal of Physiology-Heart and Circulatory Physiology, 1999. **276**(3): p. H1064-H1077.
235. Sandercock, G.R.H. and D.A. Brodie, *The role of heart rate variability in prognosis for different modes of death in chronic heart failure.* Pacing and clinical electrophysiology, 2006. **29**(8): p. 892-904.
236. Van Berlo, J.H., M. Maillet, and J.D. Molkentin, *Signaling effectors underlying pathologic growth and remodeling of the heart.* The Journal of clinical investigation, 2013. **123**(1): p. 37-45.
237. Zaza, A., R. Robinson, and D. DiFrancesco, *Basal responses of the L-type Ca2+ and hyperpolarization-activated currents to autonomic agonists in the rabbit sino-atrial node.* The Journal of physiology, 1996. **491**(2): p. 347-355.

238. Mangoni, M.E., et al., *Bradycardia and slowing of the atrioventricular conduction in mice lacking CaV3. 1/α1G T-type calcium channels.* Circulation research, 2006. **98**(11): p. 1422-1430.
239. Honjo, H., et al., *Sarcoplasmic reticulum Ca2+ release is not a dominating factor in sinoatrial node pacemaker activity.* Circulation research, 2003. **92**(3): p. e41-e44.
240. Christel, C.J., et al., *Distinct localization and modulation of Cav1. 2 and Cav1. 3 L-type Ca2+ channels in mouse sinoatrial node.* The Journal of physiology, 2012. **590**(24): p. 6327-6341.
241. Pang, C., et al., *Rem GTPase interacts with the proximal CaV1. 2 C-terminus and modulates calcium-dependent channel inactivation.* Channels, 2010. **4**(3): p. 192-202.
242. MacDonald, E.A., R.A. Rose, and T.A. Quinn, *Neurohumoral control of sinoatrial node activity and heart rate: insight from experimental models and findings from humans.* Frontiers in physiology, 2020. **11**.
243. Opthof, T., et al., *Functional morphology of the mammalian sinuatrial node.* European heart journal, 1987. **8**(11): p. 1249-1259.
244. Mackaay, A., et al., *Interaction of adrenaline and acetylcholine on cardiac pacemaker function. Functional inhomogeneity of the rabbit sinus node.* Journal of Pharmacology and Experimental Therapeutics, 1980. **214**(2): p. 417-422.
245. Li, N., et al., *Redundant and diverse intranodal pacemakers and conduction pathways protect the human sinoatrial node from failure.* Science translational medicine, 2017. **9**(400).
246. Verheijck, E.E., et al., *Pacemaker synchronization of electrically coupled rabbit sinoatrial node cells.* The Journal of general physiology, 1998. **111**(1): p. 95-112.
247. Tardif, J.-C., et al., *Efficacy of ivabradine, a new selective I f inhibitor, compared with atenolol in patients with chronic stable angina.* European heart journal, 2005. **26**(23): p. 2529-2536.
248. Yancy, C.W., et al., *2017 ACC/AHA/HFSA focused update of the 2013 ACCF/AHA guideline for the management of heart failure: a report of the American College of Cardiology/American Heart Association Task Force on Clinical Practice Guidelines and the Heart Failure Society of America.* Journal of the American College of Cardiology, 2017. **70**(6): p. 776-803.
249. Pichavaram, P., et al., *Elevated plasma catecholamines functionally compensate for the reduced myogenic tone in smooth muscle STIM1 knockout mice but with deleterious cardiac effects.* Cardiovascular research, 2018. **114**(5): p. 668-678.
250. Mathar, I., et al., *Increased catecholamine secretion contributes to hypertension in TRPM4-deficient mice.* The Journal of clinical investigation, 2010. **120**(9): p. 3267-3279.
251. Peters, C.H., E.J. Sharpe, and C. Proenza, *Cardiac pacemaker activity and aging.* Annual review of physiology, 2020. **82**: p. 21-43.
252. Larson, E.D., et al., *Depressed pacemaker activity of sinoatrial node myocytes contributes to the age-dependent decline in maximum heart rate.* Proceedings of the National Academy of Sciences, 2013. **110**(44): p. 18011-18016.

253. Kim, M.S., et al., *Heterogeneity of calcium clock functions in dormant, dysrhythmically and rhythmically firing single pacemaker cells isolated from SA node.* Cell calcium, 2018. **74**: p. 168-179.
254. Bers, D.M., *Cardiac excitation-contraction coupling.* Nature, 2002. **415**(6868): p. 198-205.
255. Zuhlke, R.D., et al., *Calmodulin supports both inactivation and facilitation of L-type calcium channels.* Nature, 1999. **399**(6732): p. 159-62.
256. Bean, B.P., M.C. Nowycky, and R.W. Tsien, *β-Adrenergic modulation of calcium channels in frog ventricular heart cells.* Nature, 1984. **307**(5949): p. 371-375.
257. Morotti, S., et al., *Theoretical study of L-type Ca2+ current inactivation kinetics during action potential repolarization and early afterdepolarizations.* The Journal of physiology, 2012. **590**(18): p. 4465-4481.
258. Lei, M., et al., *PKA phosphorylation of Cav1. 2 channel modulates the interaction of calmodulin with the C terminal tail of the channel.* Journal of pharmacological sciences, 2018. **137**(2): p. 187-194.
259. Benmocha Guggenheimer, A., et al., *Interactions between N and C termini of α1C subunit regulate inactivation of CaV1.2 L-type Ca(2+) channel.* Channels (Austin), 2016. **10**(1): p. 55-68.
260. Ivanina, T., et al., *Modulation of L-type Ca2+ channels by gbeta gamma and calmodulin via interactions with N and C termini of alpha 1C.* J Biol Chem, 2000. **275**(51): p. 39846-54.
261. Hofmann, F., *Ca2+-and voltage-dependent inactivation of the expressed L-type Cav1. 2 calcium channel.* Archives of biochemistry and biophysics, 2005. **437**(1): p. 42-50.
262. Markandeya, Y.S. and T.J. Kamp, *Rational strategy to stop arrhythmias: early afterdepolarizations and L-type Ca2+ current.* Journal of General Physiology, 2015. **145**(6): p. 475-479.
263. Grandi, E., et al., *Interplay of voltage and Ca-dependent inactivation of L-type Ca current.* Progress in biophysics and molecular biology, 2010. **103**(1): p. 44-50.
264. Naraghi, M. and E. Neher, *Linearized buffered Ca2+ diffusion in microdomains and its implications for calculation of [Ca2+] at the mouth of a calcium channel.* Journal of Neuroscience, 1997. **17**(18): p. 6961-6973.
265. Fakler, B. and J.P. Adelman, *Control of KCa channels by calcium nano/microdomains.* Neuron, 2008. **59**(6): p. 873-881.
266. Shen, M.J. and D.P. Zipes, *Role of the autonomic nervous system in modulating cardiac arrhythmias.* Circulation research, 2014. **114**(6): p. 1004-1021.
267. Bayer, K.U., et al., *Interaction with the NMDA receptor locks CaMKII in an active conformation.* Nature, 2001. **411**: p. 801-805.
268. Wang, L., et al., *Different paths, same destination: divergent action potential responses produce conserved cardiac fight-or-flight response in mouse and rabbit hearts.* The Journal of Physiology, 2019. **597**(15): p. 3867-3883.
269. Wickman, K., et al., *Abnormal heart rate regulation in GIRK4 knockout mice.* Neuron, 1998. **20**(1): p. 103-14.
270. Nikolaev, V.O., et al., *β2-adrenergic receptor redistribution in heart failure changes cAMP compartmentation.* Science, 2010. **327**(5973): p. 1653-1657.

271. Chruscinski, A.J., et al., *Targeted disruption of the beta2 adrenergic receptor gene.* J Biol Chem, 1999. **274**(24): p. 16694-700.
272. Navedo, M.F., et al., *Increased coupled gating of L-type Ca2+ channels during hypertension and Timothy syndrome.* Circulation research, 2010. **106**(4): p. 748.
273. Dukes, I. and E. Vaughan Williams, *Effects of selective alpha 1-, alpha 2-, beta 1- and beta 2-adrenoceptor stimulation on potentials and contractions in the rabbit heart.* The Journal of Physiology, 1984. **355**(1): p. 523-546.
274. Tranquillo, J.a.S., A., *Can we trust the transgenic mouse? Insights from computer simulations.* International Conference on Functional Imaging and Modeling of the Heart, 2007: p. 210-219.
275. Mitarai, S., et al., *Two distinct inactivation processes related to phosphorylation in cardiac L-type Ca2+ channel currents.* American Journal of Physiology-Cell Physiology, 2000. **279**(3): p. C603-C610.
276. Xiang, Y. and B.K. Kobilka, *Myocyte adrenoceptor signaling pathways.* Science, 2003. **300**(5625): p. 1530-1532.
277. Myagmar, B.-E., et al., *Adrenergic receptors in individual ventricular myocytes: the beta-1 and alpha-1B are in all cells, the alpha-1A is in a subpopulation, and the beta-2 and beta-3 are mostly absent.* Circulation research, 2017. **120**(7): p. 1103-1115.
278. Jimenez, M., et al., *β1/β2/β3-adrenoceptor knockout mice are obese and cold-sensitive but have normal lipolytic responses to fasting.* FEBS letters, 2002. **530**(1-3): p. 37-40.
279. Devic, E., et al., *β-adrenergic receptor subtype-specific signaling in cardiac myocytes from β1 and β2 adrenoceptor knockout mice.* Molecular pharmacology, 2001. **60**(3): p. 577-583.
280. Yang, T., A. Puckerin, and H.M. Colecraft, *Distinct RGK GTPases differentially use α 1-and auxiliary β-binding-dependent mechanisms to inhibit Ca V 1.2/Ca V 2.2 channels.* PLoS One, 2012. **7**(5): p. e37079.
281. Finlin, B. and D. Andres, *Phosphorylation-dependent association of the Ras-related GTP-binding protein Rem with 14-3-3 proteins.* Archives of Biochemistry and Biophysics, 1999. **368**(2): p. 401-412.
282. Colecraft, H.M., *Designer genetically encoded voltage-dependent calcium channel inhibitors inspired by RGK GTPases.* The Journal of physiology, 2020. **598**(9): p. 1683-1693.
283. Murata, M., et al., *Creation of a genetic calcium channel blocker by targeted gem gene transfer in the heart.* Circulation research, 2004. **95**(4): p. 398-405.
284. Ward, Y., et al., *Phosphorylation of critical serine residues in Gem separates cytoskeletal reorganization from down-regulation of calcium channel activity.* Molecular and Cellular Biology, 2004. **24**(2): p. 651-661.
285. Béguin, P., et al., *14-3-3 and calmodulin control subcellular distribution of Kir/Gem and its regulation of cell shape and calcium channel activity.* Journal of cell science, 2005. **118**(9): p. 1923-1934.
286. Bannister, R., H. Colecraft, and K. Beam, *Rem inhibits skeletal muscle EC coupling by reducing the number of functional L-type Ca2+ channels.* Biophysical journal, 2008. **94**(7): p. 2631-2638.

287. Puckerin, A.A., et al., *Similar molecular determinants on Rem mediate two distinct modes of inhibition of CaV1. 2 channels.* Channels, 2016. **10**(5): p. 379-394.
288. Man, K.N.M., et al., *Tissue-specific adrenergic regulation of the L-type Ca2+ channel CaV1. 2.* Science Signaling, 2020. **13**(663).
289. Fischer, R., et al., *Calmodulin binds to and inhibits GTP binding of the ras-like GTPase Kir/Gem.* Journal of Biological Chemistry, 1996. **271**(41): p. 25067-25070.
290. Goonasekera, S.A., et al., *Decreased cardiac L-type Ca 2+ channel activity induces hypertrophy and heart failure in mice.* The Journal of clinical investigation, 2012. **122**(1): p. 280-290.
291. Siegelbaum, S. and R. Tsien, *Modulation of gated ion channels as a mode of transmitter action.* Trends in neurosciences, 1983. **6**: p. 307-313.
292. Tsien, R., et al., *Mechanisms of calcium channel modulation by β-adrenergic agents and dihydropyridine calcium agonists.* Journal of molecular and cellular cardiology, 1986. **18**(7): p. 691-710.
293. Almagor, L., et al., *The role of a voltage-dependent Ca2+ channel intracellular linker: a structure-function analysis.* Journal of Neuroscience, 2012. **32**(22): p. 7602-7613.
294. Fukushima, Y. and S. Hagiwara, *Currents carried by monovalent cations through calcium channels in mouse neoplastic B lymphocytes.* The Journal of physiology, 1985. **358**(1): p. 255-284.
295. Feng, W., et al., *Identifying the cardiac dyad proteome in vivo by a BioID2 knock-in strategy.* Circulation, 2020. **141**(11): p. 940-942.
296. Roger, V.L., et al., *Heart disease and stroke statistics—2011 update: a report from the American Heart Association.* Circulation, 2011. **123**(4): p. e18-e209.
297. Kemp, C.D. and J.V. Conte, *The pathophysiology of heart failure.* Cardiovascular Pathology, 2012. **21**(5): p. 365-371.
298. Inamdar, A.A. and A.C. Inamdar, *Heart failure: diagnosis, management and utilization.* Journal of clinical medicine, 2016. **5**(7): p. 62.
299. Ling, H., et al., *Requirement for Ca 2+/calmodulin–dependent kinase II in the transition from pressure overload–induced cardiac hypertrophy to heart failure in mice.* The Journal of clinical investigation, 2009. **119**(5): p. 1230-1240.
300. Zima, A.V., et al., *Ca handling during excitation–contraction coupling in heart failure.* Pflügers Archiv-European Journal of Physiology, 2014. **466**(6): p. 1129-1137.
301. Gómez, A.M., et al., *Defective excitation-contraction coupling in experimental cardiac hypertrophy and heart failure.* Science, 1997. **276**(5313): p. 800-806.
302. Roos, K.P., et al., *Hypertrophy and heart failure in mice overexpressing the cardiac sodium-calcium exchanger.* Journal of cardiac failure, 2007. **13**(4): p. 318-329.
303. Houser, S.R., V. Piacentino III, and J. Weisser, *Abnormalities of calcium cycling in the hypertrophied and failing heart.* Journal of molecular and cellular cardiology, 2000. **32**(9): p. 1595-1607.
304. Luo, M. and M.E. Anderson, *Mechanisms of altered Ca(2)(+) handling in heart failure.* Circ Res, 2013. **113**(6): p. 690-708.

305. El-Armouche, A. and T. Eschenhagen, *β-Adrenergic stimulation and myocardial function in the failing heart.* Heart failure reviews, 2009. **14**(4): p. 225.
306. Stokke, T.M., et al., *Geometry as a confounder when assessing ventricular systolic function: comparison between ejection fraction and strain.* Journal of the American College of Cardiology, 2017. **70**(8): p. 942-954.
307. Faerber, G., et al., *Induction of heart failure by minimally invasive aortic constriction in mice: reduced peroxisome proliferator-activated receptor γ coactivator levels and mitochondrial dysfunction.* The Journal of thoracic and cardiovascular surgery, 2011. **141**(2): p. 492-500. e1.
308. Frey, A., et al., *Experimental heart failure causes depression-like behavior together with differential regulation of inflammatory and structural genes in the brain.* Frontiers in behavioral neuroscience, 2014. **8**: p. 376.
309. Wisløff, U., et al., *Increased contractility and calcium sensitivity in cardiac myocytes isolated from endurance trained rats.* Cardiovascular research, 2001. **50**(3): p. 495-508.
310. Bertero, E. and C. Maack, *Calcium signaling and reactive oxygen species in mitochondria.* Circulation research, 2018. **122**(10): p. 1460-1478.
311. Nickel, A., M. Kohlhaas, and C. Maack, *Mitochondrial reactive oxygen species production and elimination.* Journal of molecular and cellular cardiology, 2014. **73**: p. 26-33.
312. Lyon, A.R., et al., *SERCA2a gene transfer decreases sarcoplasmic reticulum calcium leak and reduces ventricular arrhythmias in a model of chronic heart failure.* Circulation: Arrhythmia and Electrophysiology, 2011. **4**(3): p. 362-372.
313. Tocchetti, C.G., et al., *Nitroxyl improves cellular heart function by directly enhancing cardiac sarcoplasmic reticulum Ca2+ cycling.* Circulation research, 2007. **100**(1): p. 96-104.
314. Yang, T., et al., *Rem, a member of the RGK GTPases, inhibits recombinant CaV1. 2 channels using multiple mechanisms that require distinct conformations of the GTPase.* The Journal of physiology, 2010. **588**(10): p. 1665-1681.
315. Yue, D.T., S. Herzig, and E. Marban, *Beta-adrenergic stimulation of calcium channels occurs by potentiation of high-activity gating modes.* Proceedings of the National Academy of Sciences, 1990. **87**(2): p. 753-757.
316. Miriyala, J., et al., *Role of CaVβ subunits, and lack of functional reserve, in protein kinase A modulation of cardiac CaV1. 2 channels.* Circulation research, 2008. **102**(7): p. e54-e64.
317. MOYERS, J.S., Z. Jianhua, and C.R. KAHN, *Effects of phosphorylation on function of the Rad GTPase.* Biochemical Journal, 1998. **333**(3): p. 609-614.
318. Sasaki, T., et al., *Direct inhibition of the interaction between α-interaction domain and β-interaction domain of voltage-dependent Ca2+ channels by Gem.* Journal of Biological Chemistry, 2005. **280**(10): p. 9308-9312.
319. Correll, R.N., et al., *Analysis of the Rem2-voltage dependant calcium channel β subunit interaction and Rem2 interaction with phosphorylated phosphatidylinositide lipids.* Cellular signalling, 2008. **20**(2): p. 400-408.
320. Del Villar, S.G., et al., *β-Adrenergic control of sarcolemmal CaV1. 2 abundance by small GTPase Rab proteins.* Proceedings of the National Academy of Sciences, 2021. **118**(7).

321. Cingolani, E., et al., *Gene therapy to inhibit the calcium channel β subunit: physiological consequences and pathophysiological effects in models of cardiac hypertrophy.* Circulation research, 2007. **101**(2): p. 166-175.
322. Ikeda, K., et al., *Possible involvement of endothelin-1 in cardioprotective effects of benidipine.* Hypertension Research, 2000. **23**(5): p. 491-496.
323. Zou, Y., et al., *Continuous blockade of L-type Ca2+ channels suppresses activation of calcineurin and development of cardiac hypertrophy in spontaneously hypertensive rats.* Hypertension Research, 2002. **25**(1): p. 117-124.
324. Onohara, N., et al., *TRPC3 and TRPC6 are essential for angiotensin II-induced cardiac hypertrophy.* The EMBO journal, 2006. **25**(22): p. 5305-5316.
325. Colella, M., et al., *Ca2+ oscillation frequency decoding in cardiac cell hypertrophy: role of calcineurin/NFAT as Ca2+ signal integrators.* Proceedings of the National Academy of Sciences, 2008. **105**(8): p. 2859-2864.
326. Zobel, C., et al., *Mechanisms of Ca2+-dependent calcineurin activation in mechanical stretch-induced hypertrophy.* Cardiology, 2007. **107**(4): p. 281-290.
327. Muth, J.N., et al., *A Ca2+-dependent transgenic model of cardiac hypertrophy: A role for protein kinase Cα.* Circulation, 2001. **103**(1): p. 140-147.
328. Iaccarino, G., et al., *β-adrenergic receptor kinase-1 levels in catecholamine-induced myocardial hypertrophy: regulation by β-but not α1-adrenergic stimulation.* Hypertension, 1999. **33**(1): p. 396-401.
329. Nakayama, H., et al., *Ca 2+-and mitochondrial-dependent cardiomyocyte necrosis as a primary mediator of heart failure.* The Journal of clinical investigation, 2007. **117**(9): p. 2431-2444.
330. Chen, H., et al., *Expression of Rem2, an RGK family small GTPase, reduces N-type calcium current without affecting channel surface density.* Journal of Neuroscience, 2005. **25**(42): p. 9762-9772.
331. Wang, S.-Q., et al., *Ca 2+ signalling between single L-type Ca 2+ channels and ryanodine receptors in heart cells.* Nature, 2001. **410**(6828): p. 592-596.
332. Guo, Y. and W.T. Pu, *Genetic mosaics for greater precision in cardiovascular research.* Circulation research, 2018. **123**(1): p. 27-29.
333. Reynolds, J.O., et al., *Junctophilin-2 is necessary for T-tubule maturation during mouse heart development.* Cardiovascular research, 2013. **100**(1): p. 44-53.
334. Chen, B., et al., *Critical roles of junctophilin-2 in T-tubule and excitation–contraction coupling maturation during postnatal development.* Cardiovascular research, 2013. **100**(1): p. 54-62.
335. Guo, A., et al., *Emerging mechanisms of T-tubule remodelling in heart failure.* Cardiovascular research, 2013. **98**(2): p. 204-215.
336. Janse, M.J., *Electrophysiological changes in heart failure and their relationship to arrhythmogenesis.* Cardiovascular research, 2004. **61**(2): p. 208-217.
337. Fenske, S., et al., *cAMP-dependent regulation of HCN4 controls the tonic entrainment process in sinoatrial node pacemaker cells.* Nature communications, 2020. **11**(1): p. 1-22.
338. Segura, A.M., O. Frazier, and L.M. Buja, *Fibrosis and heart failure.* Heart failure reviews, 2014. **19**(2): p. 173-185.
339. Ingwall, J.S., *Energy metabolism in heart failure and remodelling.* Cardiovascular research, 2009. **81**(3): p. 412-419.

340. Garvey, W.T., et al., *Muscle Rad expression and human metabolism: potential role of the novel Ras-related GTPase in energy expenditure and body composition.* Diabetes, 1997. **46**(3): p. 444-450.
341. Liu, J., et al., *RRAD inhibits the Warburg effect through negative regulation of the NF-κB signaling.* Oncotarget, 2015. **6**(17): p. 14982.
342. Yan, Y., et al., *Ras-related associated with diabetes gene acts as a suppressor and inhibits Warburg effect in hepatocellular carcinoma.* OncoTargets and therapy, 2016. **9**: p. 3925.
343. Quick, A.P., et al., *SPEG (striated muscle preferentially expressed protein kinase) is essential for cardiac function by regulating junctional membrane complex activity.* Circulation research, 2017. **120**(1): p. 110-119.
344. Splingard, A., et al., *Biochemical and structural characterization of the gem GTPase.* Journal of Biological Chemistry, 2007. **282**(3): p. 1905-1915.

VITA

Brooke M Ahern

EDUCATION

PhD in Physiology, University of Kentucky (Projected April 2021)

B.S. in Neuroscience, Brigham Young University (April 2016)

AWARDS

2020 Basic Cardiovascular Sciences Mentorship Program, American Heart Association

Selected by AHA-BCVS Early Career Committee as a visiting scholar in Dr. Mark Sussman's laboratory

2019-2020 AHA Predoctoral Fellowship (2 year award; $53,688)

2019-2020 Graduate Student Incentive Program Award (2 year award;$2600)

2019 Department of Physiology Hardin Award Winner 2019

Annual award to staff or trainee demonstrating dedication and enthusiasm for their work.

2019 New Investigator Travel Award, Basic Cardiovascular Sciences Scientific Sessions of the AHA ($500)

2019 Student Research Achievement Award at 63rd Annual Meeting of the Biophysical Society ($200)

2018,2019 Department of Physiology Annual Retreat Best Research Blitz Presentation

2018,2019 Department of Physiology Annual Retreat Best Graduate Student Poster Presentation

2018 Poster Competition, 2nd Place at Gill Heart Cardiovascular Research Day, University of Kentucky

2018 Research Blitz, 2nd Place at Gill Heart Cardiovascular Research Day, University of Kentucky

2017 NIGMS Grant T32GM118292 (1 year award)

PROFESSIONAL EXPERIENCE

2016-2021 Graduate Research Assistant

University of Kentucky

	Mentor: Jonathan Satin, PhD
2014-2016	Undergraduate Research Assistant
	Brigham Young University
	Mentor: Dawson Hedges, MD
2014-2016	Teaching Assistant
	Brigham Young University
	Mentor: Steven Luke, PhD
2016	Undergraduate Research Assistant
	Brigham Young University
	Mentor: Steven Luke, PhD

PUBLICATIONS

Levitan, B.M.*, **Ahern, B.M.***, Aloysius, A., Brown, L., Wen, Y., Andres, D.A. and Satin, J., (2021). Rad-GTPase contributes to heart rate via L-type calcium channel regulation. *Journal of Molecular and Cellular Cardiology*, *154*, pp.60-69.

Shindo, K., Peng, H., Donahue, R.R., **Ahern, B.M**., Levitan, B.M., Satin, J., Seifert, A.W. and Abdel-Latif, A. (2020). Evaluating spiny mice (Acomys) as a model for cardiac research. *bioRxiv*.

Miller, J.M., Meki, M.H., Ou, Q., George, S.A., Gams, A., Abouleisa, R.R., Tang, X.L., **Ahern, B.M.,** Giridharan, G.A., El-Baz, A., Hill, B.G., Satin, J., Conklin, D.J., Moslehi, J., Bolli, R., Ribeiro, A.J.S., Efimov, I.R., and Mohamed, T.M.A. (2020). Heart Slice Culture System Reliably Demonstrates Clinical Drug-Related Cardiotoxicity. *Toxicology and Applied Pharmacology,* 406,115213.

Ahern, B., Sebastian, A., Andres, D.A. and Satin, J., (2020). Myocardial RAD Deletion Increases Early L-type Calcium Current without Affecting Late Calcium Current through Multiple Mechanisms. *Biophysical Journal*, *118*(3), p.105a.

Ahern, B.M., Levitan, B.M., Veeranki, S., Shah, M., Ali, N., Sebastian, A., Su, W., Gong, M.C., Li, J., Stelzer, J.E. and Andres, D.A., (2019). Myocardial-restricted ablation of the GTPase RAD results in a pro-adaptive heart response in mice. *Journal of Biological Chemistry*, 294(28),10913-10927..

Ahern, B.M. and Satin, J., (2019). The L-type calcium channel current modulation mechanism: the plot thickens and fogs. *The Journal of Clinical Investigation*, *129*(2),496-498.

Ahern, B., Levitan, B., Veeranki, S., Shah, M., Ali, N., Sebastian, A., Li, J., Stelzer, J.E., Andres, D. and Satin, J., (2019). Rad Ablation as a Treatment to Target Cardiac Inotropy via L-type Calcium Channel Function. *Circulation Research*, *125*(Suppl_1), pp.A807.

Ahern, B., Shah, M., Sebastian, A., Andres, D.A. and Satin, J., (2019). Myocardial Rad Deletion Modulates L-Type Calcium Channel Current. *Biophysical Journal*, *116*(3), p.237a.

PRESENTATIONS

Ahern, B., Sebastian, A., Andres, D.A. and Satin, J. (2020, February). Myocardial RAD Deletion Increases Early L-type Calcium Current without Affecting Late Calcium Current through Multiple Mechanisms. Poster presentation at the 64th Annual Meeting of the Biophysical Society, San Diego, California.

.

Ahern, B., Sebastian, A., Andres, D., Satin, J. (2019, September). *Rad Deletion Increases Early $I_{Ca,L}$ without Affecting Late, Arrhythmogenic $I_{Ca,L}$ through Faster Calcium Dependent Inactivation*. Poster session presented at the Gill Heart Institute Cardiovascular Research Day at University of Kentucky, Lexington, KY.

Ahern, B., Levitan, B., Veeranki, S., Shah, M., Ali, N., Sebastian, A., Li, J., Stelzer, J., Andres, D., Satin, J. (2019, July). *Rad Ablation as a Treatment to Target Cardiac Inotropy Via L-Type Calcium Channel Function.* Poster session presented at Basic Cardiovascular Sciences Scientific Sessions, Boston, Massachusetts.

Ahern, B., Shah, M., Sebastian, A., Andres, D.A. and Satin, J., (2019, March). Myocardial Rad Deletion Modulates L-Type Calcium Channel Current. *Biophysical Journal*, *116*(3), p.237a. **Poster presentation award** at the 63rd Annual Meeting of the Biophysical Society, Baltimore, Maryland.

Ahern, B., Levitan, B., Shah, M., Sebastian, A., Bessinger, Z., Mihail, R.P., Jacobs, N., Andres, D., Satin, J. (2018, June). *Cardiac Specific Rad Ablation Enhances Cardiac Function.* Poster session presented at Cardiac Regulatory Mechanisms of Gordon Research Conferences at Colby Sawyer College, New London, New Hampshire.

Ahern, B., Levitan, B., Shah, M., Sebastian, A., Bessinger, Z., Mihail, R.P., Jacobs, N., Andres, D., Satin, J. (2018, April). *Cardiac Specific Rad Ablation Enhances Cardiac Function Long-term.* **Selected for Oral Presentation** at the Kentucky Chapter of the American Physiological Society at University of Louisville, Louisville, KY.

Ahern, B., Levitan, B., Shah, M., Sebastian, A., Bessinger, Z., Mihail, R.P., Jacobs, N., Andres, D., Satin, J. (2017, November). *Cardiac Specific Rad Deletion Enhances Cardiac Function through Safe, Stable Positive Inotropic Support*. Poster session presented at the Gill Heart Institute Cardiovascular Research Day at University of Kentucky, Lexington, KY. **Selected for Oral Presentation**.

Shah, M., Sebastian, A., Simpson, L., Andres, D., Satin, J., **Ahern, B**. (2017, November). *Cardiac Specific Rad Knockout Increases Calcium Release*. Poster session presented at the Gill Heart Institute Cardiovascular Research Day at University of Kentucky, Lexington, KY.

Levitan, B., Shah, M., Rutland, J., **Ahern, B**., Andres, D., Satin, J. (2017, October). *Novel Approach for Modifying Intrinsic Heart Rate using RRAD Deletion*. Poster session presented at the Kentucky Chapter: American College of Cardiology Annual Meeting, Louisville, Kentucky.

SERVICE

2019-2020	Graduate Student Congress Physiology Representative
2019-2020	Graduate Student Representative for Department of Physiology
2019	Bardstown High School Career Panel
2018-2020	Biomedical Graduate Student Organization Buddy Program